INSTITUTO DE INGENIERIA

GEOLOGY AND PROBABILITY IN THE ASSESSMENT OF SEISMIC RISK

LUIS ESTEVA

JANUARY 1975

E13

UNIVERSIDAD NACIONAL AUTONOMA DE MEXICO

GEOLOGY AND PROBABILITY IN THE ASSESSMENT OF SEISMIC RISK

by

LUIS ESTEVA

INSTITUTE OF ENGINEERING

NATIONAL UNIVERSITY OF MEXICO

presented at the

2nd INTERNATIONAL CONGRESS OF THE INTERNATIONAL ASSOCIATION OF ENGINEERING GEOLOGY

SAO PAULO, BRASIL, AUGUST 1974

ABSTRACT

RESUMEN

Se presenta un criterio para la evaluación probabilística de riesgo sísmico cuando se cuenta con información geotectónica y sismológica. Los procedimientos sugeridos se basan en el empleo de la evidencia geológica para la formulación de un conjunto de hipótesis alternativas sobre los modelos analíticos de sismicidad. Se asigna una distribución de probabilidades a dicho conjunto y se introduce la evidencia estadística para juzgar la validez de cada hipótesis y modificar la probabilidad asignada inicialmente a ella.

ABSTRACT

A criterion is presented for the probabilistic evaluation of seismic risk when geotectonic and seismological information is available. The procedures suggested rely on use of geological evidence for the formulation of a set of alternate hypotheses concerning analytical models of seismicity. A probability distribution is assigned to that set and statistical evidence is introduced in order to assess the probable validity of each hypothesis and to modify the initial probability initially assigned to it.

1. INTRODUCTION

Rational formulation of engineering decisions in seismic areas requires probabilistic assessment of the maximum intensities that may occur at a site in given time intervals. Unlike variables that are relevant in many other decision problems, where probabilities are estimated almost exclusively on the basis of relative frequencies of the outcomes of repetitions of a given experiment, seismic risk estimates should make use of information stemming from sources of different nature, some of which, while being the object of probabilistic evaluations, can not be interpreted in terms of relative frequencies. Thus, geologists talk of the maximum magnitude that may be generated in a given area, by looking at the dimensions of the gological accidents and by extrapolating the observations of other regions which available evidence allows to brand as similar to the one of interest. Following nearly parallel lines, some geophysicists estimate the energy that can be liberated by a single shock in a given area by making quantitative

assumptions about source dimensions, dislocation amplitude and stress drop, consistent with tectonic models of the region and, again, with comparisons with areas of similar tectonic characteristics. Statisticians, on the other hand, are prone to base their predictions of the future exclusively on the basis of observations on a sample, however scanty that sample may be.

None of these approaches, by itself, suffices to provide a satisfactory answer to the requirements of decision makers: purely statistical analysis is unacceptable because it neglects a wealth of relevant information, and it is not clear that bounds can always be assigned to magnitudes in given areas, or that, when this is feasible, those bounds are sufficiently low that designing for them is economically sound, even if they are not very likely to occur in the near future. In fact, some studies relating source dimensions, stress drop and magnitude show that, considering not unusually high stress drops, it does not take very large source dimensions to get magnitudes 8.0 and greater.

A criterion for combining the above approaches in the probabilistic assessment of seismic risk is presented in this paper. Its philosophy consists in using the geological, geophysical or any other non-statistical evidence for producing a set of alternate assumptions concerning a mathematical (stochastic process) model of seismicity in a given source area. An initial, or prior, probability is assigned to each hypothesis, and the statistical information is then used for improving that probability assignment. The criterion is based on application of Bayes theorem, also called the theorem of the probabilities of the hypotheses. A previous formulation (1) has evolved through the interaction of multidisciplinary groups in the development of seismic risk studies performed in the last few years in Mexico (2-4). Since estimates of risk depend on conceptual models of the geophysical process involved, and these are little known at present, more questions are raised here than solutions given.

2. MEASURES OF SEISMIC RISK

Let y be a measure of earthquake intensity. According to the problem at hand, y may be peak ground acceleration, velocity, spectral ordinate for a given natural period, or, shortly, any variable that determines the response of the system under study. This means that a relation can be established between the intensity of a given earthquake and the corresponding loss $D(y)$.

A commonly applied criterion assumes that seismic risk should be measured by the highest intensity that can be caused at the site by the largest-magnitude earthquake that can be generated at any of the potential seismic sources in the vicinity. However, engineering systems cannot always be designed for the worst possible condition to be expected. Instead, decisions have to be based on cost-benefit studies. When designing for earthquakes, a significant cost term is made of the value of the expected actualized cost of damage or failure, as given by the following equation:

$$E[F] = \int_0^\infty \delta_t \, e^{-\gamma t} \, dt \qquad (1)$$

Here, $e^{-\gamma t}$ is a compound interest actualization function, γ the interest rate and δ_t the expected cost of damage or failure per unit time at instant t. Its value can be obtained from Eq 2, where $\nu_t(y)$ (in general a function of t) is the mean number of earthquakes per unit time whose intensity is greater than y and D(y) is defined above*:

$$\delta_t = \int_0^\infty - \frac{\partial \nu_t(y)}{\partial y} D(y)\, dy \qquad (2)$$

From Eqs 1 and 2 and the corresponding cost-benefit studies, it is concluded that evaluation of seismic risk for engineering purposes implies the definition of function $\nu_t(y)$ (henceforth called regional seismicity). This can be done as shown in the sequel.

3. MAGNITUDES, INTENSITIES AND FREQUENCY FUNCTIONS

With the possible exception of the rare cases where the record of intensities at a site suffices for producing reliable estimates of $\nu_t(y)$, evaluation of seismic risk should include the following steps:

a) Identifying the potential sources of activity
b) Formulating mathematical models of local seismicity for each source
c) Obtaining the contribution of each source to $\nu_t(y)$ and adding up contributions of the various sources.

---

* Eqs. 1 and 2 imply that every time that some damage or failure occurs the system is repaired or rebuilt in such a manner that the function D(y) remains unchanged. Corresponding expressions can be obtained for more general conditions (19). In general they require no more information about the mathematical model of seismicity.

This section deals with step c). The rest of the paper is devoted to the more difficult problems relevant to steps *a*) and *b*).

Let $\lambda_t(M)$ (also a function of time, as is regional seismicity) be the mean number of earthquakes with magnitude greater than M generated per unit volume and per unit time in a given seismic source. If a deterministic relationship M(y, X) holds between magnitude M, intensity y at a site, and focal coordinates X of an earthquake, $\nu_t(y)$ and $\lambda_t(M)$ can be related as follows:

$$\nu_t(y) = \int_{vol} \lambda_t(M(y,X))\, dV \qquad (3a)$$

Unless some information is available concerning systematic effects related to a given origin and a given site (attributable either to local soil or to propagation path properties), the influence of X is a function only of distance R, either to the instrumental focus or to the causative fault. Eq 3 then becomes:

$$\nu_t(y) = \int_{vol} \lambda_t(M(y,R))\, dV \qquad (3b)$$

A number of empirical or semi-empirical expressions relating M, R and y have been proposed. A summary of them is given in Ref 5. The author has made use of information in Refs 6-8 in order to derive expressions relating magnitude, hypocentral distance and various measures of intensity on firm ground, such as peak ground acceleration and of velocity (respectively a, v, $\overline{A}$ and $\overline{V}$) (9). These expressions are of the form

$$y = b_1 \, e^{b_2 M} \, R'^{-b_3} \qquad (4)$$

where $R' = R + R_0$; R must be given in kilometers and b_1, b_2, b_3 and R_0 are given in Table 1, which also shows the mean m and the standard deviation σ of the natural logarithm of the ratio of observed to computed intensities.

TABLE 1. EXPRESSIONS RELATING MAGNITUDE, INTENSITY AND HYPOCENTRAL DISTANCE

Expression for:	b_1	b_2	b_3	R_0	m	σ
v (cm/sec)	32	1.0	1.7	25	0.124	0.74
a (cm/sec^2)	5 600	0.8	2.0	40	0.04	0.64
$\overline{V}$ (cm/sec)	250	1.0	1.7	60	0.058	0.64
$\overline{A}$ (cm/sec^2)	69 600	0.8	2.0	70	0	0.75

The significant dispersion of these expressions, implied by the high values of σ, is due mainly to their having been obtained from data of earthquakes originating in different sources and having different mechanisms and propagation paths. The form of Eq 4 gives place, moreover, to a faster variation of intensities with respect to magnitudes in the near field than what occurs in nature because the liberation of energy is distributed throughout volumes whose dimensions can be significant with respect to the site-to-source distance. This relatively low sensitivity of y with respect to M in the near field has been verified in practice at least for earthquakes produced by a strike-slip mechanism (10, 11). This effect can be represented by expressions as simple as Eq 4, if b_2 is taken, for instance, of the form $b_2 = A + BR/(C + R)$.

For wide zones in the earth's crust, $\lambda(M)$, the average value of $\lambda_t(M)$ over long time intervals, can be approximated as follows,

$$\lambda(M) = \alpha_1 \, e^{-\beta_1 M} \quad \text{for } M \leq M_1$$
$$\lambda(M) = \alpha_2 \, e^{-\beta_2 M} \quad \text{for } M > M_1 \qquad (5)$$

where $\beta_2 \geq \beta_1$, M_1 is a magnitude beyond which there is a higher rate of decrease of $\lambda(M)$ with magnitude; continuity at M_1 requires that α_2 equal $\alpha_1 \exp[(\beta_2 - \beta_1) M_1]$.

As a result of the statistical dispersion in the expressions relating M, X and y, Eq 3 has to be changed to the following:

$$\nu(y) = \int_{vol} \lambda[M(y,X)] \, \varphi(y, X) \, dV \qquad (6)$$

where $\varphi(y, X)$ is a corrective function that can be computed as described in Ref 21.

4. ANALYTICAL MODELS OF SEISMICITY

As has been pointed out, when engineering decisions concerning construction in seismic areas have to be made, it does not suffice to express local seismicity in terms of an upper bound for magnitudes, the probability of whose excedance is arbitrarily assumed to be negligibly small. Instead, it should be expressed in terms of the probability distribution of the maximum magnitude that can be generated at given sources during given time periods. These probabilities depend on the following functions:

a) Frequency-magnitude relations for small volumes of the earth's crust
b) Statistical correlation functions of the process of earthquake generation in time and space.

The analytical models of local seismicity postulated in this paper are stochastic processes of the renewal type: the time interval between occurrence of successive earthquakes having magnitudes greater than a given value are mutually independent random variables. Let T be any such time interval. Its probability density function will be assumed of the gamma type:

$$f_T(t) = \frac{\nu}{(k-1)!} (\nu t)^{k-1} e^{-\nu t} \qquad (7)$$

Here, ν and k are two positive numbers and a! is the factorial function of a. This distribution was adopted because a wide number of distributions can be approximated by it, if parameters ν and k are properly chosen (17). ν and k are related with the first two moments of the probability density function of T:

$$E(T) = k/\nu, \quad V(T) = 1/\sqrt{k} \qquad (8)$$

where E means expectation and V coefficient of variation.

The probability density function of the wainting time T_1, from the origin to the occurrence of the first event, differs from Eq 7, since the time elapsed between the last prior event is usually unknown. The distribution of T_1 coincides with that of the excess life in a renewal process at an arbitrary value of t that tends to infinity. The corresponding probability density function has been shown to be (18)

$$f_{T_1}(t) = \frac{1}{E(T)} [1 - F_T(t)] \qquad (9)$$

where $F_T(t)$ is the probability distribution function of the time between successive events.

An important function in decisions under seismic hazard conditions is the conditional distribution of the additional time to next event, when it is known that there have been no events for a time t_0. If t_0 is measured from the instant just following the occurrence of an event and if $\tau = (T - t_0)/E(T)$ and $u_0 = t_0/E(T)$, then

$$f_\tau(u \mid T \geq t_0) = \frac{f_{T/E(T)}(u + u_0)}{1 - F_{T/E(T)}(u_0)} \qquad (10)$$

The Poisson process is the particular case of the gamma process for which k = 1. In that instance, Eqs 7, 9 and 10 lead to

$$f_T(t) = f_{T_1}(t) = f_{T-t_0}(t \mid T \geq t_0) = f_{T_1-t_0}(t \mid T_1 \geq t_0) = \nu e^{-\nu t} \qquad (11)$$

which reflect the non-informative property of Poisson process: at any given instant the conditional probability density function of the time to next event does not depend on the time elapsed since the last one.

Explicit expressions for evaluation of the conditional and the unconditional probability density functions of T and T_1 for the general gamma process are given in the appendix.

The Poisson process assumption is ordinarily adopted in probabilistic seismic risk studies. It is difficult either to substantiate it or to reject it in general on the basis of statistical data alone, since these are scanty,

particularly in small areas or for large magnitudes. After consideration of the geophysical processes in play it is reasonable to conclude, however, that if strain energy stored in a region grows in a more or less systematic manner, the risk function should grow with the time elapsed since the last event. Preliminary statistical analysis of the waiting times between earthquakes with magnitudes 6.5 or 7.0 and greater in some seismic provinces in the southern coast of Mexico shows that if shocks occurred in the same seismic province within a few months of each other are lumped together as single events, the resulting distribution of waiting times can be approximated by a gamma function with k = 2. However, results have not been uniform. Reliable evaluations of alternate assumptions concerning k will have to rest partially on simulation of the process of storage and liberation of strain energy.

According to Eqs 1 and 2, the actualized value of the expected cost of damage or failure is a function of $\nu_t(y)$, which is a function not only of $\lambda(M)$ in the neighbouring seismic sources, but also of the probability distribution of T/E(T). The possible significance of the value of k in the variables that affect seismic design decisions can be inferred from Table 2, which compares the initial and the conditional expected values of the time to next event, as well as the actualized values of the expected cost of failure for the Poisson and the gamma processes. These quantities were computed by means of the expressions developed in the appendix. The actualized value of the expected cost of failure was obtained from the expression that follows.

$$\frac{E[F]}{D} = \int_0^\infty f_T(t+t_o \mid T \geq t_o)\, e^{-\gamma t}\, dt \qquad (12)$$

This expression is consistent with the assumptions that a structure fails when a given intensity with retum period E(T) is exceeded, that the cost of that failure is D, and that the system is not rebuilt after failure. k was taken as 2, and two values of $\gamma E(T)$ were considered: 10 and 100.

TABLE 2. COMPARISON OF POISSON AND GAMMA PROCESSES

	GAMMA PROCESS, k = 2				POISSON PROCESS		
			E(F)/D			E(F)/D	
u_o	$E(\tau \mid T \geq t_o)$	$E(\tau_1 \mid T \geq t_o)$	$\gamma E(T)=10$	$\gamma E(T)=100$	$E(\tau \mid T \geq t_o) = E(\tau_1 \mid T \geq t_o$	$\gamma E(T)=10$	$\gamma E(T)=100$
0	1.0	0.75	0.0278	0.0004			
0.1	0.92	0.73	0.0511	0.0036			
0.2	0.86	0.71	0.0675	0.0059			
0.5	0.75	0.67	0.0973	0.0100			
1	0.67	0.63	0.120	0.0132	1.0	0.0909	0.0099
2	0.60	0.58	0.139	0.0158			
5	0.54	0.54	0.154	0.0179			
10	0.52	0.52	0.160	0.0187			
00 ∞	0.50	0.50	0.167	0.0196			

This table shows very significant differences between the expected cost of failure for both processes. At small values of t_o, E(F)/D for the Poisson process is greater than that for the gamma process, but as time goes on and no earthquakes occur, E(F)/D grows gradually for the gamma process, until the actualized risk for the latter becomes nearly twice that for the Poisson process. Clearly, the problem is significant when making engineering decisions.

Improved analytical models of seismicity should also cover those observed cases where the sources of large shocks move systematically along faults. This can be done by means of Markov process models, but extensive seismological and geophysical studies are required before the range of applicability of those models can be established and their parameters estimated.

5. ELEMENTS IN THE ESTIMATION OF LOCAL SEISMICITY

Only exceptionally can frequency-magnitude relations for small valumes of the earth's crust and statistical correlation functions of the process of earthquake generation be derived exclusively from statistical analysis of recorded shocks. In most cases this information is too limited for that purpose and it often seems to contradict geological evidence. Since the latter, as well as its connection with seismicity, is beset with wide margins of uncertainty, information of a different nature has to be evaluated, its uncertainty analysed, and conclusions reached that are consistent with all pieces of information. A probabilistic criterion that accomplishes this is presented here: on the basis of geotectonic information and of conceptual models of the physical processes involved, a set of alternate assumptions can be made concerning the functions in question (frequency-magnitude, time and space correlation) and an initial probability distribution assigned to it; statistical information is used to judge about the likelihood of each assumption, and a posterior probability distribution is obtained. How statistical information contributes to the posterior probabilities of the alternate assumptions depends on the extent of that information and on the degree of uncertainty implied by the

initial probabilities. Thus, if the geological evidence supports confidence in a particular assumption or range of assumptions, statistical information should not greatly modify the initial probabilities. If, on the other hand, a long and reliable statistical record is available, it may practically determine the form and parameters of the mathematical model selected to represent local seismicity.

Analysis of geological information must consider local details as well as general structure and evolution. In some areas it is clear that all potential earthquake sources can be identified by surface faults, and their displacements in recent geological times measured. When mean displacements per unit time can be estimated, the order of magnitude of creep and of energy liberated by shocks and hence of the frequency-magnitude law can be established (12, 13), the corresponding uncertainty evaluated, and the initial probability distribution assigned. The fact that frequency-magnitude relations are only weakly correlated with the size of recent displacements is reflected in large uncertainties (14).

Application of the criterion described in the foregoing paragraph may be unfeasible or inadequate in many practical problems, as in areas where the abundance of faults of different sizes, ages and activity, and the insufficient accuracy with which focal coordinates are determined preclude a differentiation of all sources. Regional seismicity may then be evaluated under the assumption that at least part of the seismic activity is distributed in a given volume rather than concentrated in faults of different importance. The same situation would be faced when dealing with active

zones where surface evidence of motions does not exist. Hence, consideration of the overall behaviour of complex geological structures is in general more significant than the study of local details.

To the authors's knowledge, not much work has been done in the analysis of the overall behaviour of large geological structures with respect to the energy that can be expected to be liberated per unit volume and per unit time in given portions of those structures. Important research and applications should be expected, however, since, as a result of the contribution of modern plate tectonics theory to the understanding of large scale tectonic processes, the numerical values of some of the variables correlated with energy liberation are being determined, and can be used at least to obtain orders of magnitude of expected activity along plate boundaries. Far less understood are the occurrence of shocks in apparently inactive regions of continental shields and the behaviour of complex continental blocks or regions of intense folding, but even there some progress is contemplated in the study of accumulation of stresses in the crust (15).

Knowledge of the geological structure can serve to formulate initial probability distributions of seismicity even when quantitative use of geophysical information seems beyond reach. Initial probability distribution of local seismicity parameters α, β, M_1 (Eq 5) of the relatively small volumes of the earth's crust that contribute significantly to the seismic risk at a site can be assigned by comparison with the average seismicity observed in wider areas of similar tectonic characteristics or where the extent and completeness of

statistical information warrant reliable estimates of frequency-magnitude curves (1). In this manner we can, for instance, use the information about the average distribution of the depths of earthquakes of different magnitudes throughout a seismic province in order to estimate the corresponding distribution in an area of that province where activity has been low during the observation interval even though there might be no apparent geophysical reason for the difference. Likewise, the expected value and the coefficient of variation of $\lambda(M)$ in a given area of moderate or low seismicity (like a continental shield) can be obtained from the statistics of the motions originated at all the supposedly stable or aseismic regions in the world (16).

Fig. 1 illustrates the kind of concepts that one has to consider when trying to use all available information for the quantitative probabilistic analysis of seismic risk. The southern coast of Mexico is one of the regions of highest activity in the world. Large shallow shocks are produced by the interaction of the continental mass and the ocean bottom's plate (Cocos plate) that underthrusts it. Seismological data shows significant gaps of activity along the coast during the present century and not much is known about previous history. At points along those gaps seismic risk estimates based on observed intensities would be quite low. No significant difference is evident in the geological structure of these regions with respect to the rest of the coast, with the exception of some faults transverse to the coast, that divide the continental formation into several blocks. An analysis of the locations of previous large earthquakes along

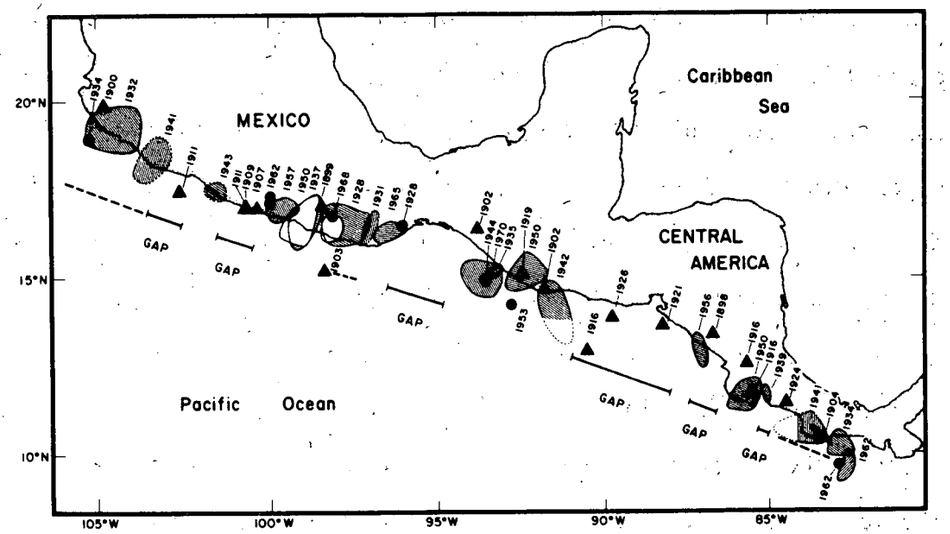

Fig. 1 Gaps of seismic activity (after Kelleher et al., Ref.20)

the coast has led Kelleher et al. (20) to conclude that those gaps are with high probability the locations of large magnitude shocks in the near future. The probabilistic evaluation of all these pices of information can be done as described in the next section.

6. SIGNIFICANCE OF STATISTICAL INFORMATION

In the proposed formulation, statistical data serve to ascertain the probable validity of each of the alternative models of local seismicity that can be postulated on the grounds of geological evidence. Any criterion that intends to weight information of different nature and different degrees of uncertainty should permit obtaining probabilistic conclusions consistent with the degree of confidence attached to each source of information. This is accomplished through use of the concepts of bayesian statistical analysis, as described in the sequel.

Let H_i, i = 1, . . . , n, be a comprehensive set of mutually exclusive assumptions concerning a given, imperfectly known phenomenon and let A be the observed outcome of such a phenomenon. Suppose also that before observing outcome A we assign an initial probability $P(H_i)$ to each hypothesis. If $P(A \mid H_i)$ is the probability of A in case hypothesis H_i is true, then Bayes' theorem states the following (17):

$$P(H_i \mid A) = P(H_i) \frac{P(A \mid H_i)}{\sum_j P(H_j)\, P(A \mid H_j)} \qquad (13)$$

The first member in this equation is the (posterior) probability that assumption H_i is true, given the observed outcome A.

In the evaluation of seismic risk problems Bayes' theorem can be used to improve the initial estimates of $\lambda(M)$, β, M_1, and variation of $\lambda(M)$ with depth in a given area.

Consider $\lambda(M)$. If a model as given by Eq 7 is adopted, we start by assuming for each M and initial probability function for the actual, but unknown, value of $\lambda(M)$. If the possible assumptions concerning the values of $\lambda(M)$ for a given M constitute a continuous interval, the initial probabilities of the alternative hypotheses can be expressed in terms sumption is made concerning the form of this probability density function, only the initial values of $E(\lambda(M))$ and $V(\lambda(M))$ have to be assumed. It is advantageous to assign to $\nu = k/E(T)$ a gamma distribution. Then, if ρ and μ

are the parameters of this initial distribution of ν, if k is assumed to be known, and if the observed outcome is expressed as the time t_n elapsed between n + 1 consecutive events (earthquakes with magnitude $\geq M$), application of Eq 13 leads to the conclusion that the posterior probability function of ν is also gamma, now with parameters $\rho + nk$ and $\mu + t_n$. The initial and the posterior expected values of ν are respectively equal to ρ/μ, and to $(\rho + nk)/(\mu + t_n)$. When initial uncertainty about ν is small ρ and μ will be relatively large and the initial and the posterior expected values of ν will not differ greatly. On the other hand, if only statistical information were deemed significant, ρ and μ should be given very small values in the initial distribution, and $E(\nu)$, and hence $\lambda(M)$, would be practically defined by n, k and t_n. This means that the initial estimates of geologists should not only include expected or most probable values of the different parameters, but also statements about ranges of possible values and degrees of confidence attached to each.

In the case studied above only a portion of the statistical information was used. In most cases, especially if seismic activity has been low during the observation interval, significant information is provided by the durations of the intervals elapsed from the initiation of observations to the first of the n + 1 events considered and from the last of those events until the end of the observation period. Here, application of Eq 13 leads to expressions slightly more complicated than those obtained when only information about t_n is used.

The particular case when the statistical record reports no events during time t_0 comes up frequently in practical problems. Expressions applicable to

that situation are presented in the appendix. Here, consider their application to one of the seismic gaps in Fig 1. An initial set of assumptions and corresponding probabilities was adopted as described in the following. From previous studies referring to all the southern coast of Mexico, local seismicity in the gap area (measured in terms of λ for $M \geq 6.5$) was represented by a gamma process with k = 2. An initial probability density function for ν was adopted in such a manner that the expected value of $\lambda(6.5)$ for the region coincided with its average throughout the complete seismic province. Two values of ρ were considered: 2 and 10, which correspond to coefficients of variation of 0.71 and 0.32, respectively. The values in Table 3 were obtained for the ratio of the final to the initial expected values of ν, in terms of u_o, the ratio of the length of the observation interval to the initial expected value of the return perior, E(T).

TABLE 3. BAYESIAN ESTIMATES OF SEISMICITY IN ONE SEISMIC GAP

$u_o = t_o/E(T)$	$E''(\nu)/E'(\nu)$		$E''(\tau_1 \mid T_1 \geq t_o)$	
	$\rho = 2$	$\rho = 10$	$\rho = 2$	$\rho = 10$
0	1.0	1.0	0.75	0.75
0.1	0.95	0.99	0.76	0.74
0.5	0.75	0.94	0.91	0.71
1	0.58	0.87	1.14	0.73
5	0.20	0.54	3.11	1.05
10	0.11	0.36	5.47	1.55
20	0.06	0.22	10.50	2.48

The last two columns of the table contain the ratios of the computed values of $E(T_1)$ and E(T) when ν is taken equal respectively to its initial or to its

posterior expected value. This table shows that, for $\rho = 10$, that is, when uncertainty attached to the geologically based assumptions is low, the expected value of the time to next event keeps decreasing, in accordance with the conclusions of Ref 20. However, as time goes on and no events occur the statistical evidence leads to a reduction in the estimated risk, which shows in the increased conditional expected values of τ_1. For $\rho = 2$ the geological evidence is less significant and risk estimates decrease at a faster rate.

Bayesian estimation of other parameters would run along the same lines. The most important problems emerging in practical applications are related to the bayesian analysis of jointly distributed variables (21).

7. CONCLUDING REMARKS

A common difficulty encountered in the solution of problems by interdisciplinary groups is the need to establish a clear formulation of the objectives and a framework that permits unified analysis of all viewpoints. In seismic risk evaluation different especialists have in their minds different models of seismicity. However, the objetive must be the same: estimation of probabilities that given intensities are exceeded at a site in given time intervals. As suggested in this paper, those probabilities are estimated from stochastic process models of the generation of earthquakes in different seismic sources. Since neither present geophysical knowledge nor statistical data warrant adoption of a specific analytical model, decisions are based on the

consideration of a set of alternate hypotheses concerning that model, and a probability distribution attached to that set. Establishment of this distribution can be done by application of bayesian statistical theory to the processing of all relevant pieces of information.

The analytical models presented here serve only to illustrate the possibilities. More general models should be studied as they are suggested by considerations about the physical processes involved (21).

8. ACKNOWLEDGEMENT

The author wishes to recognize the valuable comments of E. Rosenblueth and R. G. Sexsmith.

9. REFERENCES

1. L. Esteva, Seismicity prediction: a bayesian approach, *Procs., 4th World Conference on Earthquake Engineering*, Santiago (1969)

2. J. L. Trigos and L. Esteva, Riesgo sísmico en Las Truchas (México), *Institute of Engineering*, National University of Mexico (1973)

3. J. L. Trigos and L. Esteva, Riesgo sísmico en Managua, Nicaragua, *Ministry of Public Works*, México (1973)

4. J. L. Trigos and L. Esteva, Riesgo sísmico en El Sumidero (México), *Institute of Engineering*, National University of Mexico (1973)

5. N. N. Ambraseys, Dynamics and response of foundation materials in epicentral regions of strong earthquakes, *Procs., 5th World Conference on Earthquake Engineering*, Rome (1973)

6. D. E. Hudson, Analysis of strong motion earthquake accelerograms, Vol. III, Response spectra, part A, *EERL, Caltech*, Pasadena, Calif. (1972)

7. D. E. Hudson, Ed., Strong motion instrumental data on the San Fernando earthquake of February 9, 1971, *EERL, Caltech*, Pasadena, Calif. (1971)

8. D. E. Hudson, Strong motion earthquake accelerograms, digitized and plotted data, Vol. III, corrected accelerograms and integrated ground velocity and displacement curves, Part A, *EERL, Caltech*, Pasadena, Calif. (1971)

9. L. Esteva and R. Villaverde, Seismic risk, design spectra and structural reliability, *Procs., 5th World Conference on Earthquake Engineering*, Rome (1973)

10. J. H. Dietrich, A deterministic near-field source model, *Procs., 5th World Conference on Earthquake Engineering*, Rome (1973)

11. M. D. Trifunac, Characterization of response spectra by parameters governing the gross nature of the earthquake source mechanisms, *Procs., 5th World Conference on Earthquake Engineering*, Rome (1973)

12. R. E. Wallace, Earthquake recurrence intervals on the San Andreas Fault, *Bull. Geological Society of America*, Vol.81 (oct 1970)

13. G. F. Davies and J. N. Brune, Regional and global fault slip rates from seismicity, *Nature Physical Science*, Vol. 229, No 4 (jan 1971)

14. B. A. Petrushevsky, The geological fundamentals of seismic zoning, *Scientific Translation Service*, order 5032, Ann Arbor, Mich (1966)

15. E. Artyushkov (Institute of Physics of the Earth, USSR Academy of Sciences), personal communication.

16. L. Esteva, Bases para la formulación de decisiones de diseño sísmico, *Institute of Engineering*, National University of Mexico (1968)

17. H. Raiffa and R. Schlaifer, Applied statistical decision theory, *MIT Press*, Cambridge, Mass (1969)

18. E. Parzen, Stochastic processes, *Holden Day*, San Francisco (1962)

19. E. Rosenblueth, Optimum design for infrequent disturbances, submitted for publication to ASCE (1974)

20. J. Kelleher, L. Sykes and J. Oliver, Possible criteria for predicting earthquake locations and their application to major plate boundaries of the Pacific and the Caribeean, *Journal of Geophysical Research*, Vol. 78, No. 14 (may 1973)

21. L. Esteva, Probabilistic models of seismicity based on seismotectonic evidence, *Institute of Engineering*, National University of Mexico (1974)

APPENDIX 1. PARTICULAR GAMMA PROBABILITY FUNCTIONS

Explicit expressions for evaluation of some of the functions introduced in the text can be obtained in closed form when k is an integer. Some of these cases are studied here. The expressions obtained are used in the examples contained in the body of the paper.

Probability density function of T_1. Substitution of Eq 7 into Eq 9 and integration by parts lead to

$$f_{T_1}(t) = \frac{1}{k} \sum_{m=1}^{k} \frac{\nu}{(m-1)!} (\nu t)^{m-1} e^{-\nu t} \qquad (A1)$$

whose expected value is

$$E(T_1) = \frac{k+1}{2k} E(T) \qquad (A2)$$

Conditional probability density functions of T *and* T_1. The denominator of the second member of Eq 10 can be obtained in closed form when k is an integer. In that case,

$$f_r(u|T \geq t_o) = \frac{\frac{k}{(k-1)!} (k(u+u_o))^{k-1}}{\sum_{m=1}^{k} \frac{1}{(m-1)!} (k u_o)^{m-1}} e^{-ku} \qquad (A3)$$

The corresponding conditional probability density function for T_1 is

$$f_{\tau_1}(u|T_1 \geq t_o) = \frac{\sum_{m=1}^{k} \frac{k}{(m-1)!} [k(u+u_o)]^{m-1}}{\sum_{m=1}^{k} \sum_{n=1}^{m} \frac{1}{(n-1)!} (k u_o)^{n-1}} e^{-ku} \qquad (A4)$$

where $\tau_1 = (T_1 - t_o)/E(T)$.

The conditional expectations of T and T_1 can be obtained from weighting of T and T_1 with respect to the probability density functions of Eqs A3 and A4:

$$E(\tau \mid T \geq t_o) = (A - Bu_o)/B \qquad (A5)$$

$$E(\tau_1 | T_1 \geq t_o) = (A_1 - B_1 u_o)/B \qquad (A6)$$

where

$$A = \sum_{m=1}^{k+1} \frac{1}{(m-1)!} (k u_o)^{m-1} e^{-ku_o} \qquad (A7)$$

$$B = \sum_{m=1}^{k} \frac{1}{(m-1)!} (k u_o)^{m-1} e^{-ku_o} \qquad (A8)$$

$$A_1 = \frac{1}{k} \sum_{m=1}^{k} \sum_{n=1}^{m+1} \frac{m}{k(n-1)!} (k u_o)^{n-1} e^{-ku_o} \qquad (A9)$$

$$B_1 = \frac{1}{k} \sum_{m=1}^{k} \sum_{n=1}^{m} \frac{1}{(n-1)!} (k u_o)^{n-1} e^{-ku_o} \qquad (A10)$$

APPENDIX 2. BAYESIAN ESTIMATION OF ν WHEN $T_1 \geq t_o$

Suppose that the initial probability density function of ν in a given area is gamma with parameters ρ and μ, and that no events have occurred in the area for t_o years. The probability of this outcome given ν is equal to the probability that $T_1 \geq t_o$. From integration of Eq A1 one obtains,

$$P(T_1 \geq t \mid \nu, k) = \frac{1}{k} \sum_{m=1}^{k} \sum_{n=1}^{m} \frac{1}{(n-1)!} (\nu t_o)^{n-1} e^{-\nu t_o} \qquad (A11)$$

Application of Eq 13 in this case can be expressed as

$$f''(\nu | T_1 > t_o) = \frac{f'(\nu) P(T_1 \geq t_o | \nu, k)}{\int f'(\nu) P(T_1 \geq t_o | \nu, k) \, d\nu} \qquad (A12)$$

Here, f' and f'' stand for the initial and posterior probability density functions of ν and $f'(\nu)$ adopts the form of a gamma function with parameters ρ and μ. After performing all substitutions and integrations, the following is obtained:

$$f''(\nu \mid T_1 \geq t_o) = K^{-1} \sum_{m=1}^{k} \sum_{n=1}^{m} B_n \, g_n(\nu) \qquad (A13)$$

Here,

$$K = \sum_{m=1}^{k} \sum_{n=1}^{m} B_n \qquad (A14)$$

$$B_n = \frac{(n + \rho - 2)!}{(\rho - 1)!\ (n - 1)!} \cdot \frac{\mu^{\rho}\, t_o^{n-1}}{(t_o + \mu)^{n+\rho-2}} \qquad \text{(A15)}$$

and $g_n(v)$ is the gamma probability density function with parameters $t + \mu$, $n + \rho - 1$.

Instituto de Ingeniería
Research Division of the School of Engineering

Universidad Nacional Autónoma de México
Ciudad Universitaria, México 20, D. F.
MEXICO

PROGRAMA DE DESARROLLO DEL CURSO

SISMOLOGIA Y SISMICIDAD

Duración: 18 h, del 5 al 21 de julio

Clases: Martes y jueves de 17 a 20 h en el auditorio DESFI

5 de julio: Dr. Cinna Lomnitz - de 17 a 18:30 h
Temas: Origen y distribución de los temblores
Estructuras de la tierra. Tectónica global, regional y local. Tectónica del continente americano. Mecanismos sísmicos. Ondas sísmicas.

M en I J. Abraham Díaz R. - de 18:30 a 20 h

Tema: Efectos sísmicos en suelos granulares

7 de julio: Dr. Cinna Lomnitz
Temas:
Propagación de ondas en la tierra. Atenuación. Instrumentos para registrar temblores. Magnitud e intensidad. Isosistas. Determinación instrumental de la magnitud de un temblor. Sismicidad de la tierra. Predicción de temblores.

12 de julio: Dr. Gustavo Ayala - de 17 a 18:30 h
Temas: Propagación de ondas en un medio siminfinito. Propagación de ondas en un medio estratificado.

Dr. Octavio A. Rascón Chávez - de 18:30 a 20 h

Temas: Propiedades de los temblores
Relaciones entre magnitud, intensidad y distancia. Tipos de temblores. Propiedades estadísticas de los temblores.

14 de julio: Dr. Octavio A. Rascón Chávez - de 17 a 18:30 h

Temas: Elaboración de espectros de diseño. Procesamiento de acelerogramas. Componentes de traslación y rotación del suelo durante un sismo.

Dr. Luis Esteva - de 18:30 a 20 h

Temas: Sismicidad y riesgo sísmico
Teoría de decisiones en diseño estructural. El proceso estocástico de Poisson

19 y 21 de julio: Dr. Luis Esteva

Temas: La ocurrencia de temblores como proceso estocástico. Modelos analíticos. Estadística bayesiana en la estimación de riesgo sísmico. Aplicaciones. Regionalización sísmica. Sismicidad de la República Mexicana. Microregionalización sísmica.

DIRECTORIO DE PROFESORE DEL CURSO SIMOLOGIA Y SISMICIDAD

DR. GUSTAVO AYALA M.
Coordinador
Mecánica Aplicada
Instituto de Ingeniería ,UNAM
Tel.: 548.97.94

DR. LUIS ESTEVA MARABOTO
Investigador
Instituto de Ingeniería, UNAM
Tel.: 548.97.94

DR. EZIO FACCIOLI

DR. CINNA LIMNITZ
CONSULTOR
DIRAC, S.A.

DR. OCTAVIO A. RASCON CHAVEZ
Jefe de la División de Estudios Superiores
Facultad de Ingeniería, UNAM
Tel.: 548.09.50

'edcs. 21,VII.77.

centro de educación continua
división de estudios superiores
facultad de ingeniería, unam

SISMOLOGIA

Dr. Cinna Lomnitz

Julio de 1977

III CURSO INTERNACIONAL DE INGENIERIA SISMICA

SISMOLOGIA

C LOMNITZ

5 Y 7 DE JULIO DE 1977

INTRODUCCION

Desde el punto de vista del ingeniero, los sismos representan un riesgo importante que debe ser considerado en el diseño de toda estructura. En muchas regiones el riesgo de falla de la estructura por sismo puede llegar a dominar otras consideraciones de diseño. Por lo tanto, es necesario conocer ciertos aspectos básicos de sismología para fines de estimación del riesgo sísmico local.

Las presentes conferencias tratarán de los siguientes aspectos, que de ninguna manera agotan el tema de la sismología; pero se han seleccionado por ser relevantes en el marco de este curso.

A. Sismología y Sismotectónica

B. Sismología observacional

C. Predicción de temblores

Ante todo, es indispensable precisar que no conocemos la causa y el mecanismo de generación de los temblores. Existen ciertas hipótesis y se ha avanzado mucho en los últimos diez o quince años; pero se trata de fenómenos muy complejos cuya naturaleza exacta aún no llega a ser totalmente comprendida por la ciencia.

A. SISMOLOGIA Y SISMOTECTONICA

Observemos la distribución geográfica de los temblores en un globo (fig 1). Veremos que la actividad sísmica va rodeando y delineando ciertas grandes unidades geográficas, que son placas de la litósfera. Se cree que estas placas pueden tener movimientos absolutos y relativos, ya que descansan en una capa viscosa: astenósfera. Cuando dos placas se van alejando mutuamente, el hueco es rellenado por materiales que suben desde la astenósfera. En cambio, cuando dos placas se van acercando su choque mutuo es acomodado mediante la subducción, es decir, la absorción de una placa (la placa oceánica) por debajo de la otra (la placa continental). Si ambas placas en proceso de colisión son continentales se produce una compresión que pliega el borde continental y los deja como un acordeón (ejemplo: los Himalayas); los temblores se originan principalmente en los bordes de placas, debido a estos procesos de tensión o compresión entre las placas

Hay también sismos en el interior de las placas, ya que éstas no son homogéneas y, por el contrario, contienen numerosas imperfecciones que son otras tantas causas de concentración de esfuerzos. Algunos de estos sismos "intra-placas" pueden ser altamente destructivos. Sin embargo, la mayor proporción de la energía sísmica se localiza en los bordes de las placas litosféricas.

Fallas y fracturas. Una falla es un plano de discontinuidad mecánica entre dos unidades geológicas; en cambio, un contacto es un plano de discontinuidad deposicional (fig 2). Por ejemplo, una falla puede desplazar un contacto, pero no viceversa. El desplaza-

miento de los contactos a uno y otro lado de una falla, indica la actividad de la falla.

Prácticamente toda la superficie de la tierra ha sufrido deformación intensa; por lo tanto, existen fallas en todas partes. La sismología estudia la configuración de las unidades geológicas en relación a los sismos, y la sismotectónica estudia la deformación que dichas unidades han sufrido y su actividad sísmica.

Un sismo es una ruptura sobre un plano. Todo sismo se produce sobre una falla, generalmente una falla pre-existente. El largo de una falla y su importancia regional, indican la magnitud potencial del sismo que puede generar.

Pero antes hay que determinar si la falla es activa. Esta tarea es de crítica importancia y debe ser realizada por un geólogo experimentado. Consiste en analizar las relaciones entre la falla y las formaciones cenozoicas, muy particularmente las del cuaternario: desplazamiento del curso de los ríos, formación de terrazas, erosión y depósitos deltaicos, y otros indicios.

Hay fallas activas que atraviesan toda la corteza terrestre (fallas corticales), o toda la litósfera, como la Falla de San Andrés que es un borde de placas. Para poder determinar la importancia relativa de una placa, es necesario complementar la sismogeología regional con estudios geofísicos específicos sobre la estructura de la corteza. Por ejemplo, si existe una fuerte anomalía gravitacional, y si los estudios sismológicos revelan espesores diferentes de la corteza a ambos lados de la falla, podrá concluirse que la falla

compromete todo el espesor de la corteza.

Existen sismos destructores que se han originado en fallas cortas. La Falla de Tiscapa, que produjo el sismo de Managua de 1972, tiene un largo de unos 15-20 km. Sin embargo, la magnitud del sismo fue solamente de 6 en la escala de Richter. Los daños desproporcionados se debieron a la cercanía del epicentro y al tipo de construcciones.

Como ejemplo, veremos el análisis sismogeológico y sismotectónico del terremoto de Tangshan (China), en 1976.

B. SISMOLOGIA OBSERVACIONAL

Las ondas sísmicas se propagan en cualquier medio, excepto en el vacío, y su detección se limita únicamente a la sensibilidad de los aparatos y al ruido sísmico ambiente.

El sismógrafo es un instrumento que utiliza el principio del micrófono: transforma vibraciones mecánicas en impulsos eléctricos. El sistema inercial del sismómetro se compone de una masa suspendida mediante resortes o hilos: se mide la posición relativa del centro de masa con respecto al suelo. Hay una gran variedad de tipos y modelos de sismómetros, según la dirección del movimiento (de la suspensión) y el rango de frecuencias.

TIPOS DE SISMOMETROS

(a) Frecuencia:

Acelerógrafos	2 - 20 Hz
Sismómetros de periodo corto	1 Hz
Sismómetros de periodo largo	0.01 - 0.1 Hz

(b) Tipo de suspensión:

Vertical

Horizontal

Las características de amplificación de un sismómetro pueden regularse eléctricamente, es decir, variando la impedancia del circuito de salida y las características del equipo de registro. En principio es posible obtener amplificaciones máximas del orden de 10^6 en términos de desplazamiento a frecuencias de 1Hz (la amplificación se refiere al factor de escala en el sismograma). En la práctica, el ruido sísmico ambiente reduce la amplificación útil a una fracción de la sensibilidad del equipo. La mayoría de las buenas estaciones operan a una amplificación del orden de 50,000 a frecuencias de 1Hz.

Ondas sísmicas. En sismología, las ondas compresionales (sonido), se denominan "Ondas P"; y las transversales (rotacionales o de cizalle), se denominan "Ondas S". Las velocidades de estas ondas son muy diferentes entre sí y varían de un material a otro. Si ρ es la densidad del material y λ, μ son los números de Lamé (parámetros elásticos), las velocidades de P y S se expresan como sigue:

$$v_p = \sqrt{(\lambda + 2\mu)/\rho}$$

$$v_s = \sqrt{\mu/\rho}$$

Además de las ondas P y S, que se denominan "ondas de cuerpo", existen las ondas superficiales que se dan solamente en la interfase entre dos medios diferentes. Las amplitudes de las ondas superficiales decaen rápidamente desde la superficie hacia el interior del medio. Existen ondas Rayleigh (en las que cada partícula de la superficie

sigue una elipse retrógrada en el plano vertical); y ondas Love (en que la trayectoria de la partícula transversal a la dirección de propagación y está en el plano de la interfase). Las ondas superficiales son dispersivas y sus componentes de alta frecuencia se amortiguan rápidamente. Suelen adquirir amplitudes mucho mayores para las ondas de cuerpo, y desempeñan un papel importante desde el punto de vista del daño sísmico.

Predicción. A partir de 1966 se inició en China un programa oficial de predicción de temblores. Por ser el primer programa de este género en el mundo merece un análisis detallado.

El sistema chino de predicción se basa en las siguientes premisas:

1. Las causas directas de los sismos se desconocen.
2. La interacción de estas causas con la estructura geológica da margen a un cuadro muy complejo de síntomas y efectos.
3. En una región dada la configuración general de estos síntomas y efectos es estable y tiende a repetirse.
4. Para predecir temblores es necesario disponer de una información muy amplia y detallada, que permita al sismólogo abstraer el cuadro general de fenómenos premonitores y analizar su significado.
5. Esto significa que es necesario cubrir la región, y especialmente la posible zona epicentral, con una densa red de estaciones de observación.

Los chinos enfocan la lucha contra los sismos como un programa de alta prioridad, en todo similar a una campaña militar. Han movili-

zado a cientos de miles de voluntarios que construyeron aparatos sencillos en sus lugares de trabajo y los controlan diariamente. En consecuencia, ya las brigadas y los burós sismológicos provinciales han aprendido a interpretar las características de sus respectivas regiones, que las ayudan a diagnosticar las anomalías al momento de presentarse y a implementar medidas que ya han salvado muchos miles de vidas.

Las mediciones que actualmente se hacen en China para detectar efectos premonitores de los sismos abarcan más de diez diferentes fenómenos, en su mayoría relacionados con variaciones en el campo de esfuerzos de la tierra:

observaciones geodésicas
desplazamientos en fallas geológicas
inclinación del suelo
cambios de resistividad en rocas
corrientes telúricas
geomagnetismo
campo gravitacional
mediciones geoquímicas
fluctuación del nivel de agua en pozos
efecto piezoeléctrico en sondeos
cambios de velocidad sísmica en rocas
cambios en la ocurrencia de sismos menores
cambios en el caudal de los manantiales
cambios en el comportamiento animal

La mayoría de estos efectos son cuantitativos e instrumentales; unos cuantos son cualitativos y dependen de observadores humanos. Existen cuatro etapas de predicción, y cada etapa utiliza otras clases de fenómenos predictores.

A. Predicción a largo plazo

B. Predicción a mediano plazo

C. Predicción a corto plazo

D. Predicción inmediata

Para la predicción inmediata se utilizan los cambios en el campo geomagnético, en la resistividad de las rocas, en el nivel de los pozos, en la inclinación del suelo, en el comportamiento animal y, sobre todo, la ocurrencia de sismos premonitores. La predicción inmediata es la más delicada ya que depende generalmente de la eficiencia y decisión de un pequeño grupo local, muchas veces de sismólogos voluntarios.

Sin embargo, los éxitos reportados por el programa son impresionantes. Se presentará un estudio de caso para aclarar el método utilizado.

Bibliografía

C. Lomnitz, Global Tectonics and Earthquake Risk (Elsevier, 1974).

F. Press y R. Siever, Earth (W.H. Freeman, 1976)

E. Rosenblueth, Predicción en Ingeniería Sísmica en China, Soc. Mex. Ing. Sísmica, Diciembre 1976.

X. Le Pichon, J. Franchetean y J. Bonnia, Plate Tectonics (Elsevier, 1973).

EFECTOS SISMICOS EN SUELOS GRANULARES

por

Abraham Díaz Rodríguez*

INTRODUCCION

El comportamiento adecuado de los suelos y las cimentaciones durante la ocurrencia de temblores es escencial para evitar daños severos a toda clase de estructuras.

Las condiciones bajo las cuales los suelos (como parte de la cimentación o como material de construcción) pierden una parte significativa de su resistencia, conduciendo a fallas inducidas por temblores, no son, al menos hasta la fecha (junio, 1977) completamente entendidas y constituyen un campo fertil de investigación y de gran utilidad para la práctica profesional de la Ingeniería Civil.

La importancia de los efectos que los sísmos pueden inducir en los suelos granulares se debe a los graves daños que se han observado en numerosas ocasiones durante los temblores pasados.

---

* Investigador, Instituto de Ingeniería, UNAM

* Profesor, División de Estudios Superiores, Facultad de Ingeniería, UNAM

De 1881 a 1946 se ha informado de 229 deslizamientos, que causaron el desplazamiento total de 25 millones de m^3 de arena. En Holanda, a orillas de los numerosos estrechos que existen, ha habido gran cantidad de deslizamientos que provocaron el rompimiento de diques y, por tanto, la inundación de grandes extensiones.

Durante el temblor de Chile, en 1960, se formaron extensas zonas de falla. La tierra fue arrastrada hacia el mar a lo largo de la costa de 600 m, llevando consigo todas las estructuras de retención; las paredes del muelle con secciones de 5 m de concreto reforzado fueron abatidas y luego arrastradas. En este mismo temblor, falló una presa debido a la licuación del suelo de cimentación.

En México existen evidencias de que durante el sismo de 1959 (Marsal, 1961), un gran tramo de la margen izquierda del río Coatzacoalcos tuvo desplazamientos verticales y horizontales de importancia. Muchas instalaciones de la zona de astilleros sufrieron hundimientos bajo la cimentación y el asentamiento general fue notable después del sismo. Algunos tramos de los muelles cimentados sobre pilotes metálicos de 10 m de longitud sufrieron desplazamientos apreciables en dirección horizontal. Uno de los muelles se desplazó hacia el río más de 1/2 m. Tales movimientos se han atribuido al fenómeno de licuación en los mantos arenolimosos y limoarenosos que allí se encuentran entre 0 y 8 m de profundidad. En vista de las altas relaciones de vacíos y de la granulometría uniforme de dichos suelos, no puede descartarse esta posibilidad.

En Alaska, en 1964 (Seed, 1969), se produjo un deslizamiento debido a la licuación del suelo que movió 70 millones de m^3 de material, destruyendo muchas de las instalaciones de la bahía de Anchorage. La superficie del terreno fue completamente devastada por los desplazamientos, produciéndose una nueva superficie irregular. El 40 por ciento de las casas y edificios comerciales fueron seriamente dañados debido a las fisuras que se extendían bajo las construcciones.

Durante junio de 1964, en Niigata, Japón (Seed y Lee, 1966), hubo daños muy graves causados por licuación de la arena. Muchas estructuras se asentaron más de 1 m y se inclinaron notablemente; hubo un edificio que giró 80° (fig 1), quedando prácticamente tendido en el suelo. Además de estas fallas, hubo otras evidencias físicas de licuación. Poco después del sismo se observó que brotaba agua del suelo por grietas que se formaron, en las cuales llegaron a hundirse casas y automóviles; al mismo tiempo, se veía emerger a la superficie estructuras que debían permanecer bajo el suelo, como fue el caso de un tanque para tratamiento de aguas negras.

Durante este sismo, en la extensa zona licuada se produjeron daños en edificios, puentes, caminos, muelles, vías de ferrocarril, etc. Debido al asentamiento que se produjo, la parte de la ciudad cercana al río quedó completamente inundada. Se estima que en este sismo 2,130 edificios sufrieron falla total, 6,200 fueron seriamente dañados y 31 200 sufrieron daños ligeros (Seed y Lee, 1967).

FENOMENOS INDUCIDOS POR SISMOS

El comportamiento dinámico de los suelos granulares constituye, dentro de la dinámica de suelos, uno de los problemas que actualmente está lejos de ser comprendido totalmente y es mucho lo que falta por dilucidar en torno a ello, al grado que es posible ver interpretaciones diferentes y aún contradictorias de los hechos experimentales disponibles, y por lo tanto, constituye un campo fertil para la investigación en ingeniería sísmica.

Dos de los principales fenómenos que la ocurrencia de temblores, pueden inducir en depósitos de suelos granulares son:

1. Cambios de volumen (Densificación-asentamientos)
2. Reducción de la resistencia al esfuerzo cortante (Aumento de la presión de poro-licuación)

En lo que sigue se tratará de dar un breve panorama del estado de conocimiento que guardan estos dos temas. No se ha pretendido en estas notas hacer un análisis exahustivo y completo. Para mayores detalles se ha elaborado una lista de referencias actualizada (junio de 1977) para que sirva de guía a aquellas personas que esten interesadas en profundizar en el tema.

ESTUDIOS DE DENSIFICACION

Es un hecho bien establecido que la aplicación de carga cíclica a una muestra de arena, da como resultado un decrecimiento progresivo de volumen, aún en el caso de arenas densas, las cuales se comportarían dilatantes bajo carga unidireccional o monotónica. Varias técnicas, tanto de laboratorio como de campo, se han desarrollado (Broms y Forssblad, 1969).

El uso de vibraciones verticales para producir la densificación de muestras de arena se ha utlizado en el pasado (D'Appolonia y D'Appolonia, 1967; Whitman y Ortigosa, 1968), estos estudios han mostrado que los cambios de peso volumétrico de las muestras son pequeños para aceleraciones menores de 1 g (figs 4 y 5).

Los cambios tanto de volumen como de características friccionantes de arenas secas inducidos por grandes aceleraciones horizontales y un gran número de ciclos de pequeña amplitud se han investigado utilizando cajas de corte montadas sobre mesas vibradoras (Barkan, 1962; Youd, 1970), ver fig 6.

Otros estudios basados en ensayes de corte simple y mesas vibradoras, con niveles de aceleración y amplitudes de deformación semejantes a los esperados en temblores intensos, han mostrado que: la amplitud de deformación, compacidad relativa y número de ciclos de carga son los principales factores que gobiernan la compactación de suelos granulares secos o saturados bajo condiciones drenadas (Silver y Seed, 1969; Youd, 1972) ver fig 7.

Pyke, Seed y Chan (1974), realizaron una serie de ensayes de corte simple tanto en una (x) como en dos (x,y) direcciones. Se utilizaron dos patrones básicos de movimiento, en los ensayes bidireccionales.

Los resultados de los ensayes utilizando movimientos aleatorios se resumen en la fig 8, en donde se encuentra el asentamiento para 10 ciclos de carga como función de la relación, $\tau h/\sigma_v$, en donde, τh, es el máximo esfuerzo cortante horizontal y, σ_v, es el esfuerzo vertical aplicado. Estas pruebas confirmaron las conclusiones de Silver y Seed (1971), que para un nivel de deformaciones cortantes el asentamiento inducido es independiente del esfuerzo vertical. Sin embargo, si se realiza una prueba bajo condiciones de esfuerzo controlado, las deformaciones cortantes cíclicas,y por lo tanto los asentamientos, se incrementan con el incremento de la relación de esfuerzos. Para un valor dado de la relación de esfuerzos se puede ver que el asentamiento causados por dos componentes de movimiento es aproximadamente igual a la suma de los asentamientos causados por cada una de las componentes.

Sobre la base de estos resultados parece razonable postular que para arenas saturadas ensayadas bajo condiciones no drenadas, el incremento de la presión de poro será aproximadamente dos veces más rápida bajo dos componentes de movimiento que bajo una sola.

Tomando en cuenta todo lo anterior, se puede concluir que los aspectos más importantes relacionados con los cambios de volumen de suelos granulares, son los siguientes:

a) Los esfuerzos cortantes cíclos constituyen el medio más efectivo de densificación

b) Para un peso volumétrico dado, la amplitud de las deformaciones cortantes es el parámetro más importante que afecta la velocidad y magnitud de la densificación

c) A mayores esfuerzos de sobrecarga la velocidad de densificación generalmente resulta menor

d) La densificación es independiente de la frecuencia del movimiento

CALCULO DE ASENTAMIENTO

La acción de los sismos puede causar asentamientos considerables en depósitos de suelos granulares. Durante el temblor de San Fernando, ocurrido el 9 de febrero de 1971, se tuvieron asentamientos de edificios, los cuales variaron de 10 a 15 cm (aprox. 4 a 6 pulgadas).

Mayores asentamientos e incluso inclinación de edificios pueden ocurrir debido a la licuación de los depósitos de arena saturada, pero este problema se tratará en el capítulo siguiente.

Los asentamientos de depósitos de arena seca, resultantes del movimiento del terreno son rara vez uniformemente distribuidos, y, en general causan asentamientos diferenciales en las estructuras, los cuales, en algunos casos, pueden llegar a clasificarse como daños mayores. Daños severos de grandes estructuras en Skopje durante

el temblor de 1963, fueron atribuidos a los asentamientos diferenciales causados por la densificación de lentes de arena suelta bajo las cimentaciones (Seed and Silver, 1972).

Los asentamientos de edificios cimentados sobre arena seca, considerando la acción de cargas estáticas, se estima empíricamente y generalmente, se pone poca atención a los posibles asentamientos debidos a los movimientos del terreno inducidos por sísmos.

Se han propuesto dos procedimientos semi-empíricos para estimar los asentamientos provocados por temblores. Uno de éstos propuesto por Seed y Silver (1972) permite estimar el asentamiento de arenas secas, Pyke et al (1974) amplió el método para tomar en cuenta movimientos multi-direccionales. Lee y Albaisa (1974) propusieron un método aplicable a arenas saturadas.

El procedimiento de Seed y Silver (1972) para estimar el asentamiento de un estrato de arena debido a carga sísmica, consiste de los siguientes pasos:

a) Calcular la historia de deformaciones de cortante en varias capas del estrato, usando un método de análisis dinámico lineal.

b) Convertir la historia de deformaciones de cortante en cada capa a un número equivalente de ciclos de deformación cortante de amplitud constante.

c) Aplicar el número de ciclos de deformación cortante, determinado en (b) a muestras de arena ensayadas bajo condiciones de corte simple y determinar las deformaciones volumétricas a deformaciones verticales resultantes.

d) Repetir el porcedimiento de (c) para cada capa del estrato e integrar las deformaciones verticales para obtener el asentamiento total.

El paso (b) involucra una aproximación. Martin et al. (1975) ha demostrado que el efecto de una historia irregular de deformaciones de cortante depende no únicamente de la magnitud de los pulsos en el registro, como también del orden en que ellos son aplicados. El procedimiento para determinar el número equivalente de ciclos no toma en cuenta el hecho antes mencionado.

Al expresar analíticamente la relación entre deformaciones de cortante y los cambios de volumen, se pueden eliminar los pasos b, c y d como sucede con el método de Martin et al (1975), el cual es aplicable al cálculo de asentamientos de estratos de arena seca o parcialmente saturada.

PERDIDA DE RESISTENCIA DE SUELOS GRANULARES

- LICUACION DE ARENAS -

Probablemente uno de los efectos más costosos y espectaculares que se puedan encontrar en ingeniería sísmica se deban al fenómeno de la licuación de arenas.

El fenómeno es complejo y aún no es claro y completamente comprendido, al grado que es posible encontrar interpretaciones diferentes y aún contradictorias de los hechos experimentales existentes.

La discrepancia empieza con la propia definición del término licuación. Mientras que para H.B. Seed (1966) el término "licuación inicial" es la condición de una muestra de arena en la cual la presión de poro inducida por la aplicación de carga cíclica alcanza el valor de la presión de confinamiento y el término "licuación total" es la condición correspondiente a que la muestra alcance una amplitud de deformación del 20%; A. Casagrande en 1969, utiliza los términos licuación y mobilidad cíclica que después modifica (Casagrande,1976) definiendo por "licuación real" a la respuesta de una muestra de arena suelta y saturada cuando se le somete a deformaciones o impactos que dan como resultado una pérdida sustancial de resistencia y en casos extremos a flujo de taludes, y por "licuación cíclica" la respuesta de un espécimen dilatante de arena cuando se le ensaya en cámara triaxial cíclica y la presión de poro se eleva en forma incremental hasta alcanzar la presión de confinamiento.

En esta plática entenderemos por "licuación de arenas" al fenómeno mediante el cual una arena saturada pierde una gran parte de su resistencia al esfuerzo cortante (debido a carga monotónica o cíclica) y fluye o se comporta como un líquido hasta que los esfuerzos cortantes actuantes en la masa de suelo disminuyen a valores compatibles con la resistencia del suelo licuado, el movimiento se detiene, y el suelo recupera su resistencia y estabilidad.

Por lo tanto, un talud que se licúa llega a estabilizarse, cuando la pendiente se ha reducido a pocos grados.

Descripción del Fenómeno

El fenómeno de licuación de arenas es causado por el desarrollo de grandes presiones en el agua que ocupa los poros del suelo. Estas grandes presiones de poro son inducidas cuando se aplican a la masa de suelo esfuerzos o deformaciones de cortante, en condiciones tales que no se permite su disipación inmediata, es decir prácticamente a volumen constante. La forma de aplicación de los esfuerzos cortantes puede ser monotónica, cíclica o transitoria.

Factores que influyen en la ocurrencia de licuación

Los factores más importantes que influyen en la ocurrencia de licuación son:

a) Tipo de suelo

Los suelos uniformemente graduados son más susceptibles de sufrir licuación que los suelos bien graduados; dentro de los primeros, las arenas finas se licuan más facilmente que las gravas o suelos

arcillosos aluviales. En el temblor de Alaska se observó que las estructuras de puentes cimentadas sobre arena sufrieron grandes desplazamientos, mientras que las cimentadas en grava no tuvieron daños.

En la fig 9 se muestran las envolventes de las curvas granulométricas de los suelos que se han licuado.

b) Compacidad relativa (C_r) o relación de vacíos (e)

Un depósito de arena suelta es más susceptible de sufrir licuación que un depósito de arena densa.

En el temblor de Niigata hubo licuación en zonas cuya C_r era del orden del 50 por ciento, o menor, en tanto que en las zonas con una C_r > 70 por ciento no se presentó ningún daño.

En la fig 10 se ilustra el concepto de compacidad relativa.

c) Esfuerzo confinante inicial

La susceptibilidad de licuación disminuye al aumentar el esfuerzo confinante. Ensayes de laboratorio han mostrado que para una relación de vacíos inicial, el esfuerzo cortante requerido para comenzar la licuación bajo condiciones de carga repetida, se incrementa con el aumento de la presión de confinamiento.

d) Magnitud del esfuerzo repetido

Cualquier depósito con una relación de vacíos mayor que su $e_{mín}$ es susceptible de sufrir pérdida parcial o total de resistencia, si la excitación es de intensidad suficiente.

Evidencias de campo demuestran que depósitos de arena suelta han resistido sismos de poca intensidad (0.005g) y se han licuado ante la acción de sismos intensos (0.16g), (Seed, Idriss, 1971).

La resistencia a la licuación decrece al aumentar la magnitud del esfuerzo.

e) Número de ciclos de esfuerzo

Todos los estudios de laboratorio indican que en una muestra sujeta a carga repetida, con un nivel de esfuerzo o deformación prescrito, el inicio de la licuación dependerá de la aplicación de un número requerido de ciclos de esfuerzo.

Esto se confirmó en Anchorage, durante el temblor de 1964, ya que los deslizamientos ocurrieron después de 90 seg de iniciado el movimiento.

TRABAJOS EXPERIMENTALES

Desde el punto de vista experimental, el fenómeno de licuación ha sido estudiado por varios investigadores utilizando diversos aparatos (triaxial, triaxial cíclica, corte simple cíclico, torsión cíclica y mesa vibradora).

El concepto de relación de vacíos crítica

La evidencia experimental ha demostrado que las arenas "sueltas" disminuyen su volumen bajo la acción de esfuerzos cortantes y que, por el contrario las arenas "densas" lo aumentan.

Tomando en cuenta lo anterior, A. Casagrande llegó a la conclusión de que el decremento de volumen de una arena suelta y el incremento de volumen de una arena densa tenderían a la misma relación de vacíos, en la cual la arena puede deformarse sin cambio de volumen, a la cual denominó "relación de vacíos crítica".

Puesto que la curva de relación de crítica divide el comportamiento dilatante (bajo la curva) y contractivo (arriba de la curva), Casagrande la propuso como una medida para investigar la susceptibilidad de licuación de una arena.

Posteriormente Casagrande al analizar la falla de la presa de Fort Peck se dio cuenta que la curva de relación de vacíos crítica no dividía realmente el comportamiento contractivo y dilatante de las arenas.

Castro (1969) modificó el concepto de relación de vacíos crítica y obtuvo, a partir de resultados de pruebas triaxiales consolidadas-no drenadas con medición de presión de poro (pruebas $\overline{cu}$), la curva de estado crítico. En la fig 11 se muestran las líneas e_f de estado crítico para varias arenas.

Prueba triaxial cíclica

Seed y Lee (1966) fueron los primeros en utilizar cámara triaxial cíclica, con objeto de reproducir la condición de esfuerzos a que se halla sujeto un elemento de suelo durante un temblor (atribuyendo el estado de deformaciones del suelo a la propagación de ondas de cortante).

Si la superficie del terreno es horizontal, antes del temblor no hay esfuerzos cortantes en planos horizontales (fig 12a). Durante el temblor, los esfuerzos normales permanecen constantes, pero se generan esfuerzos cortantes (figs 12b y 12c).

En una cámara triaxial cíclica, la condición de esfuerzos señalada antes se produce en un plano a 45°, como se indica en la fig 13.

El comportamiento de las muestras de arena suelta, sometidas al ensaye propuesto por Seed y Lee, se caracteriza por un aumento gradual de la presión de poro sin que haya deformación axial apreciable, hasta que se produce el incremento que eleva la presión de poro al mismo valor de la presión confinante, momento a partir del cual la muestra se deforma subitamente más del 20%. Las arenas en estado compacto exhiben un comportamiento similar al de las arenas sueltas, pero al llegar a la "licuación inicial" no se presenta una deformación grande en forma súbita, sino que la deformación se incrementa gradualmente.

Según el concepto de Seed y Lee, cualquier espécimen de arena es susceptible de licuarse no importando su compacidad relativa. Los parámetros más importantes según estos investigadores son: el número de ciclos de esfuerzo (Nd_c) para alcanzar la condición $u = \bar{\sigma}_3$, la relación entre el esfuerzo cortante máximo y el esfuerzo confinante, $\frac{\sigma_{dc}}{2\bar{\sigma}_3}$ y la relación de vacíos.

Castro (1969) al realizar sus ensayes en cámara triaxial cíclica observó que durante la prueba se desarrollan heterogeneidades en las muestras, de manera especial en la zona superior. Atribuye a

estas heterogeneidades, inducidas por el ensaye, el que especímenes densos alcancen la condición $u = \bar{\sigma}_3$.

Al comparar los ensayes realizados por Castro y por Seed y Lee, se aprecia que la frecuencia de aplicación de carga hace que el comportamiento de prueba Quasi estática sea diferente al de prueba cíclica.

Prueba de corte simple cíclico

La prueba de corte simple cíclico se desarrolló con la idea de conseguir mayor aproximación a las condiciones de campo que la lograda con cámara triaxial.

Uno de los primeros aparatos de corte simple fue el desarrollado por Swedish and Norwegian Geotechnical Institutes (Kjellman,1951). Sin embargo, este aparato tenía el inconveniente de utilizar muestras cilíndricas (los esfuerzos cortantes en una sección horizontal no pueden ser uniformes).

Roscoe (1953) modificó el aparato, utilizando muestras de sección rectangular y paredes rígidas.

En la Universidad de California, en Berkeley, Peacock y Seed (1968) desarrollaron un aparato de corte simple, que utilizaron para examinar la tendencia a licuarse de una muestra de arena sometida a este tipo de esfuerzo. También en la Universidad de British Columbia, Pickering y Finn (1969), Finn et al (1970 y 1971) han utilizado corte cíclico simple para el estudio de licuación.

En las figs 14 y 15 se ilustran los resultados obtenidos por Peacock y Seed.

Este tipo de ensayes generalmente consiste en colocar un recipiente o caja con arena saturada, sobre una mesa vibradora y medir la aceleración de la mesa a la cual ocurre la licuación. Estos valores se relacionan con las medidas de aceleración en el campo [illegible]

Whitman (1970) menciona los factores que afectan los resultados y su influencia en la interpretación de los mismos:

1. Frecuencia de vibración
2. Duración de vibración
3. Tamaño y geometría del recipiente
4. Características de deformación del recipiente
5. Método de colocación de la muestra
6. Control del drenaje
7. Aparatos de medición de deformaciones
8. Presión confinante

Finn, Emery y Gupta (1971) mencionan las ventajas de usar grandes muestras y mesa vibradora.

Tal vez la principal objeción al uso de recipientes rígidos sobre mesa vibradora es que no representan las condiciones de campo.

Con objeto de superar esta dificultad Díaz, Weckmann e Iturbe (1973) proponen combinar la utilidad de las condiciones de corte simple (inciso b) y la ventaja de utilizar muestras grandes (30 x 60 x 90 cm)

en un recipiente de paredes móviles para ensayar arena saturada en mesa vibradora.

METODOS PARA EVALUAR LA SUSCEPTIBILIDAD A LA LICUACION DE LOS SUELOS

En relación a la predicción de la susceptibilidad a la licuación de depósitos de suelos granulares saturados considerable cantidad de investigación se ha dirigido hacia el desarrollo de mejores métodos de predicción y técnicas de ensaye.

Los métodos se pueden clasificar en tres categorías:

1. Métodos empíricos, basados en la comparación de las condiciones de los sitios en donde ocurrió o no licuación con las condiciones del sitio que se desea analizar.

   Dentro de esta categoría se clasifican los primeros cuatro métodos que se describirán en este capítulo.

2. Métodos simplificados. Consisten básicamente en comparar la resistencia obtenida en pruebas de laboratorio, con los esfuerzos que provocará el sismo.

   En esta categoría se clasifican los métodos propuestos por Seed e Idriss (1970) y por Casagrande (1976).

3. Métodos de análisis de respuesta del terreno. Son más refinados que los anteriores, utilizan programas de computadora.

Criterio del WES (Waterways Experimental Station)

Este criterio fue desarrollado para analizar la estabilidad de terraplenes a lo largo del Río Mississipi, en el que se producen flujos de material producidos por el incremento de la presión de poror originada por los cambios del nivel del río.

Criterio de Florin e Ivanov

Esté criterio, desarrollado en Rusia, permite estimar la susceptibilidad a la licuación de suelos por medio de pruebas de campo. Se investigan los 10 m superiores de suelo haciendo explotar sucesivamente tres cargas de dinamita de 5 kg colocadas a una profundidad media de 4.5 m y determinando después de cada explosión, el asentamiento medio de la superficie dentro de un radio de 4.5 m. La cantidad y profundidad a la que se coloca el explosivo se eligen de forma que no haya expulsión de suelo durante la explosión. Si el asentamiento promedio es menor de 8 a 10 cm y la relación de asentamientos entre explosiones sucesivas es menor que 0.6 se puede afirmar que ese suelo no es susceptible a licuación.

Criterio de Kishida

Este criterio está basado en el análisis de las condiciones del suelo de 3 sitios en los que ocurrió licuación, (Kishida,1969). Bajo sismos de igual magnitud, puede ocurrir licuación si el nivel freático está cerca de la superficie, si las características granulométricas satisfacen las relaciones: $2mm > D_{50} > .074$ mm; $C_u < 10$ y

además se cumplen las siguientes condiciones:

- El espesor del estrato de suelo no licuable, arriba del estrato, licuable es menor que 8 m.
- La relación de los espesores del estrato no licuable al licuable es menor que 1.

Kishida también concluye que los suelos no son susceptibles a la licuación si:

- La presión efectiva de confinamiento es superior a 2 kg/cm^2 o,
- La compacidad relativa es superior a 75%.

Criterio de Oshaki

Este criterio (Oshaki, 1969) establece que los suelos con nivel freático cercano a la superficie pueden licuarse si se presentan las siguientes características granulométricas:

$$2 \text{ mm} > D_{60} > 0.2 \text{ mm}; \quad D_{10} < 0.1 \text{ mm}$$

Adicionalmente, establece que estos suelos tendrán poca probabilidad de licuarse si el número de golpes N_{sp} en prueba de penetración estándar es mayor que 2z, en que z es la profundidad en metros.

Método de Seed e Idriss

Este método consiste en comparar los esfuerzos inducidos por el sismo en los estratos licuables con los que puede resistir el suelo sin que ocurra licuación. Para determinar los esfuerzos inducidos in situ, debe contarse con el acelerograma del sismo de diseño, la estratigrafía y las propiedades índice y mecánicas de los suelos. Seed e Idriss proponen un procedimiento simplificado para estimar

la magnitud de los esfuerzos que origina el sismo. La magnitud de los esfuerzos que pueden provocar licuación en el suelo se obtiene a partir de pruebas de laboratorio, tanto triaxiales como de corte simple, con esfuerzos repetidos o bien se estima con gráficas de diseño obtenidas por Seed e Idriss. La comparación de los esfuerzos inducidos por el sismo con los que provocan licuación del suelo permite juzgar la susceptibilidad de un suelo a sufrir este fenómeno.

Se calcula el esfuerzo cortante máximo ($\tau_{máx}$) a una profundidad z, conocida la aceleración máxima ($a_{máx}$) en la superficie del terreno, y suponiendo que la masa de suelo se comporta como un cuerpo rígido, mediante la expresión:

$$\tau_{máx} = \frac{\gamma z}{g} a_{máx}$$

$a_{máx}$ aceleración máxima en la superficie del terreno

γz presión vergical total a la profundidad z

g aceleración de la gravedad

$\tau_{máx}$ esfuerzo cortante máximo a la profundidad z

Como el terreno es deformable, en general se tendrá que:

$$\tau_{máx} = \frac{\gamma z}{g} a_{máx}\ r_d$$

siendo r_d un factor de corrección, menor que 1.

El análisis de varios sismos en sitios que presentan un estrato de arena en los 15 m superiores ha mostrado que r_d cae dentro del intervalo de valores de la fig 16.

Seed e Idriss proponen calcular el esfuerzo cortante promedio τ_p que, en un número dado de ciclos, produce el mismo efecto que el sismo con la expresión:

$$\tau_p = 0.65 \frac{\gamma z}{g} a_{máx} r_d$$

Por su parte, el número de ciclos significativos en el comportamiento del material dependerá de la duración del sismo. Para fines prácticos se puede usar la siguiente tabla:

Magnitud del sismo	N° de ciclos significativos, N
7	10
7 1/2	20
8	30

Previamente a la realización de pruebas de laboratorio, es preciso conocer la compacidad relativa del material in-situ. Para ello se utilizan los resultados de las investigaciones hechas por Holtz y Gibbs. En la fig 17 se presenta una gráfica modificada por Seed e Idriss que permite conocer la compacidad relativa.

Los esfuerzos que provocarán la licuación en un suelo a una compacidad relativa dada, se pueden deducir en forma aproximada de los experimentos llevados a cabo por diversos investigadores, tanto en cámaras triaxiales como en aparatos de corte simple. A partir de pruebas en cámaras triaxiales se han obtenido gráficas que permiten estimar si ocurrirá licuación en un suelo sometido a cierto número de ciclos (10 ó 30 usualmente) para una relación de esfuerzos $(\frac{\sigma_{dc}}{2\sigma_c})$

dada y determinado tamaño de las partículas (representado por el D_{50}). En las figs 14 y 15 se presentan estas gráficas para una compacidad relativa de 50%.

Para determinar la relación de esfuerzos correspondiente a otra compacidad relativa se usa el hecho experimental de que la relación de esfuerzos $(\frac{\sigma_{dc}}{2\sigma_c})$ es aproximadamente proporcional a la compacidad relativa (fig 14 y 15). En las mismas figuras, se observa que el material menos resistente corresponde a un $D_{50} = 0.074$ mm.

Tomando en cuenta que el esfuerzo más significativo, en la licuación de un suelo bajo la acción de un temblor, es el esfuerzo cortante actuante en el plano horizontal; la prueba de corte simple es la que mejor asemeja las condiciones de deformación in-situ. Es por tanto importante correlacionar los resultados anteriores, obtenidos en cámaras triaxiales, con los obtenidos en pruebas de corte. Las investigaciones llevadas a cabo por Seed e Idriss, permitieron concluir que, para fines prácticos:

$$(\frac{\tau_{xy}}{\sigma_y})_{\text{corte simple}} \simeq c_r (\frac{\sigma_{dc}}{2\sigma_c})_{\text{triaxial}}$$

en que c_r depende de la compacidad relativa (fig 18).

Comparando los esfuerzos producidos en el terreno por un temblor y los esfuerzos que el material es capaz de soportar, es posible determinar si el suelo presentará o no el fenómeno de licuación, para las condiciones particulares supuestas.

Seed e Idriss presentan un procedimiento simplificado que permite aplicar el método anterior en forma expedita mediante gráficas de

penetración estándar contra la profundidad, elaboradas para 2 profundidades típicas del nivel freático y para 2 aceleraciones máximas del terreno (figs 19 y 20). En estas gráficas se delimitan tres zonas: una, en la cual no habra licuación; otra, en la que podría o no presentarse licuación dependiendo de las características granulométricas del material y de la magnitud del temblor; y la tercera en la cual es muy probable que el material se licúe. Las fronteras entre las zonas anteriores se determinaron para una compacidad relativa de 50% y corresponden a condiciones extremas en cuanto al número de ciclos significativos producidos por un temblor y a la granulometría del material. La frontera a la izquierda de la cual se concluye que habrá licuación fue obtenida usando el mínimo número de ciclos razonable (N_{sp} = 10) combinado con la granulometría del material menos susceptible a la licuación (D_{50} = 2 mm); la frontera a la derecha de la cual se dice no habrá licuación se obtuvo combinando el máximo número de ciclos razonable (N_{sp} = 30) con la granulometría del material mas susceptible (D_{50} = .074 mm).

Método de Casagrande

En esencia el procedimiento consta de los siguientes pasos:

1. Se ejecutan pruebas triaxiales con aplicación de carga monotónica (o cíclica, dependiendo de la compacidad relativa de la arena), en muestras inalteradas labradas de bloques obtenidos manualmente, y se determina su respuesta. De preferencia las pruebas deben ejecutarse en un equipo que disponga de extremos lubricados y los especímenes deben estar consolidados con una relación de esfuerzos principales de 2.

2. Se determina la línea de estado crítico, línea e_f, si es que los resultados de las pruebas lo permiten.

3. A partir de pruebas de compresión unidimensional, se estiman las combinaciones de esfuerzos efectivos y compacidad relativa (relación de vacíos) susceptibles de desarrollarse en el campo.

4. Se compara la posición de los puntos estimados en el paso anterior con la posición de la línea e_f. Los puntos situados arriba y a la derecha de la línea e_f son susceptibles de experimentar licuación. Puntos situados a la izquierda de y sobre la línea e_f, no son susceptibles de experimentar licuación.

5. En suelos no susceptibles de experimentar licuación por su posición en relación con la línea e_f, es posible estimar el incremento de presión de poro inducido por la aplicación de cargas cíclicas para un cierto número de ciclos. A. Casagrande estima que el número de ciclos necesario para inducir presiones de poro superiores al 50% de la presión de confinamiento in situ, es superior a cuatro veces el número de ciclos observados en el laboratorio (valor a partir del cual la influencia del fenómeno de movilidad cíclica en los resultados, es muy importante).

6. Si se requiere una estimación de las deformaciones inducidas por carga cíclica en el campo, es necesario ejecutar mediciones precisas de las deformaciones en el laboratorio, hasta que la presión de poro alcanza el 50% de la presión de confinamiento, y utilizar estas mediciones como una guía de las posibles deformaciones in situ, teniendo en cuenta que solo una fracción de las deformaciones medidas en el laboratorio son causadas por el mecanismo que controla el desarrollo de presiones de poro y deformaciones en el campo.

CONCLUSIONES

1. La licuación se presenta fundamentalmente en arenas finas, uniformes, de origen reciente y aluvial, y con compacidades relativas inferiores a 40 ó 50% dependiendo de la presión de confinamiento. La experiencia de que se dispone indica que arenas con una compacidad relativa > 50% no son susceptibles de experimentar licuación.

2. Para estimar la susceptibilidad a la licuación de arenas existen procedimientos empíricos y analíticos. Ambos hacen uso de la experiencia, y el segundo tipo hace uso de los resultados de pruebas de laboratorio ejecutadas sobre muestras representativas del suelo.

3. Los procedimientos empíricos relacionan el comportamiento del suelo con factores tales como el espesor de los estratos bajo consideración, sus características granulométricas, etc. Su aplicación es limitada a condiciones similares a las que les dieron origen.

4. Los procedimientos analíticos hacen uso de la experiencia, la teoría, y los resultados de pruebas de laboratorio en donde se determina la respuesta de muestras del suelo, sujetas a condiciones de esfuerzo y deformación que se supone duplican las condiciones existentes in situ.

5. Los procedimientos analíticos responden a dos enfoques principales: (a) el basado en el concepto de relación de vacíos crítica; aplicable para identificar la susceptibilidad a la licua

ción de arenas bajo carga monotónica y cíclica, y (b) el basado en los resultados de pruebas cíclicas; de utilidad para estimar el aumento en la presión de poro y las deformaciones in situ después de considerar que el mecanismo que controla el desarrollo de estas variables in situ es diferente al mecanismo que controla el desarrollo de estas mismas variables en el laboratorio.

6. Parece ser que un enfoque diferente y realista al problema de la licuación de arenas consistiría en efectuar investigaciones detalladas de depósitos naturales.

REFERENCIAS

Ambraseys, N. N., 1970. Factors controlling the earthquake response of foundation materials. *Proc. Third European Symp. Earthq. Engrg.*, Sofia, Bulgaria, pp 309-323.

Ambraseys, N. N., 1973. Dynamics and response of foundation materials in epicentral regions of strong earthquakes. *Proc. Figth World Conf. Earthq. Engrg.*, Rome, Italy, pp CXXVI-CXLVIII.

Ambraseys, N. N., and Sarma, S., 1969. Liquefaction of soils induced by earthquakes. *Bull. Seism. Soc. Am.*, 59:651-664.

Barkan, D. D., 1962. *Dynamics of Bases and Foundations*. McGraw-Hill, New York, 434 pp.

Bazaraa, A., 1967. Use of the standard penetration test for estimating settlements of shallow foundations on sand. *Doctoral thesis, Dept. of Civil Engrg., University of Illinois*, Urbana,Illinois.

Broms, B. B., and Forssblad, L., 1969. Vibratory compaction of cohesionless soils. *Proc. Specialty Session No. 2, Seventh Interntl. Conf. Soil Mech. Found. Engrg.*, Mexico City, pp 101-118.

Casagrande, A., 1936. Characteristics of cohesionless soils affecting the stability of slopes and earth fills. *J. of the Boston Society of Civil Engineers*, January, pp 257-276.

Casagrande, A., 1938. The Shearing Resistance of Soils and its Relation to the Stability of Earth Dams., *Proc. Soils and Foundation Conference of the U. S. Engineer Department*, Boston, Mass.

Casagrande, A., and Shannon, W. L., 1948. Stress-deformation and strength characteristics of soils under dynamic loads. *Proc. Second Interntl. Conf. Soil Mech.*, Rotterdam, Holland, V, pp 29-34.

Casagrande, A., 1965. Role of the Calculated Risk in Earthwork and Foundation Engineering. *Journal of the Soil Mechanics and Foundation Engineering Division*, ASCE.

Casagrande, A. y Rendon, F., 1976. Reciprocating and Gyratory Shear Apparatus-Design, Testing Procedures and Tests on Saturated Sand. *Report to WATERWAYS EXPERIMENTAL STATION*, Vicksburg, Miss.

Casagrande. A., 1976. Liquefaction and Cyclic Deformation of Sands: A Critical Review. Harvard Soil Mechanics Series No. 88.

Castro, G., 1969. Liquefaction of sands. *Report 81, Harvard Soil Mechanics Series, Harvard University*, Cambridge, Massachusetts.

Castro, G., 1975. Liquefaction and cyclic mobility of saturated sands. *Proc. ASCE, J. Geotechnical Engrg. Div.*, Vol 101.

Castro, G. and Christian, J.T., 1976. Shear Strength of Soils and Cyclic Loading. *Proc. ASCE, 102 (GT9): 887-894.*

Castro, G. and Poulos, S.J., 1977. Factors Affecting Liquefaction and Cyclic Mobility. *Proc. ASCE, 103 (GT6): 501-506.*

Cervantes, R., Esteva, L., and Alduncin, G., 1973. Riesgo sísmico en formaciones estratificadas. *Internal Report, Instituto de Ingeniería, Universidad Nacional Autónoma de México*, Mexico City.

Corps of Engineers, U.S. Department of the Army. 1939. Report on the Slide of a Portion of the Upstream Face at Fort Peck Dam. *U.S. Goverment Printing Office*, Washington, D.C.

Cuellar, V., Bazant, Z.P., Krizek, R.J. and Silver, M.L., 1977. Densification and Hyteresis of Sand Under Cyclic Shear. *Proc. ASCE, 103 (GT5): 399-416.*

D'Appolonia, D.J., and D'Appolonia, E., 1967. Determination of the maximum density of cohesionless soils. *Proc. Third Asian Regional Conf. on Soil Mech. and Foundation Engrg.*, Haifa, Israel, pp 266-268.

De Alba, P., Chan, C.K. and Seed, H.B., 1975. Determination of Soil Liquefaction Characteristics by Large-Scale Laboratory Tests. *Report No. EERC 75-14.* University of California. Berkeley, California.

Díaz, A., Weckmann, O. Iturbe, R., 1973. Licuación de Arenas, Primera Parte. Instituto de Ingeniería, UNAM, Informe 319.

Donovan,N.C., 1971. A stochastic approach to the seismic liquefaction problem. Presented at *First Interntl. Conf. on Applications of Statistics and Probability to Soil and Structural Engineering*, Hong-Kong.

Faccioli, E. and Resendiz, D., 1975. Soil Dynamics Behavior Including Liquefaction. *Report E 15, Instituto de Ingeniería, UNAM.* México.

Finn, W.D.L., Pickering, D.J., and Bransby, P.L., 1969. Sand Liquefaction in triaxial and simple shear tests. *Report 11, Soil Mechanics Series, Dept. of Civil Engrg., University of British Columbia,* Vancouver, Canada.

Finn, W.D.L., Bransby, P.L., and Pickering, D.J., 1970. Effect of strain history of liquefaction of sand. *Proc. ASCE, 96 (SM6): 1917-1934.*

Finn, W.D.L., Emery, J.J., and Gupta, Y.P., 1971. Liquefaction of large samples of saturated sand on a shaking table. *Proc. First Canadian Conf. on Earthq. Engrg.*, Vancouver, Canada, pp 97-110.

Finn, W.D.L. and Byrne, P.M., 1976. Estimating Settlement in Dry Sands During Earthquakes. *Canadian Geotechnical J., Vol. 13, Number 4: 355-363.*

Finn, W.D.L., Lee, K.W. and Martin, G.R., 1977. An Effective Stress Model for Liquefaction. *Proc. ASCE, 103 (GT6): 517-533.*

Florin, V.A. and Ivanov, E.L., 1973. Liquefaction of Saturated Sandy Soils. *Proc., 5th International Conference on Soil Mechanics and Foundations Engineering*, Paris, France.

Gibbs, H.J., and Holtz, W.G., 1957. Research on determining the density of sands by spoon penetration testing. *Proc. Fourth Interntl. Conf. Soil Mech. Found. Engrg.*, London, England, 1, pp 35-39.

Hardin, B.O., and Drnevich, V.P., 1972a. Shear modulus and damping in soils: measurement and parameter effects. *Proc. ASCE, 98 (SM6): 603-624.*

Hardin, B.O., and Drnevich, V.P., 1972b. Shear modulus and damping in soils: design equation and curves. *Proc. ASCE, 98 (SM7): 667-692.*

Huang, Wen-Xi, 1961. Investigations on Stability of Saturated Sand Foundations and Slopes Against Liquefaction. *Proc. 5th ICSMFD.* Vol 2.

Idriss, I.M., and Seed, H.B., 1968b. Seismic response of horizontal soil layers. *Proc. ASCE, 94 (SM4): 1003-1031.*

Ishibashi, I., and Sherif, M.A., 1974. Soil liquefaction by torsional simple shear device. *Proc. ASCE, 100 (GT8): 871-888.*

Ishihara, K., and Li, S., 1972. Liquefaction of saturated sand in triaxial torsion shear test. *Soils and Foundations, 12(2):19-40.*

Ishihara, K. and Yasuda, S., 1972. Sand Liquefaction Due to irregular Excitation, *Soil and Foundations, Vol. 12, No. 4.*

Ishida, H., 1970. Characteristics of liquefaction of level sandy ground during the Tokachioki earthquake. *Soil and Foundations,* 10(2): 103-111.

Ladd, R.S., 1977. Specimen Preparation and Cyclic Stability of Sand. *Proc. ASCE, 103 (GT6): 535-547.*

Lee, K.L., and Seed, H.B., 1967. Cyclic stress conditions causing liquefaction of sand. *Proc. ASCE, 93 (SM1): 47-70.*

Lee, K.L., and Fitton, J.A., 1968. Factors affecting the cyclic loading strength of soil. In: *Symposium on Vibration Effects of Earthquakes on Soils and Foundations, ASTM Spec. Techn. Publ. 450, pp 71-95.*

Lee, K.L., and Albaisa, A., 1974. Earthquake induced settlements in saturated sands. *Proc. ASCE, 100 (GT4): 387-406.*

Liou, C.P., Streeter, V.L. and Richart, F.E. Jr., 1977. Numerical Model for Liquefaction. *Proc. ASCE, 103 (GT6): 589-606.*

Marsal, R.J., 1961. Behavior of a Sandy Uniform Soil During the Jaltipan Earthquake, México. *Procs 5th International Conference on Soil Mechanics and Foundation Engineering, Vol I, pp 224-233.*

Martin, G.R., Fenn, W.D. and Seed, H.B., 1975. Fundamentals of Liquefaction under Cyclic Loading. *Journal of the Geotechnical Engineering Division, No. GT5.*

Martin, R.E., 1977. Estimating Foundation Settlements in Residual Soils. *Proc. ASCE, 103 (GT3): 197-212.*

Middlebrooks, T.A., 1942. Fort Peck Slide. *ASCE Transactions, Vol 107.*

Mulilis, J.P., Seed, H.B., Chan, C.K., Mitchell, J.K. and Arulanandan, K., 1977. Sample Preparation Sand Liquefaction. *Proc. ASCE, 103 (GT2): 91-108.*

Ohsaki, Y., 1966. Niigata earthquakes, 1964, building damage and soil condition. *Soils and Foundations, 6(2): 14-37.*

Ohsaki, Y., 1970. Effects of sand compaction on liquefaction during the Tokachioki earthquake. *Soils and Foundations, 10(2): 112-128.*

Papadakis, C.N., 1973. Soil transients by characteristics method. *Doctoral thesis, Dept. of Civil Engrg., University of Michigan,* Ann Arbor, Michigan.

Peacock, W.H., and Seed, H.B., 1968. Sand liquefaction under cyclic loading simple shear conditions. *Proc. ASCE, 94 (SM3): 689-708.*

Poulos, S.J., 1971. The stress-strain curves of soils. *Mimeographed pamphlet.*

Pike, R., Chan, C.K., and Seed, H.B., 1974. Settlement and liquefaction of sands under multi-directional shaking. *Report EERC 74-2, Earthq. Engrg. Res. Center, University of California,* Berkeley, California.

Schnabel, P.B., Lysmer, J., and Seed, H.G., 1972b. SHAKE: a computer program for earthquake response analysis of horizontally layered sites. *Report EERC 72-12, Earthq. Engrg. Res. Center, University of California,* Berkeley, California.

Seed, H.B., 1960. Soil strength during earthquakes. *Proc. Second World Conf. Earthq. Engrg.,* Tokyo and Kyoto, Japan, I, pp 183-194.

Seed, H.B., 1969. The influence of local soil conditions on earthquake damage. *Soil Dynamics Speciality Conference, VII ICSMFD,* México.

Seed, H.B., 1970. Soil problems and soil behavior. In: R.L. Wiegel (Editor), *Earthquake Engineering.* Prentice-Hall, Englewood Cliffs, New Jersey, pp 227-252.

Seed, H.B., and Lee, K.L., 1966. Liquefaction of saturated sands during cyclic loading. *Proc. ASCE, 92 (SM6): 105-134.*

Seed, H.B., and Idriss, I.M., 1967. An analysis of the soil liquefaction in the Niigata earthquake. *Proc. ASCE, 93(SM3): 83-108.*

Seed, H.B., and Idriss, I.M., 1969. Influence of soil conditions on ground motions during earthquakes. *Proc. ASCE, 95 (SM1): 99-137.*

Seed, H.B., and Idriss, I.M., 1970b. A simplified procedure for evaluating soil liquefaction potential. *Report EERC 70-9, Earthq. Engrg. Res. Center, University of California*, Berkeley, California.

Seed, H.B., and Idriss, I.M., 1970c. Soil moduli and damping factors for dynamic response analyses. *Report EERC 70-10, Earthq. Engrg. Res. Center, University of California*, Berkeley, California.

Seed, H.B. and Silver, M.L., 1972. Settlement of dry sands during earthquakes. *Proc. ASCE, 98 (SM4): 381-397.*

Seed, H.B., Lee, K.L., Idriss, I.M. and Makdisi, F.I., 1973. Analysis of the Slide in the San Fernando Dams during the Earthquake of Feb. 9, 1971. *EERC, Report No. EERC 73-2, University of California*, Berkeley, California.

Seed, H.B., Mori, K. and Chan, C.K., 1975. Influence of Seismic History on the Liquefaction Characteristics of Sands. *Report No. 75-25. University of California*, Berkeley, California.

Seed, H.B., Martin, P.P. and Lysmer, J., 1975. The Generation and Dissipation of Pore Water Pressures During Soil Liquefaction. *Report No. EERC 75-26, University of California*, Berkeley, California.

Seed, H.B., Arango, I. and Chan, C.K., 1975. Evaluation on Soil Liquefaction Potential During Earthquakes. *Report No. EERC 75-28, University of California*, Berkeley, California.

Seed, H.B., Pyke, R. and Martin, G.R., 1975. Effect of Multi-directional Shaking on Liquefaction of Sands. *Report No. EERC 75-41, University of California*, Berkeley, California.

Seed, H.B. and Booker, J.R., 1976. Stabilization of Potentially liquefiable Sand Deposits Using Gravel Drain Systems.

Shannon & Wilson, Inc., and Agbabian-Jacobsen Associates, 1971. Soil behavior under earthquake loading conditions. *Report prepared for U.S.A.E.C.*, Contract W-7405-eng-26.

Shockley, W.C. y Ahluin, R.C., 1960. Non-Uniform Conditions in Triaxial Test Specimens, *Research Conference on Shear Strength of Cohesive Soils*, ASCE. Boulder, Colorado.

Silver, M.L., and Seed, H.B., 1969. The behavior of sands under seismic loading conditions. *Report EERC 69-16, Earthq. Engrg. Res. Center, University of California*, Berkeley, California.

Streeter, V.L., Wylie, E.B., and Richart, F.E., 1973. Soil motion computations by characteristics method. *ASCE Natl. Struct. Engrg. Meeting*, San Francisco, California, Preprint 1952.

Thiers, G.R., and Seed, H.B., 1968a. Cyclic stress-strain characteris tics of clay. *Proc. ASCE, 94(SM2): 555-569.*

Valera, J.E. and Donovan, N.C., 1977. Soil Liquefaction Procedures-A Review. *Proc. ASCE 103 (GT6): 607-625.*

Watson, J.D., 1970. Stress-deformation characteristics of cohesionless soils from triaxial compression tests. *Doctoral thesis, Harvard University*, Cambridge, Massachusetts.

Whitman, R.V., and Ortigosa, P., 1968. Densification of sand by vertical vibrations. *Technical paper T68-5, Dept. of Civil Engrg., Massachusetts, Institute of Technology*, Cambridge, Massachusetts.

Yegian, M.K., 1976. Resk analysis for Earthquake-induced ground failure by liquefaction, M.I.T. *Publication No. R76-22.*

Youd, T.L., 1970. Densification and shear of sand during vibration. *Proc. ASCE, 96 (SM3): 863-880.*

Youd, T.L., 1972. Compaction of sands by repeated shear straining. *Proc. ASCE, 98 (SM7): 709-726.*

Youd, T.L. and Hoose, S.N., 1976. Liquefaction During 1906 San Fran cisco Earthquake. *Proc. ASCE, 102 (GT5): 425-439.*

Zeevaert, L., 1967. Free vibration torsion tests to determine shear modulus of elasticity of soils. *Proc. Third Panamerican Conf. Soil Mech. and Found Engrg.*, Caracas, Venezuela, I. 111-129.

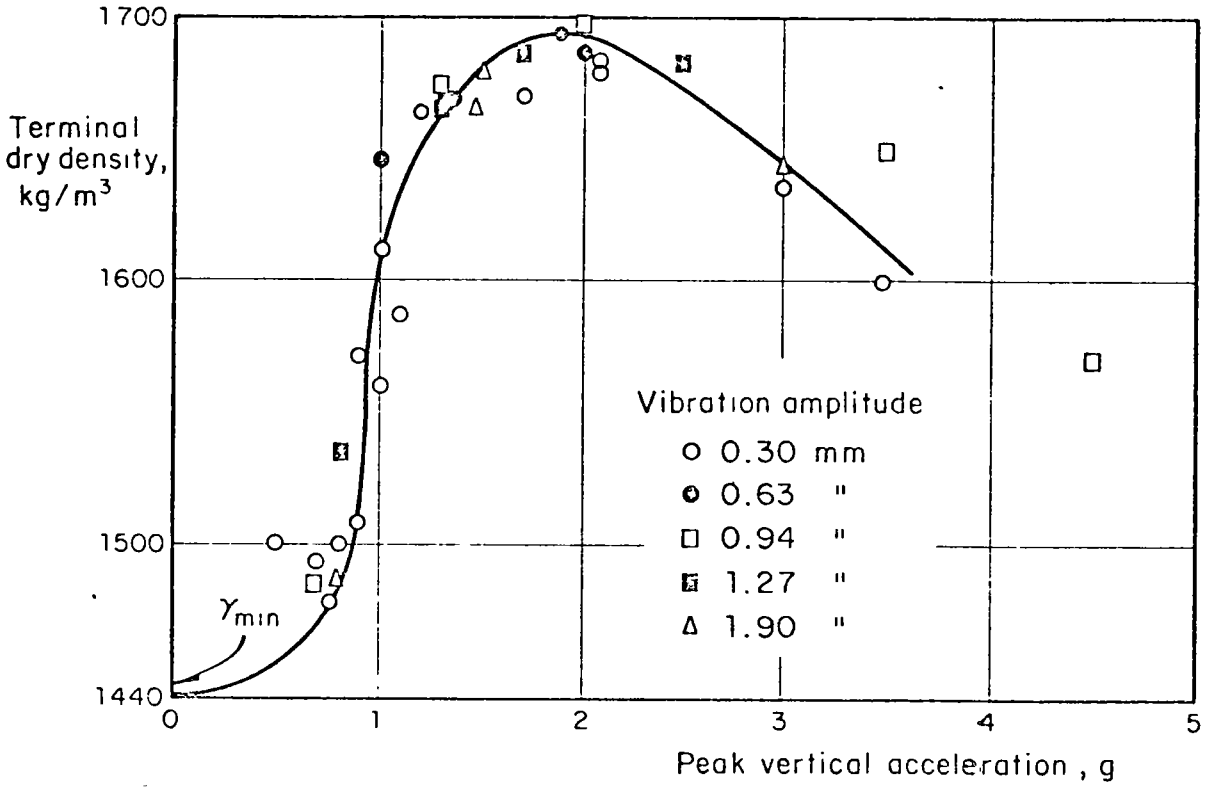

Fig 4 — *Effect of acceleration intensity on densification of sand in vertical shaking table tests.* After D'Appolonia and D'Appolonia (1967).

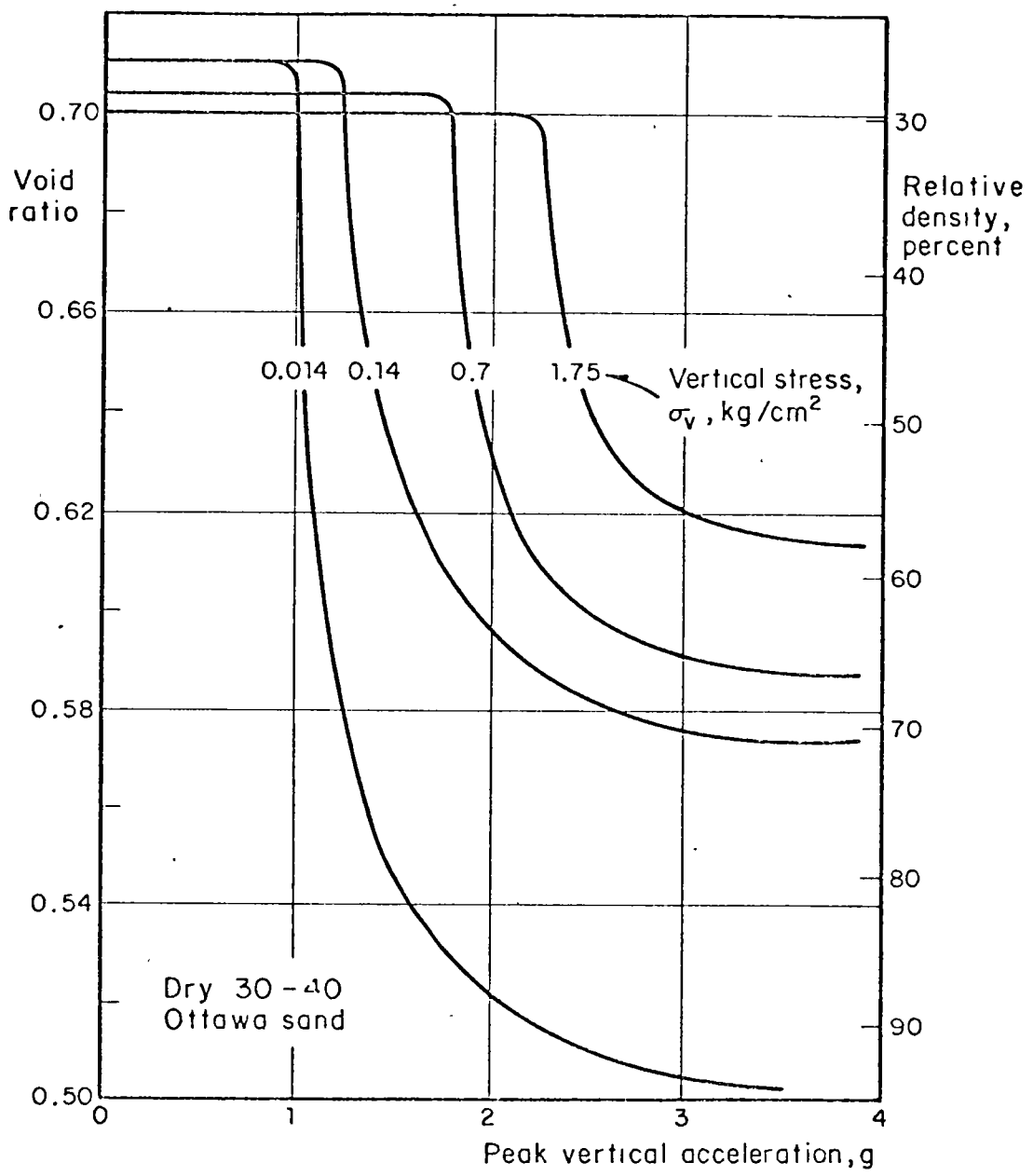

Fig. 5. *Effects of acceleration intensity and confining stress on densification of dry Ottawa sand in vertical shaking table tests.* After Whitman and Ortigosa (1968).

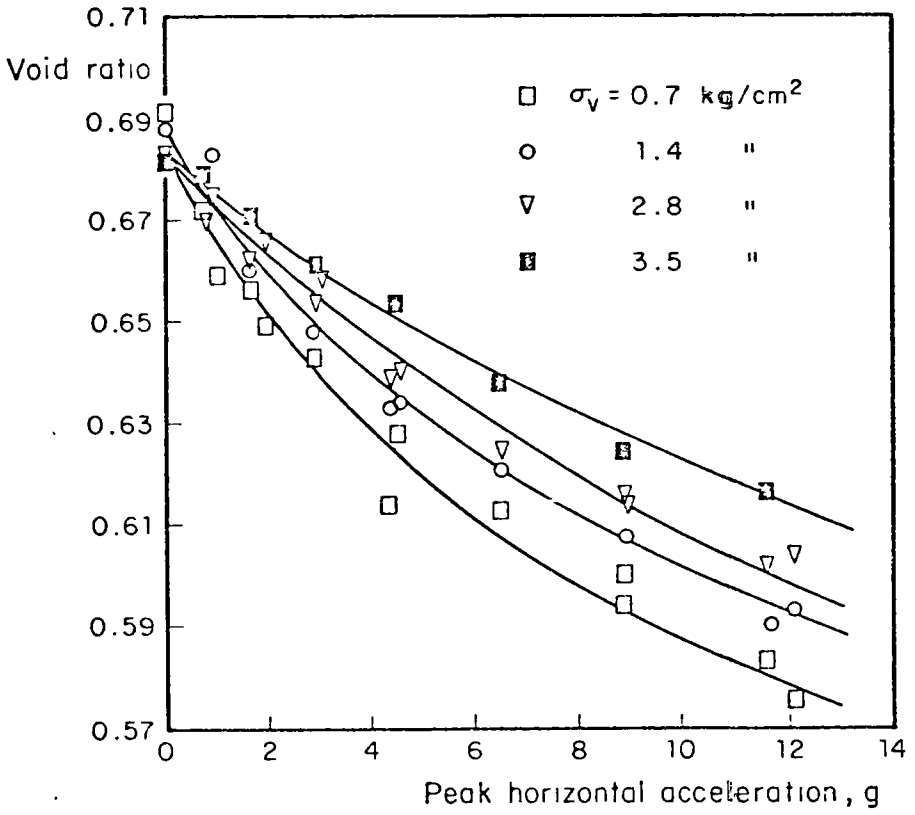

Fig 6 Effects of acceleration intensity and confining stress on final void ratio of dry Ottawa sand in shear vibration tests. After Youd (1970).

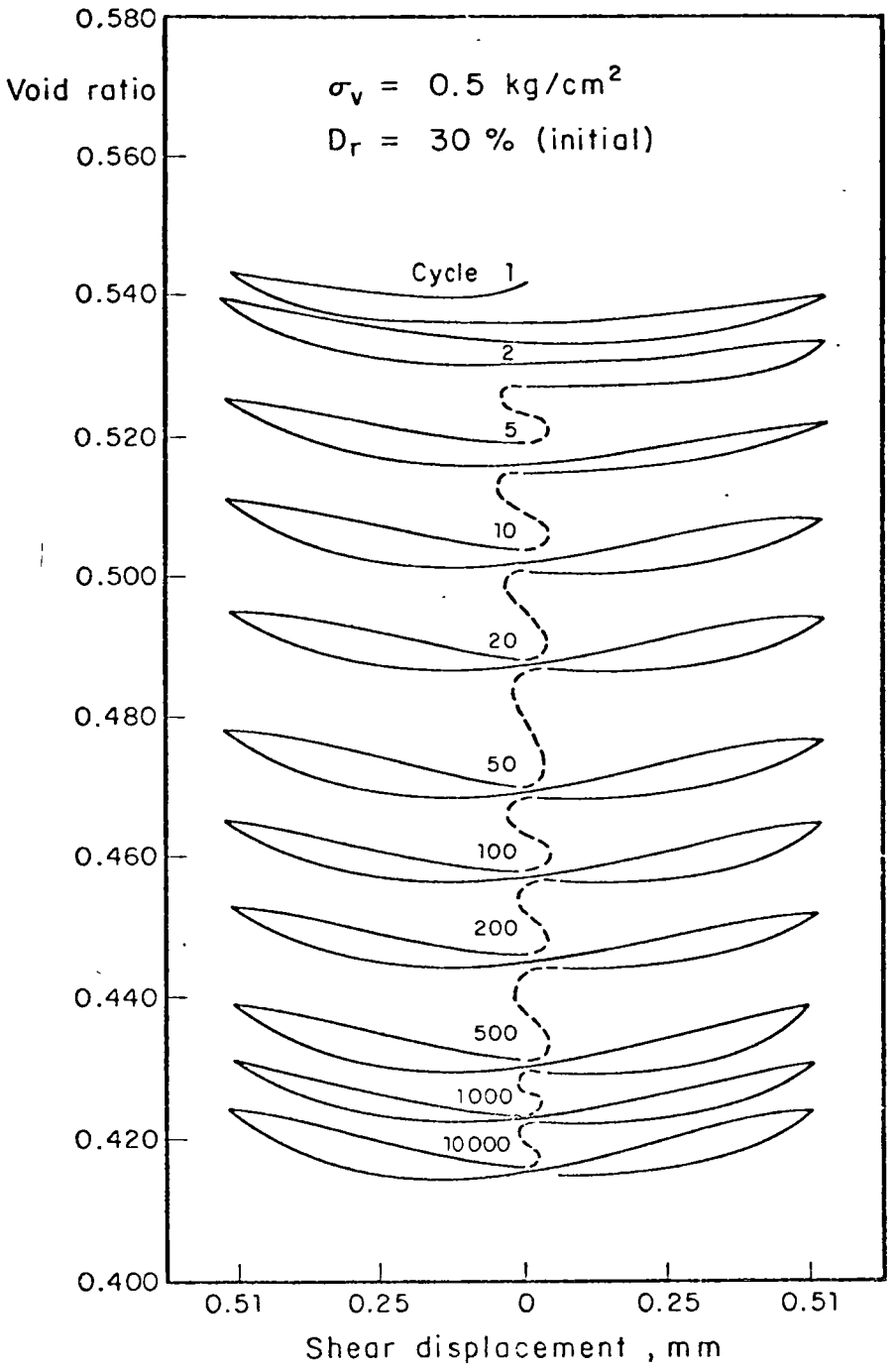

Fig 7 : *Compaction vs. shear-strain history in a cyclic shear test on saturated, drained Ottawa sand.* After Youd (1972).

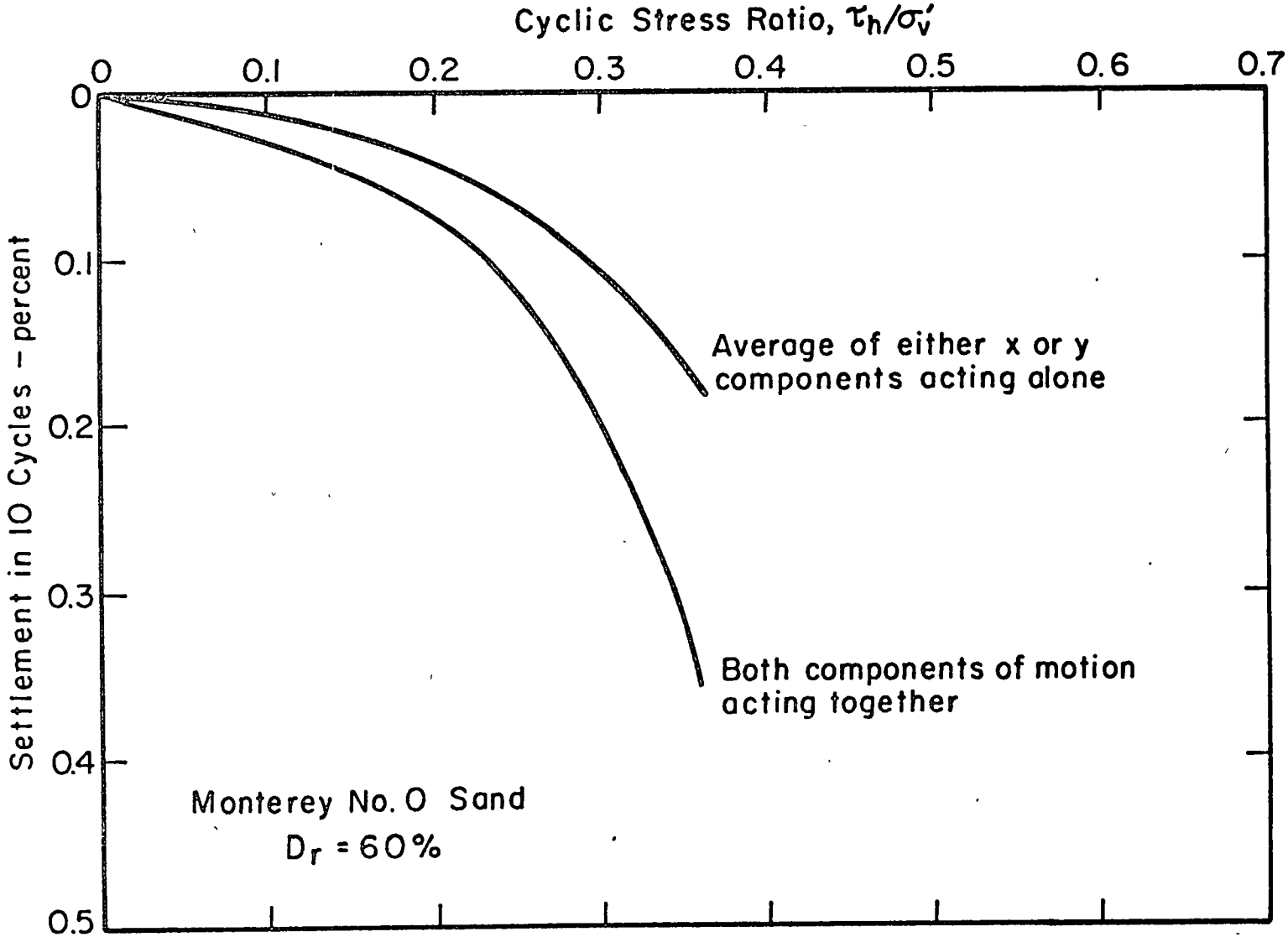

Fig. 8 SETTLEMENT OF DRY SAND UNDER UNIDIRECTIONAL AND MULTIDERECTIONAL SHAKING

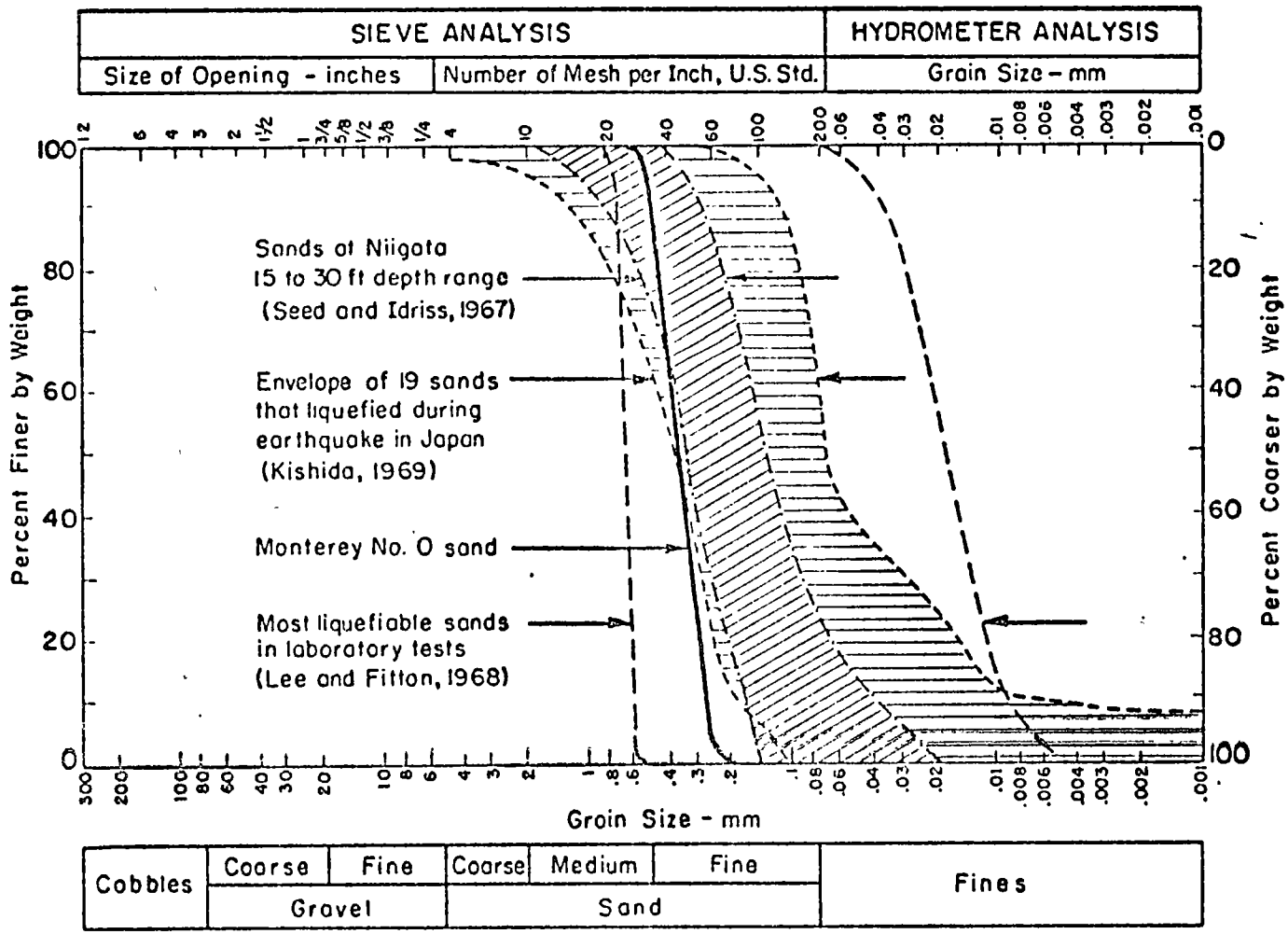

Fig. 9. SOILS SUSCEPTIBLE TO LIQUEFACTION

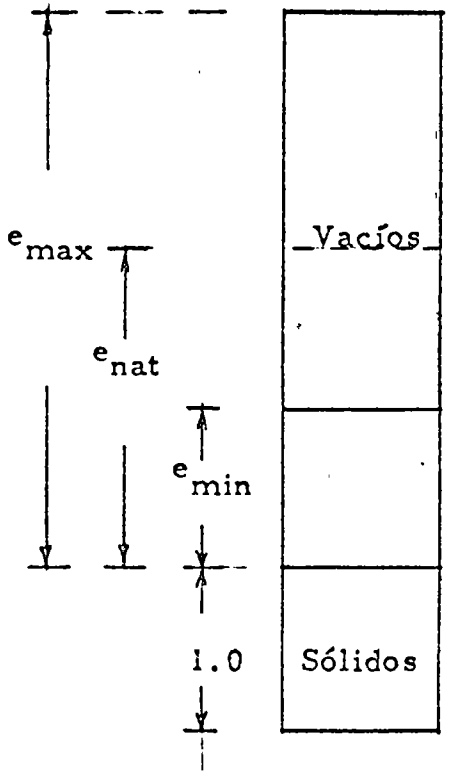

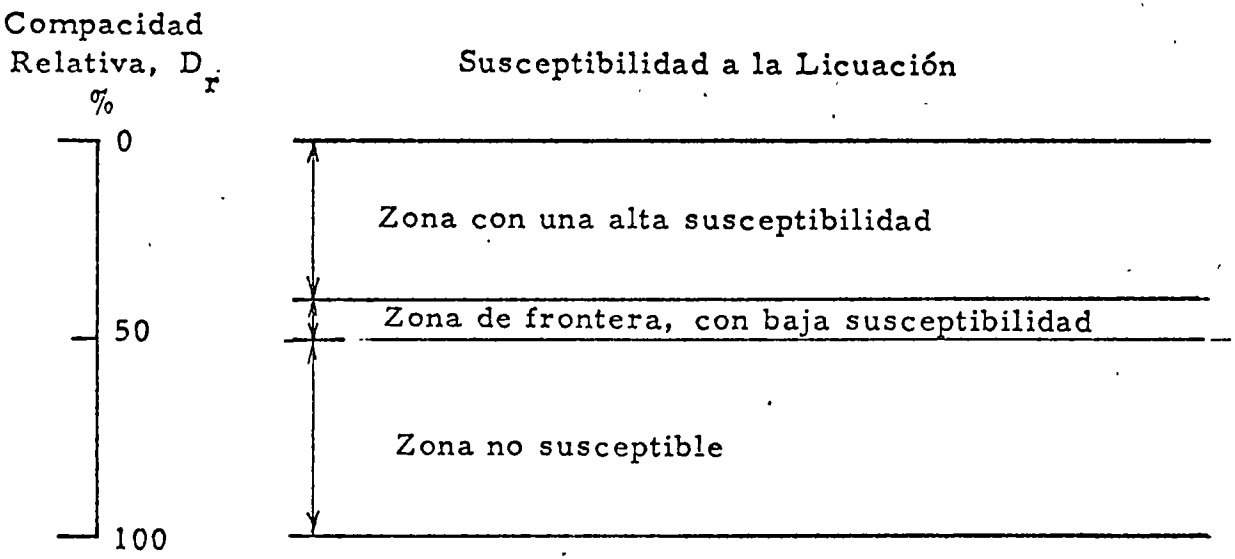

$$\text{Compacidad Relativa } D_r\ (\%) = \frac{e_{max} - e_{nat}}{e_{max} - e_{min}} \times 100$$

Fig. 10 Concepto de Compacidad Relativa

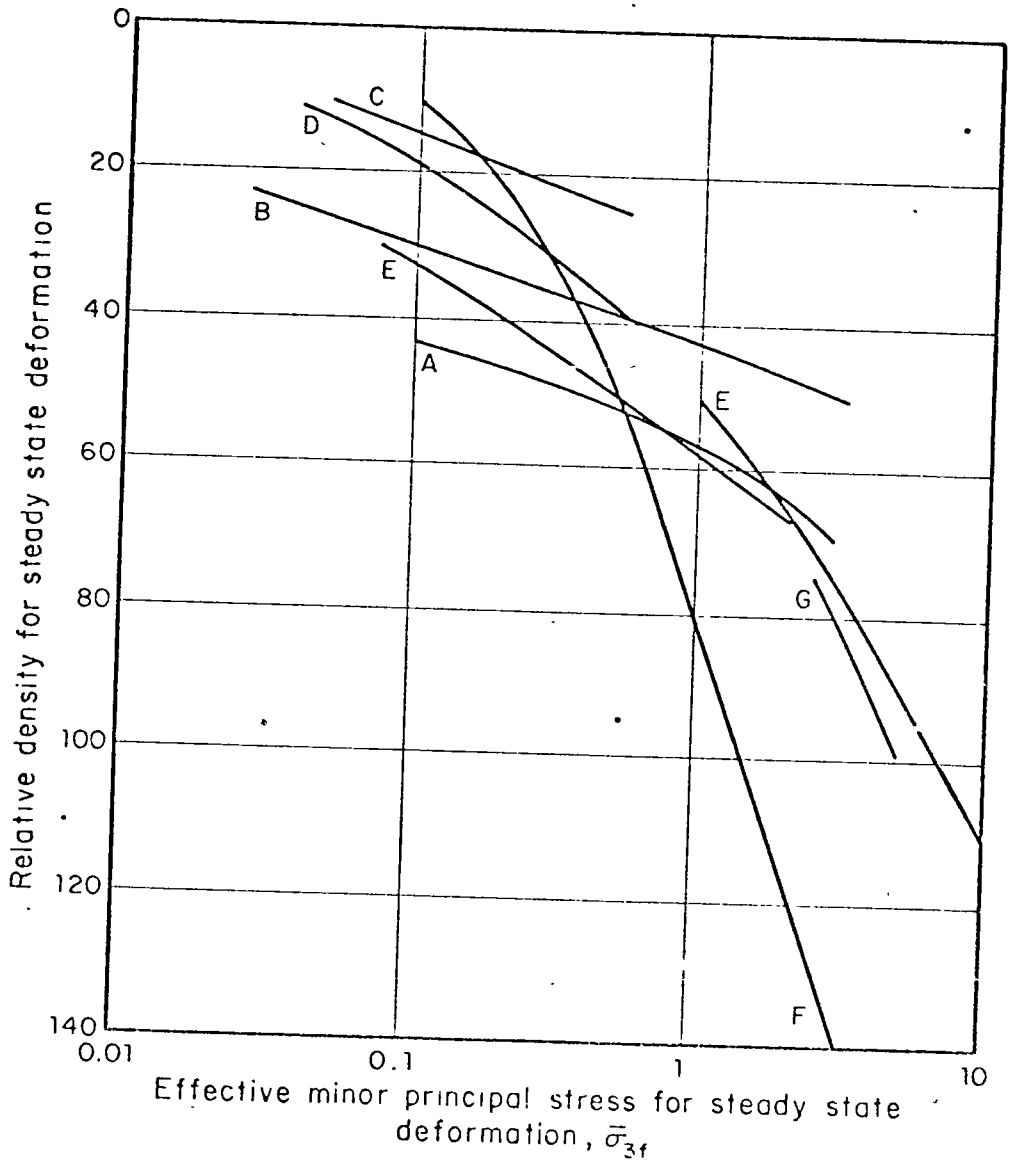

Fig. 11. Critical state lines (e_f-lines) of sands described in Table 4.2 (Castro, 1972).

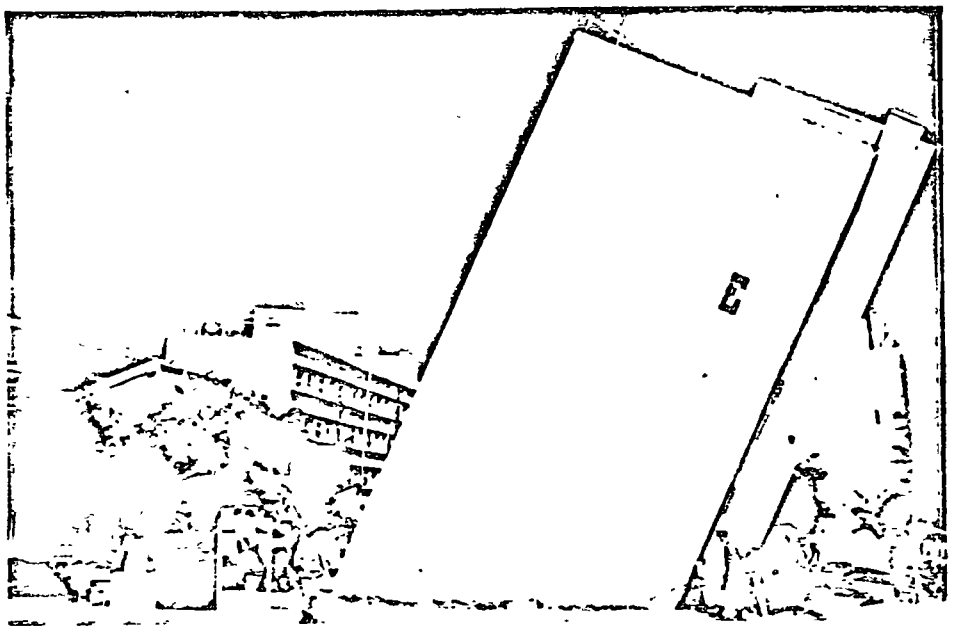

Fig 1. Inclinación de edificios durante el temblor de Niigata, 1964

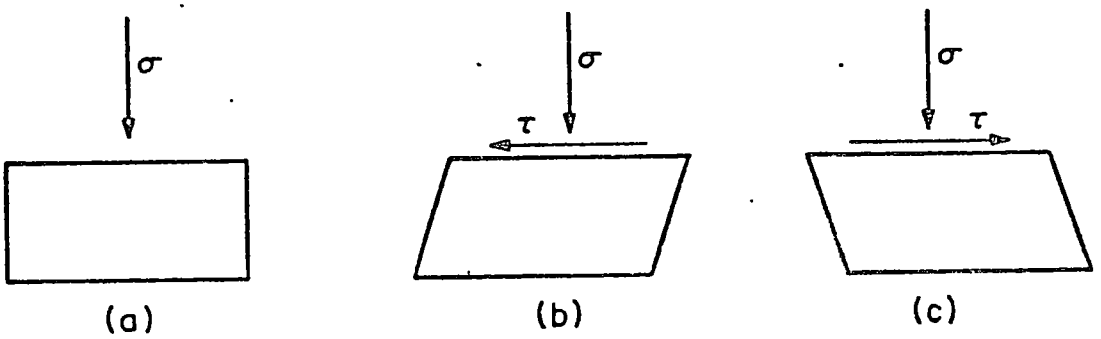

Fig 12. Condición idealizada de esfuerzos para un elemento de suelo en el interior de un depósito, durante un temblor

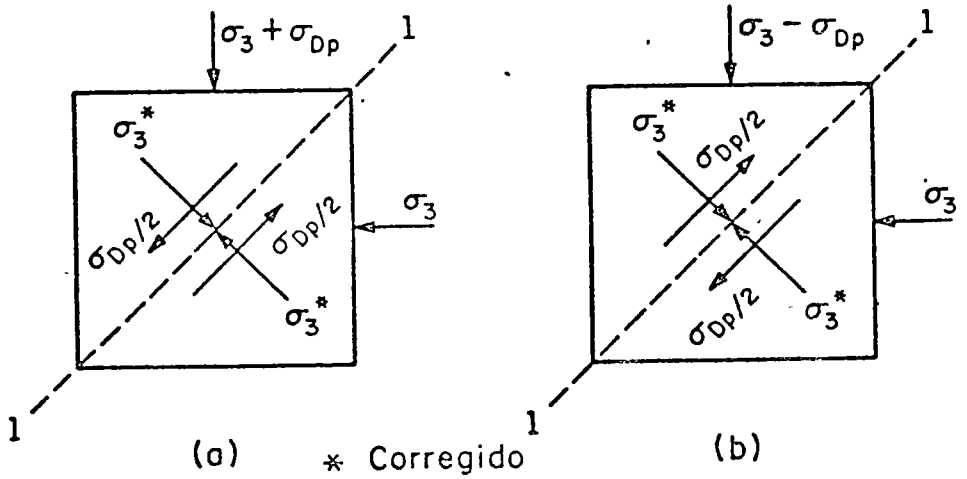

Fig 13. Prueba de compresión triaxial cíclica

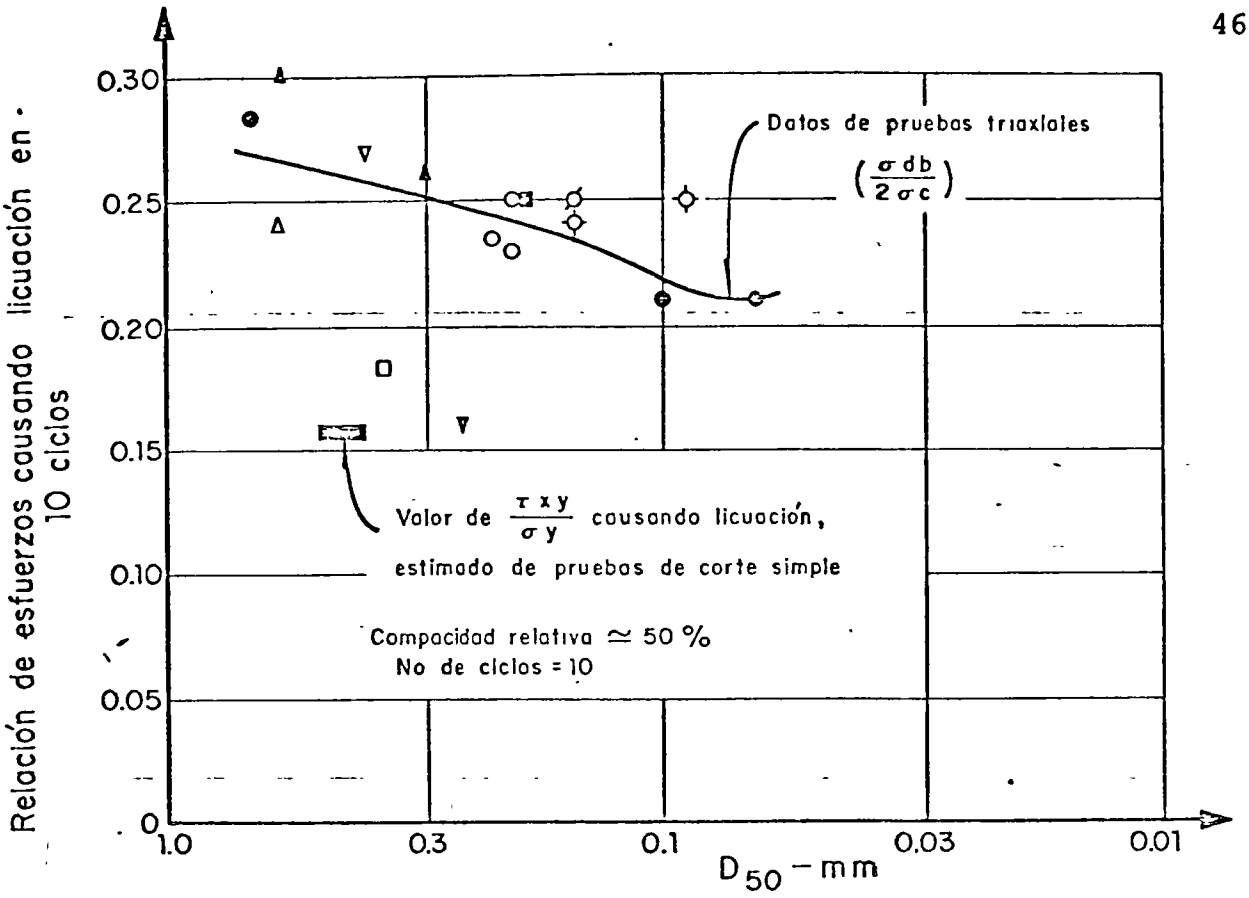

Fig 14 Condiciones de esfuerzo causando licuación de arenas en 10 ciclos

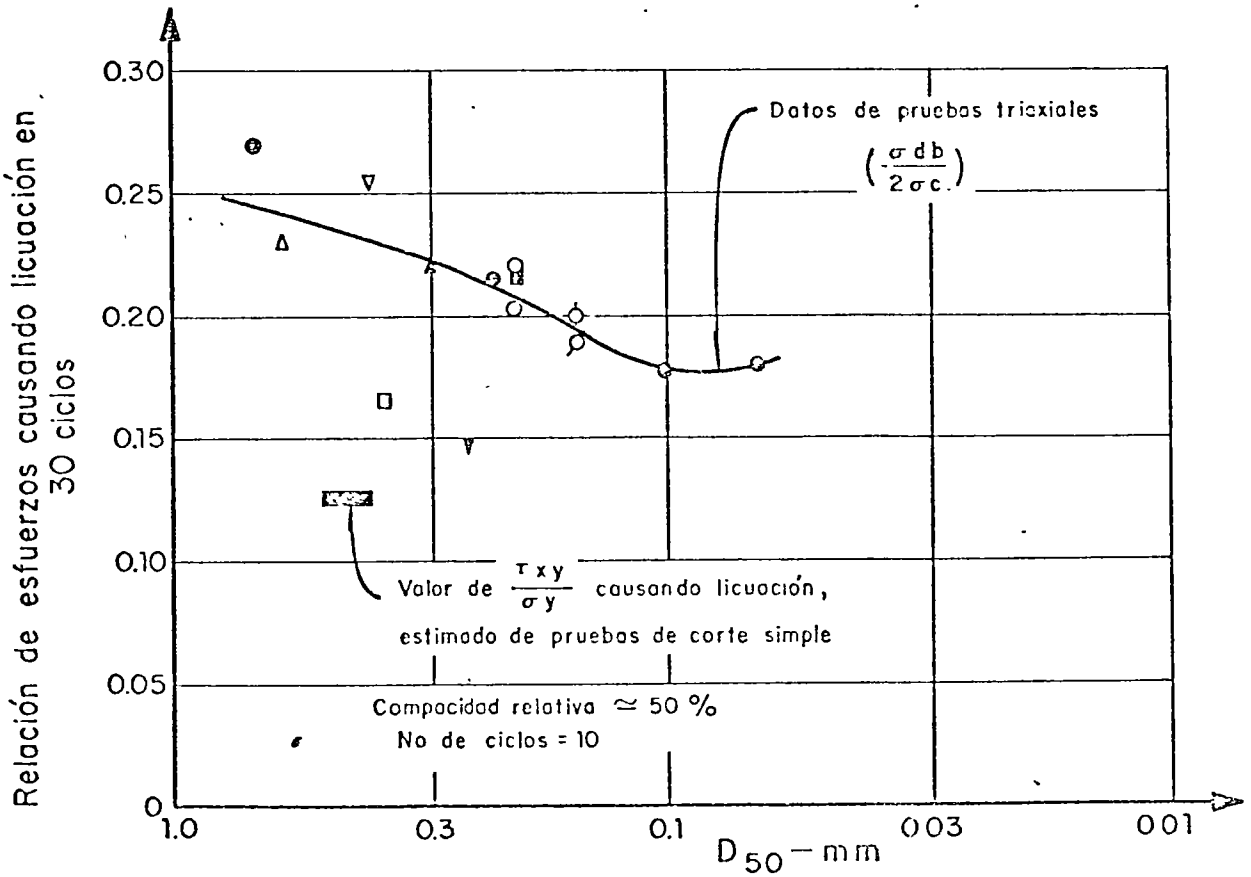

Fig 15 Condiciones de esfuerzo causando licuación de arenas en 30 ciclos

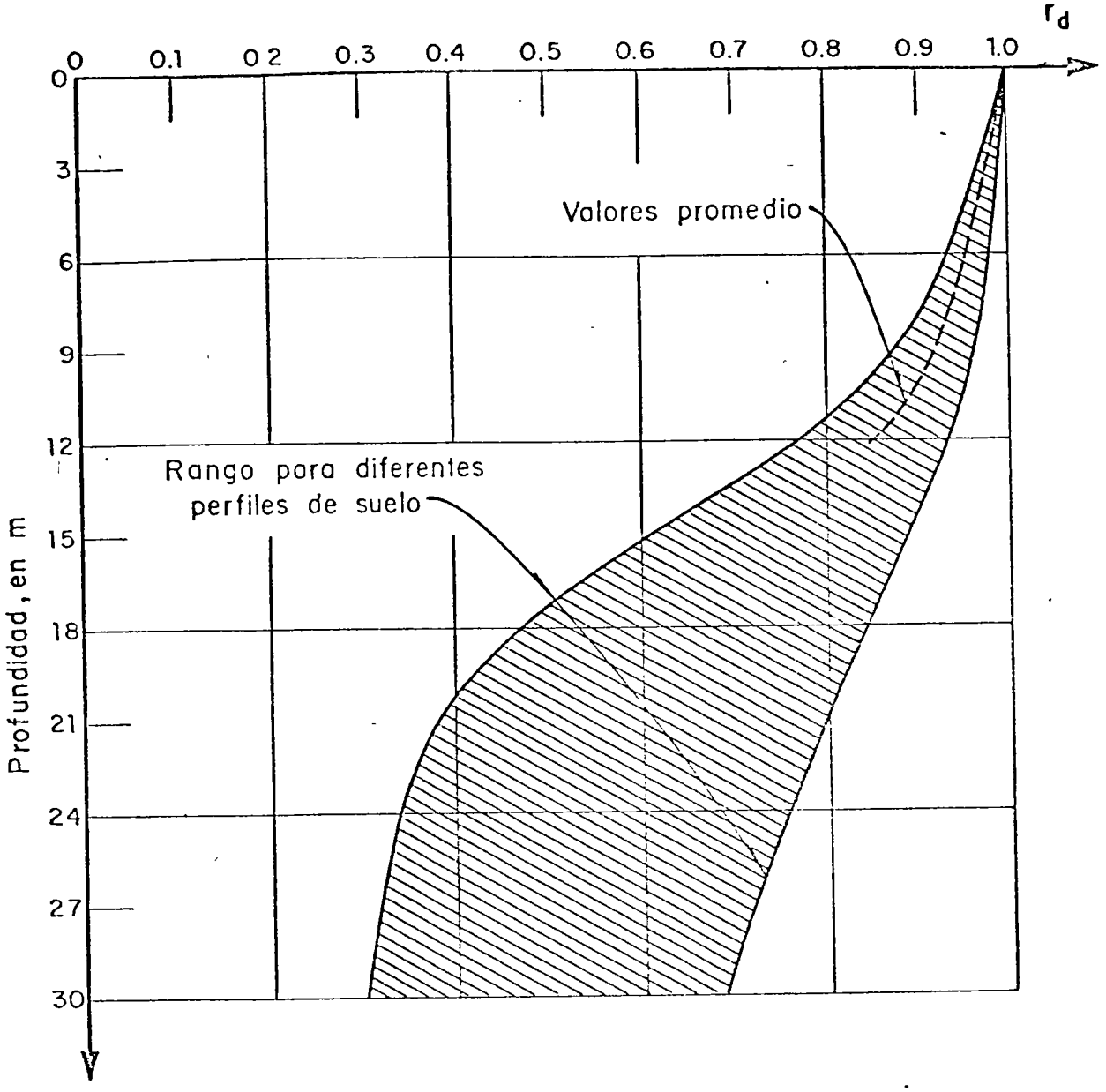

Fig 16 Rango de valores de r_d para diferentes perfiles de suelo

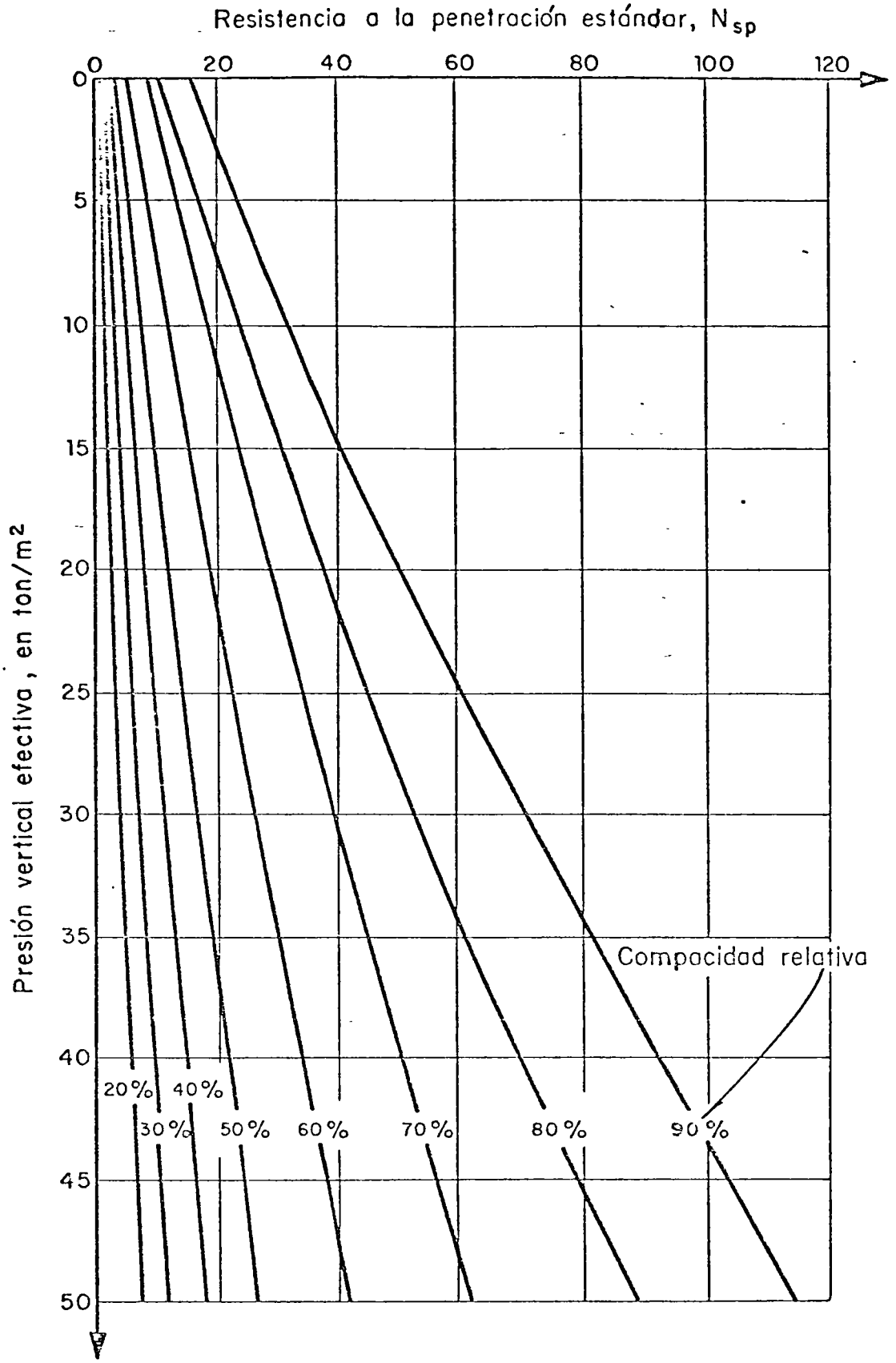

Fig 17 Relación entre la resistencia a la penetración, compacidad relativa y presión vertical

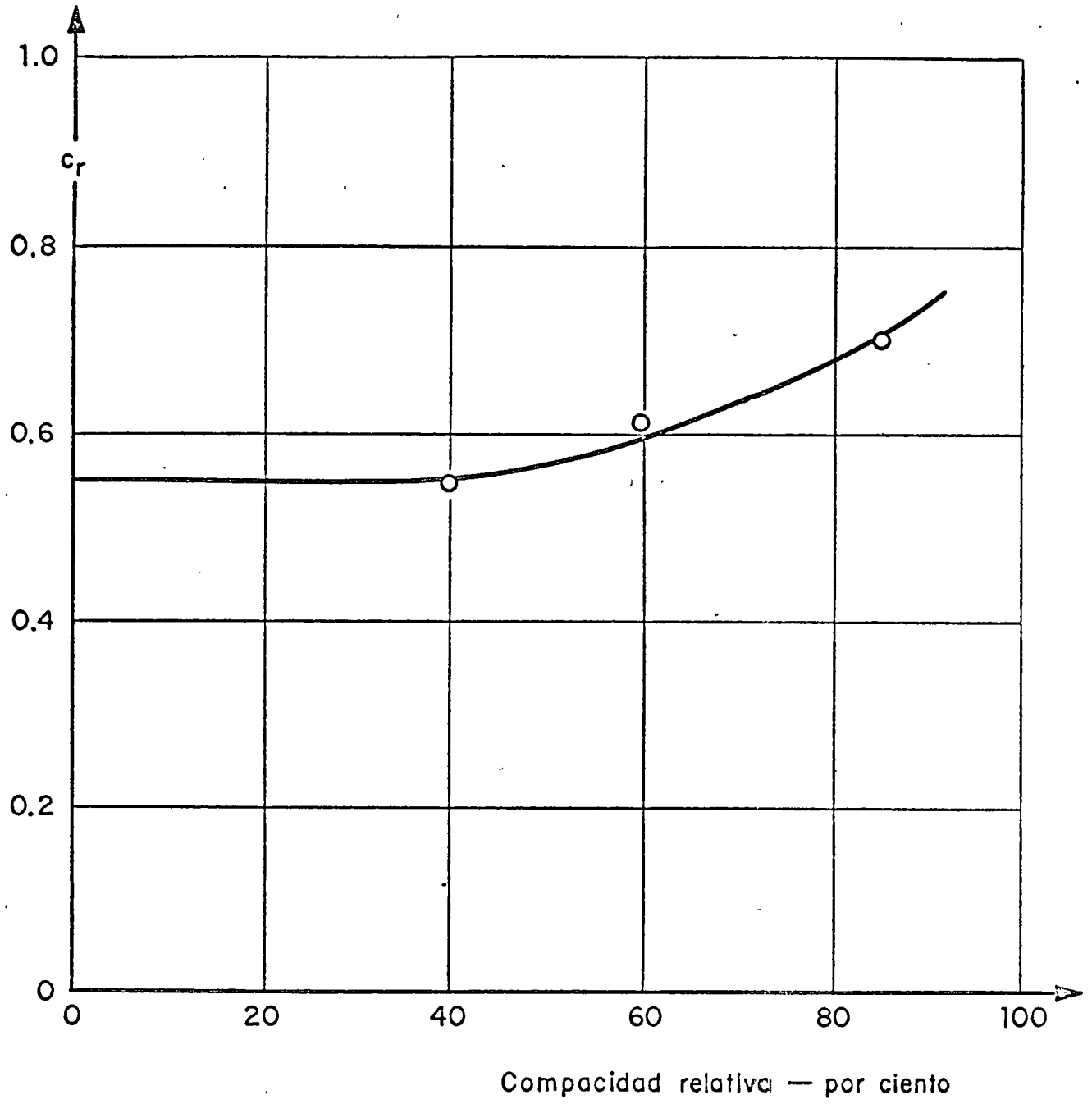

Fig 18 Relación entre c_r y la compacidad relativa

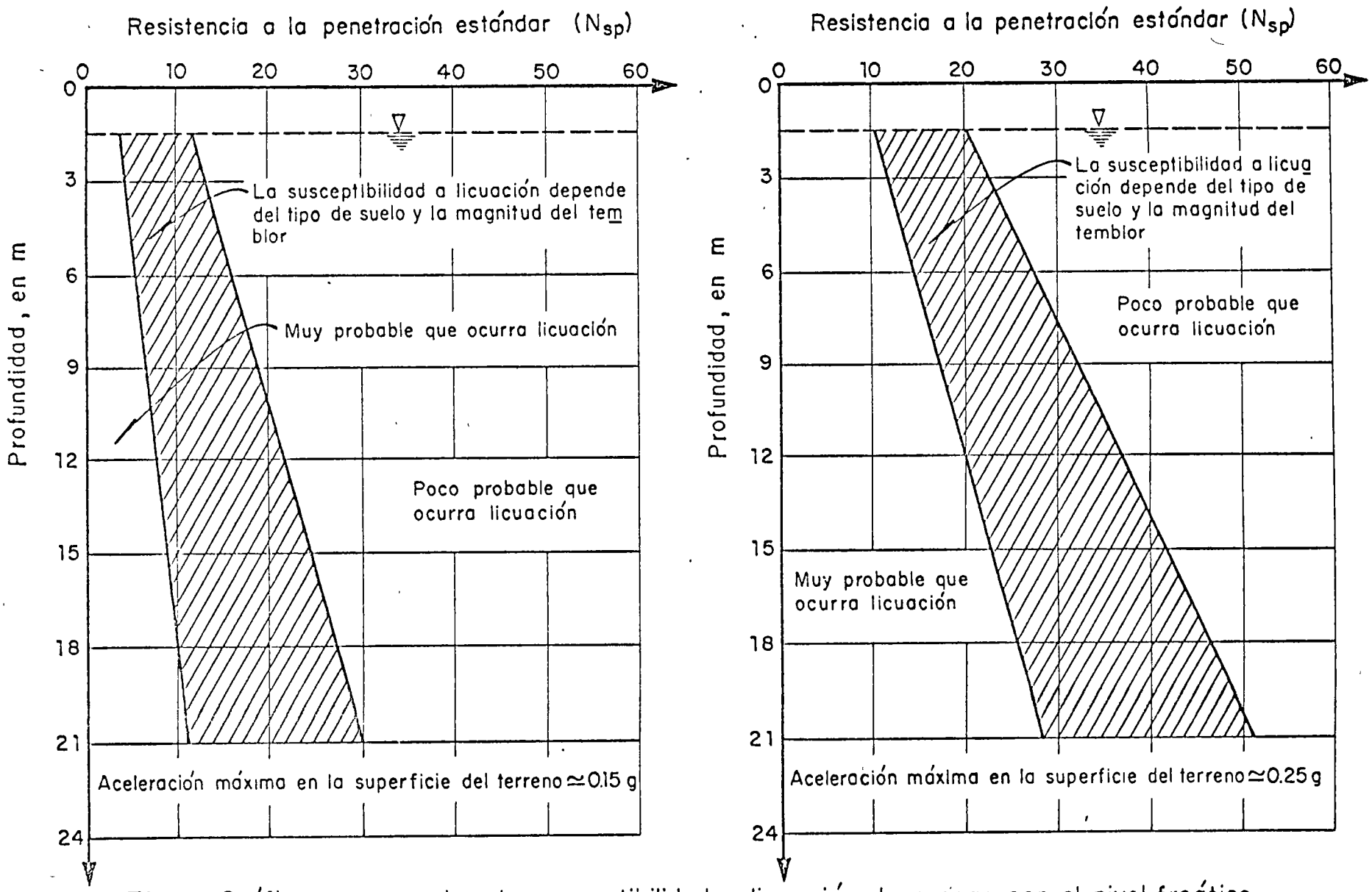

Fig 19 Gráficas para evaluar la susceptibilidad a licuación de arenas con el nivel freático a una profundidad aproximada de 1.5 m

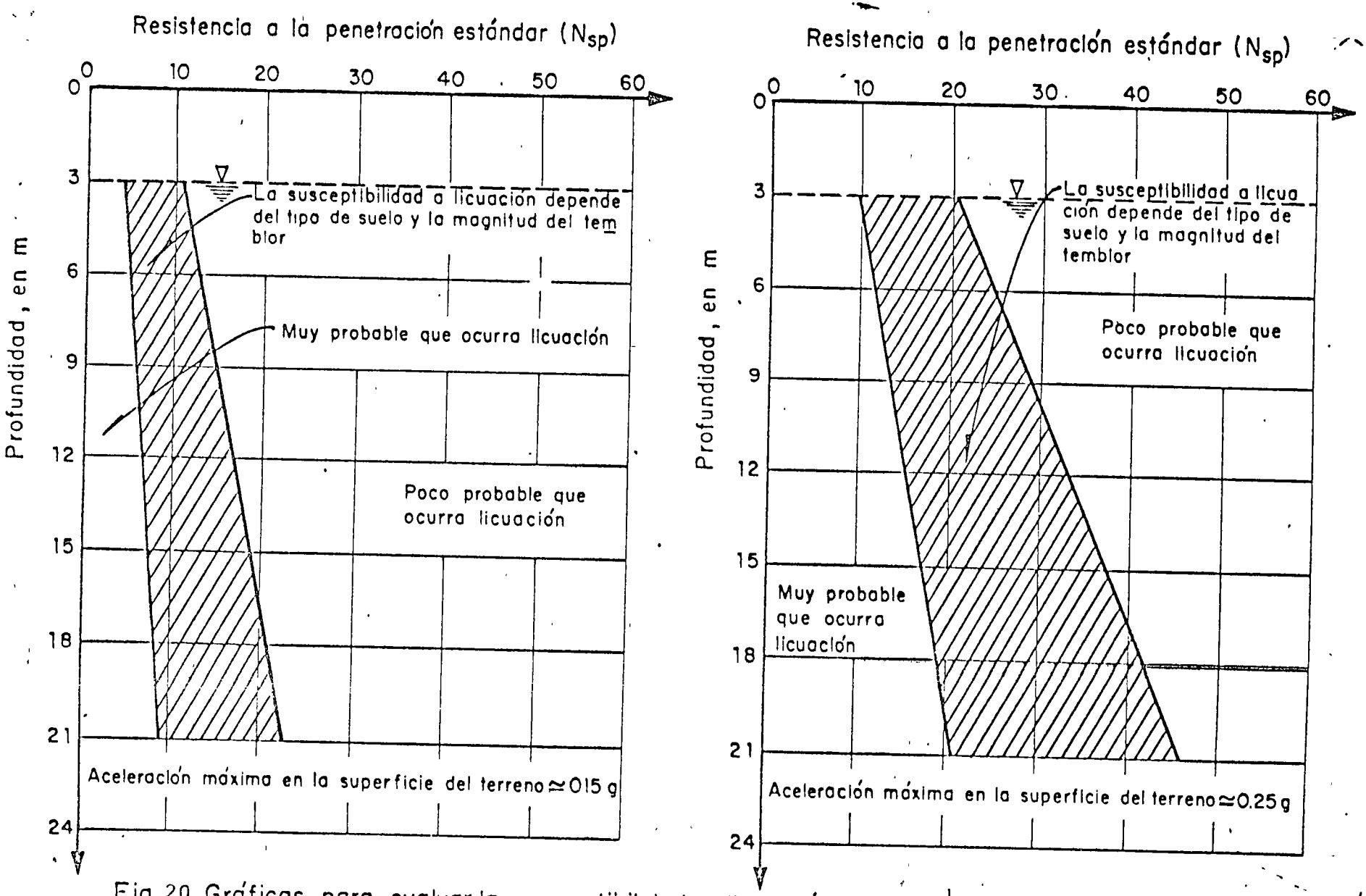

Fig 2.0 Gráficas para evaluar la susceptibilidad a licuación de arenas con el nivel freático a una profundidad aproximada de 3.0m

centro de educación continua
división de estudios superiores
facultad de ingeniería, unam

II CURSO INTERNACIONAL DE INGENIERIA SISMICA

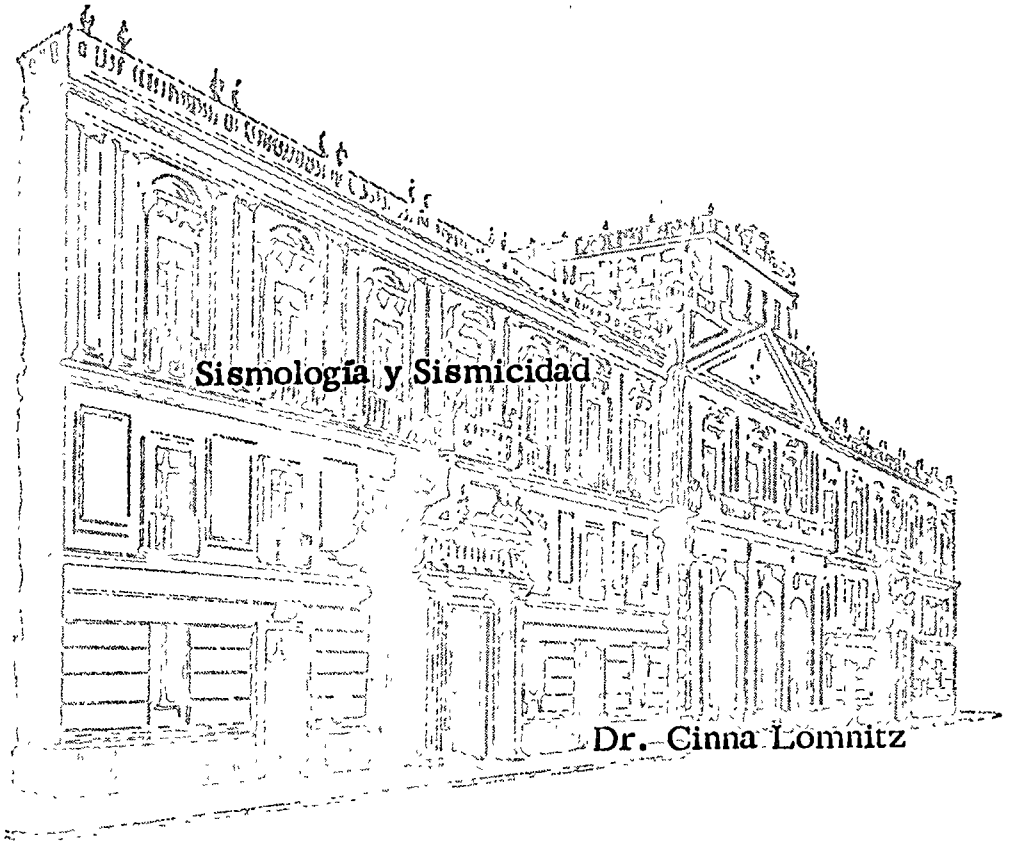

Sismología y Sismicidad

Dr. Cinna Lomnitz

Chapter 10

SEISMOLOGICAL INSTRUMENTATION

THOMAS V. MCEVILLY

Department of Geology and Geophysics, University of California, Berkeley, Calif., U.S.A.

10.1 INTRODUCTION

This chapter presents general information and guideline hopefully useful in selecting instruments for seismological research and engineering applications. Two main aspects are considered: (1) defining the measurement requirements in a particular situation; (2) understanding the principles and capabilities of available sensing, signal conditioning, and recording systems and the degree to which requirements can be met by available equipment. Emphasis is on widely used conventional seismological equipment. Special devices, such as strain gages, seismoscopes, and digital acquisition systems are mentioned where appropriate.

10.2 APPLICATIONS

The following stand out among the many applications of seismological instruments in the assessment of seismic risk and in providing bases for the making of engineering decisions.

— Seismotectonic investigations: use of earthquake source parameters and spatial distribution of hypocenters to infer local or regional tectonic characteristics such as principal stress directions, extent of potential earthquake zones, deformation rates, depth range of crustal or upper-mantle earthquakes, and temporal variations of earthquake source parameters or medium properties.

— Monitoring of fault creep: detection and measurement of long-term aseismic slip on potentially active recent fault traces.

— Earthquake prediction research: monitoring temporal variations in earthquake characteristics and physical properties in the source region.

— Short-range seismicity studies: use of portable or temporary equipment in gathering spatial and temporal data on occurrence of small local earthquakes, detecting and mapping active faults, or monitoring effects of reservoir loading behind dams.

— Shallow subsurface investigation: use of a variety of active or passive seis-

mological methods in measuring soil properties, overburden thickness, lateral variation in near-surface geology, depth of water table, etc.

- Aftershock sequence study: study of characteristics of aftershock sequences, the nature of faulting, and local ground effects.
- Strong-motoin recording: detection and broadband recording of moderate to strong ground motion in seismic regions for specifying bases of structural design in the area.
- Determination of dynamic properties of structures: measurement of structural responses to static or dynamic perturbations including, among the latter, impulsive excitation of free vibrations, forced harmonic or quasiharmonic excitation, ambient disturbances, blasts, and earthquakes.
- Model studies: monitoring of shaking-table motions and of the responses of models to dynamic excitation.

These applications require the measurement of motion or force either at a point (e.g., an accelerometer) or between two points (e.g., a strain gage). We shall concentrate on the former class of requirement and will thus treat the conventional inertial seismometer in some detail. Strain monitoring techniques for structures or across fault zones are well-covered in specialized texts. A series of papers presented at the 5th World Conference on Earthquake Engineering (1973) provide an excellent review of earthquake instrumentation for recording strong motion.

10.3 REQUIREMENTS: GENERAL

The nature of a particular application will usually specify the type of sensor required, the frequency range of interest, the accuracy and resolution of the record produced, and any requirements for possible interconnection of instruments, remote data telemetry, or provisions for automatic processing. Additional constraints are always present in the available budget as well as in the operational and maintenance conditions.

An important early decision involves recording requirements. At times a simple measurement of the peak value if sufficient — in other applications the time history of the parameter variation must be retained. Ordinarily direct measurement of peak values is far less expensive than time-based recording. We consider next a group of special-purpose instruments, including peak-reading devices, and follow with a more extensive discussion of widely used conventional inertial seismometers and seismographs.

10.4 PEAK-READING INSTRUMENTS

10.4.1 Peak ground motion

The information contained in the peak value of a ground-motion parameter (maximum displacement, velocity, or acceleration) is usually insuffi-

cient for much analysis beyond threshold monitoring or event counting. Instruments measuring such peak values serve frequently as complements of standard seismographs capable of supplying full time histories of ground motion. In some applications, however, these data are of great value. A prime example is the simple low-cost shock (acceleration) indicator widely used to monitor the vibration environment during commercial transportation of delicate equipment. Another application is the peak velocity indicator used to monitor damage potential of vibrations from blasting and heavy construction. Simple counting of microearthquakes larger than a given magnitude also provides a valuable activity indicator for volcanoes.

For strong-motion recording, interest is ordinarily centered on the peak horizontal ground acceleration or the peak responses of oscillators with specific periods and damping ratios. A precise measurement of peak ground acceleration is not sought. In keeping with the goals of low-cost and simplicity, and in view of the unsophisticated analysis of the resulting data, a rough estimate of peak acceleration is usually adequate. This can be obtained from several types of devices.

A falling-pin set is a primitive vibration-indicating instrument consisting of a set of slender, rigid prismatic rods of different heights, standing on a horizontal surface. Roughly, the rod slenderness determines the horizontal acceleration required to topple it. If b = diameter of rod base, h = rod height, and g = gravity, a statistically applied horizontal acceleration of bg/h is required to topple the rod. While the peak earthquake acceleration actually required to topple the rod in an earthquake may differ substantially from this value, by noting which rods have toppled over we get a gross idea of a range in which lies the maximum horizontal acceleration. The maximum and minimum values of peak ground acceleration in which we are interested determine the range of rod slenderness and the precision with which we wish to bracket the peak acceleration governs the number of rods used.

A seismoscope is an instrument which records the occurrence of an earthquake. A widely used model due to Wilmot (shown in Fig. 10.1) is a damped two-degree-of-freedom oscillator capable of recording the pendulum trajectory in the horizontal plane. Recording by stylus on a smoked watch glass, the instrument traces a hodogram representing the response of a lightly damped pendulum to the earthquake excitation. A reasonable model of a typical structure is embodied in a natural period of 0.75 sec and a damping factor of 0.1 critical. Having no time (nor frequency) scale, the seismoscope record cannot be reduced to ground motion, i.e., the same record can be produced by an infinite family of widely differing ground motions. At high-frequency excitation, the seismoscope trace deflection is proportional to ground displacement, while at low frequencies it is proportional to ground acceleration. For any excitation, however, it fulfills the intended purpose of providing a point (0.75 sec period, 0.1 damping) on the response spectrum for the earthquake motion recorded. A series of such seismoscopes

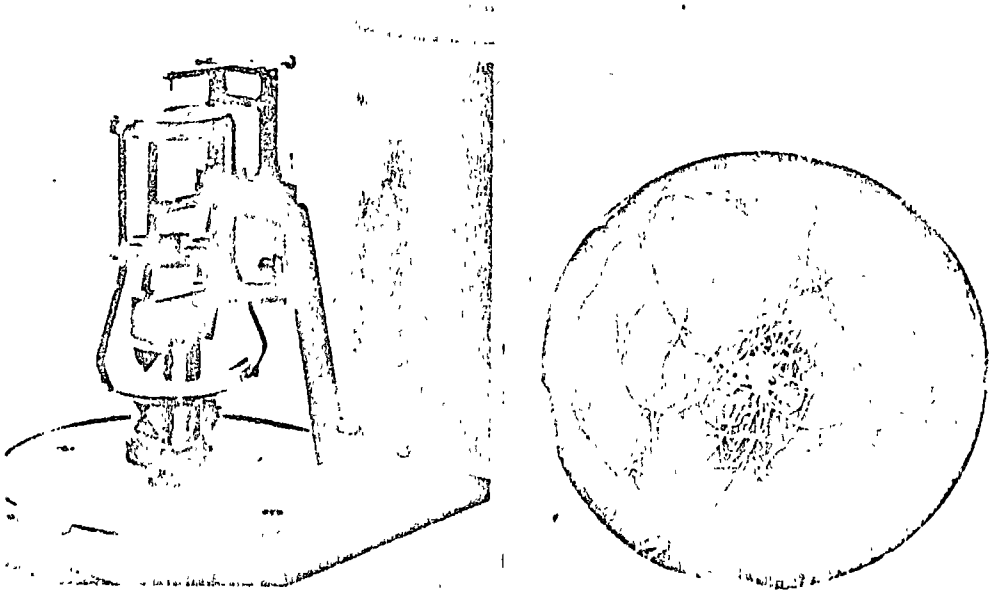

Fig. 10.1 Wilmot seismoscope (left, courtesy Kinemetrics, Inc.) and seismogram written in 1971 San Fernando earthquake (courtesy Seismological Field Survey, NOAA).

with different periods and damping can be used to obtain several points on the response spectrum directly.

Seismoscopes with natural frequencies above about 20 Hz produce, for typical earthquakes, records with amplitude directly proportional to ground acceleration and can thus be calibrated as peak-reading accelerometers. Various designs exist based on different types of oscillation, e.g., pendulums with stylus and smoked glass, cantilevers with magnetic indication of maximum deflection, elastic spheres writing ink impressions on a confining box upon flattening due to acceleration, etc.

10.1.2 Peak structural motion

When conducting harmonic-excitation tests of a structure, often only the motion amplitudes at different points are of interest for various excitation frequencies. The oscillations are usually of sufficiently low frequency and large amplitude; they can be measured directly at the seismometer output. When the structure is man-excited, visual observation of the seismometer output allows the operators to control their swaying. For earthquake excitation, any of the devices described in the previous section can, of course, be installed at various points within the structure.

In cases where the structure's damping ratio is to be measured, an accurate

record of the decay of free oscillations must be made and peak-reading devices are inadequate. With modern instrumentation it should be easy to obtain natural frequencies and damping factors for structures to an accuracy of a few percent — quite adequate for such measurements within the linear-response range of structures.

One of the most significant structural response parameters in earthquakes is the maximum acceleration developed at selected points. Using the peak-reading accelerometers discussed in the previous section, such measurements should be possible with errors of 10% or less.

10.4.3 Peak structural deformations

We are often interested in measuring a building's maximum interstory relative displacements and the strains at selected sections of structural members or at joints. The former have been successfully recorded by using the device depicted in Fig. 10.2. It consists of a diagonal bar extending the whole story height, connected at the lower end to a lever that magnifies relative displacements five-fold. The lever has a pen that records on a drum possessing a clock mechanism which requires rewinding once a week. Records are obtained on paper replaced when rewinding the clock mechanism. The reason for the rotating drum in lieu of a stationary scratch device is that temperature changes and wind effects cause some story drifts which it is desirable to isolate from earthquake response. The latter is confined to such a short time interval on the record that it is impossible to derive a response-history record but the accuracy with which maximum drifts are read is quite sufficient for practical purposes.

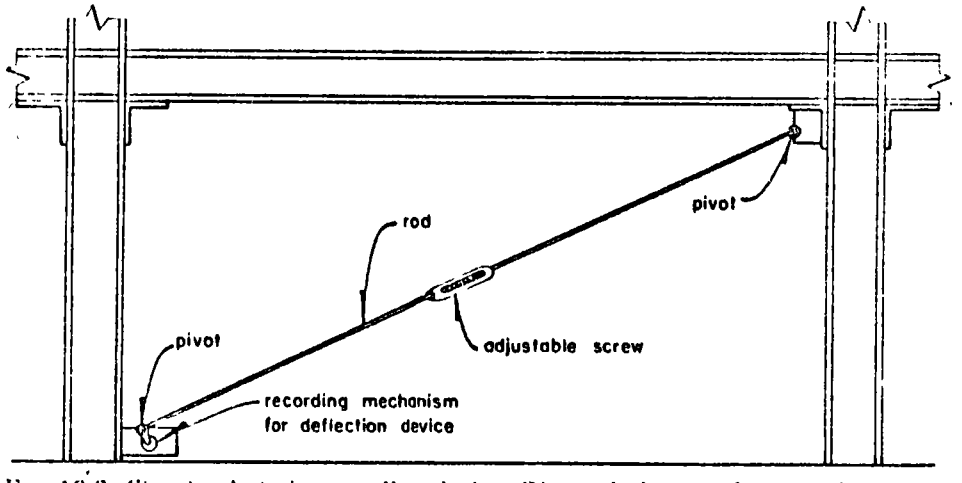

Fig. 10.2 Structural strain recording device. Diagonal element detects relative motion across entire story in building (after Zeevaert and Newmark, 1956).

Fig. 10.3. Scratch strain gage. The circular target, 2.5 cm in diameter, is rotated by the strains. End attachment plates may be separated several meters (courtesy Prewitt Associates).

When strains due to phenomena other than earthquakes are negligible relative to earthquake-caused strains, a very convenient, inexpensive, and compact instrument is the scratch strain gage, shown in Fig. 10.3. This is essentially a bar connecting two fixed plates attached to a member up to several meters apart. A simple magnifying device, ending in a stylus which scratches on a smoked glass or metal plate, is incorporated in the connecting rod and provides a permanent record of the strain. The record is ordinarily read through a microscope or a powerful magnifying glass.

Although the instruments described provide only peak values and their accuracy is not high, their costs are so many times smaller than those of more conventional and complex equipment that a great many can be installed in a structure for the price of a single sophisticated instrument. It would seem that there is much to recommend the use of these simple instruments.

10.5 CONVENTIONAL SEISMOGRAPHIC SYSTEM — DESIGN CONSIDERATIONS

10.5.1 Basic design parameters

Bandwidth, *sensitivity*, and *dynamic range* are the basic parameters one must define in specifying a seismographic system. A difficulty lies in their interdependence. Bandwidth is the frequency interval of greatest interest; dynamic range is the span of the largest (full scale) to the smallest (system noise) usable signal recorded and is expressed as the ratio (often in dB) of these two signals; and sensitivity refers to the absolute gain (magnification) of the seismograph within the range. Generally all three cannot be optimized simultaneously in a reasonably simple instrument. For example, the special, high-gain, long-period seismographs used in the detection of teleseismic surface waves from small nuclear explosions and earthquakes exhibit very high gain (ca. 10^5 magnification) in a very narrow frequency band around 40 sec

(0.02—0.03 Hz). The same long-period seismograph, operating at the same site, but in the conventional WWSSN (world-wide seismographic station network) long-period mode (15—100 sec) would be capable of operating at maximum magnification of the order of $3 \cdot 10^3$, giving the same amplitude of background motion on a record as produced by the high-gain configuration. On the other hand, if we could faithfully record the basic seismometer input with a dynamic range of 10^6, we would capture the information in both of the foregoing configurations and we could produce either record through an appropriate playout.

A second example of parameter control can be seen in the recording methods commonly used for local earthquake motion. The bandwidth required for recording strong ground motion near the source of a major earthquake is essentially the same as that used in microearthquake recording — about 0.1—30 Hz. The actual ground motion, however, will be several centimeters for the former and several nanometers (10^{-9} m) for the latter, a ratio of 10^7. A single instrument designed to do both measuring tasks simultaneously would demand a dynamic range of 10^7, or 150 dB (20 dB is a factor of 10). This design near-impossibility gives rise to the two different system types in common use.

10.5.2 Bandwidth

Bandwidth can usually be specific early-on in the consideration of a seismographic system design. The required frequency range of ground motion is generally clear from the intended use of the data. Modern instruments allow great flexibility in this selection. However, if the recording medium is a visible record (as opposed to digital or analog magnetic tape to be processes later), one must take care not to attempt extreme wideband recording, as the resulting earthquake records would be of ragged appearance and difficult to interpret. Background noise amplitude also increases with bandwith, often obscuring small events that could be seen clearly on a visible record from a narrower-band instrument. An obvious example is the 6—8 sec microseism band, which is effectively avoided in the conventional short-period/long-period seismographs employed in most observatories.

If both bandwidth and visible records are required, it is often possible to split the output from a single seismometer into several desirable frequency bands, with individual gain adjustments, and to record the bands separately. A pertinent example lies in the use of the commercially available force-balance accelerometer for moderate-to-strong-motion recording. Such units exhibit flat response to ground acceleration over the frequency range 0—50 Hz with the limiting instrumental noise background smaller than 10^{-6} g (g = gravity) for high-quality units having a full-scale capability of 1 g. Any desired frequency bands can be derived from its output on visible records at gains consistent with the inherent device output noise. Another illustration

of modern wideband sensors is the new series of long-period seismometers capable of operating at natural periods of 50 sec or more in conventional environments. Equipped with appropriate transducers these instruments can produce simultaneous records of solid-earth tides (period of about 12 hours), free oscillations and mantle surface waves (100—3000 sec), conventional long-period waves (5—100 sec), conventional short-period waves (0.2—5 sec), and microearthquake signals (2—20 Hz). This exemplified the need for separate records of the different bandwidth signals, with individual gains and recording speeds, if visible records are the prime data medium. It is clear that use of digital or analog magnetic tape for primary recording provides a means of recovering the desired bandwidth in postprocessing and this reduces the requirements for continuous visible monitoring of all bands.

10.5.3 Sensitivity

Selection of the operating sensitivity for a seismograph would appear straightforward once the bandwidth is specified. In most applications the seismologist or engineer can define the maximum and minimum signals to be recorded; the interdependence of the fundamental design parameters of sensitivity and dynamic range is apparent here.

Modern high-quality inertial seismometers with moving coil transducers have inherent dynamic range capabilities of 10^5—10^6 (100—120 dB) over which the output is an adequately linear and undistorted representation of the input ground motion. Only the most sophisticated and state-of-the-art recording systems (such as the digital systems in exploration seismology or in large nuclear detection arrays, with 16—19 bit word lengths) approach these values. Conventional seismographs use only a part of this dynamic range of the sensor itself.

A good quality, conventional, visible seismograph has a dynamic range of 40—50 dB (roughly, a measurement resolution in the trace position of about 0.2—0.5 mm and a full-scale swing of 50 mm). The best analog FM magnetic tape recorders exhibit roughly the same dynamic range, but generally over a wider frequency bandwidth. With digital recording the range depends on the number of bits in a data word, while the bandwidth is set by the sampling rate and seismometer response. Ten- to twelve-bit words are commonly used in seismology for dynamic requirements of about 54 and 66 dB, respectively.

In this discussion we have assumed that the fundamental noise limitation is imposed by the recording systems, i.e., that the inherent seismometer noise (not ground noise) and the noise in the signal-processing elements (galvanometer or amplifier) are at or below the recorder noise level or resolution. This situation should be a design criterion to avoid wasting part of the usable recorder range on system noise.

Having selected the recording medium and its dynamic range, we can now

specify the sensitivity required or our overall system. This is often done easily at the small-signal end of the range, where we can usually define the smallest motion we want to detect. Frequently this level is simply set at the local microseismic background level. However, in some applications it is important that earthquakes of a given size be recorded without "clipping" the record. This is particularly true for strong-motion recording where, for example, we may wish to stay on scale up to 1 or 1.5 g. If the recorder range is not large, this requirement will result in records with no visible microseismic background. This should be carefully considered in setting the system sensitivity. Having established the operating sensitivity, its realization is a simple matter of gain between seismometer and recorder.

Finally, some scheme must exist in order that the system response can be measured in its operating configuration. This is important both in the initial set up and in the maintenance program where periodic checks of performance are made with the system installed and operational.

10.5.4 Response curve

A reasonable estimate of the nature of the motion to be recorded by a proposed system thus allows specification of the fundamental instrument parameters. These characteristics are embodied in the instrument response curve, which contains all the relevant information about the seismograph's behavior under excitation. The common representation of the system response is a magnification curve $M(f)$, where f is frequency, in hertz, of the excitation motion, assumed harmonic. M is the ratio of record amplitude to excitation displacement; it is thus a displacement sensitivity. The record amplitude can be measured in many ways, such as millimeters of trace displacement on a record or film viewer, output voltage from an amplifier or tape recorder on playback, or the numerical value of a digital word generated by an analog-to-digital converter. The denominator in M can equally well be excitation velocity or acceleration. These choices define than $V(f) = M(f)/2\pi f$ = velocity sensitivity, and $A(f) = M(f)/(2\pi f)^2$ = acceleration sensitivity, where we have used the relation $|dx/dt| = 2\pi|x|f$ in harmonic motion.

In complete statements about magnification curves lend themselves to confusion. M, V, and A curves can apply to the same instrument, differing solely by factors $2\pi f$. It is important that the precise meaning of the ordinates of the magnification curve be made explicit. This source of confusion is related to the practice of referring to some seismographs as "velocity meters" and to others as "accelerometers". This terminology applies to the frequency range of interest. If the $M(f)$ curve is flat in this frequency range, the instrument is termed a "displacement meter"; if $V(f)$, a velocity meter; and if $A(f)$ is flat, an accelerometer. Figure 10.4 shows a set of generalized M, V, and A curves for a hypothetical seismograph; this single instrument may be called a displacement meter, velocity meter, or accelerometer, de-

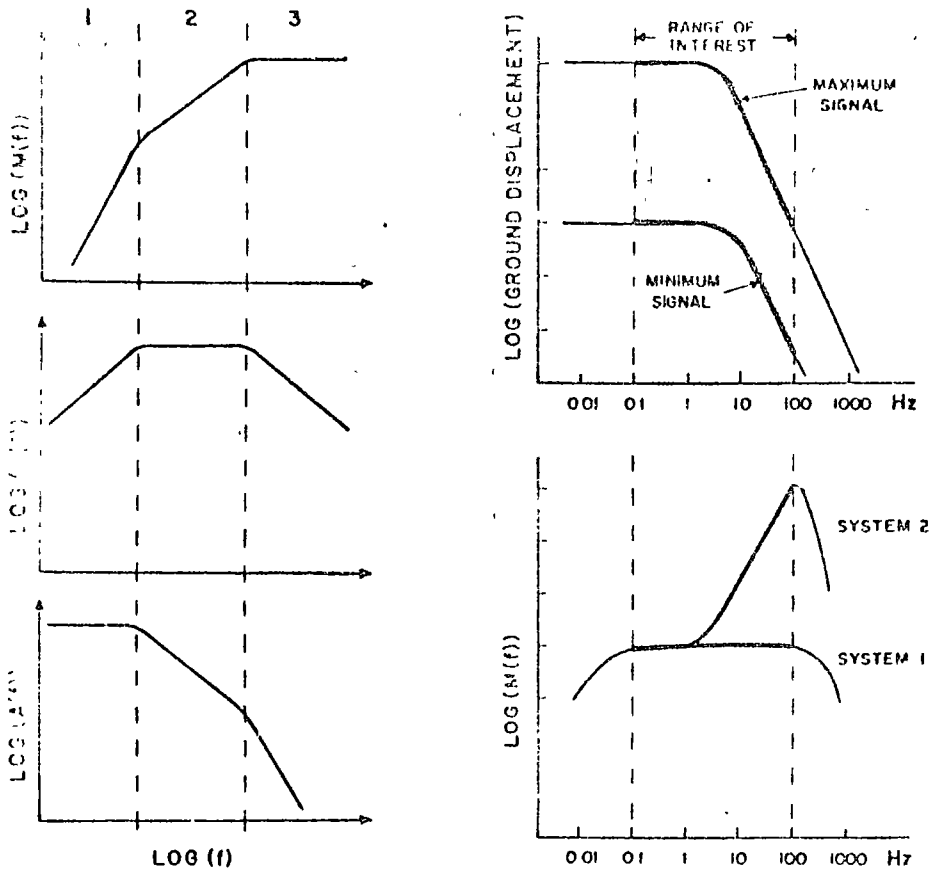

Fig. 10.4. Magnification (M), velocity sensitivity (V), and acceleration sensitivity (A) response curves for a seismograph, generalized to straight line segments. The seismograph may be described as an accelerometer, a velocity meter, or a displacement meter in the frequency ranges 1, 2, and 3, respectively.

Fig. 10.5. Top. Approximate spectral range, 0.1–100 Hz, of ground displacement expected from earthquakes in the magnitude range 2–5. Bottom. Alternate system magnification curves to record shaded signal range in top figure, requiring 100 dB dynamic range ('flat' response of system 1) or 60 dB ('pre-whitened' response of system 2).

pending on whether we are interested in frequency ranges 3, 2, or 1 respectively.

Analysis of the intended application of a required seismographic system should lead to the design response curve, both in shape and in absolute level. The shape reflects the bandwidth of the motion to be measured and, if possible, it should compensate for any severe frequency-dependence in its expected motion (it should "pre-whiten" the input, in the sense of making its spectrum essentially flat in the frequency range of interest). The latter consi-

Geration is more important the smaller the available dynamic range of the system and the wider the bandwidth desired. The response curve's absolute level is the system sensitivity and must be set recognizing the expected range of the motions to be recorded. There are upper and lower limits to the size of the motions to be recorded (their ratio being the required minimum dynamic range). Figure 10.5 illustrates these concepts with a generalized range of expected earthquake signals at two possible response curves for the bandwidth. The figure displays an earthquake-like displacement spectrum assuming that recording over three orders of earthquake magnitude is required. From the maximum signal at low frequency to the minimum at high frequency there are five orders of magnitude (100 dB). If we attempted to record in accordance with the desired bandwidth and signal range for response curve 1, we would need a resolution of 10^{-5} of full scale to detect the minimum signal of interest. After prewhitening the response (curve 2), we require only a resolution of 10^{-3} of full scale to record the same motions. Most visible records offer little more than two orders of magnitude, and the ground-displacement spectrum is typical for earthquakes. Hence it is not surprising that difficulty is encountered in trying to record wideband earthquake ground-motion data (in the 0.05—50 Hz band, say) on systems with limited dynamic range. Even digital recording with system response curve 1 in the figure would need an 18-bit word length for the full 10^5 range while 12 bits would suffice for the shaped response of curve 2.

Another step in defining the required response curve for a given application lies in identifying potential noise sources, in the ground or in the system, that might limit the sensitivity. The classic example of such noise problem is the 6—8 sec microseism so prominent in most seismograms. With magnitudes up to 10 mm during high activity, these ubiquitous surface waves have resulted in the traditional long-period/short-period division in seismometry, which effectively avoids high gain in the troublesome range.

The wide variation often resulting in response curves as we attempt to cover the useful frequency range of earthquake ground motion is illustrated in Figs. 10.6—10.8. The figures display a range of magnification curves of systems operating within the observatories of the University of California Seismographic Stations and are representative of current techniques for wide-range applications. An entire complex of instruments for recording earthquakes in the magnitude (M) range of -3 to 9 covers a phenomenal span of ground amplitudes and frequencies: 10^{-10} to 10^{-1} m or more in displacements and $3 \cdot 10^{-4}$ to 10^{2} Hz in frequencies, where we are excluding earth tides, fault creep, fault rupture, and secular strains at the low-frequency extreme, and high-frequency acoustic waves at the high end.

10.5.5 Setting specifications

The application for which a seismographic system is to be designed defines the key instrumental parameters required to furnish the data sought, as we

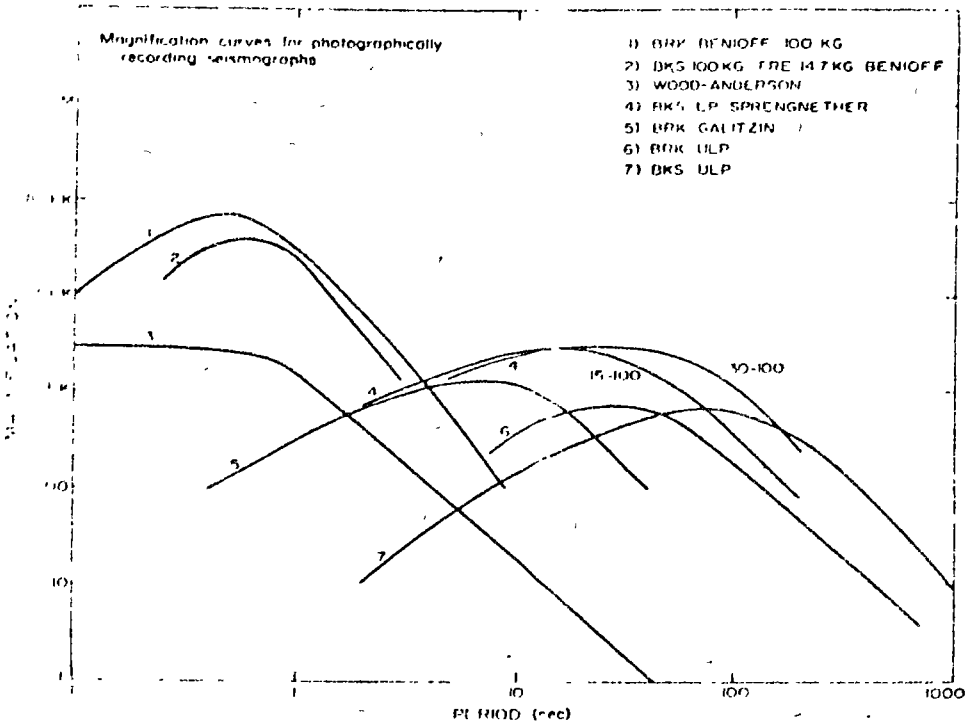

Fig. 10.6. Suite of magnification curves applicable to photographically recording seismographs in station network of University of California, Berkeley. Note wide range of maximum magnification and period of the maximum, from the conventional short-period system (curve 1) to the ultra-long period (ULP) system (curve 7).

have discussed. bandwidth, sensitivity (with possible variations over the bandwidth), and dynamic range. These result in a response curve, the absolute sensitivity levels, the required resolution at the small-signal extreme, and the full-scale capability. Bandwidth and sensitivity parameters are matters of mechanical and electrical characteristics of the seismometers and signal conditioning devices. Dynamic range, along with timing resolution and constraints on record duration format, sets additional requirements on the recording system.

The most important admonition in setting specifications for seismographic systems is to ascertain as completely as possible the nature of the ground motions we wish to record. Manufacturers of seismological equipment should not be placed in the position of interpreting requests for quotations on "short-period seismograph systems", for a "strong-motion sensor", or a broadband seismograph". The result can be a purchased system that does not do the job or that is far more elaborate and thus more expensive than needed.

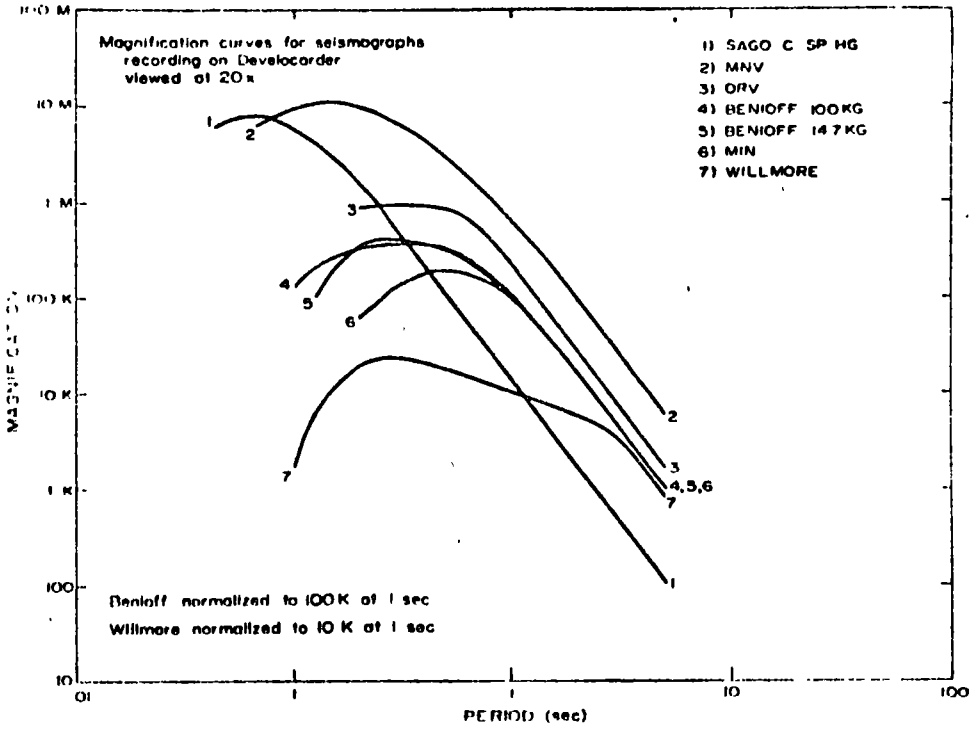

Fig. 10.7. Suite of magnification curves applicable to telemetered short-period seismographs in the University of California network which record on a single 16-mm film recorder.

A common mistake is the assumption that one should apply a "safety factor" of, say, two to the requirements in all directions to be sure of getting the system actually needed. This is seriously objectionable because seismographic design does not use a continuous spectrum of building-block components. The components are widely spaced in capabilities and in cost, and a factor of two in sensitivity and bandwidth may necessitate major steps in several components of the system and imply an order of magnitude cost increase.

When the particular application allows some flexibility in system parameters it is advisable to request quotations on packages designed for the extremes in the acceptable range. The manufacturer usually also suggests an intermediate system as optimum. On the other hand, if one knows precisely the required instrumental parameters for the application, it is well to state them exactly from the beginning. This will ordinarily insure that the most economical design will be adopted.

In this discussion of system specification we must also mention the existence of "standard" seismographs — widely used systems developed in re-

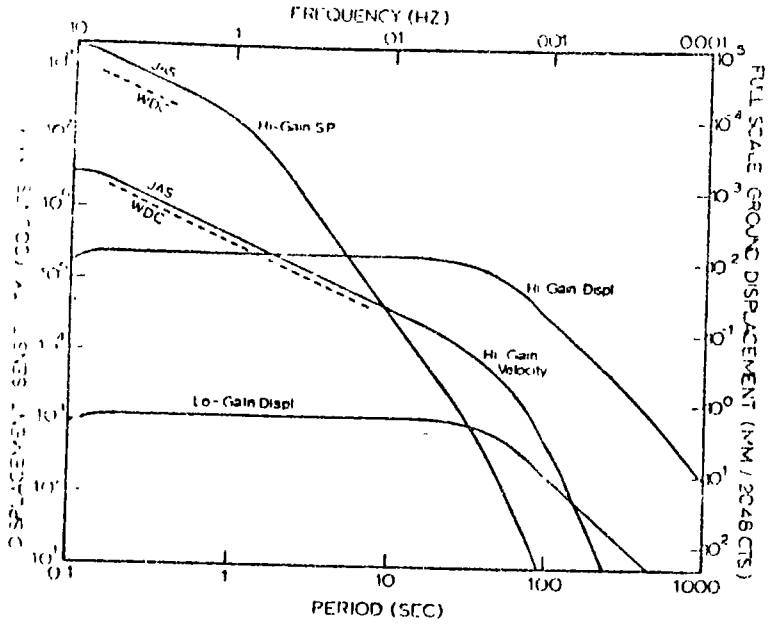

Fig. 10.8 Suite of displacement sensitivity curves applicable to telemetered broadband seismographs in the University of California network which record on FM magnetic tape at Berkely and are digitized on playback. JAS, WDC are station named, SP is short period channel, Displ., Velocity indicate transducer used. The four response types shown are taken simultaneously from a single seismometer by appropriate selection of transducer, amplifier gain, and filter.

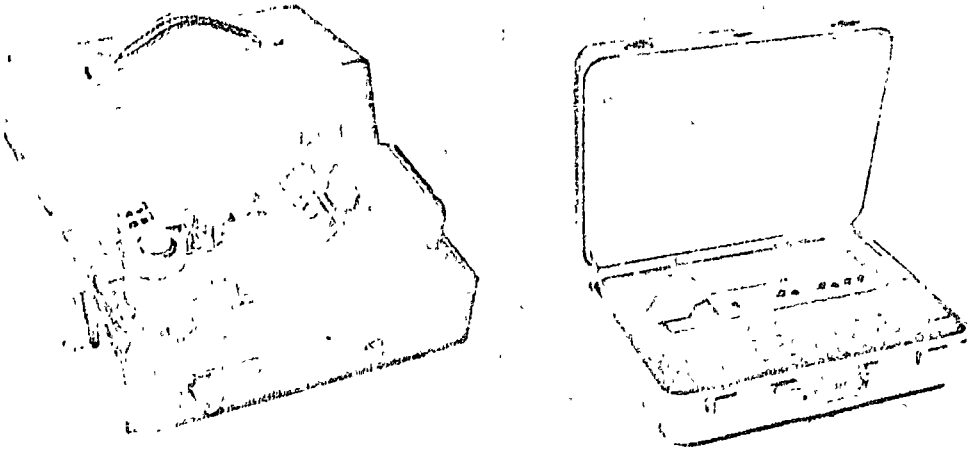

a b

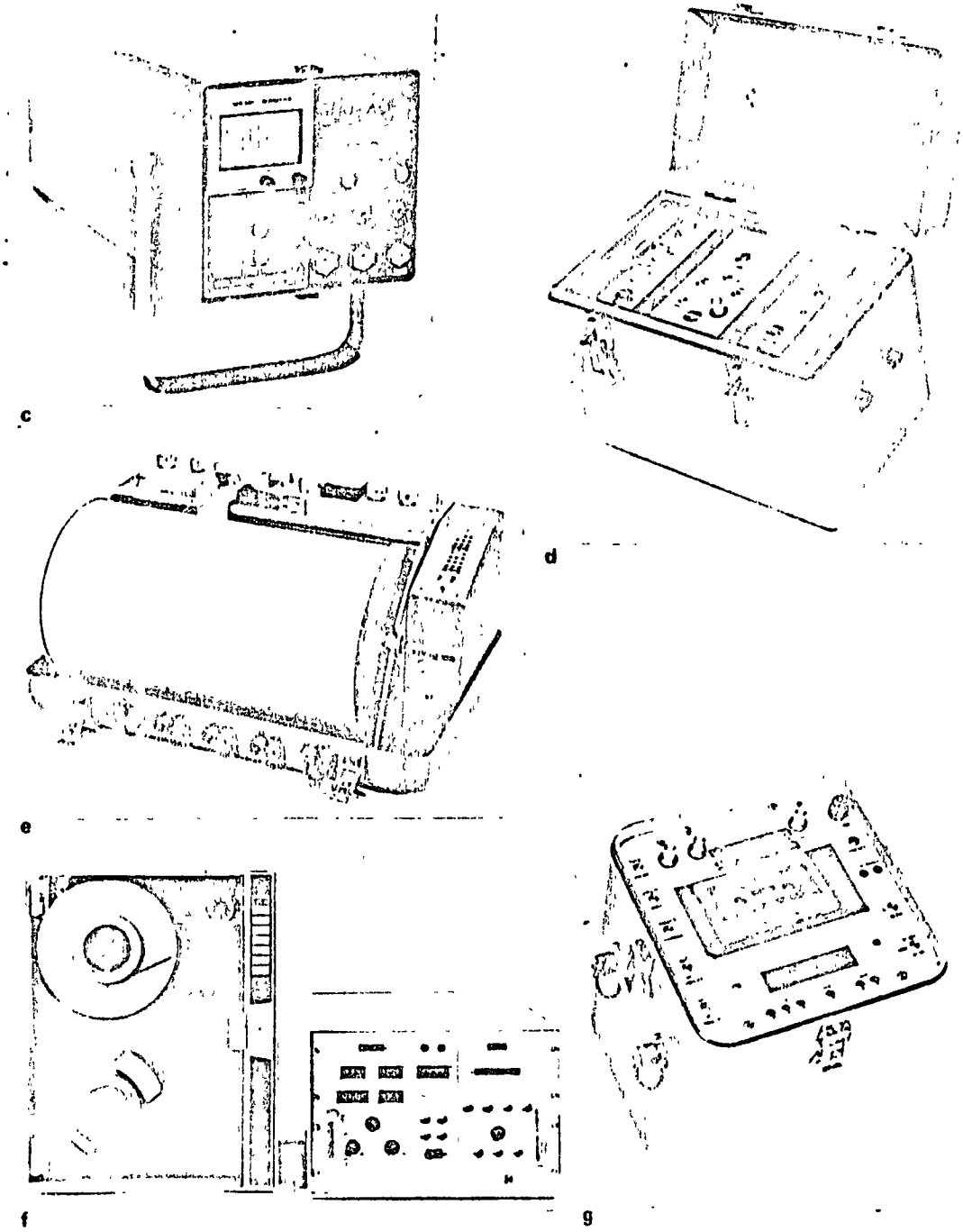

Fig. 10.9. Examples of commercially available specially packaged seismographic systems: a) strong-motion accelerometer; b) 6-channel engineering seismograph; c) signal-enhancement refraction seismograph; d) field station for FM telemetry with amplifier, voltage controlled oscillator, calibrator, and RF transmitter (inside case); e) portable microearthquake seismograph; f) digital data acquisition system with 1/2 in. magnetic tape; g) digital event recording system with memory and cassette magnetic tape (courtesy Kinemetrics (a,f), Nimbus Instruments (b,c), Sprengnether Instrument (d,e,g)).

use to particular applications and which consequently offer maximum performance for their cost. Several are illustrated in Fig. 10.9. It is often economically advantageous to use such packages when their specifications cover the requirements of the application in mind.

10.5.6 *Peripheral considerations*

The preceding discussion dealt with what can be called the fundamental instrumental parameters. There are usually several additional considerations in selecting a seismographic system for a given application. The more specific the application, the more significant these peripheral considerations may become. The following list provides some examples.

- Timing. One should state the required precision and resolution of the timing system. Precision involves stability of the clock, generally crystal-controlled, and its absolute time error. Resolution involves both the increment of reference pulses from the clock and the speed of the recording system.
- Record duration. This includes the time elapsed from the physical changing of the paper, film, or magnetic tape.
- Physical size. The total volume and weight of the complete system are often important, especially for instruments for recording structural responses, and the matter becomes paramount in office and commercial buildings.
- Power requirements. Electrical-power consumption is crucial when one must operate the system on batteries in remote locations or with portable instruments. When maintenance costs for more conventional solutions are particularly high, use of solar cells can be appropriate.
- Telemetry. It is becoming commonplace to transmit data from a remote installation to a central or convenient recording site using land line, telephone line, or low-power radio links. There are many advantages in this practice:

(1) Reduced maintenance costs for instruments at locations of difficult accessibility.

(2) The use of a common time base for an entire network of stations.

(3) Continuous monitoring of the instruments' operation, which allows immediate detection of conditions requiring attention.

(4) Continuous recording of all data on a common medium. If magnetic tape, the uninteresting portions may be erased, retaining complete records of events only, thus avoiding the use of excessive lengths of paper, film, or tape while attaining excellent timing resolution.

(5) Reduced system costs due to elimination of local clocks, recorders, and elaborate vaults, with attendant power requirements. For station networks, these cost savings are usually not compensated by telephone-line charges, resulting in a net cost reduction for the telemetered system.

- Recording system. There is much variety in this system component. One

may select smoked glass or paper; photographic film; pen and helical recording on drum; strip chart; cassette; 1/4", 1/2", or 1" reel-to-reel magnetic tape, analog or digital. The user generally has several constraints that incline his preference toward a particular recorder. Thus, magnetic-tape recording adds the expensive requirement of a playback system and associated hardware but in many applications it is well justified in view of the increased dynamic rangem bandwidth, and timing resolution along with conciseness in processing.

— Triggering and memory. Modern sensors and circuitry allow a wide selection of triggering thresholds and background noise/signal ratios to be incorporated into systems designed to record only sporadic events of interest. Inexpensive semiconductor memories are available that permit retention of the initial portion of the signal; yet their use is by no means widespread at present. In the coming years, however, such systems promise to become standard in seismology where the information desired consists of discrete events. Many shortcomings in present triggered seismographs, due primarily to missing the onset of the event, are eliminated by the incorporation of such memory systems.

— Instrumental protection. Instruments used at construction or near blasting sites or installed in locations exposed to vandalism or mere curiosity demand special considerations concerning their protection.

The foregoing and other additional considerations are necessary ingredients in the selection of a system configuration once the fundamental parameters have been specified. Often they drastically reduce the number of alternative system types for a given application.

10.6 CONVENTIONAL SEISMOGRAPHIC SYSTEMS — COMPONENT ELEMENTS

10.6.1 General constraints

The preceding section treated the general problem of specifying performance and physical characteristics in a seismograph. The following discussion dealt with available components used in the design of specific seismographic systems. Upon cursory analysis, it would appear that virtually any desired response curve is attainable. In theory this is the case. Any seismometer, of arbitrary natural frequency, damping, mass, and sensitivity, produces a non-zero output in response to ground motion of any amplitude and frequency. Conceivably one need merely select, by some signal conditioning method (amplification and selective filtering), the sensitivity and bandwidth of interest. The concept is perfectly correct. The neglected factor is noise. As long as a system so designed will produce, in response to ground motion at the desired detection threshold, an output sufficiently above system noise, the design concept is sound. Unfortunately, this condition is not easily ob-

tained when high sensitivity and low frequencies are involved. If it were, seismologists would need only an inexpensive exploration-type geophone, an amplifier, and a variable filter to work the entire seismic band from solid-earth tides to blast vibrations.

Realizable (as opposed to ideal) designs for seismographs are based on careful consideration and definition of the system requirements, as discussed earlier, followed by a common-sense evaluation of performance capacilities in components available for use. There will always be more than one design to accomplish a given measurement task. Satisfaction comes in optimizing the interplay of capability, complexity, and cost with the requirements of the application. Variations in the resulting solutions are evident when one considers, as an example, the wide range of seismographs in routine use worldwide as "long period" instruments. Subsequent discussions outline information on system components that, hopefully, will be helpful to the seismologist, geologist, or engineer faced with the task of specifying a seismograph for a particular use.

10.6.2 The complete seismograph

The basic elements integral to a seismograph are three. The *sensor*, normally a seismometer of some description, produces a measurable signal in response to a motion of its base. The response of a seismometer is characterized typically in terms of a sensitivity and some frequency dependence. This fundamental behavior can be stated compactly in its transfer function, i.e., the output (in whatever units are appropriate — e.g., volts, amperes, deflection of an optical or mechanical lever, etc.) per unit excitation (again in appropriate units — e.g., ground displacement, velocity, accelaration, strain, rotation, etc.), as a function of the frequency (in Hz) of the excitation. Generally, the transfer function is presented for convenience as a complex function of angular frequency, e.g., $S(\omega)$, where ω is in radians per second ($\omega = 2\pi f$ where f is in Hz or cycles per second). The complex nature of $S(\omega)$ indicates that the output of the sensor may be out of phase with the excitation, and $S(\omega)$ could be given as $|S(\omega)|e^{i\phi(\omega)}$, where $\phi(\omega)$ is the phase lag. $S(\omega)$ completely defines the response characteristics of a seismometer. For the conventional design using a spring-mass mechanical oscillator, $S(\omega)$ can be written in terms of its natural frequency, damping, and sensitivity.

The second element in the seismograph acts on the output of the sensor and is loosely described as the *signal conditioning device*. It may be no more than a mechanical or optical system of levers, or, more often in modern instruments, an electronic circuit or galvanometer providing amplification and filtering of the electrical output of the sensor. In any case, the signal conditioning element can also be characterized by its transfer function, say $C(\omega)$, giving output/input as a function of frequency in appropriate units. While we shall see that most $S(\omega)$ are very similar in form, $C(\omega)$, on the

other hand, can range from the simplicity of a numerical constant to the intricacy of an involved chain of amplifiers with low- and high-pass filters, yielding a complicated, complex functional representation. Despite potential complexity in $C(\omega)$, it is usually a straightforward procedure to write the mathematical expression for it.

The third and final element in a complete seismograph records the conditioned output of the sensor. The output of the *recorder* is a record. In its simplest form it is the deflection (e.g., in mm) of a trace from some zero position on a sheet of recording paper, film or glass. It may alternatively be a digital word (in counts) an FM tone (in Hz) or voltage written on magnetic tape. The recorder also may have a characteristic frequency response. We define its transfer function as $R(\omega)$, in the same sense as for the two previous elements. The output of the recorder is the seismogram, the fundamental medium of data presentation in seismology.

Assuming the system elements are themselves linear systems, we can define the response of the complete seismograph in terms of its components. The transfer function $T(\omega)$ of the complete seismograph is:

$$T(\omega) = S(\omega)C(\omega)R(\omega)$$

where $T(\omega)$ is the output of the recorder divided by the input to the sensor, in the appropriate units for the system. Virtually always a complex quantity, $T(\omega)$ is usually presented as $|T(\omega)|$, the amplitude response, in a magnification, velocity sensitivity, or acceleration sensitivity curve (see Fig. 10.4), along with $\phi(\omega)$, the phase response.

$T(\omega)$ completely describes the performance of a seismograph, except for system noise. It is sufficient to produce synthetic seismograms from a known input, $I(\omega)$ (where $I(\omega)$ is simply the Fourier transform, or spectrum of $I(t)$, the input ground motion time function). It serves as well to recover the input motion (in the frequency range where the input ground motion exceeds the equivalent system noise) from the recorded output $O(t)$, or its spectrum $O(\omega)$. The nature of the system transfer function is thus seen clearly in its definition:

$$O(\omega) = I(\omega)T(\omega)$$

or:

$$I(\omega) = O(\omega)/T(\omega)$$

It is evident at this stage that, in designing a required system response, all three system elements, S, C, and R, must be considered in shaping $T(\omega)$. With regard to the system noise level, each element also contributes. Either a level of background noise (e.g., from an amplifier) or a basic resolution (e.g., the smallest measurable signal in a recording medium) will characterize each element. These limiting values, which generally are frequency-depen-

dent, can be "taken through" the system transfer function to give the operating noise level or resolution in $O(\omega)$.

We shall discuss the system elements in turn.

10 6.3 Seismometers

The seismometer is the basic sensor of ground motion, say $u(x, y, z, t)$. For inertial (spring-mass) type seismometers, the measurement is made of relative distance between the seismometer frame (ground) and an inertial reference point on the suspended mass. Normally only one component of u, say u_x, is detected with a given seismometer. The seismometer output is thus proportional in some way to $u_x(t)$, and it may, depending on the design and on the type transducer used to detect the relative motion, actually produce a signal very nearly proportional to $u_x(t)$ or the time derivatives $\dot{u}_x(t)$ or $\ddot{u}_x(t)$ in the bandwidth of interest (see Section 10.5.5).

Extensometers or strain gages, on the other hand, measure the change in one of the components of u, usually in the direction of the measured component, e.g., $\partial u_x(t)/\partial x$, usually denoted as the extensional strain component e_{xx}. Again, depending on the transducer, which is the integral part of a seismometer converting mechanical motion into a usable output signal, the actual output may be a time derivative of $e_{xx}(t)$, e.g., $\dot{e}_{xx}(t)$.

The response equations for the conventional inertial seismometer are easily developed. For convenience in analyzing data, we desire the response in a form $S(\omega)$, where ω is angular frequency of the excitation (see Section 10.6.2).

The equilibrium equation for a damped single degree of freedom seismometer, responding to ground motion $u_x(t)$, can be written:

$$m\ddot{x} + c\dot{y} + ky = 0$$

where, as shown in Fig. 10.10, x is the absolute displacement of m, $y = x - u_x$, the measurable relative displacement of m, m is mass of the system, c is the damping coefficient (force/velocity), and k is the spring constant (force/displacement).

Rewriting the equation in the familiar form:

$$\ddot{y} + 2\zeta\omega_n\dot{y} + \omega_n^2 y = -\ddot{u}_x$$

where $\omega_n = \sqrt{k/m}$, the undamped natural frequency of the system in radian/sec, and $\zeta = c/2m\omega_n$, the damping factor, i.e., the fraction of critical damping for the oscillator.

The solution to the equation of motion is readily obtained by application of the Laplace transform, i.e.:

$$Y(s) = \frac{y(0) + \dot{y}(0)(s + 2\omega_n)}{s^2 + 2\zeta\omega_n s + \omega_n^2} + \frac{F(s)}{s^2 + 2\zeta\omega_s + \omega_n^2}$$

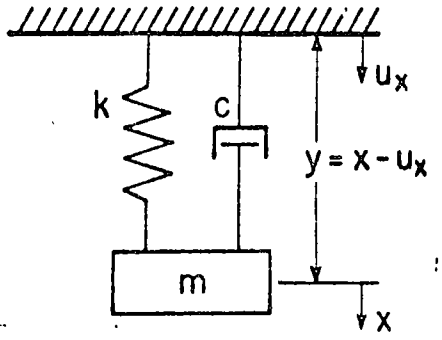

Fig. 10.10. Mechanical schematic of conventional inertial seismometer.

where $s = i\omega$, $Y(s)$ is the Laplace transfor of $y(t)$, and $F(s)$ is the Laplace transfor of $-u_x(t)$.

The first term is the complementary solution, representing transient motion due to initial conditions at $t = 0$, while the second is the particular solution for the forcing acceleration $-\ddot{u}_x(t)$.

The transient motion, or natural vibration of the oscillator can be transformed back to the time domain, giving:

$$y(t) = \exp(-\zeta\omega_n t)\left[y(0)\cos\mu\omega_n t + \left(\frac{y(0)}{\mu\omega_n} + \frac{y(0)\zeta}{\mu}\right)\sin\mu\omega_n t\right]$$

where $\mu = (1-\zeta^2)^{1/2}$.

The physical significance of critical damping ($\zeta = 1$) is clear in this form as the value of c ($= 2\zeta m\omega_n$) for which the natural vibration ceases and the motion becomes a simple exponential decay as $y(0)e^{-\omega_n t}$. This is termed critical damping. For $\zeta > 1$, the natural motion is described by exponentially decaying functions, always taking a longer time to reach a given amplitude reduction than for the critically damped case. In most seismograph designs, the natural frequency ω_n of the seismometer falls within the frequency band of the ground motion to be recorded by the system. In such cases, damping is usually set near-critical to eliminate prolonged transient oscillations which tend to mask the desired response to the ongoing forcing ground motion.

Similarly transforming the forced motion back to time yields, for a general form of $-\ddot{u}_x(t)$:

$$y(t) = \frac{-1}{\mu\omega_n}\int_0^t \ddot{u}_x(t)\exp[-\zeta\omega_n(t-\tau)]\sin[\mu\omega_n(t-\tau)]\,d\tau$$

This is the familiar convolution integral seen in the analysis of linear system response. It is clear that the output at a given time depends on the total prior time history of excitation. With damping near-critical, however, the response to a given input is reduced significantly by times of the order of several times the natural period.

Rather than a general form of u_g, it is convenient to consider the seismometer response to sinusoidal excitation at a particular frequency. For harmonic ground motion of the form:

$$u_g(t) = A \sin \omega_e t$$

or,

$$u_g(t) = \frac{A}{\omega_e^2} \sin \omega_e t$$

where ω_e is the angular frequency of forcing motion (radians per second), the steady-state response (neglecting transient motion) is:

$$y(t) = \frac{A}{[(\omega_n^2 - \omega_e^2)^2 + (2\zeta\omega_n\omega_e)^2]^{1/2}} \sin(\omega_e t + \phi)$$

where:

$$\phi = \tan^{-1} \frac{2\zeta\omega_n\omega_e}{\omega_e^2 - \omega_n^2}$$

gives the phase shift.

This expression represents the basic measurable motion in a seismometer. Ignoring for the moment any effects of the transducer which detects this motion, we can define the basic seismometer displacement sensitivity, or magnification $M(\omega_e)$, as:

$$M(\omega_e) = \frac{|y(t)|}{|u_g(t)|} + \text{the phase lag } \phi(\omega_e)$$

$$= \frac{\omega_e^2}{[(\omega_n^2 - \omega_e^2)^2 + (2\zeta\omega_n\omega_e)^2]^{1/2}}$$

Similarly, the velocity sensitivity is:

$$V(\omega_e) = \frac{M(\omega_e)}{\omega_e} + \text{additional } \pi/2 \text{ phase lag over } M$$

$$= \frac{\omega_e}{[(\omega_n^2 - \omega_e^2)^2 + (2\zeta\omega_n\omega_e)^2]^{1/2}}$$

and the acceleration sensitivity is:

$$A(\omega_e) = \frac{M(\omega_e)}{\omega_e^2} + \text{additional } \pi \text{ phase lag over } M$$

$$= \frac{1}{[(\omega_n^2 - \omega_e^2)^2 + (2\zeta\omega_n\omega_e)^2]^{1/2}}$$

The equivalent expressions in the form of complex transfer functions are:

$$S_M(\omega) = \frac{s^2}{s^2 + 2\zeta\omega_n s + \omega_n^2}$$

$$S_V(\omega) = \frac{-is}{s^2 + 2\zeta\omega_n s + \omega_n^2}$$

$$S_A(\omega) = \frac{-1}{s^2 + 2\zeta\omega_n s + \omega_n^2}$$

where $s = i\omega$.

These fundamental sensitivity curves are presented for various damping factors in Fig. 10.11. The corresponding phase curves are shown in Fig. 10.12. Note that an arbitrary specification of phase must be made, corresponding

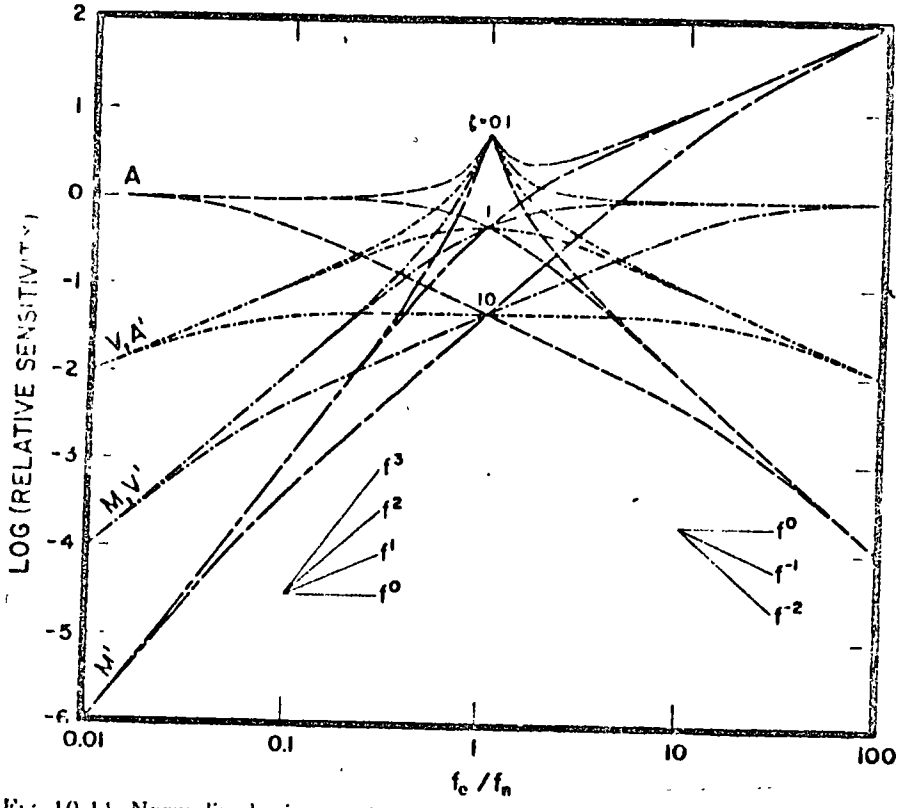

FIG. 10.11. Normalized seismometer response curves for three damping factors in terms of magnification (M), velocity sensitivity (V), and acceleration sensitivity (A) vs. frequency of excitation (f_c) relative to seismometer natural frequency (f_n). Unprimed symbols for seismometer with displacement transducer, primed symbols for velocity transducer, insets give asymptotic slopes.

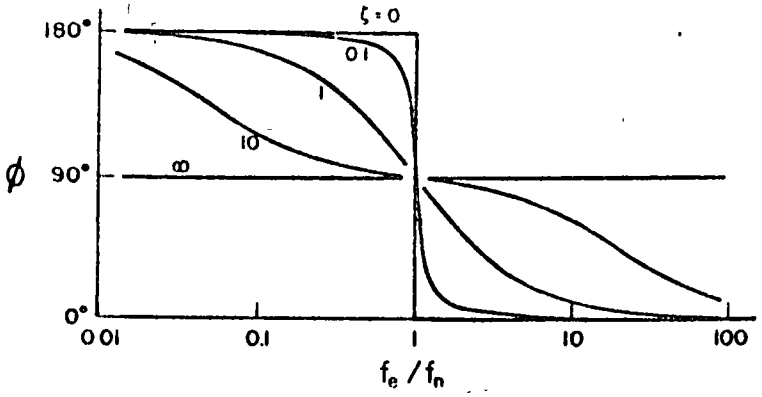

Fig. 10.12. Phase response (ϕ) for the magnification curve M in Fig. 10.11 for four damping values. High-frequency asymptotes are set by convention at 0°.

to the sign definition on y relative to x and u_x in Fig. 10.10. In seismometry it is conventional to specify the asymptotic phase-delay value as zero for high-frequency displacement sensitivity; i.e., we usually tap the seismometer in a given direction and identify the output polarity with the tap direction. This convention produces the phase relations shown in Fig. 10.12 for y relative to u_x, and illustrated for high frequencies in Fig. 10.13.

The seismometer thus provides us with the measurable quantity y, which is related to the ground motion u_x as shown in Figs. 10.11 and 10.12. Signal conditioning, as will be discussed in the next section, is normally applied to y in the form of amplification and filtering. A very common form of such

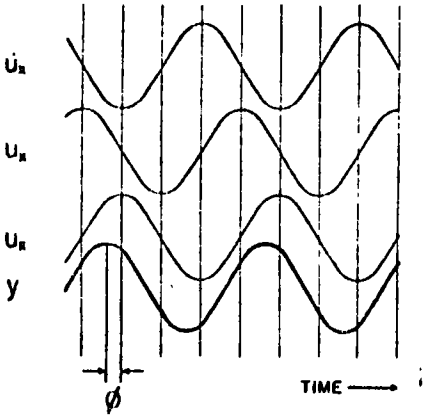

Fig. 10.13. Illustration of high-frequency ($f_e > f_n$) phase response of seismometer displacement y to steady-state sinusoidal ground displacement u_x, velocity $\dot{u}_x$, and acceleration $\ddot{u}_x$. High-frequency limit is 0° by convention.

conditioning is applied within the seismometer in the process of measuring y. The device which performs this measurement within the seismometer is termed the transducer. Transducer in general use are designed to measure either y (the displacement of the inertial reference) or $\dot{y}$. The former type, the displacement transducer, consists normally of either a passive lever system (optical or mechanical), or of an active (requiring external electrical power) electronic circuit to measure change in capacitance between a fixed and a moving plate. The velocity transducer is typically a coil of wire moving in a fixed magnetic field generated by a permanent magnet, and producing an output voltage directly proportional to the relative velocity $\dot{y}$. In this case the seismometer output is differentiated, and the response curves M, V, and A in Fig. 10.11 are multiplied by $\omega_e = 2\pi f_e$, shown as M', V', and A' in the figure. Note that it is not possible to obtain a flat magnification curve from the velocity-transducer output, unless further shaping is applied to the signal.

All the response curves in Fig. 10.11 exhibit asymptotic demands with slopes proportional to f_e^n where n is a positive or negative integer or zero (see insert in figure). Furthermore, these asymptotes always intersect at $f_e/f_n = 1$, i.e., at the natural frequency of the seismometer. Note also that, for heavy damping (see curves for $\zeta = 10$), a third straight segment appears around $f_e/f_n = 1$. This segment extends from $f_n/2\zeta$ to $2\zeta\, f_n$, and is often used in response shaping. For example, Soviet strong-motion instruments use the curve A' ($\zeta \approx 10$) while U.S. designs use the curve A ($\zeta \approx 1$). Willmore (1961) and Rodgers (1967) present a complete disc of the graphical representation of response curves.

10.6.4 Signal conditioning

We have reviewed the nature of basic output signals presented by conventional seismometers. If the shape (frequency response) and absolute level (sensitivity) of one of these curves if essentially that required for a particular application, we need only record the signal. More often we have need for a different shape and/or sensitivity and must investigate methods of signals conditioning.

In virtually every requirement for a seismograph there exists a range of frequencies to be recorded with reasonable difelity. This specification almost always implies injection of unwanted background noise (from either the system or the ground). In Fig. 10.14 we show a generalized background noise curve for a very quiet site. Superimposed on roughly a f_e^{-1} or f_e^{-2} wideband noise distribution are the microseism peaks, particularly the 5–8 sec band related to ocean waves. It is this curve which has had the greatest influence on high-gain seismograph design. The common long-period–short-period division is obviously motivated by the necessity of minimizing response around 6-sec period. The rationale for sharp peaking of the response at 35–40 sec in the modern high-gain long-period systems likewise is based

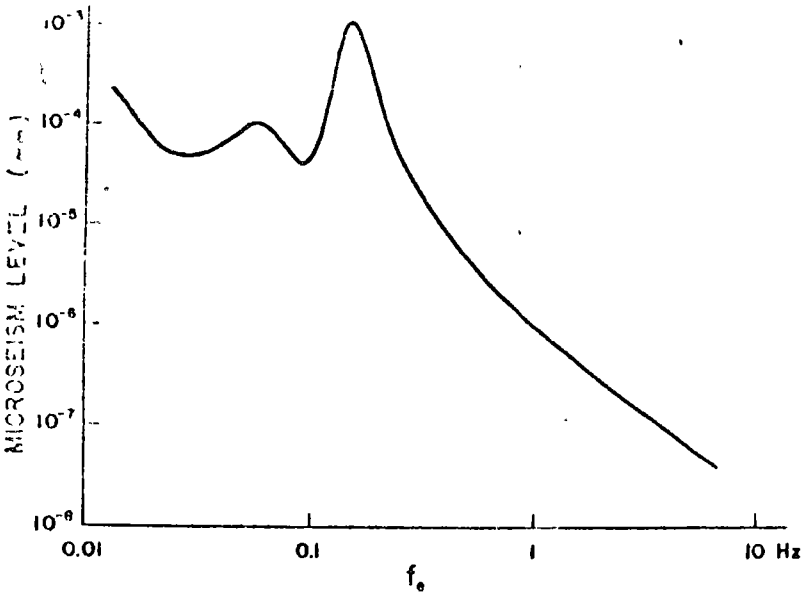

Fig. 10.14. Average background microseism for a very quiet site, in mm of ground displacement, as a function of frequency.

on background motion considerations. Peterson and Orsini (in press) describe these considerations in the design of the modern Seismic Research Observatories (SRO) which are being installed in the world-wide network.

The degree of conditioning necessary in a system will depend on the subsequent recording of the signal. As discussed earlier in this chapter, the conventional visible seismogram used in routine seismological observations has limited dynamic range. Such records are more readable with correspondingly narrower bandwidths than are more broadband seismograms. At the other extreme, a digitally recording system with very wide dynamic range, say 100 dB, can record with a wide frequency range.

Signal conditioning in its most common implementation consists of amplification and/or filtering of the signal to produce the desired sensitivity and bandwidth. Basic parameters to be considered in conditioning are the inherent noise levels at the seismometer output and in the conditioning device.

A typical moving-coil velocity transducer with several hundred ohms resistance will have a generator constant G of around 100 volts per meter per second, or 100 newtons per ampere. This quantity is a fixed property of the permanent magnet and coil, equal to the product of the flux density B (webers/m^2) and the length of conductor L (m) in the magnetic field. The quantities $Vm^{-1}s^{-1}$, N/A, or Wb/m are numerically and dimensionally identical, and all specify G. From Fig. 10.10, the typical background velocity at a quiet site at 1 Hz is $2\pi \cdot 10^{-6}$ mm/sec or $2\pi m\mu$/sec (or nm/sec), producing

a peak voltage of 0.6 μV. The inherent Johnson noise in the coil by virtue of its resistance is smaller by more than two magnitude than this voltage in a bandwidth of a few hertz, yielding a fairly clear and uncontaminated signal from the smallest ground motions we might wish to measure in the short period range. With f_c^{-1} ground noise, the background particle velocity will remain essentially constant except for microseism peaks, and, so long as $y \approx u$, $(f_c > f_n)$, the velocity-transducer output gives the most noise-free measurement of y over a relatively wide frequency bandwidth.

A conventional displacement transducer using capacitance plates is inherently a device with greater noise than a coil by virtue of the fact that it is an active electronic circuit measuring small capacitance changes, thus subject to noise contributions from its components, power supply, etc. In bandwidths of a few hertz, with very careful design utilizing phase-sensitive detection, noise levels equivalent to 10^{-7} mm have been achieved. For the older-style design using balanced resonant circuits, a practical equivalent noise level would appear to be 10^{-5}—10^{-6} mm. See Dratler (in press) for a discussion of capacitance-displacement transducers.

Modern amplifiers are capable of operating over bandwidths of several hertz with equivalent input noise levels of something less than 0.1 μV for discrete components, and less than 1 μV for the best integrated circuit amplifiers (cost about $25). Clearly, the state-of-the-art now allows substitution of solid-state amplifiers for galvanometers where high sensitivity is required and DC power (typically much less than 1 watt) is available. This development, in very recent years, has provided a new dimension in flexibility for seismograph design.

Until around the middle 1960's there was no substitute for the galvanometer as a low-noise amplifier. Equivalent input noise levels below 0.1 μV were readily available. Equally important, the galvanometer derives its driving power directly from the moving-coil transducer, with external power required only for the light source. It is this combination of low noise and high gain (2 to 20 mm/μV) that sets the seismometer—galvanometer combination as the standard electromagnetic seismograph for many years. It also led to the phototube amplifier (PTA) when high-level electrical signals were required for subsequent visible or tape recording and other signal processing or transmission.

A conclusion apparent in the preceding discussion is important in the design of signal-conditioning electronics following a seismometer output. It is that available velocity or displacement transducers can be used with equally satisfactory results in the range of frequencies about 0.01—10 Hz, where the seismometer relative displacement y can be made essentially equal to the ground displacement u_x, i.e., where the M-curve is essentially flat. In this range either transducer can be designed with inherent noise levels equivalent to ground displacements well below background in the quietest sites. At frequencies above about 10 Hz, by virtue of decreasing ground noise, the dis-

placement-transducer noise approaches levels equivalent to background. At low frequencies, however, by virtue of the more rapid decrease in velocity (*y*) than in displacement (*y*) (f_c^3 vs. f_c^2) with longer-period ground motion (compare *M'* with *M* in Fig. 10.7), the displacement transducer rapidly becomes the better detector and is the logical choice for measurement of mantle surface waves, free oscillations, gravity, earth strain, and solid-earth tides.

The above considerations of noise limitations in signal conditioning become more important as higher sensitivities are required. For most strong-motion and engineering-seismology applications, however, the ground motions to be measured are sufficiently large that noise levels in signal conditioning devices are not normally a serious concern.

The basic rule governing selection of signal-conditioning components is that the full dynamic range of the recording device is used for ground motion in the bandwidth of interest. An example would be in digital recording, where one would want the least significant bit in the digital data word to represent ground motion and not system noise. Similarly, the mechanical and optical design in a conventional strong-motion accelerometer should be sufficiently clean that the smallest measurable deflection of the photographic trace represents seismometer mirror deflection due to ground motion and not spurious noise in the mechanical film drive or optical systems.

10.6.5 Recording

The decision as to recording method for a seismograph is usually reached early in the systems design procedure. Dictated by the planned use of the data, as well as by the form and quality of the signal available for recording, the recorder selection is normally straightforward. Frequency bandwidth, dynamic range, and record length, in addition ot physical and electrical constraints, are the principal parameters governing the choice.

The major division in commonly used recording systems separates visible, or hard-copy, recorders from those which record the signal on magnetic tape of some type. The former designation includes: (1) devices in which a stylus inscribes the record on smoked or otherwise coated paper, glass, or metal; (2) pen and ink recorders; (3) heated stylus on special paper; and (4) light spot on photographic film or paper. Dynamic range is limited to about 40–50 dB in the best cases. The highest frequency measurable depends on the speed of the recording medium relative to the stylus, pen, or light spot, as well as on the actual size of the trace being written. Typical recordings speeds range from 0.1 mm/sec for frequencies about 0.05 Hz, up to 10 mm/sec for frequencies as high as 20–50 Hz (depending on trace width). In general, the finest trace, about 0.1 mm wide, is written by a stylus on smoked paper or glass. The problem of pen friction and associated deadband is eliminated in photographic recording where high contrast is also obtained.

The convenience of pen-ink recorders, using inexpensive paper, is often preferred in a tradeoff analysis considering resolution, contrast, and friction along with cost and convenience. A compromise with the convenience of pen and paper, but improved resolution and contrast over ink, is the heated stylus on special coated paper, which is naturally more expensive than the plain paper used with ink. A popular multi-channel recorder uses 16-mm film which is processed in the unit. Unless the seismograph is designed for a specific recording technique (e.g., the 70-mm film in many strong-motion systems), the selection of visible recorders is normally based as much on personal preference as on details in specifications.

Visible recorder, in general, are designed for low cost plus the convenience of viewing and monitoring at least one day's data on a single record. They allow measurement of time and amplitude, only estimations of frequency content, and by and large are not well suited for digitization and subsequent processing. An exception is the high-quality strong-motion accelerograph film record, which contains a single event on three well-spaced traces at relatively high recording speed.

Magnetic-tape systems constitute the other principal class of recorders commonly used in seismological measurements. Developments in low-power analog and digital circuitry during the 1970's, plus the increasing access of workers to analog playback facilities and to small computers with magnetic-tape playback capabilities, have resulted in greatly increased application of magnetic-tape recording in a wide range of seismological efforts. Recording is accomplished in three fundamentally different modes: (1) analog direct; (2) analog FM (frequency modulated); and (3) digital.

In direct recording the analog signal is converted directly into a proportional magnetization on the tape. A consequence of the dependence on tape to head velocity in the playback process is that DC signals cannot be recorded and recovered on playback, thus the method has a low-frequency cutoff of several hertz. Very low recording speeds of around 0.1 mm/sec with up to 30 dB dynamic range have been used to record data at frequencies up to 20–30 Hz. For ½-in tape with seven data tracks this is a very efficient mode of data storage. The lack of DC response and relatively low dynamic range are the major limitations of direct analog recording.

FM analog magnetic-tape recording offers the advantages of DC response, precise amplitude information, and 40—50 dB dynamic range, at a tradeoff in tape speed. 0–10 Hz bandwidth can be obtained at 1 mm/sec tape speed. Considering again seven data tracks on a ½-in tape at this slow speed, a single reel of tape can contain several weeks data from up to seven seismographs. While such recorders are used widely in seismology, they are in reality precision laboratory devices not well-suited to the rigors of field installations unless maintained constantly by qualified technicians.

Digital magnetic-tape recording suffered initially from the low information density possible relative to analog methods. For example, a 12-bit word

(66 dB dynamic range) at 25 samples per second (barely adequate for 10 Hz response, with adequate anti-alias filtering), recording on the same ½-in 7-track tape, with seven data channels multiplexed (each at 10 Hz bandwidth), would require a tape speed over 1 cm/sec — an order of magnitude less information density than for FM. Even though the lower density is balanced by an order of magnitude improvement in dynamic range, the required frequency of tape change for multi-station continuous recording poses a severe problem for seismographic data acquisition.

Two recent developments may well revolutionize the use of digital magnetic-tape recording in seismology. These are the advent of low-cost reliable digital cassette transports along with the development of integrated circuit shift register modules whereby thousands of bits of information can be held in memory on a single printed circuit board, providing a delay in the data stream while the decision is being made regarding its significance and the necessity of recording it permanently on tape. Such "self-editing" data systems, which can be used with low-cost cassette or ¼-in tape recorders for event recording, have finally brought the unquestioned superior fidelity of digital recording to routine seismographic recording where the desired data consist of discrete events, comprising but a fraction of the total monitoring time. Ambuter and Solomon (1974) and Prothero (1976) describe systems of this type.

As a final suggestion to those who would design systems based on magnetic tape as the prime recording medium — a monitor record of some type, recording continuously, is invaluable in the task of identifying, locating, and processing the events stored on the tape.

10.6.6 Timing

Timing systems commonly used in seismographs are of two types: (1) a precision oscillator driving a clock; or (2) continuous reception of a radio time signal. Even in the case of the oscillator and clock, regular radio reception is needed for time check.

Crystal oscillators with temperature compensation for time bases are available at relatively low cost and low power drain with long-term stability of $5 \cdot 10^{-8}$ at constant temperature. This stability makes available simple timing systems which exhibit drift rates in normal service of as little as 0.1 sec per month. The complete timing program derived from such an oscillator can be as simple as a series of minute and hour pulses for visible recorders, or as complex as a digital time code with day, hour, minute, second information repeated once per second. The basic precision is the same in either case.

Radio time signals exist in a variety of forms. Perhaps the most common is the WWV-type periodic or continuous time data transmission in the 2.5—20 MHz standard time broadcast bands. These short-wave signals can usually be received, with adequate equipment, anywhere in the world, at some time of

the day. While adequate for chronometer time checks, these signals are too erratic in reception quality for use as a primary time signal. Low-frequency time broadcasts in the 15—100 Hz range, such as WWVB, can be received reliably enough for continuous recording over areas of continental dimensions. Another source of continuous time data lies in the navigational broadcasts such as the Loran system. In many areas, standard broadcast stations (500—1500 Hz) trasnmit daily reference signals at regular times. A micropower timer can be incorporated easily and at very low cost into field systems to turn on a pretuned receiver daily at a present time stable to a few seconds per month.

There is the occasional system that does not require synchronization to universal time. Special-purpose microearthquake networks, such as those used in geothermal site investigations, recording events seen only by that network, are on example. Another example is the array of deformation and pressure gages often installed in large dams or structures to record response to strong earthquake shaking. In these cases a system is adequate which provides a reference for relative timing among data channels, and sufficient precision for the analysis comtemplated (e.g., high-resolution response spectra).

10.6.7 Telemetry

In many cases it is advantageous to emplace the seismometer some distance from the recording site. The distance may be as little as 1—2 km, where cultural noise is unacceptable high in the recorder area, or as much as hundreds of kilometres when central recording of a network of stations is desired. Modern techniques of data telemetry, FM or digital, provide a simple reliable solution to this need.

The most commonly used telemetry system for seismological data is based on frequency modulation (FM) in the audio range of 300—3000 Hz which is readily transmitted by commercial voice-grade telephone lines. Typically, seismometer signals in the 0—25 Hz range are converted by a voltage-controlled oscillator (VCO) to tones in the audio band modulated ±125 Hz by the signal. Up to nine (but preferably seven or less) independent tones (multi-components at one station, different gains, or multiple stations) can then be multiplexed onto one telephone line. At the receiver, the tones are demodulated by narrow-band discriminators which deliver the original analog seismometer signal. Dynamic range of 50—60 dB can be obtained with relatively simple system. The signals are then available at the central recording site for recording and processing. A variation on this method uses intermediate recording of the multiplexed tone bundles on magnetic tape at 15/16 ips (24 mm/sec), with demodulation upon playback. This is probably the most dense packing of information available in magnetic tape recording.

The telemetry link may consist alternatively of low power (0.1—0.5 watt) radio pairs, typically transmitting in FM mode somewhere in the 50—500

MHz range, requiring line-of-sight path, and effective up to 100 km distance in favorable circumstances. With radio telemetry, as with special land lines, the 300—3000 Hz bandwidth limitation on voice-grade telephone lines can be extended, allowing more channels per link.

If the requirement exists to telemeter data with a dynamic range greater than about 60 dB, digital techniques should be investigated. While digital data telemetry is not presently in widespread use for modest seismological installations, the rapid advances in the field of digital data transmission and acquisition virtually assures that such methods are coming is seismological practice.

10.7 CALIBRATION

After careful consideration of the requirements and components of a proposed seismographic system has produced detailed specifications and the resulting equipment has been installed, the inevitable question is asked, "What is the system response?" This question frequently arises, sometimes as soon as the system is operational; in other cases it may be months, or even years, before data from the instruments are processed in such a manner that any more than a rough magnification value is required. Nevertheless, this question will arise sooner or later in the case of virtually any modern installation of seismographic instrumentation.

In this final section the two general and most effective approaches to answering the question of system calibration will be outlined. The two methods are: (1) theoretical, a consideration of the expected response of each element in the system and their syntheses into the overall system response; and (2) empirical, a direct measurement of the system response to an input equivalent to a known ground motion. In the former approach we need to know all the parameters which define the response of each component, must be known, i.e., seismometer natural frequency, damping, coil resistance and inductance, transducer sensitivity, amplifier and filter characteristics, and recording-system constants. Many or all of these will have to be measured in the laboratory, to a precision consistent with the desired accuracy of the theoretical response calculation. In the latter empirical method, only the means to inject a known equivalent ground-motion input, with the required precision, into the system is needed. The standard modern approach to this is the use of an independent calibration coil on the seismometer. A current passed through the coil, whose electromagnetic constant is known or can be easily measured, produces a known force on the inertial mass of the seismometer which is equivalent to an acceleration of the ground. While many apparently differing schemes for calibration are used, they are, virtually without exception, simply variations or combinations of these two methods.

With careful procedures, either approach to calibration is capable of pro-

ducing response curves accurate to better than 5%. Having performed such a calibration, it is common good practice to check system response periodically with a simple weight lift or known electrical signal in the calibration coil. Variations in the system response are seen easily as changes in the response ("cal-pulse") of the system to this standard test input.

REFERENCES

Ambuter, B.P. and Solomon, S.C., 1974. An event-recording system for monitoring small earthquakes. *Bull. Seismol Soc. Am.*, 64: 1181—1188.

Dratler, J., Jr., in press. An inexpensive linear displacement transducer using a low-power lock-in amplifier.

Hudson, D.E., 1958. The Wilmot survey type strong-motion earthquake recorder. Earthquake Eng. Res. Lab., Calif. Inst. of Technol., Pasadena.

Newmark, N.M. and Rosenblueth, E., 1971. Fundamentals of Earthquake Engineering. Prentice-Hall, New Jersey, 640 pp.

Peterson, J. and Orsini, N.A., in press. Seismic research observatories — upgrading the world-wide network. *EOS Trans. Am. Geophys. Union.*

Prothero, W.A., 1976. A portable digital seismic recorder with event-recording capability. *Bull. Seismol. Soc. Am.*, 66.

Rodgers, P.W., 1967. Overdamped second-order response. *Control Eng.*, March 1967: 77—78.

Willmore, P.L., 1961. Some properties of heavily-damped electromagnetic seismographs. *Geophys. J. R. Astron. Soc.*, 4: 389—404.

Zeevaert, L., and Newmark, N.M., 1956. Aseismic design of Latino Americana Tower in Mexico City. Proc. 1st World Conf. Earthquake Eng., Berkeley, Calif., 35: 1—11.

Nociones Elementales — Dr. Gustavo Ayala M.

Para ilustrar el problema de propagación estudiemos primeramente el caso unidimensional. La ecuación que gobierna este movimiento es la llamada 'ecuación de onda unidimensional' y se escribe como

$$\frac{\partial^2 \phi}{\partial x^2} = \frac{1}{c^2} \frac{\partial^2 \phi}{\partial t^2} \qquad (1)$$

donde ϕ es por ejemplo la elevación de una onda en el agua y c es un coficiente conocido como celeridad o velocidad de propagación.

Para obtener la solución general de la ec 1 es conveniente hacer el siguiente cambio de variables,

$$u = x - ct$$
$$\text{y} \qquad (2)$$
$$v = x + ct.$$

este método conocido como de D'Alembert conduce a las siguientes transformaciones

$$\frac{\partial \phi}{\partial x} = \frac{\partial \phi}{\partial u} + \frac{\partial \phi}{\partial v} \quad , \quad \frac{\partial^2 \phi}{\partial x^2} = \frac{\partial^2 \phi}{\partial u^2} + 2\frac{\partial^2 \phi}{\partial u \partial v} + \frac{\partial^2 \phi}{\partial v^2}$$

$$\frac{\partial \phi}{\partial t} = -c\frac{\partial \phi}{\partial u} + c\frac{\partial \phi}{\partial v} \quad \text{y} \quad \frac{\partial^2 \phi}{\partial t^2} = c^2\left(\frac{\partial^2 \phi}{\partial u^2} - 2\frac{\partial^2 \phi}{\partial u \partial v} + \frac{\partial^2 \phi}{\partial v^2}\right) \qquad (3)$$

mismas que al substituirse en la ec (1) dan la ecuación

$$\frac{\partial^2 \phi}{\partial u \, \partial v} = 0 \qquad (4)$$

La solución general se escribe como

$$\phi = f(u) + g(v) \qquad (5)$$

o bien de las ecs 2 se tiene

$$\phi = f(x-ct) + g(x+ct) \qquad (6)$$

donde f y g son funciones arbitrarias de sus argumentos.

De la interpretación física de la ec 6 se tiene que para un tiempo dado la función $f(x-ct)$ representa una perturbación moviendose en la dirección positiva del x con una velocidad de propagación c. Similarmente la función $g(x+ct)$ representa una perturbación que se mueve con una velocidad c en dirección negativa del eje x.

La anterior interpretación física se ilustra en la siguiente figura

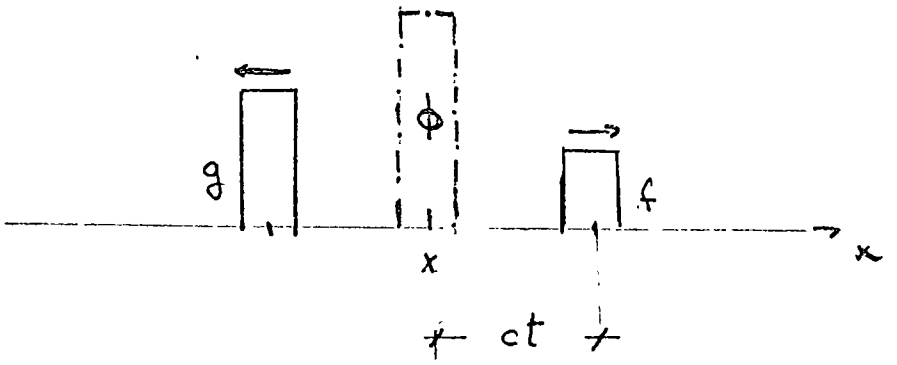

Fig 1

Para definir algunos parámetros de interés en el problema de propagación consideremos, sin perdida de generalidad una onda armónica que se mueve con una velocidad de propagación constante y sin cambiar de forma en la dirección positiva del eje x. Así

$$\phi = a \operatorname{sen} m(x - ct) \qquad (7)$$

Definiciones:

- A el valor máximo de la perturbación, en este caso 'a', se le denomina amplitud.
- A la forma de la perturbación cuando $t = 0$ se le denomina 'perfil de onda'.
- A la distancia para la cual se repite el perfil de onda, 'λ', se le denomina longitud de onda. En este caso

$$\lambda = \frac{2\pi}{m} \qquad (8)$$

o sea la (7) se puede escribir como:

$$\phi = a \operatorname{sen} \frac{2\pi}{\lambda}(x - ct) \qquad (9)$$

- El Tiempo que toma una onda en pasar por un punto se llama periodo y se escribe como.

$$T = \frac{\lambda}{c} \qquad (10)$$

- La frecuencia ν, es el número de ondas que pasan

por un punto fijo en una unidad de tiempo, esto es

$$n = \frac{1}{T} \qquad (11)$$

- a el numero de ondas en una distancia entera, k, se le llama número de onda y resulta ser

$$k = \frac{1}{\lambda} \qquad (12)$$

Las definiciones anteriores son válidas para cualquier perturbación cuyo perfil de onda se repite regularmente.

Ondas Planas

La generalización de la solución dada por la ec 6 á un problema Tridimensional permite la definición de ondas planas, esto es, ondas para las cuales la perturbación es constante en todos los puntos contenidos en cada plano perpendicular a la dirección de propagación. Frente de onda. Así si la dirección de propagación se define por sus cosenos directores l, m, n, la ec 6 en un espacio Tridimensional se escribe como

$$\phi = f(lx + my + nz - ct) + g(lx + my + nz + ct) \qquad (13)$$

Ondas esféricas.

Si estamos interesados en la solución de la ecuación de onda para problemas que poseen simetría esférica. Se tiene que la

ecuación que gobierna al problema es

$$\frac{\partial^2 \phi}{\partial r^2} + \frac{2}{r}\frac{\partial \phi}{\partial r} = \frac{1}{c^2}\frac{\partial^2 \phi}{\partial t^2} \qquad (14)$$

o bien

$$\frac{\partial^2 (r\phi)}{\partial r^2} = \frac{1}{c^2}\frac{\partial^2 (r\phi)}{\partial t^2} \qquad (15)$$

De los conceptos establecidos anteriormente se demuestra que la ec. 15 tiene la solución general

$$\phi = \frac{1}{r} f(r-ct) + \frac{1}{r} g(r+ct) \qquad (16)$$

donde f y g son nuevamente funciones arbitrarias de sus argumentos. Notese que la amplitud de las ondas esfericas decrece con $\frac{1}{r}$.

Se puede demostrar que, en el caso de ondas cilindricas con simetría axial, la atenuación de las ondas es con $\frac{1}{\sqrt{r}}$

Propagación de Ondas en un Medio Infinito

Las ecuaciones que gobiernan el movimiento de un medio elástico lineal, homogeneo e isotropo, conocidas como ecuaciones de Navier, se pueden escribir como

$$\begin{aligned}
\rho \frac{\partial^2 u}{\partial t^2} &= (\lambda + G)\frac{\partial e}{\partial x} + G\nabla^2 u + \rho X \\
\rho \frac{\partial^2 v}{\partial t^2} &= (\lambda + G)\frac{\partial e}{\partial y} + G\nabla^2 v + \rho Y \qquad (17) \\
\rho \frac{\partial^2 w}{\partial t^2} &= (\lambda + G)\frac{\partial e}{\partial z} + G\nabla^2 w + \rho Z
\end{aligned}$$

donde u, v y w son las componentes del vector desplazamiento, λ y G los coficientes elásticos del material, ρ la densidad de masa, X Y y Z las componentes del vector de fuerzas de cuerpo por unidad de masa y e la dilatación definida como

$$e = \frac{\partial u}{\partial x} + \frac{\partial v}{\partial y} + \frac{\partial w}{\partial z} \qquad (18)$$

El sistema de ecuaciones de movimiento se puede desacoplar si el vector desplazamiento se define como

$$\underset{\sim}{u} = \text{grad}\,\phi + \text{rot}\,\underset{\sim}{\Psi} \qquad (19)$$

donde $\underset{\sim}{u}$ es el vector desplazamiento con componentes u, v y w, ϕ y $\underset{\sim}{\Psi}$ son potenciales, uno escalar y otro vectorial ambos conocidos como potenciales de Helmholtz.

De las ecs 17 y 19 se encuentra que las ecs 17 se satisfacen simultaneamente si los potenciales ϕ y $\underset{\sim}{\Psi}$ son soluciones de las ecuaciones de onda

$$\nabla^2 \phi = \frac{1}{C_p^2} \frac{\partial^2 \phi}{\partial t^2} \qquad (20)$$

y

$$\nabla^2 \underset{\sim}{\Psi} = \frac{1}{C_s^2} \frac{\partial^2 \underset{\sim}{\Psi}}{\partial t^2} \qquad (21)$$

donde

$$C_p = \sqrt{\frac{\lambda + 2G}{\rho}} \quad \text{y} \quad C_s = \sqrt{\frac{G}{\rho}} \qquad (2.^{a})$$

De simples transformaciones se puede demostrar que las ecs 20 y 21 se pueden escribir respectivamente como

$$\nabla^2 e = \frac{1}{c_p^2} \frac{\partial^2 e}{\partial t^2} \qquad (23)$$

y

$$\nabla^2 \underset{\sim}{w} = \frac{1}{c_s^2} \frac{\partial^2 \underset{\sim}{w}}{\partial t^2} \qquad (24)$$

donde $\underset{\sim}{w}$ es el vector rotación.

Usando los conceptos establecidos en el capítulo anterior se observa que las ecs 23 y 24 son ecuaciones de onda asociadas a ondas de tipo dilatacional o P y distorcionales o S, respectivamente. De aquí se concluye que en un medio elástico de extensión infinita solo puede existir dos tipos de ondas, las ondas dilatacionales que se propagan con una velocidad c_p y las distorcionales que se propagan con una velocidad c_s.

Con el objeto de discutir más ampliamente el problema de propagación de ondas en un medio infinito sin fuerzas de cuerpo, investigemos algunas soluciones particulares...

Sea la solución asociada a una onda plana viajando

en la dirección positiva del eje x

$$u = a \operatorname{sen} \frac{2\pi}{\lambda}(x - ct)$$

$$v = 0 \qquad (25)$$

$$w = 0$$

Esta solución satisface las ecs 17 si y solo si $c = c_p$. y representa un tren de ondas planas distantacionales propagandose con una velocidad c_p. Notese que para este tipo de ondas el movimiento de la partícula coincide con la dirección de propagación y que además este tipo de movimiento no produce cambios volumétricos

Consideremos ahora las soluciones

$$u = w = 0$$

$$v = a \operatorname{sen} \frac{2\pi}{\lambda}(x - ct) \qquad (26)$$

o'

$$u = v = 0$$

$$w = a \operatorname{sen} \frac{2\pi}{\lambda}(x - ct) \qquad (27)$$

De la substitución de cualquiera de las soluciones anteriores en las ecs 17 se puede concluir que estas representan una solución si y solo si $c = c_s$. Además se observa que en el caso de ondas S el movimiento de la partí-

cula es normal a la dirección de propagación

Las ondas distorcionales son generalmente polarizadas*, esto es, ondas SH ... en las que el movimiento de la partícula es horizontal y ondas SV en las que el movimiento de la partícula ocurre en el plano vertical. En los casos en que el medio tiene isotropía transversal, como es el caso de muchas formaciones geológicas, en una perturbación propagandose en dirección horizontal la onda SH se propaga mas rápido que la onda SV.

* La existencia de distintas velocidades de propagación asociadas distintos tipos de onda se puede conducir una propiedad importante de las ondas sísmicas, esta es, que una onda plana arbitraria compuesta de movimientos P y S no se puede propagar. En cada instante las distintas ondas viajan diferentes distancias y es de esta propiedad que la velocidad de propagación de las ondas P y S a cualquier profundidad es facilmente calculable.

<u>Propagación de Ondas en un Semiespacio Elástico</u>

Consideremos ahora el caso de propagación de ondas en un

medio que consiste de un semiespacio elástico. Por conveniencia en la formulación escogamos el eje z dirigido verticalmente hacia abajo. Así, la superficie del semiespacio está definida por el plano $z=0$. Esta superficie está libre de esfuerzos por lo que las condiciones de frontera son

$$\tau_z = \sigma_{zx} = \sigma_{zy} \equiv 0 \qquad (28)$$

Si consideramos una onda plana dilatacional incidiendo con un ángulo i a la superficie del terreno se puede demostrar que esta produce 2 ondas reflejadas una P y una SV

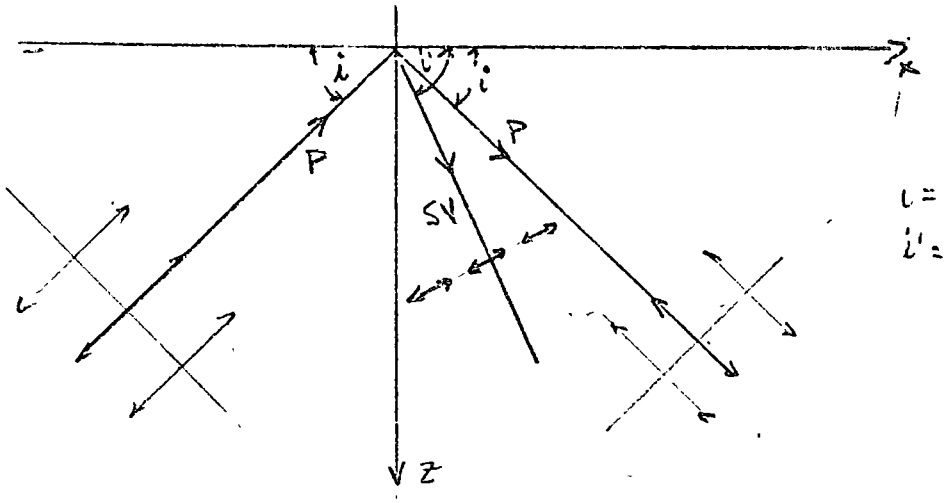

i = ángulo de incidencia
i' = ángulo de reflexión

Así para las ondas dilatacionales se tiene

$$e = \underbrace{f\left(t - \frac{x\cos i - z\,\mathrm{sen}\, i}{c_p}\right)}_{\text{incidente}} + \underbrace{Af\left(t - \frac{x\cos i + z\,\mathrm{sen}\, i}{c_p}\right)}_{\text{reflejada}}, \qquad (29)$$

y para las ondas distorsionales

$$w_2 = \underbrace{Bf\left(t - \frac{x\cos i' + z\,\mathrm{sen}\, i'}{c_s}\right)}_{\text{reflejadas}}, \qquad (30)$$

las condiciones de frontera dadas por las ecs 28 nos

permiten determinar los coeficientes desconocidos A y B, dados como

$$A = \frac{4\sqrt{\xi^2-1}\sqrt{k^2\xi^2-1} - (\xi^2-2)^2}{4\sqrt{\xi^2-1}\sqrt{k^2\xi^2-1} + (\xi^2-2)}$$

$$B =$$

$$B = \frac{4\sqrt{k^2\xi^2 - 1}\,(\xi^2 - 2)}{4\sqrt{\xi^2 - 1}\sqrt{k^2\xi^2 - 1} + (\xi^2 - 2)^2}$$

donde

$$\xi = \frac{1}{\cos i'} \qquad y \qquad k\xi = \frac{1}{\cos i}$$

Casos Particulares

1)- Si $i = \frac{\pi}{2} \Rightarrow i' = \frac{\pi}{2}$

$$A = -1$$

$$B = 0$$

2) Con $\frac{c_p^2}{c_s^2} = \frac{1}{3}$ $\quad A = 0$

Si

$$\xi = \begin{cases} 2 & \approx \quad i = 30^\circ \\ \sqrt{2\left(1 + \frac{1}{\sqrt{3}}\right)} & \approx \quad i = 18.8^\circ \\ \sqrt{2\left(1 - \frac{1}{\sqrt{3}}\right)} & < 1.0 \end{cases}$$

Nota

La tercera raiz ($\frac{1}{\cos i} < 1$) corresponde a una onda de Rayleigh en un semi espacio

ONDA SV INCIDENTE

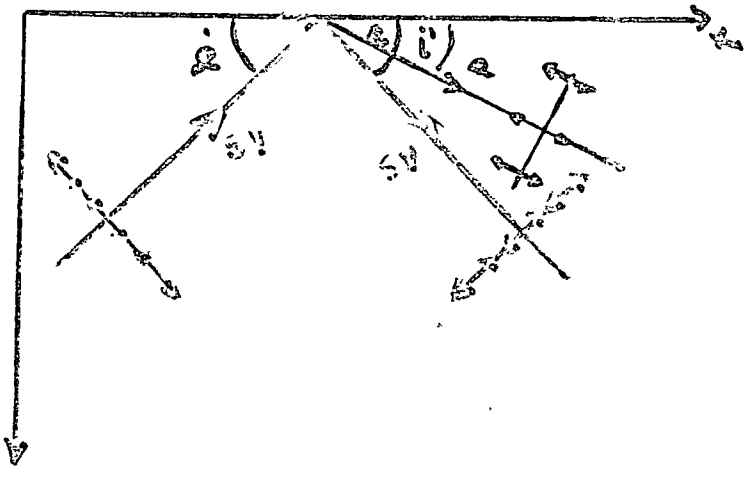

Onda P

$$\phi = C f\left(t - \frac{x \cos i' + z \operatorname{sen} i'}{c_p}\right)$$

Onda S

$$\psi = f\left(t - \frac{x \cos i - z \operatorname{sen} i}{c_s}\right) + D f\left(t - \frac{x \cos i + z \operatorname{sen} i}{c_s}\right)$$

con

$$C = -\frac{4\sqrt{\xi^2 - 1}\,(\xi^2 - 2)}{\sqrt{\xi^2 - 1}\,\sqrt{k^2 \xi^2 - 1} + (\xi^2 - 2)^2}$$

y

$$D = A$$

Casos Particulares

1) Si $i = \frac{\pi}{2} \Rightarrow i' = \frac{\pi}{2}$

$$C = 0$$
$$D = -1$$

2) Para $i = \operatorname{arc\,cos} \frac{c_s}{c_p} \Rightarrow i' = 0$

o sea la onda P reflejada se convierte en una onda

propagandose a lo largo de la superficie.

Onda SH Incidente

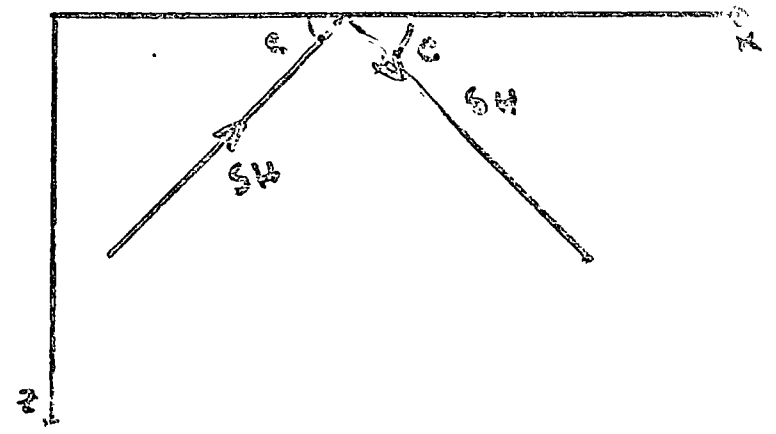

Es importante hacer notar que no solo existen ondas de Rayleigh en un semiespacio elastico, sino tambien en un semiespacio estratificado. En este caso la velocidad de propagacion $c_R = c_R(\omega)$

PROPAGACION DE ONDAS EN UN MEDIO ESTRATIFICADO

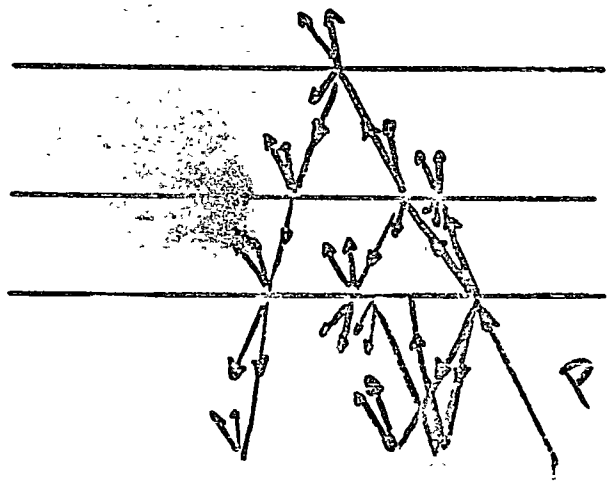

ONDAS DE LOVE

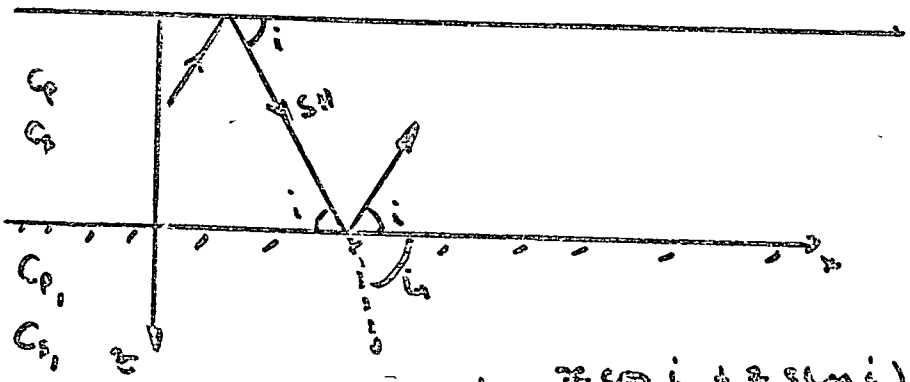

$$\nabla^2 v = \frac{1}{c_s^2}\frac{\partial^2 v}{\partial t^2}$$

$$v = A' e^{i\omega\left(t - \frac{x\cos i + z\,\mathrm{sen}\, i}{c_s}\right)} + B' e^{i\omega\left(t - \frac{x\cos i - z\,\mathrm{sen}\, i}{c_s}\right)}$$

$$c = \frac{c_s}{\cos i} \qquad \mathrm{sen}\, i = \sqrt{1 - \frac{c_s^2}{c^2}}$$

$$v = (A \cos sz + B \operatorname{sen} sz)\, e^{i\omega}$$

donde

$$s = \frac{\omega \sqrt{1 - \frac{c_1^2}{c^2}}}{c_s}$$

$$\frac{A}{B} = B' + A'$$

$$\frac{B}{B} = \sqrt{-1}\,(B' - A')$$

La onda reflectada es

$$v_1 = N e^{i\omega\left(t - \frac{x \cos i_1 + z \operatorname{sen} i_1}{c_{s_1}}\right)}$$

N es el coeficiente de transmisión

$$\tanh \frac{\omega}{c_s} \sqrt{\frac{c^2}{c_s^2} - 1} = \frac{c_{s_1} \rho_1 \sqrt{1 - \frac{c_{s_1}^2}{c^2}}}{c_s \rho \sqrt{\frac{c^2}{c_s^2} - 1}}$$

$$c_s < c < c_{s_1}$$

(distortional) propagates at the same velocity ($v_S = \sqrt{G/\rho}$) in both the rod and the infinite medium.

3.3 Waves in an Elastic Half-Space

In Sec. 3.2 it was found that two types of waves were possible in an infinite elastic medium—waves of dilatation and waves of distortion. In an elastic half-space, however, it is possible to find a third solution for the equations of motion which corresponds to a wave whose motion is confined to a zone near the boundary of the half-space. This wave was first studied by Lord Rayleigh (1885) and later was described in detail by Lamb (1904). The elastic wave described by these investigators is known as the *Rayleigh wave* (*R*-wave) and is confined to the neighborhood of the surface of a half-space. The influence of the Rayleigh wave decreases rapidly with depth.

Rayleigh-Wave Velocity

A wave with the characteristics noted above can be obtained by starting with the equations of motion (Eqs. 3-42, 3-43, and 3-44) and imposing the appropriate boundary conditions for a free surface. We define the surface of the half-space as the x-y plane with z assumed to be positive toward the interior of the half-space, as shown in Fig. 3-12. For a *plane wave* traveling in the x-direction, particle displacements will be independent of the y-direction. Displacements in the x- and z-directions, denoted by u and w respectively, can be written in terms of two potential functions Φ and Ψ:

$$u = \frac{\partial \Phi}{\partial x} + \frac{\partial \Psi}{\partial z} \quad \text{and} \quad w = \frac{\partial \Phi}{\partial z} - \frac{\partial \Psi}{\partial x}$$

The dilatation $\bar{\epsilon}$ of the wave defined by u and w is

$$\bar{\epsilon} = \frac{\partial u}{\partial x} + \frac{\partial w}{\partial z} = \frac{\partial}{\partial x}\left(\frac{\partial \Phi}{\partial x} + \frac{\partial \Psi}{\partial z}\right) + \frac{\partial}{\partial z}\left(\frac{\partial \Phi}{\partial z} - \frac{\partial \Psi}{\partial x}\right) = \nabla^2 \Phi$$

and the rotation $2\bar{\omega}_y$ in the x-z plane is

$$2\bar{\omega}_y = \frac{\partial u}{\partial z} - \frac{\partial w}{\partial x} = \frac{\partial}{\partial z}\left(\frac{\partial \Phi}{\partial x} - \frac{\partial \Psi}{\partial z}\right) - \frac{\partial}{\partial x}\left(\frac{\partial \Phi}{\partial z} - \frac{\partial \Psi}{\partial x}\right) = \nabla^2 \Psi$$

Now it can be seen that the potential functions Φ and Ψ have been chosen

$(v_S \quad \sqrt{G/\rho})$ in both the rod

of waves were possible in an
nd waves of distortion. In an
a third solution for the equa-
whose motion is confined to a
is wave was first studied by
d in detail by Lamb (1904).
ors is known as the *Rayleigh*
hood of the surface of a half-
creases rapidly with depth.

e can be obtained by starting
and 3-44) and imposing the
face. We define the surface
d to be positive toward the
. For a *plane wave* traveling
be pendent of the *y*-
ions, denoted by u and w
ial functions Φ and Ψ:

$$\frac{\partial \Phi}{\partial z} - \frac{\partial \Psi}{\partial x}$$

is

$$\frac{\partial \Phi}{\partial z} - \frac{\partial \Psi}{\partial x}\right) = \nabla^2 \Phi$$

$$\frac{\partial \Phi}{\partial z} - \frac{\partial \Psi}{\partial x}\right) = \nabla^2 \Psi$$

and Ψ have been chosen

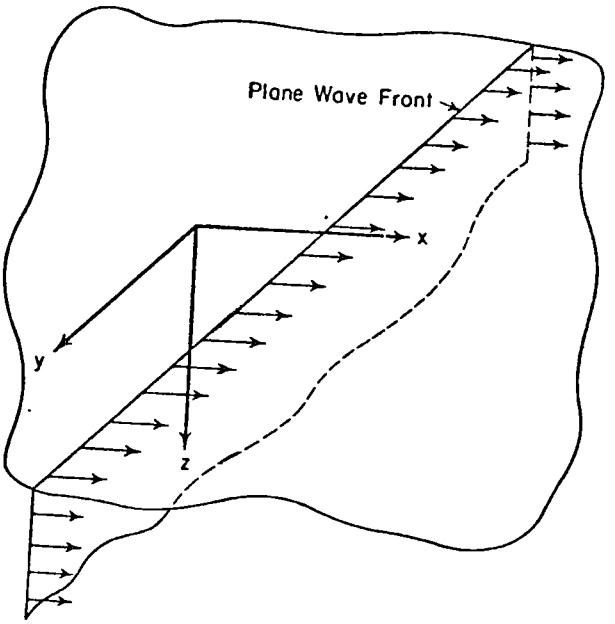

Figure 3-12 Coordinate convention for elastic half-space.

such that Φ is associated with dilatation of the medium and Ψ associated with rotation of the medium.

Substituting u and w into Eqs. (3-42) and (3-44) yields

$$\rho \frac{\partial}{\partial x}\left(\frac{\partial^2 \Phi}{\partial t^2}\right) + \rho \frac{\partial}{\partial z}\left(\frac{\partial^2 \Psi}{\partial t^2}\right) = (\lambda + 2G)\frac{\partial}{\partial x}(\nabla^2 \Phi) + G\frac{\partial}{\partial z}(\nabla^2 \Psi) \quad (3\text{-}49)$$

and

$$\rho \frac{\partial}{\partial z}\left(\frac{\partial^2 \Phi}{\partial t^2}\right) - \rho \frac{\partial}{\partial x}\left(\frac{\partial^2 \Psi}{\partial t^2}\right) = (\lambda + 2G)\frac{\partial}{\partial z}(\nabla^2 \Phi) - G\frac{\partial}{\partial x}(\nabla^2 \Psi) \quad (3\text{-}50)$$

Equations (3-49) and (3-50) are satisfied if

$$\frac{\partial^2 \Phi}{\partial t^2} = \frac{\lambda + 2G}{\rho}\nabla^2 \Phi = v_P^2 \nabla^2 \Phi \quad (3\text{-}51)$$

and

$$\frac{\partial^2 \Psi}{\partial t^2} = \left(\frac{G}{\rho}\right)\nabla^2 \Psi = v_S^2 \nabla^2 \Psi \quad (3\text{-}52)$$

Now, by assuming a solution for a sinusoidal wave traveling in the positive x-direction, expressions for Φ and Ψ can be written

$$\Phi = F(z) \exp [i(\omega t - Nx)] \quad (3\text{-}53)$$

and

$$\Psi = \mathrm{G}(z) \exp\,[i(\omega t - Nx)] \tag{3-54}$$

The functions $\mathrm{F}(z)$ and $\mathrm{G}(z)$ describe the variation in amplitude of the wave as a function of depth, and N is the wave number defined by

$$N = \frac{2\pi}{L}$$

where L is the wave length.

Now, substituting the expressions for Φ and Ψ from Eqs. (3.53) and (3-54) into Eqs. (3-51) and (3-52) yields

$$-\frac{\omega^2}{v_P^2}\mathrm{F}(z) = -N^2\mathrm{F}(z) + \mathrm{F}''(z) \tag{3-55}$$

and

$$-\frac{\omega^2}{v_S^2}\mathrm{G}(z) = -N^2\mathrm{G}(z) + \mathrm{G}''(z) \tag{3-56}$$

By rearranging Eqs. (3-55) and (3-56), we get

$$\mathrm{F}''(z) - \left(N^2 - \frac{\omega^2}{v_P^2}\right)\mathrm{F}(z) = 0 \tag{3-57}$$

and

$$\mathrm{G}''(z) - \left(N^2 - \frac{\omega^2}{v_S^2}\right)\mathrm{G}(z) = 0 \tag{3-58}$$

where $\mathrm{F}''(z)$ and $\mathrm{G}''(z)$ are derivatives with respect to z. Now, letting

$$q^2 = \left(N^2 - \frac{\omega^2}{v_P^2}\right) \tag{3-59}$$

and

$$s^2 = \left(N^2 - \frac{\omega^2}{v_S^2}\right) \tag{3-60}$$

Eqs. (3-57) and (3-58) can be rewritten as

$$\mathrm{F}''(z) - q^2\mathrm{F}(z) = 0 \tag{3-61}$$

and

$$\mathrm{G}''(z) - s^2\mathrm{G}(z) = 0 \tag{3-62}$$

$- Nx)]$ (3-54)

ation in amplitude of the wave
ber defined by

Φ and Ψ from Eqs. (3.53) and

$+ \mathbf{F}''(z)$ (3-55)

$+ \mathbf{G}''(z)$ (3-56)

$(z) = 0$ (3-57)

$(z) = 0$ (3-58)

spect to z. Now, letting

(3-59)

(3-60)

$= 0$ (3-61)

$= 0$ (3-62)

The solutions of Eqs. (3-61) and (3-62) can be expressed in the form

$$\mathbf{F}(z) = A_1 \exp(-qz) + \boldsymbol{B}_1 \exp(qz) \tag{3-63}$$

$$\mathbf{G}(z) = A_2 \exp(-sz) + \boldsymbol{B}_2 \exp(sz) \tag{3-64}$$

A solution that allows the amplitude of the wave to become infinite with depth cannot be tolerated; therefore,

$$B_1 = B_2 = 0$$

and Eqs. (3-53) and (3-54) become

$$\Phi = A_1 \exp[-qz + i(\omega t - Nx)] \tag{3-65}$$

and

$$\Psi = A_2 \exp[-sz + i(\omega t - Nx)] \tag{3-66}$$

Now, the boundary conditions specifying no stress at the surface of a half-space imply that $\sigma_z = 0$ and $\tau_{xy} = 0$ at the surface $z = 0$. Therefore, at the surface,

$$\sigma_z = \lambda\bar{\epsilon} + 2G\epsilon_z = \lambda\bar{\epsilon} + 2G\frac{\partial w}{\partial z} = 0$$

and

$$\tau_{zx} = G\gamma_{zx} = G\left(\frac{\partial w}{\partial x} + \frac{\partial u}{\partial z}\right) = 0$$

Using the definitions of u and w and the solutions for Φ and Ψ from Eqs. (3-65) and (3-66), the above equations for boundary conditions can be written

$$\sigma_{z\,z=0} = A_1[(\lambda + 2G)q^2 - \lambda N^2] - 2iA_2GNs = 0 \tag{3-67}$$

and

$$\tau_{zx\,z=0} = 2iA_1Nq + A_2(s^2 + N^2) = 0 \tag{3-68}$$

Upon rearranging, Eqs. (3-67) and (3-68) become

$$\frac{A_1}{A_2}\frac{(\lambda + 2G)q^2 - \lambda N^2}{2iGNs} - 1 = 0 \tag{3-69}$$

and

$$\frac{A_1}{A_2}\frac{2qiN}{(s^2 + N^2)} - 1 = 0 \tag{3-70}$$

Now we add these two equations to get

$$\frac{(\lambda + 2G)q^2 - \lambda N^2}{2iGNs} = -\frac{2qiN}{s^2 + N^2} \tag{3-71}$$

and cross-multiply in Eq. (3-71) to obtain

$$4qGsN^2 = (s^2 + N^2)\,[(\lambda + 2G)q^2 - \lambda N^2] \tag{3-72}$$

Squaring both sides of Eq. (3-72) and introducing q from Eq. (3-59) and s from Eq. (3-60), we get

$$16G^2N^4\left(N^2 - \frac{\omega^2}{v_P^2}\right)\left(N^2 - \frac{\omega^2}{v_S^2}\right) = \left[(\lambda + 2G)\left(N^2 - \frac{\omega^2}{v_P^2}\right) - \lambda N^2\right]^2\left[N^2 + \left(N^2 - \frac{\omega^2}{v_S^2}\right)\right]^2 \tag{3-73}$$

Now, dividing through by G^2N^8, we obtain

$$16\left(1 - \frac{\omega^2}{v_P^2N^2}\right)\left(1 - \frac{\omega^2}{v_S^2N^2}\right) = \left[2 - \left(\frac{\lambda + 2G}{G}\right)\left(\frac{\omega^2}{v_P^2N^2}\right)\right]^2\left(2 - \frac{\omega^2}{v_S^2N^2}\right)^2 \tag{3-74}$$

Then, using the following relationships derived in the footnote* gives

$$\frac{\omega^2}{v_P^2N^2} = \frac{v_R^2}{v_P^2} = \alpha^2K^2 \tag{3-75}$$

$$\frac{\omega^2}{v_S^2N^2} = \frac{v_R^2}{v_S^2} = K^2 \tag{3-76}$$

$$\frac{\lambda + 2G}{G} = \frac{1}{\alpha^2} = \frac{2 - 2\nu}{1 - 2\nu} \tag{3-77}$$

* By definition,

$$N = \frac{2\pi}{L}$$

or

$$L = \frac{2\pi}{N}$$

(Let L_R and v_R be the wave length and velocity, respectively, of the surface wave.)

SEC. 3.3

Eq. (3-74) can be written

$$16(1 - \alpha^2K^2)($$

After expansion and rearra

$$K^6 - 8K^4 +$$

Equation (3-79) can be cor
solutions can be found for gi
between the velocity of the

Also,

and, from above,

therefore,

and

Let K and α be defined such that

$$\frac{v_R^2}{v_S^2} =$$

Then

and

Substitution of v_S and v_P from Eq

$$\frac{1}{\alpha^2} =$$

and using

we get

$$\lambda$$

Eq. (3-74) can be written

$$16(1 - \alpha^2K^2)(1 - K^2) = \left(2 - \frac{1}{\alpha^2}\alpha^2K^2\right)^2(2 - K^2)^2 \qquad (3\text{-}78)$$

After expansion and rearrangement, Eq. (3-78) becomes

$$K^6 - 8K^4 + (24 - 16\alpha^2)K^2 + 16(\alpha^2 - 1) = 0 \qquad (3\text{-}79)$$

Equation (3-79) can be considered a cubic equation in K^2 and real valued solutions can be found for given values of ν. The quantity K represents a ratio between the velocity of the surface wave and the velocity of the shear wave.

Also,

$$L_R = \frac{v_R}{f} = \frac{2\pi v_R}{\omega}$$

and, from above,

$$L_R = \frac{2\pi}{N} = \frac{v_R 2\pi}{\omega}$$

therefore,

$$N = \frac{\omega}{v_R}$$

and

$$N^2 = \frac{\omega^2}{v_R^2}$$

Let K and α be defined such that

$$\frac{v_R^2}{v_S^2} = K^2 \quad \text{and} \quad \frac{v_R^2}{v_P^2} = \alpha^2K^2$$

Then

$$\frac{\omega^2}{v_P^2N^2} = \frac{v_R^2}{v_P^2} = \alpha^2K^2$$

and

$$\frac{\omega^2}{v_S^2N^2} = \frac{v_R^2}{v_S^2} = K^2$$

Substitution of v_S and v_P from Eqs. (3-46) and (3-48) gives

$$\frac{1}{\alpha^2} = \frac{v_P^2}{v_S^2} = \frac{\dfrac{\lambda + 2G}{\rho}}{\dfrac{G}{\rho}} = \frac{\lambda + 2G}{G}$$

and using

$$\nu = \frac{\lambda}{2(\lambda + G)}$$

we get

$$\frac{\lambda + 2G}{G} = \frac{2 - 2\nu}{1 - 2\nu} = \frac{1}{\alpha^2}$$

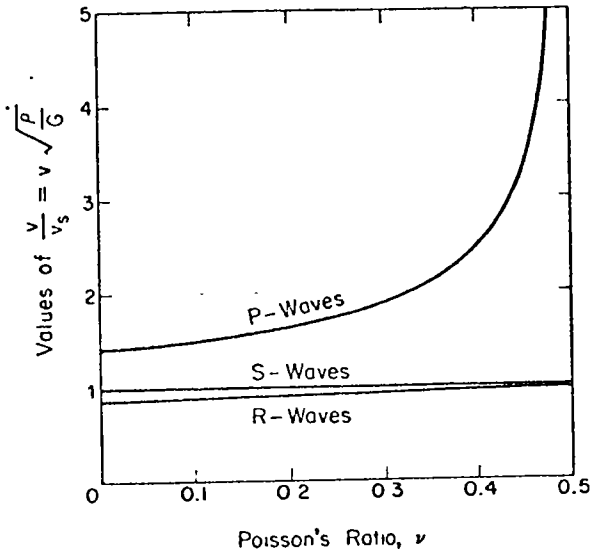

Figure 3-13. Relation between Poisson's ratio, ν, and velocities of propagation of compression (P), shear (S), and Rayleigh (R) waves in a semi-infinite elastic medium (*from Richart, 1962*).

From this solution it is clear that K^2 is independent of the frequency of the wave; consequently, the velocity of the surface wave is independent of frequency and is nondispersive.

Ratios of v_R/v_S and v_P/v_S can be obtained from Eq. (3-79) for values of Poisson's ratio ν from 0 to 0.5. Curves of these ratios as a function of ν are shown in Fig. 3-13.

Rayleigh-Wave Displacement

So far, a relationship for the ratio of the Rayleigh-wave velocity to the shear-wave velocity has been obtained, but additional information about the Rayleigh wave can be determined by obtaining the expressions for u and w in terms of known quantities. Upon substituting the expressions for Φ and Ψ from Eqs. (3-65) and (3-66) into the expressions for u and w, we get

$$u = \frac{\partial \Phi}{\partial x} + \frac{\partial \Psi}{\partial z}$$
$$= -A_1 iN \exp[-qz + i(\omega t - Nx)] - A_2 s \exp[-sz + i(\omega t - Nx)] \tag{3-80}$$

and

$$w = \frac{\partial \Phi}{\partial z} - \frac{\partial \Psi}{\partial x}$$
$$= -A_1 iN \exp[-qz + i(\omega t - Nx)] + A_2 iN \exp[-sz + i(\omega t - Nx)] \tag{3-81}$$

From Eq. (3-70) we can get

and substitution of A_2 into E

$$u = A_1\left[-iN \exp(-qz)\right.$$

and

$$w = A_1\left[\frac{2qN^2}{s^2 + N^2} \exp(-s\right.$$

Equations (3-82) and (3-83)

$$u = A_1 N\left\{-\exp\left[-\frac{q}{N}(zN\right.\right.$$

and

$$w = A_1 N\left\{\frac{2\frac{q}{N}}{\frac{s^2}{N^2} + 1} \exp\left[-\frac{s}{N}\right.\right.$$

Now, from Eqs. (3-84) and
expressed as

$$U(z) = -\exp\left[-\right.$$

and

$$W(z) = \frac{2\frac{q}{N}}{\frac{s^2}{N^2} + 1} e$$

* The significance of the pre
in the expression for u (Eq. 3-8
phase with the u-component of

From Eq. (3-70) we can get

$$A_2 = -\frac{2qiNA_1}{s^2 + N^2}$$

and substitution of A_2 into Eqs. (3-80) and (3-81) gives

$$u = A_1\left[-iN\exp(-qz) + \frac{2iqsN}{s^2+N^2}\exp(-sz)\right]\exp i(\omega t - Nx) \quad (3\text{-}82)$$

and

$$w = A_1\left[\frac{2qN^2}{s^2+N^2}\exp(-sz) - q\exp(-qz)\right]\exp i(\omega t - Nx) \quad (3\text{-}83)$$

Equations (3-82) and (3-83) can be rewritten

$$u = A_1 Ni\left\{-\exp\left[-\frac{q}{N}(zN)\right] + \frac{2\frac{q}{N}\frac{s}{N}}{\frac{s^2}{N^2}+1}\exp\left[-\frac{s}{N}(zN)\right]\right\}$$

$$\times \exp i(\omega t - Nx) \quad (3\text{-}84)$$

and

$$w = A_1 N\left\{\frac{2\frac{q}{N}}{\frac{s^2}{N^2}+1}\exp\left[-\frac{s}{N}(zN)\right] - \frac{q}{N}\exp\left[-\frac{q}{N}(zN)\right]\right\}$$

$$\times \exp i(\omega t - Nx) \quad (3\text{-}85)^*$$

Now, from Eqs. (3-84) and (3-85), the variation of u and w with depth can be expressed as

$$U(z) = -\exp\left[-\frac{q}{N}(zN)\right] + \frac{2\frac{q}{N}\frac{s}{N}}{\frac{s^2}{N^2}+1}\exp\left[-\frac{s}{N}(zN)\right] \quad (3\text{-}86)$$

and

$$W(z) = \frac{2\frac{q}{N}}{\frac{s^2}{N^2}+1}\exp\left[-\frac{s}{N}(zN)\right] - \frac{q}{N}\exp\left[-\frac{q}{N}(zN)\right] \quad (3\text{-}87)$$

* The significance of the presence of i in the expression for u (Eq. 3-84) and its absence in the expression for w (Eq. 3-85) is that the u-component of displacement is 90° out of phase with the w-component of displacement.

The functions $U(z)$ and $W(z)$ represent the spatial variations of the displacements u and w. Equations (3-59) and (3-60) can be rewritten

$$\frac{q^2}{N^2} = 1 - \frac{\omega^2}{N^2 v_P^2} \tag{3-88}$$

and

$$\frac{s^2}{N^2} = 1 - \frac{\omega^2}{N^2 v_S^2} \tag{3-89}$$

and then, using Eqs. (3-75) and (3-76), Eqs. (3-88) and (3-89) can be reduced to

$$\frac{q^2}{N^2} = 1 - \alpha^2 K^2 \tag{3-90}$$

and

$$\frac{s^2}{N^2} = 1 - K^2 \tag{3-91}$$

Now, $U(z)$ and $W(z)$ can be evaluated in terms of the wave number N for any given value of Poisson's ratio. For example, if $\nu = \frac{1}{4}$, $U(z)$ and $W(z)$ are given by

$$U(z) = -\exp[-0.8475\,(zN)] + 0.5773 \exp[-0.3933\,(zN)] \tag{3-92}$$

and

$$W(z) = 0.8475 \exp[-0.8475(zN)] - 1.4679 \exp[-0.3933(zN)] \tag{3-93}$$

Figure 3-14 shows curves for $U(z)$ and $W(z)$ vs. distance from the surface in wave lengths of the Rayleigh wave (L_R) for Poisson's ratios of 0.25, 0.33, 0.40, and 0.50.

Wave System at Surface of Half-Space

In preceding paragraphs expressions have been determined for the wave velocities of the three principal waves which occur in an elastic half-space. Knowing these velocities, we can easily predict the order in which waves will arrive at a given point due to a disturbance at another point. In addition to predicting the order of arrival of the waves along the surface, Lamb (1904) described in detail the surface motion that occurs at large distances from a point source at the surface of an ideal medium.

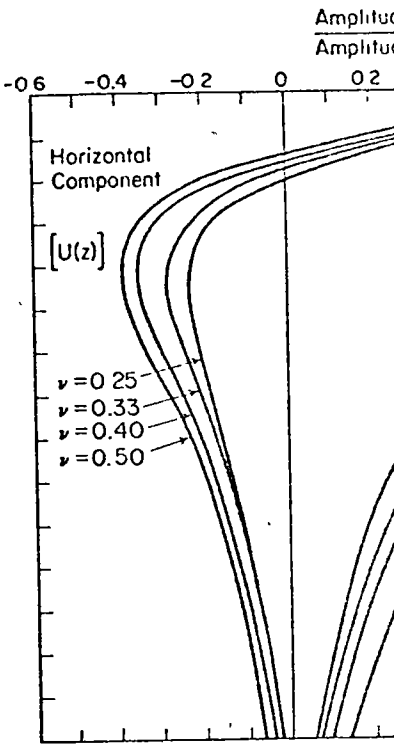

Figure 3-14. Amplitude ratio

Under the conditions consi
from the point source in the fo
The initial form of this wave sy
if the input is of short duration,
3-15 will develop. This wave sys
to the arrivals of the *P*-wave.
vertical components of particle
A particle at the surface first e
oscillation at the arrival of the
leading up to another oscillatio
are referred to by Lamb as the *m*
magnitude oscillation, the *major*

The time interval betwee
amplitude of the oscillations be
the source. In addition, the min
tremor. It is evident, therefore,
turbance along the surface of a
source, may be the only clearly

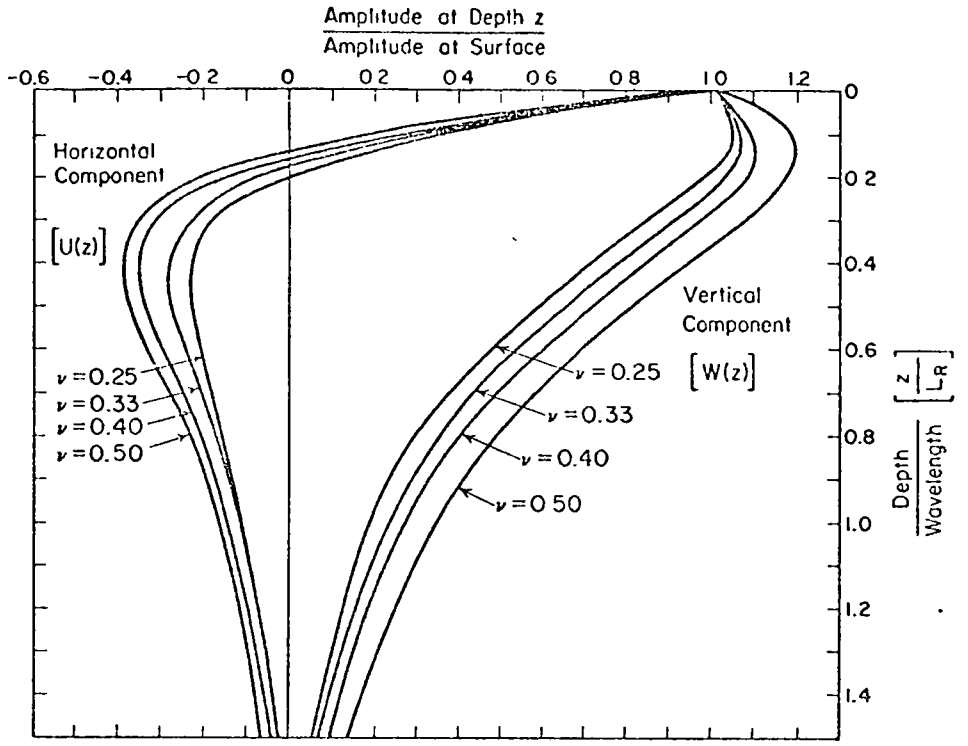

Figure 3-14 Amplitude ratio vs. dimensionless depth for Rayleigh wave.

Under the conditions considered by Lamb, a disturbance spreads out from the point source in the form of a symmetrical annular-wave system. The initial form of this wave system will depend on the input impulse; but if the input is of short duration, the characteristic wave system shown in Fig. 3-15 will develop. This wave system has three salient features corresponding to the arrivals of the *P*-wave, *S*-wave, and *R*-wave. The horizontal and vertical components of particle motion are shown separately in Fig. 3-15. A particle at the surface first experiences a displacement in the form of an oscillation at the arrival of the *P*-wave, followed by a relatively quiet period leading up to another oscillation at the arrival of the *S*-wave. These events are referred to by Lamb as the *minor tremor* and are followed by a much larger magnitude oscillation, the *major tremor*, at the time of arrival of the *R*-wave.

The time interval between wave arrivals becomes greater and the amplitude of the oscillations becomes smaller with increasing distance from the source. In addition, the minor tremor decays more rapidly than the major tremor. It is evident, therefore, that the *R*-wave is the most significant disturbance along the surface of a half-space and, at large distances from the source, may be the only clearly distinguishable wave.

7.10. LOVE WAVES

In the Rayleigh waves examined in the previous section the material particles move in the plane of propagation. Thus, in Rayleigh waves over the half-space $y > 0$ along the surface $y = 0$, propagating in the x-direction, the z-component of displacement w vanishes. It may be shown that surface waves with displacements perpendicular to the direction of propagation (the so-called *SH waves*) is impossible in a homogeneous half-space. However, *SH* surface waves are observed as prominently on the Earth's surface as other surface waves. Love showed that a theory sufficient to include *SH* surface waves can be constructed by having a homogeneous layer of a medium M_1 of uniform thickness H_1, overlying a homogeneous half-space of another medium M.

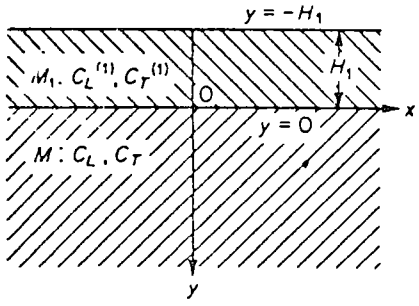

Fig. 7.10:1. A layered half-space.

Using axes as in Fig. 7.10:1, we take $u = v = 0$, and

$$(1) \qquad w = A \exp\left[-k\sqrt{1 - \frac{c^2}{c_T^2}}\, y\right] \exp\left[ik(x - ct)\right]$$

in M, and

$$(2) \qquad w = \left\{A_1 \exp\left[-k\sqrt{1 - \left(\frac{c}{c_T^{(1)}}\right)^2}\, y\right] + A_1' \exp\left[k\sqrt{1 - \left(\frac{c}{c_T^{(1)}}\right)^2}\, y\right]\right\} \times \exp\left[ik(x - ct)\right]$$

in M_1. It is easily verified that these equations satisfy the Navier's equations. If $c < c_T$, then $w \to 0$ as $y \to \infty$, as desired.

The boundary conditions are that w and σ_{zy} must be continuous across the surface $y = 0$, and σ_{zy} zero at $y = -H_1$. On applying these conditions to (1) and (2), we obtain

$$(3) \qquad A = A_1 + A_1',$$

$$(4) \qquad GA[1 - (c/c_T)^2]^{1/2} = G_1(A_1 - A_1')[1 - (c/c_T^{(1)})^2]^{1/2},$$

$$(5) \qquad A_1 \exp\{kH_1[1 - (c/c_T^{(1)})^2]^{1/2}\} = A_1' \exp\{-kH_1[1 - (c/c_T^{(1)})^2]^{1/2}\}.$$

Eliminating A from (3) and (4), and then using (5) to eliminate A_1 and A_1', we have

$$\frac{G[1 - (c/c_T)^2]^{1/2}}{G_1[1 - (c/c_T^{(1)})^2]^{1/2}} = \frac{A_1 - A_1'}{A_1 + A_1'} = i \tan\{ikH_1[1 - (c/c_T^{(1)})^2]^{1/2}\}.$$

Hence, we have

$$(6) \qquad G[1 - (c/c_T)^2]^{1/2} - G_1[(c/c_T^{(1)})^2 - 1]^{1/2} \tan\{kH_1[(c/c_T^{(1)})^2 - 1]^{1/2}\} = 0$$

as the equation to give the *SH* surface wave velocity c in the present conditions.

If $c_T^{(1)} < c_T$, Eq. (6) yields a real value of c which lies in the range $c_T^{(1)} < c < c_T$ and depends on k and H_1 (as well as on G, G_1, c_T, and $c_T^{(1)}$), because for c in this range the values of the left-hand-side terms in (6) are real and opposite in sign. Thus, *SH* surface waves can occur under the stated boundary conditions, provided the shear velocity $c_T^{(1)}$ in the upper layer is less than that in the medium M. These waves are called *Love waves*.

Love waves of general shape may be derived by superposing harmonic Love waves of the type (2) with different k. The dependence of the wave speed c on the wave number k introduces a dispersion phenomenon which will be considered later.

PROBLEMS

7.2. Derive Navier's equation in spherical polar coordinates.

7.3. From data given in various handbooks, determine the longitudinal and shear wave speeds in the following materials:

(a) Gases: air at sea level, and at 100,000 ft altitude.

(b) Metals: iron, a carbon steel, a stainless steel, copper, bronze, brass, nickle, aluminium, an aluminium alloy, titanium, titanium carbide, berylium, berylium oxide.

(c) Rocks and soils: a granite, a sandy loam.

(d) Wood: spruce, mahogany, balsa.

(e) Plastics: lucite, a foam rubber.

7.4. Sketch the instantaneous wave surfaces, particle velocities, and particle paths of a Love wave.

7.5. Investigate plane wave propagations in an anisotropic elastic material. Apply the results to a cubic crystal. *Note:*

$$\rho \frac{\partial^2 u_i}{\partial t^2} = C_{ijkl} \frac{\partial u_l}{\partial x_j \partial x_k}, \qquad u_l = A_l\, e^{-i(\omega t - k_j x_j)}$$

where $\mathbf{k}(k_1, k_2, k_3)$ is the wave vector normal to the wave front.

7.6. Determine the stress field in a rotating, gravitating sphere of uniform density.

CENTRO DE EDUCACION CONTINUA

DIVISION DE ESTUDIOS SUPERIORES

FACULTAD DE INGENIERIA

III CURSO INTERNACIONAL DE INGENIERIA SISMICA

SISMOLOGIA Y SISMICIDAD

DR. OCTAVIO A. RASCON CH.

JULIO, 1977

CORRELACIONES ENTRE DIVERSOS PARAMETROS DE LOS TEMBLORES

M = MAGNITUD EN LA ESCALA DE RICHTER

R = DISTANCIA FOCAL (EN KM)

$v_{máx}$ = VELOCIDAD MAXIMA DEL TERRENO (CM/SEG)

$a_{máx}$ = ACELERACION MAXIMA DEL TERRENO (CM/SEG^2)

$V_{máx}$ = VELOCIDAD ESPECTRAL MEDIA MAXIMA, CM/SEG (PARA $\varsigma=0$)

$A_{máx}$ = ACELERACION ESPECTRAL MEDIA MAXIMA, EN CM/SEG^2 (PARA $\varsigma=0$)

I = INTENSIDAD EN ESCALA DE MERCALLI MODIFICADA

W = ENERGIA DISIPADA, EN ERGS

$$v_{máx} = 32e^{M}(R + 25)^{-1.7}$$

$$a_{máx} = 5{,}600\ e^{0.8M}(R + 40)^{-2}$$

$$V_{máx} = 250e^{M}(R + 60)^{-1.7}$$

$$A_{máx} = 69{,}600e^{0.8M}(R + 70)^{-2}$$

NOTA: ESTAS CORRELACIONES CORRESPONDEN A LAS COMPONENTES HORIZONTALES DE TEMBLORES REGISTRADOS EN TERRENO DURO.

$$I = 1.45M - 5.7\ LOG_{10}\ R + 7.9$$

$$I = \frac{LOG\ 14\ v_{máx}}{LOG\ 2}$$

APROPIADA PARA $I \leq 10$. PARA $I > 10$ SE SOBRESTIMA I.

$$LOG_{10}W = 11.4 + 1.5M$$

Bulletin of the Seismological Society of America (Oct., 1974)

Tomado de:

Por D.L. Orphal y J.A. Lahoud

between the reported observations and calculations is good. The two measurements deviating most from the calculations were recorded at Lima and Koyna. It is noted that peak accelerations measured at Lima have been interpreted by Cloud and Perez (1971) to be anomalously high.

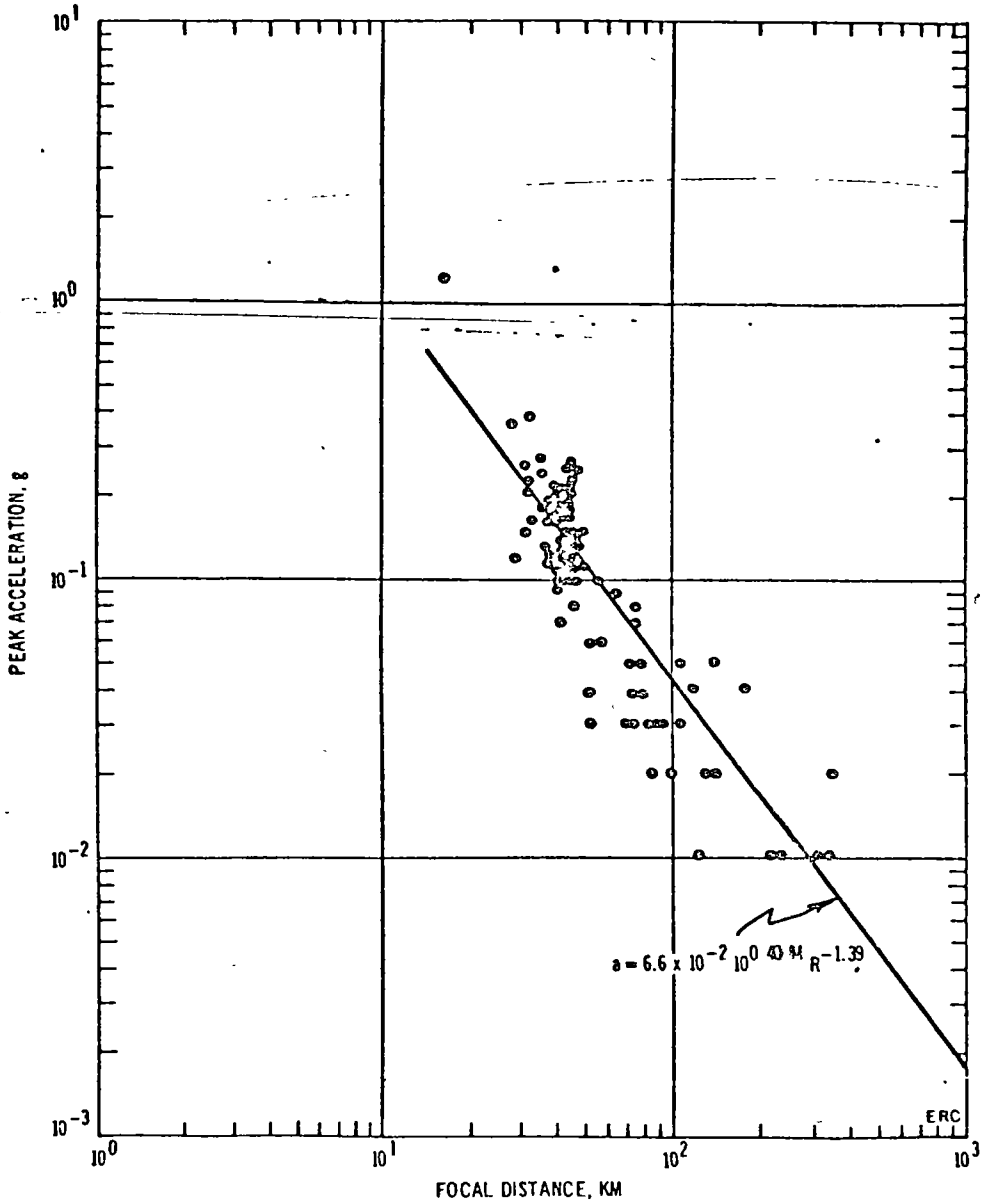

FIG. 3. Comparison between peak acceleration versus distance observed from San Fernando earthquake and calculated from equation (6).

The comparisons shown in Figures 3 through 5 are encouraging and suggest that equation (6) may be useful in predicting peak earthquake accelerations for a reasonably wide range of magnitudes, epicentral locations, focal depths and focal distances. As new earthquake ground-motion data are recorded, it is hoped that more extensive analyses will confirm the usefulness of equation (6) as well as delineate its range of validity.

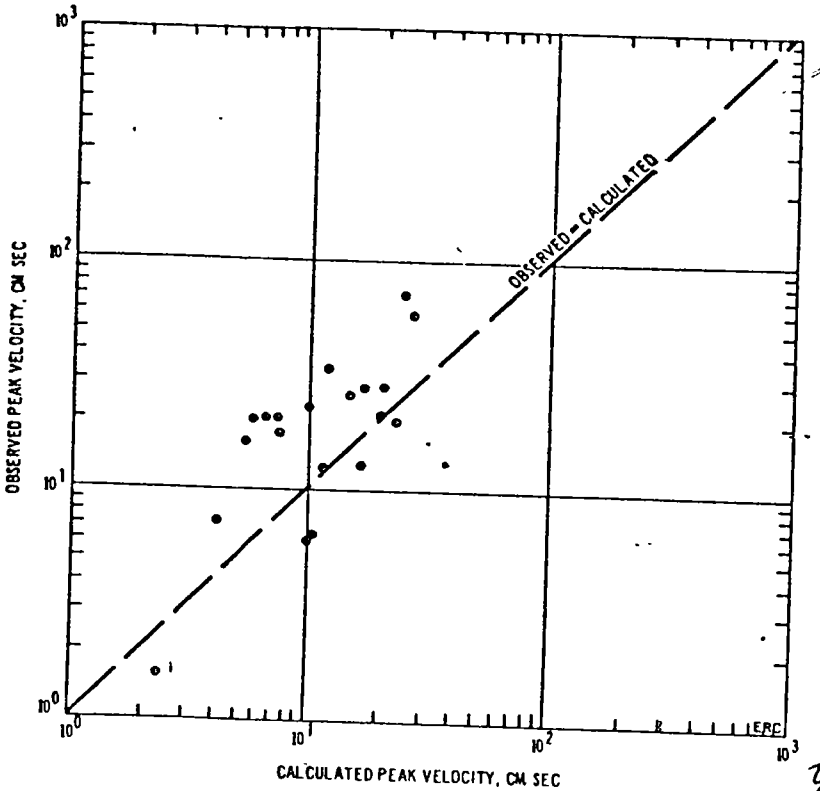

$V_{max} = 0.726 \times 10^{0.52M} R^{-1.34}$

FIG. 7. Comparison between 20 recorded peak velocities (Ambraseys, 1969) and corresponding calculations using equation (7).

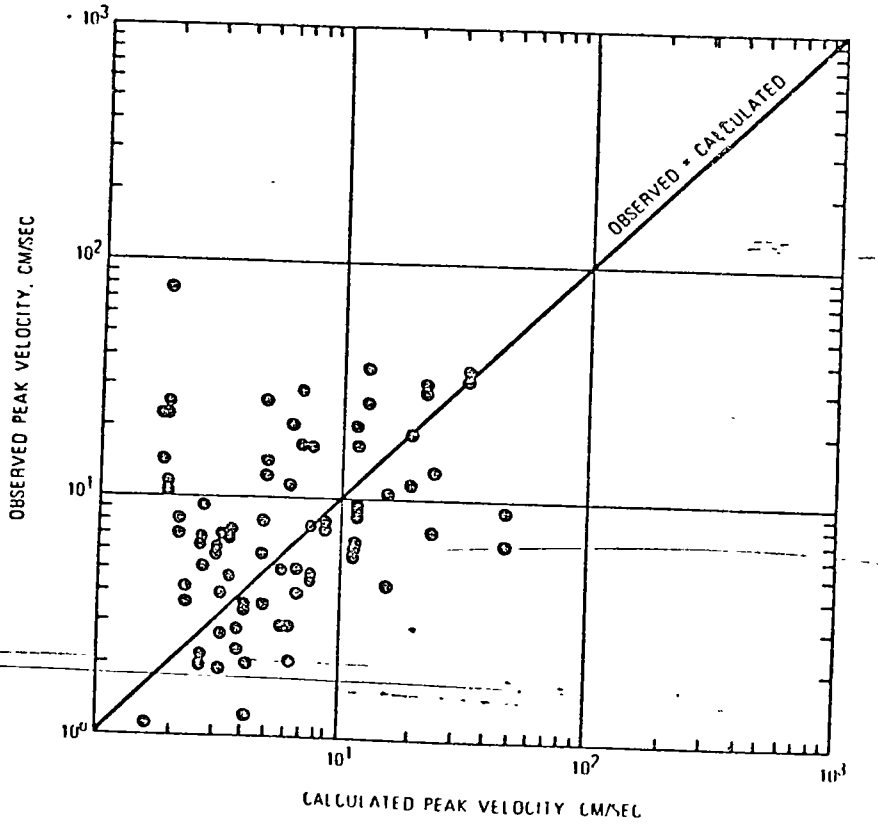

FIG. 8. Comparison between peak velocities derived from the CALTECH strong-motion accelerograms and corresponding calculations using equation (7).

motion accelerograms versus the corresponding data computed using equation (8). For this data sample, although there is considerable scatter, equation (8) generally underestimates the mean of the data by about a factor of two The reason for this discrepancy is not known and requires further study However, analysis of the data and the fact that the discrepancy between the data and equation (8) is approximately a constant factor suggests that the scaling of peak displacement with magnitude and focal distance is not substantially in error. The discrepancy may be due to an inaccurate determination of the

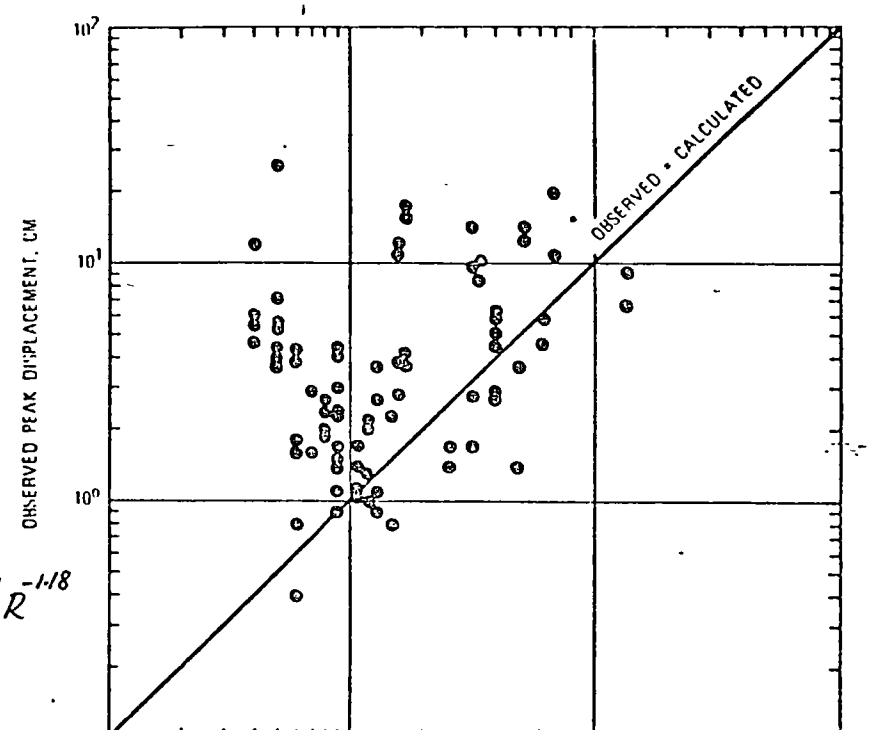

$d_{max} = 0.0471 \times 10^{0.57M} R^{-1.18}$

FIG. 9. Comparison between peak displacements derived from the CALTECH strong-motion accelerograms and corresponding calculations using equation (8)

constant factor in equation (8) or to the influence of local site amplification effects in the CALTECH data, an effect not included in this analysis.

DISCUSSION

It is of interest to examine equations (6), (7), and (8) in terms of the classical correlations between earthquake magnitude and epicentral intensity, radius of perceptibility, and maximum epicentral acceleration.

Gutenberg and Richter (1956) suggested that earthquake intensity is best related to peak ground acceleration. Using the Gutenberg-Richter intensity-acceleration equation and equation (6), assuming a focal depth of 15 km, one derives an equation relating magnitude and epicentral intensity. The equation so derived differs significantly from Gutenberg and Richter's empirical relationship. This suggests that earthquake intensity may not be closely related to peak acceleration, a suggestion that has been made previously by many researchers.

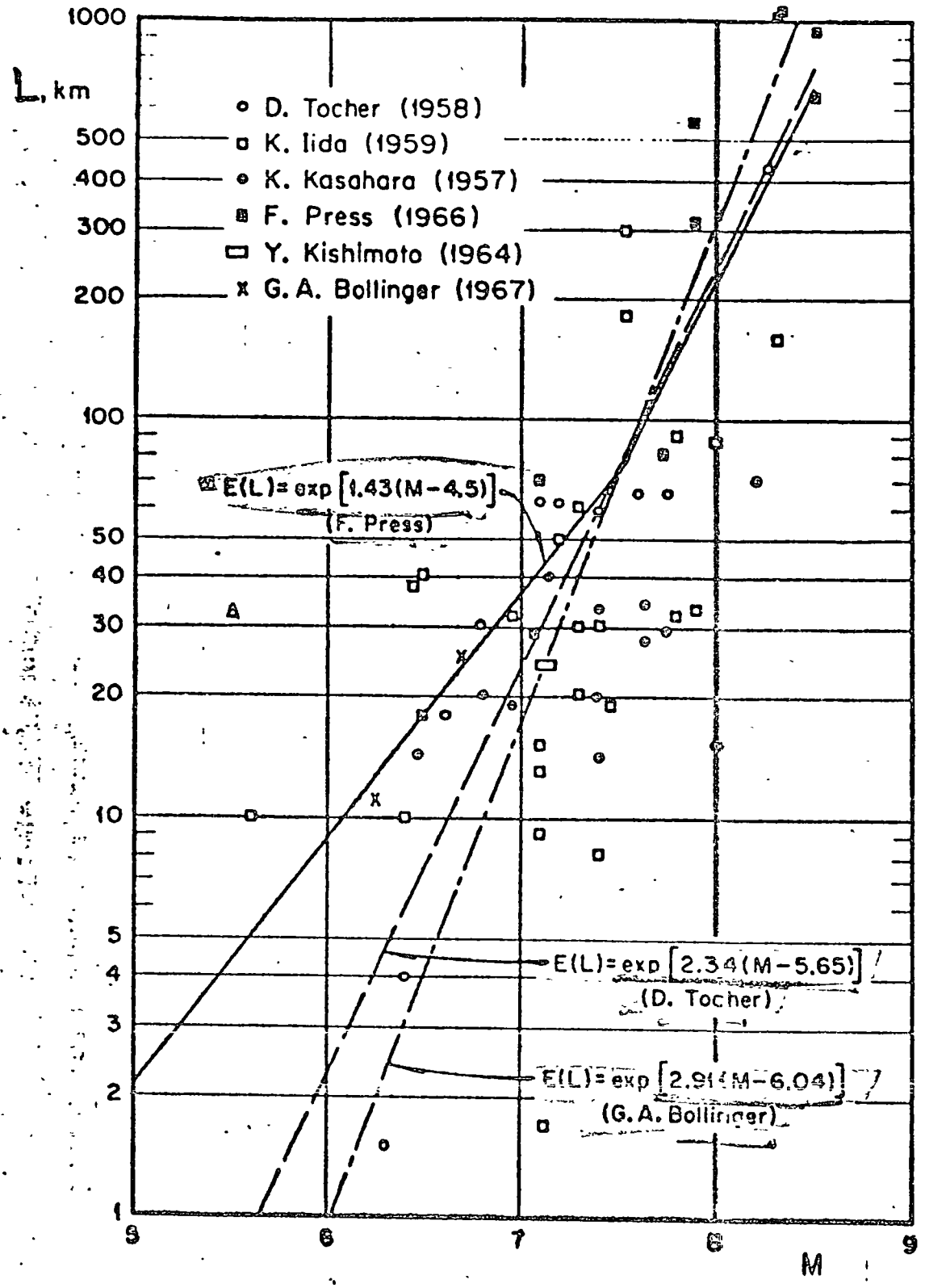

Fig. 3.1 Correlación entre la longitud de la falla y la magnitud del sismo

(Según G.A. Bollinger)

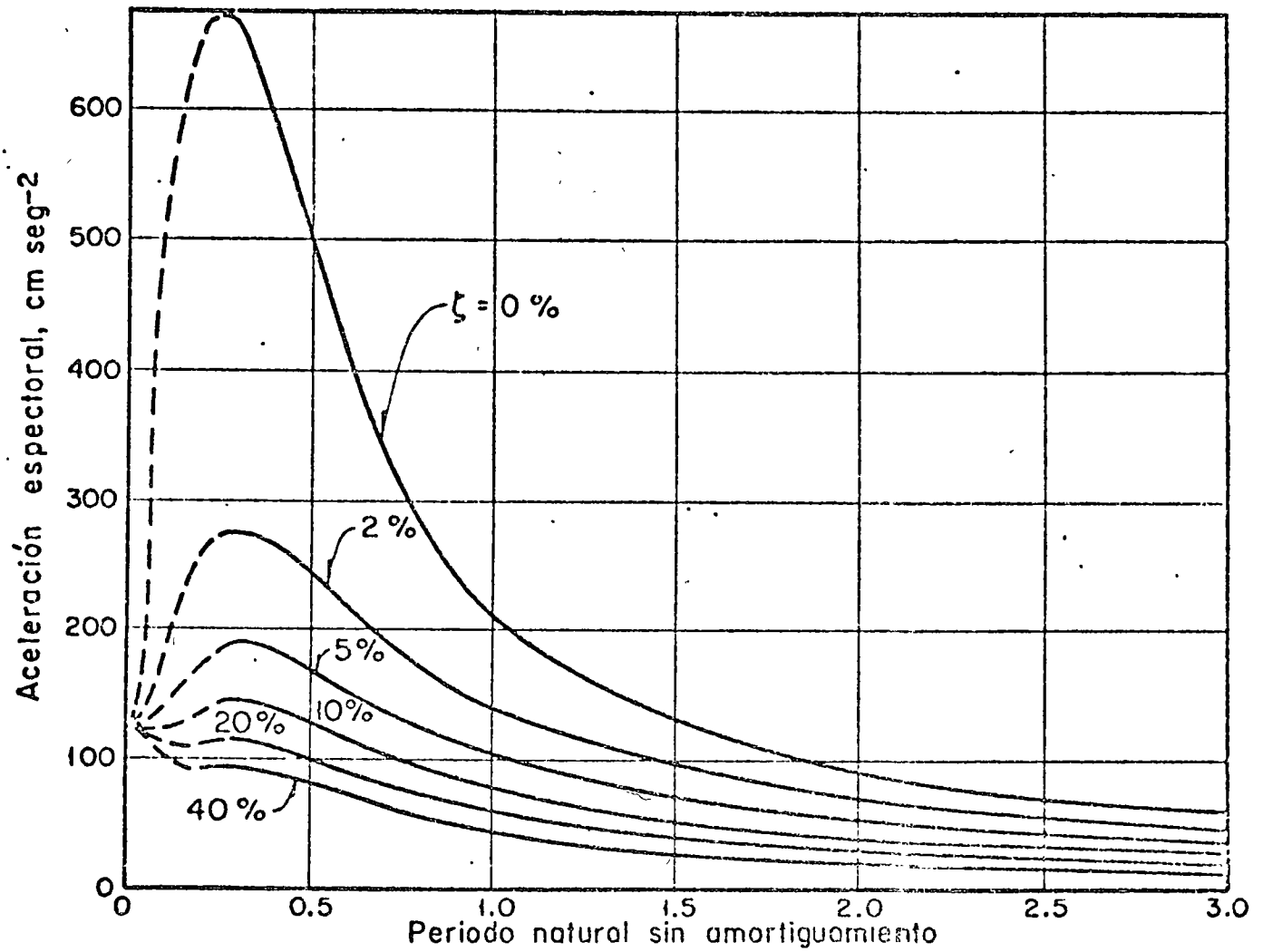

Fig. 16 Espectros de la aceleración media normalizada para los temblores de California
(Según G.W. Housner)

TRAZO DE ESPECTROS DE DISEÑO ELASTICO

RECORDEMOS QUE LA ECUACION QUE RELACIONA LAS ORDENADAS ESPECTRALES SUAVIZADAS PARA UN AMORTIGUAMIENTO ζ CON EL DE AMORTIGUAMIENTO NULO ES

$$\frac{D_\zeta}{D_o} = \frac{A_\zeta}{A_{\zeta=0}} = \left(1 + 3.77 \frac{\zeta S}{T}\right)^{-0.45} = R_\zeta \qquad (1)$$

DONDE S = DURACION DEL SISMO = $0.04e^{0.74M}+0.3R$

ζ = RELACION DE AMORTIGUAMIENTO

T = PERIODO NATURAL

CONSIDERANDO QUE EL ESPECTRO PARA $\zeta = 0.20$ COINCIDE EN PROMEDIO CON LAS LINEAS QUE DEFINEN LA ENVOLVENTE DEL MOVIMIENTO DEL SUELO SE TIENE QUE

DE (1): $A_{\zeta=0} = R_{0.20}\, A_{0.20}$ (2)

SUSTITUYENDO LA EC. (2) EN LA (1) SE PUEDE OBTENER EL ESPECTRO PARA CUALQUIER VALOR DE ζ

$$A_\zeta = (R_{0.20}\, A_{0.20})\left(1 + 3.77 \frac{\zeta S}{T}\right)^{-0.45} \qquad (3)$$

PARA ESPECTROS ELASTOPLASTICOS DE DISEÑO BASTA CON DIVIDIR EL ESPECTRO ELASTICO ENTRE μ O ENTRE $\sqrt{2\mu - 1}$, SEGUN EL CRITERIO QUE SE ELIJA PARA ELLO.

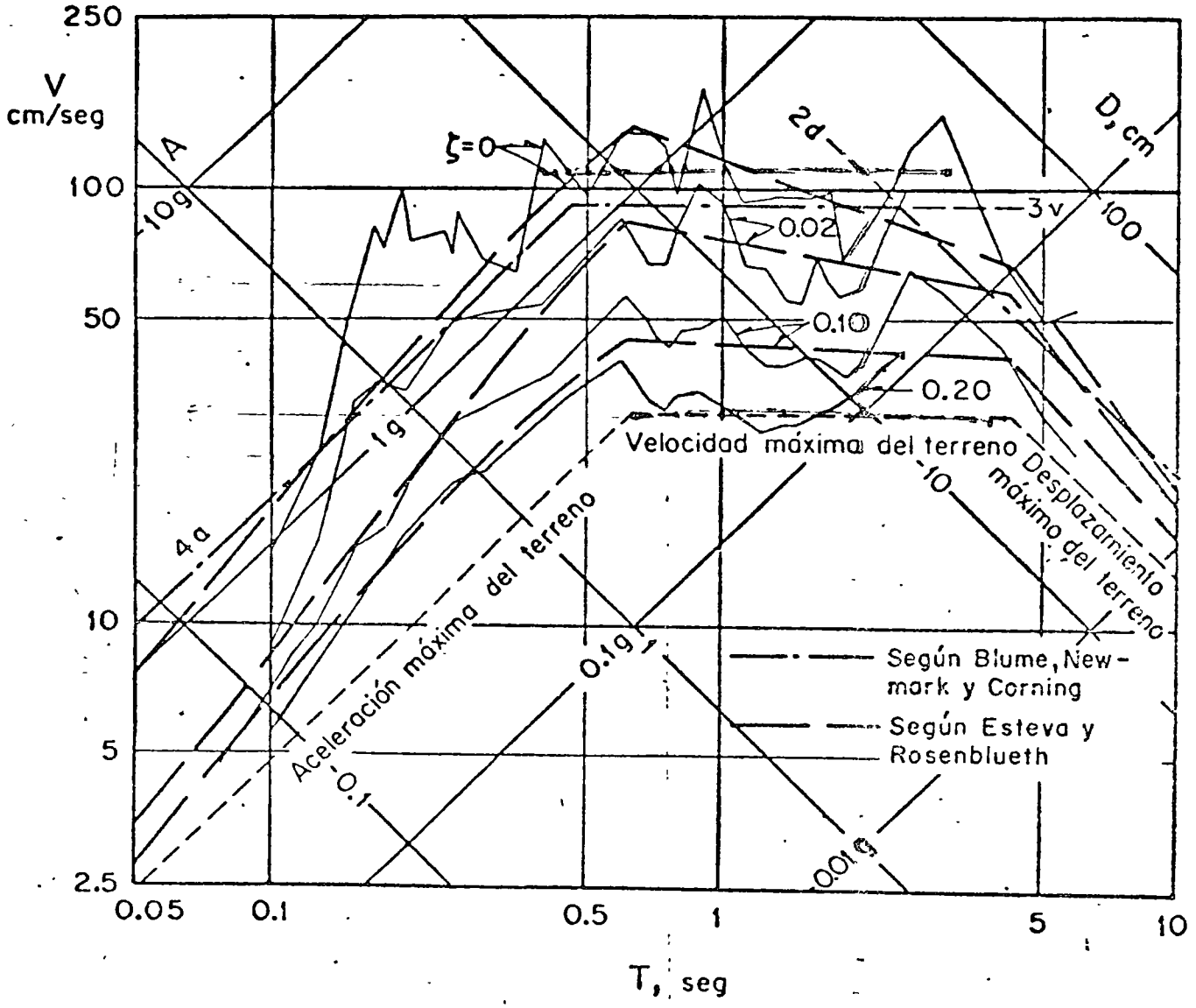

Relación entre movimiento del terreno y ordenadas espectrales

Tomada de: Regionalización Sísmica de México para fines de Ingeniería por L. Esteva, Informe 246, Instituto de Ingeniería, UNAM (abr. 1970)

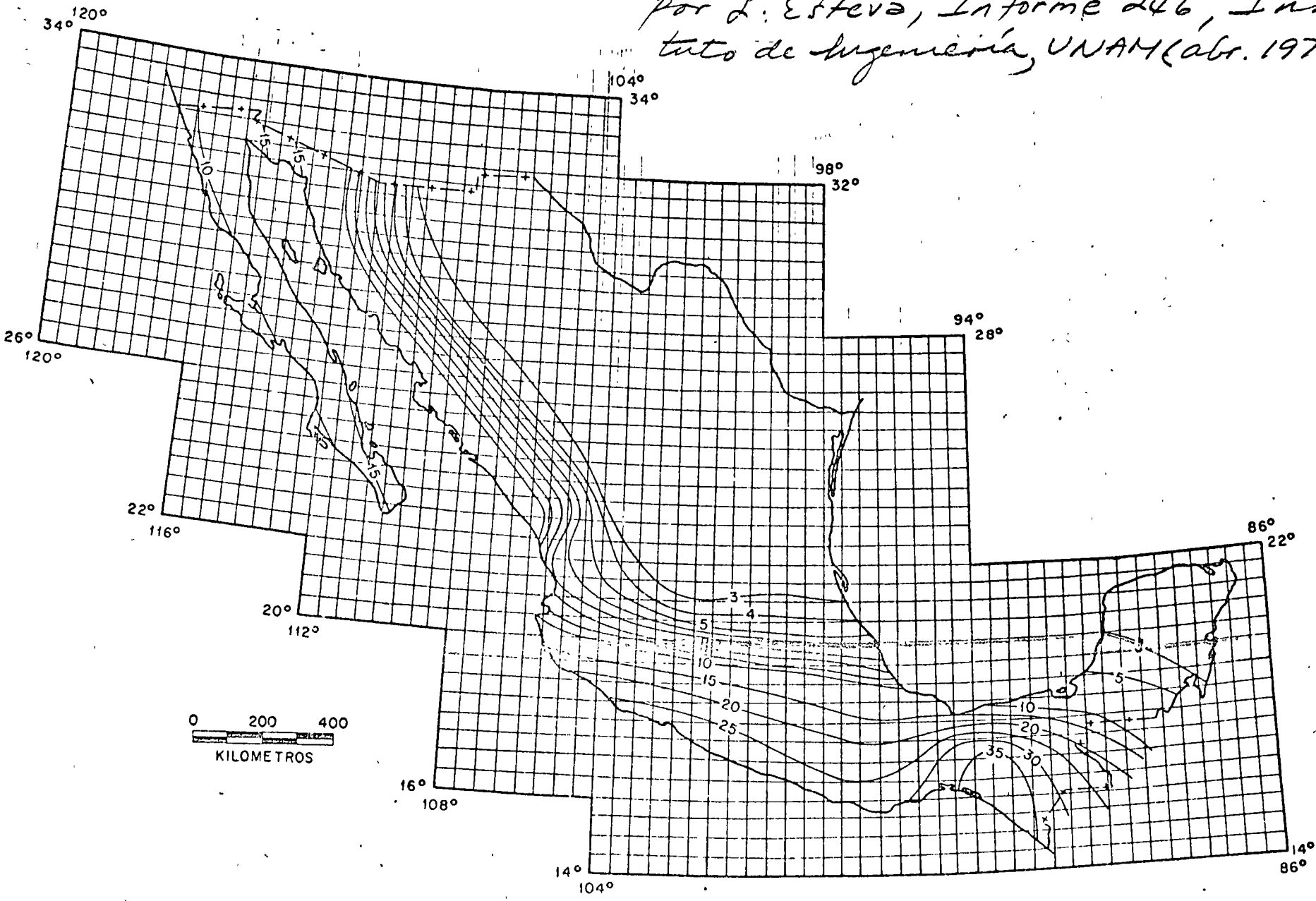

Fig 3. Velocidades máximas del terreno con periodo de recurrencia igual a 50 años

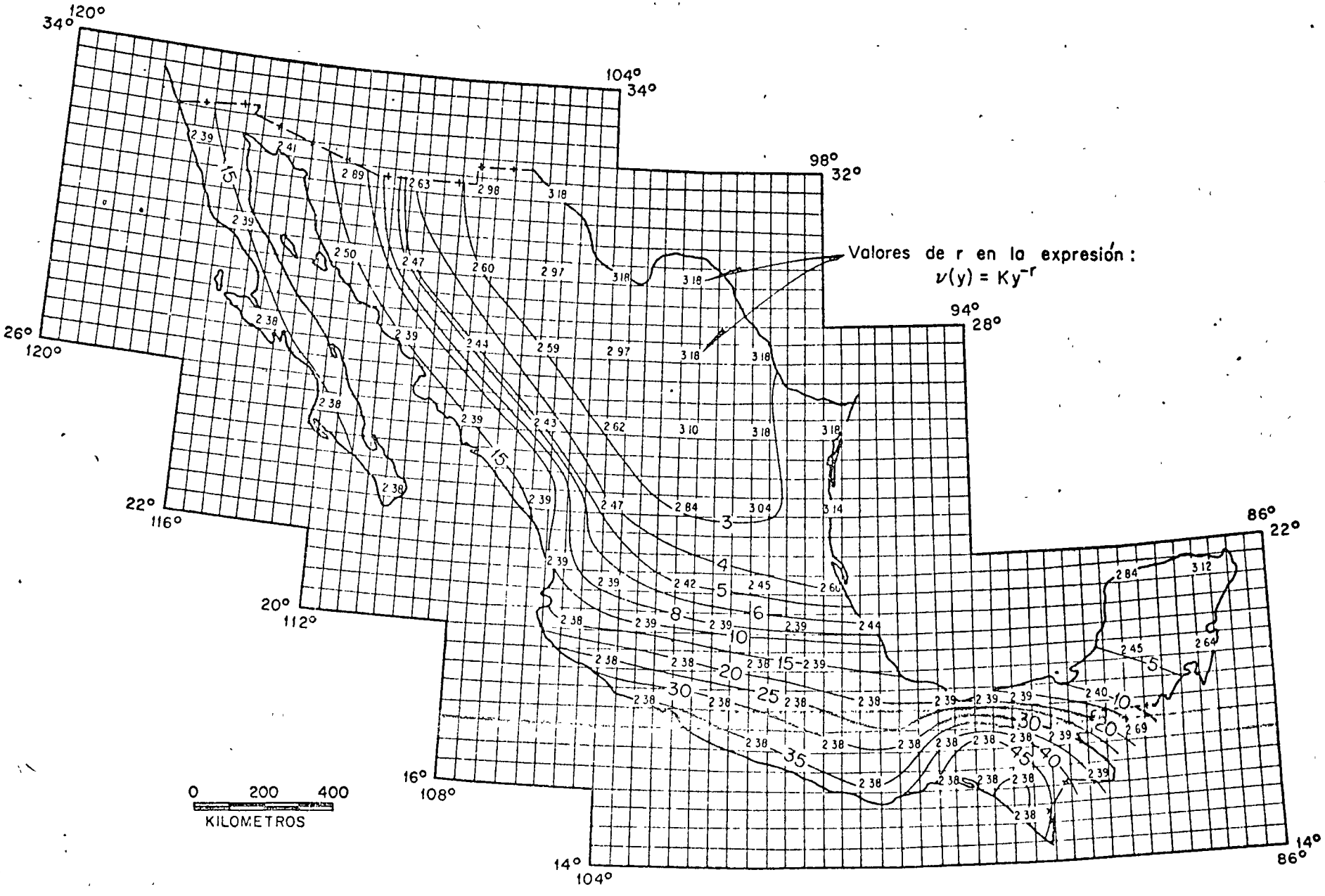

Fig 4. Velocidades máximas del terreno con periodo de recurrencia igual a 100 años

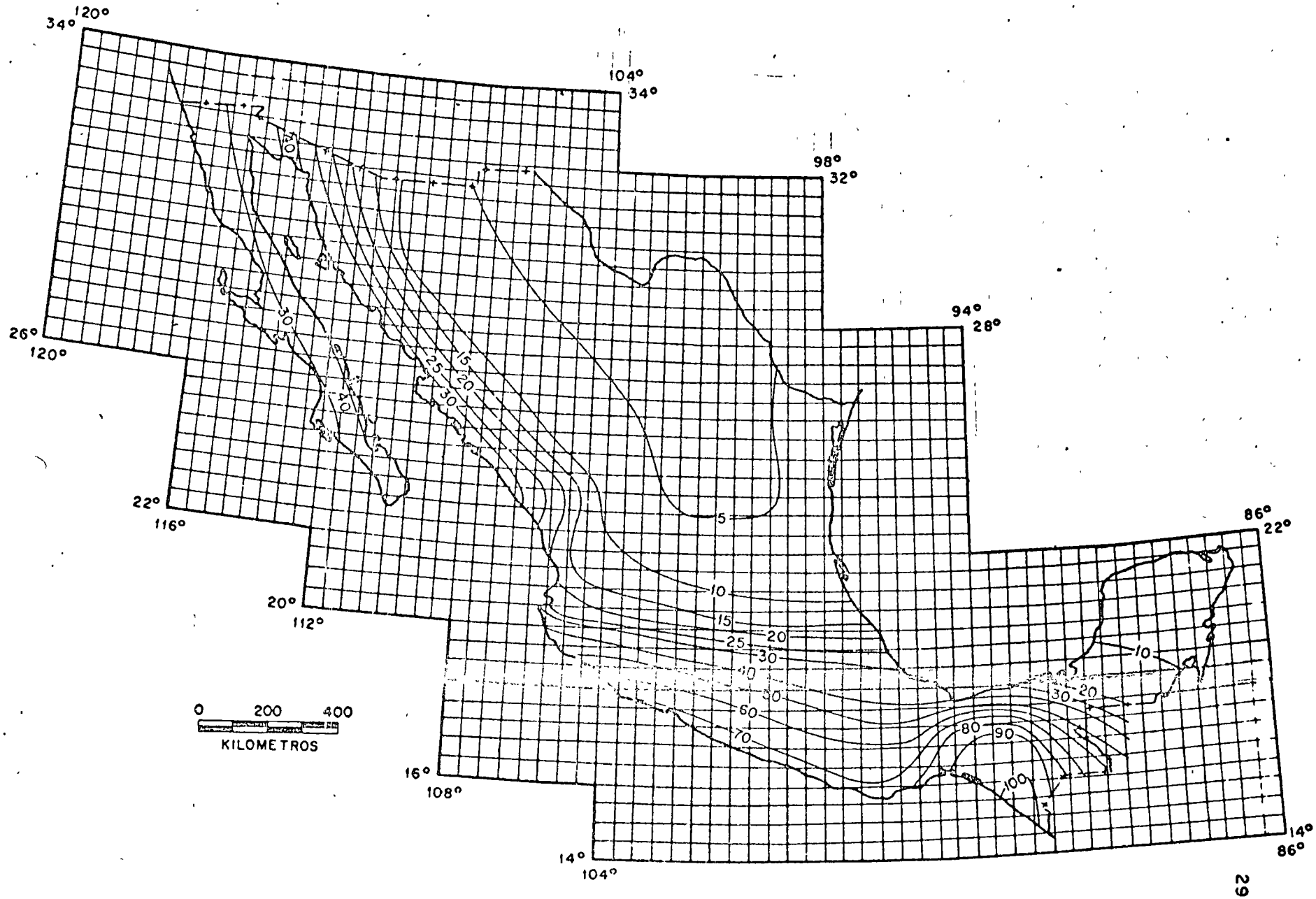

Fig 5. Velocidades máximas del terreno con periodo de recurrencia igual a 500 años

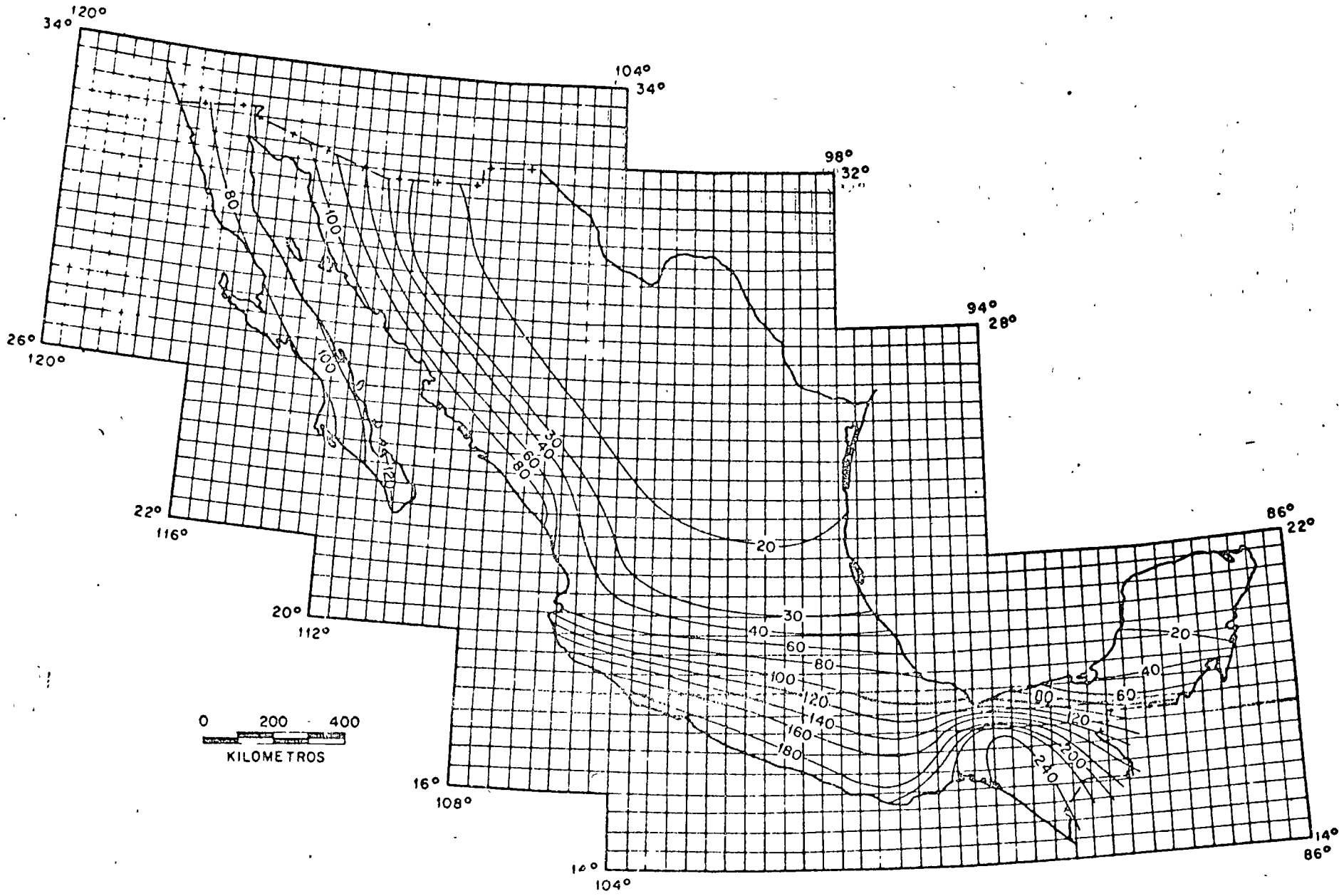

Fig 6. Aceleraciones máximas del terreno con periodo de recurrencia igual a 50 años

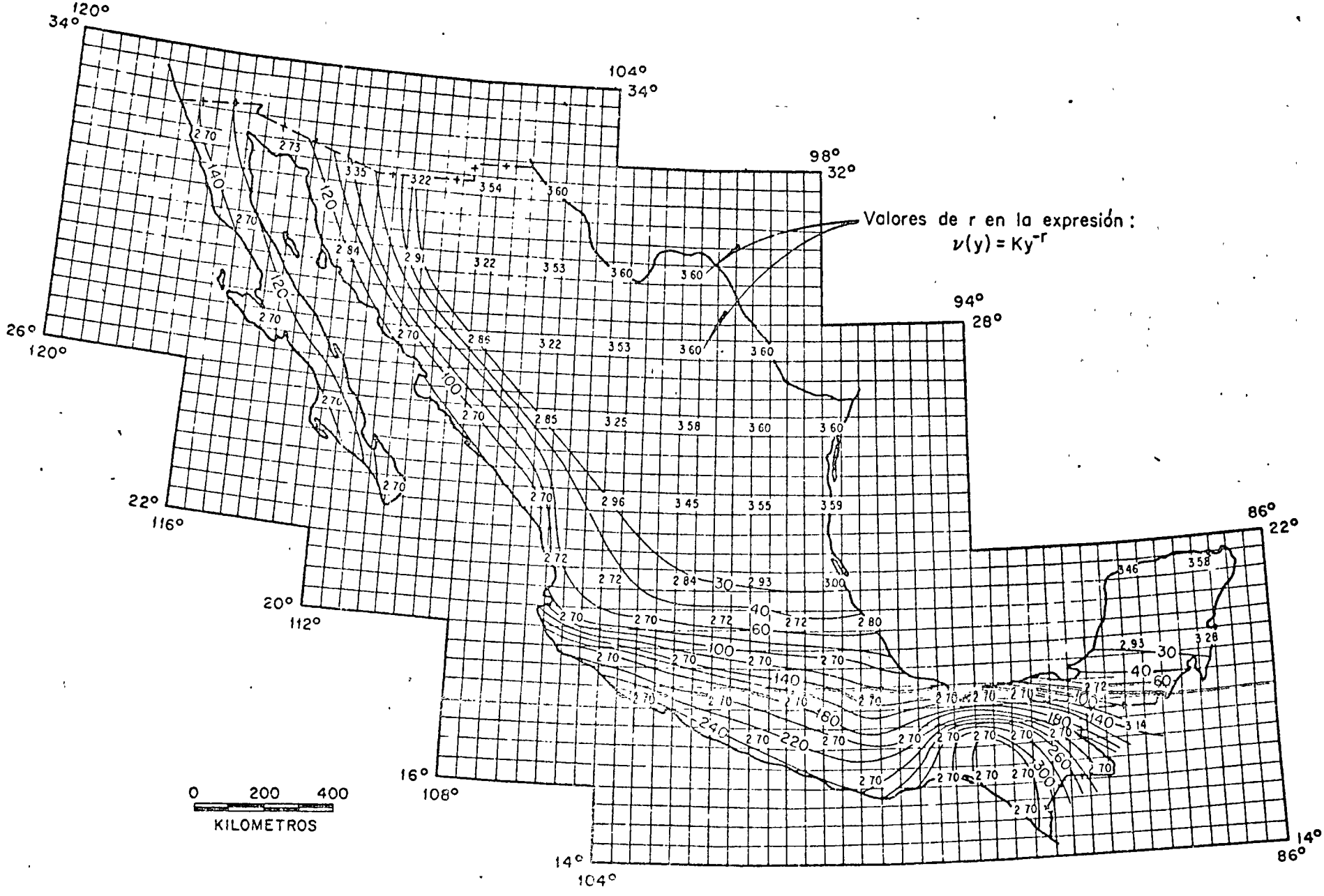

Fig 7. Aceleraciones máximas del terreno con período de recurrencia igual a 100 años

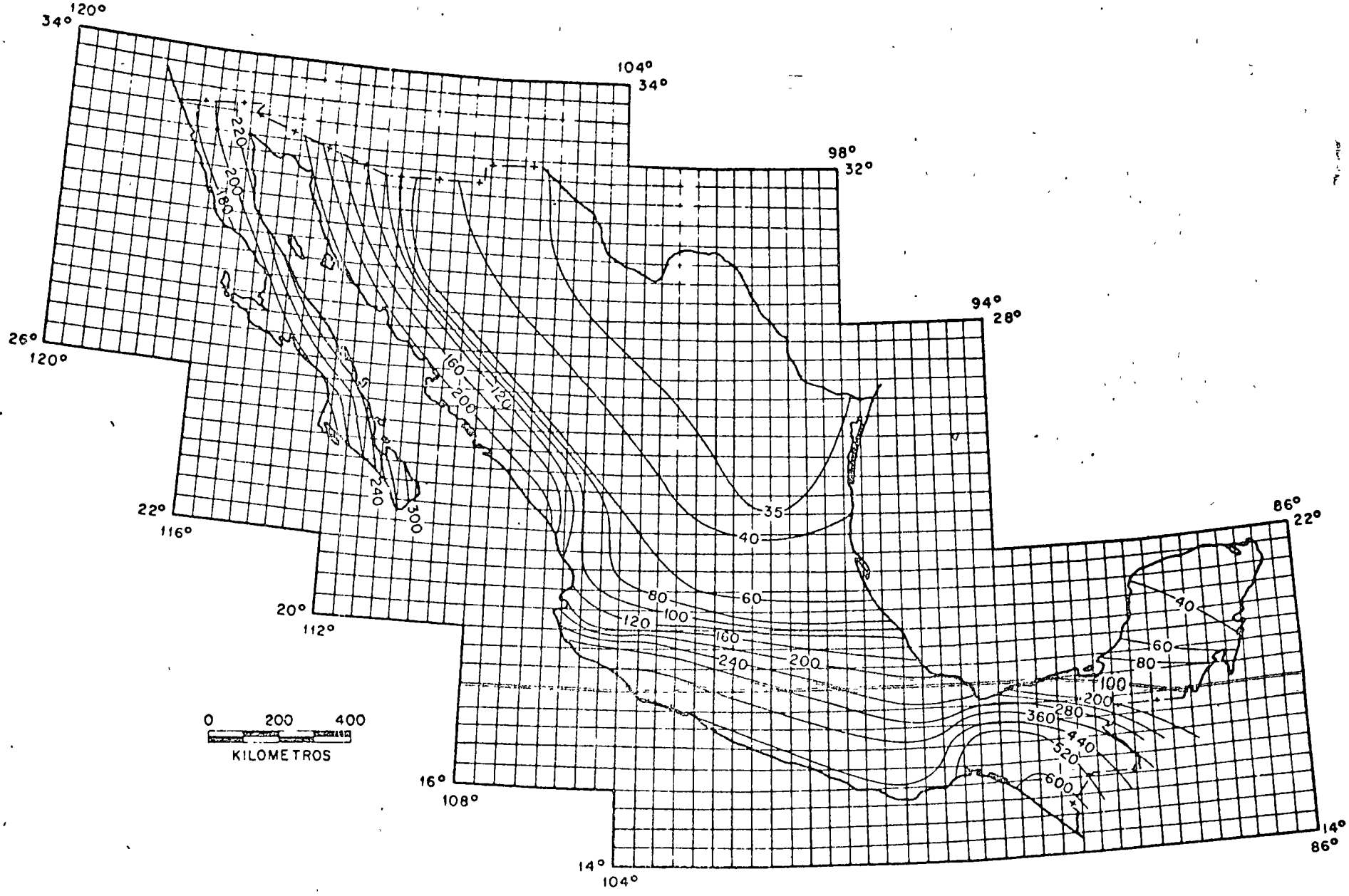

Fig 8. Aceleraciones máximas del terreno con periodo de recurrencia igual a 500 años

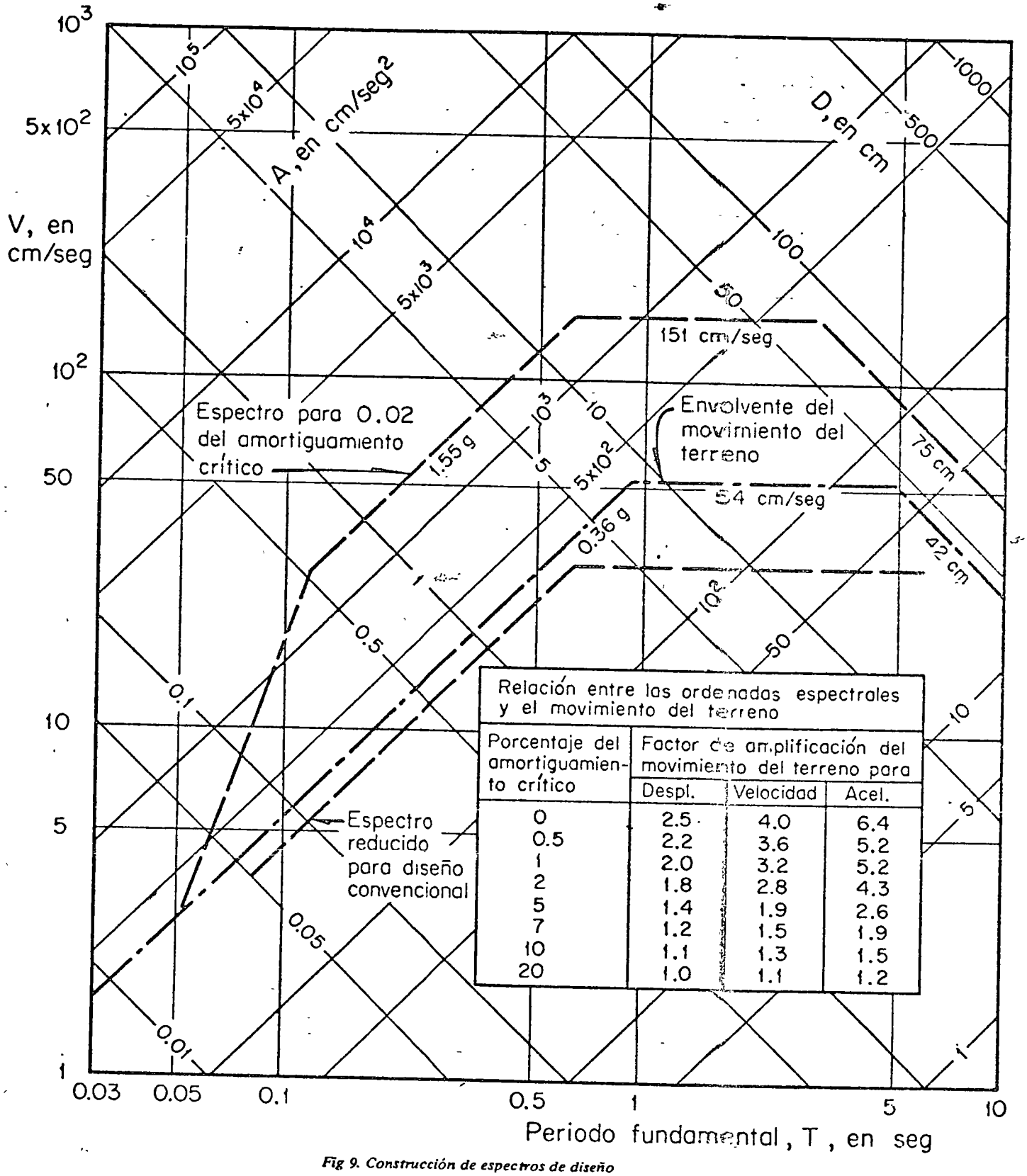

Fig 9. Construcción de espectros de diseño

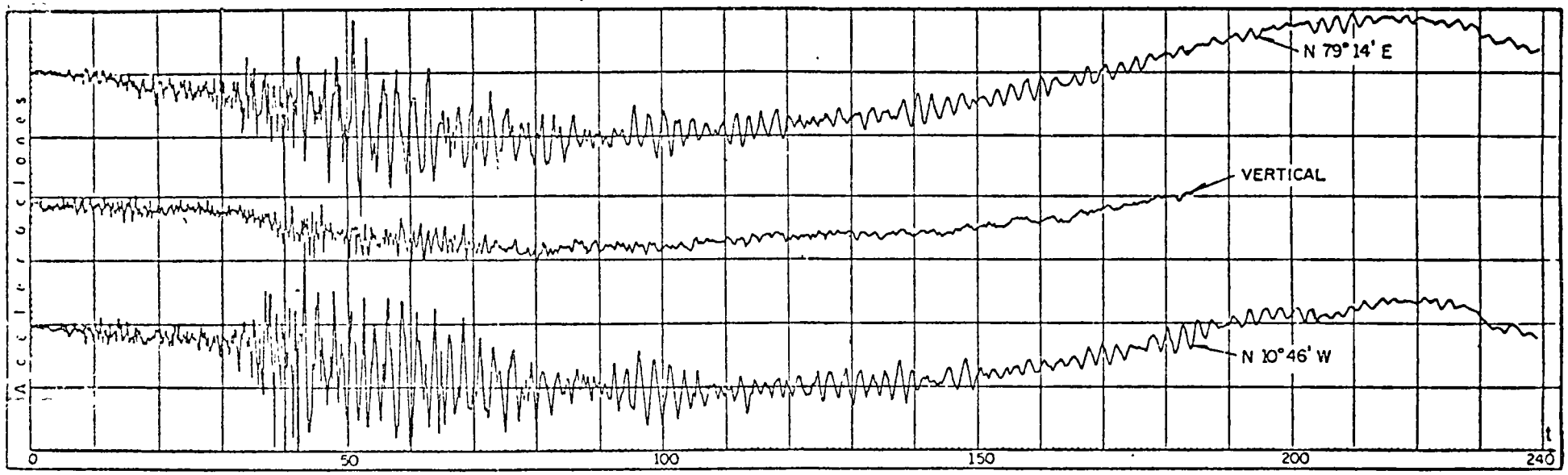

Fig 1 . Acelerogramas originales del sismo registrado el 11-V-1962 en la ALAMEDA CENTRAL, Méx, D. F.

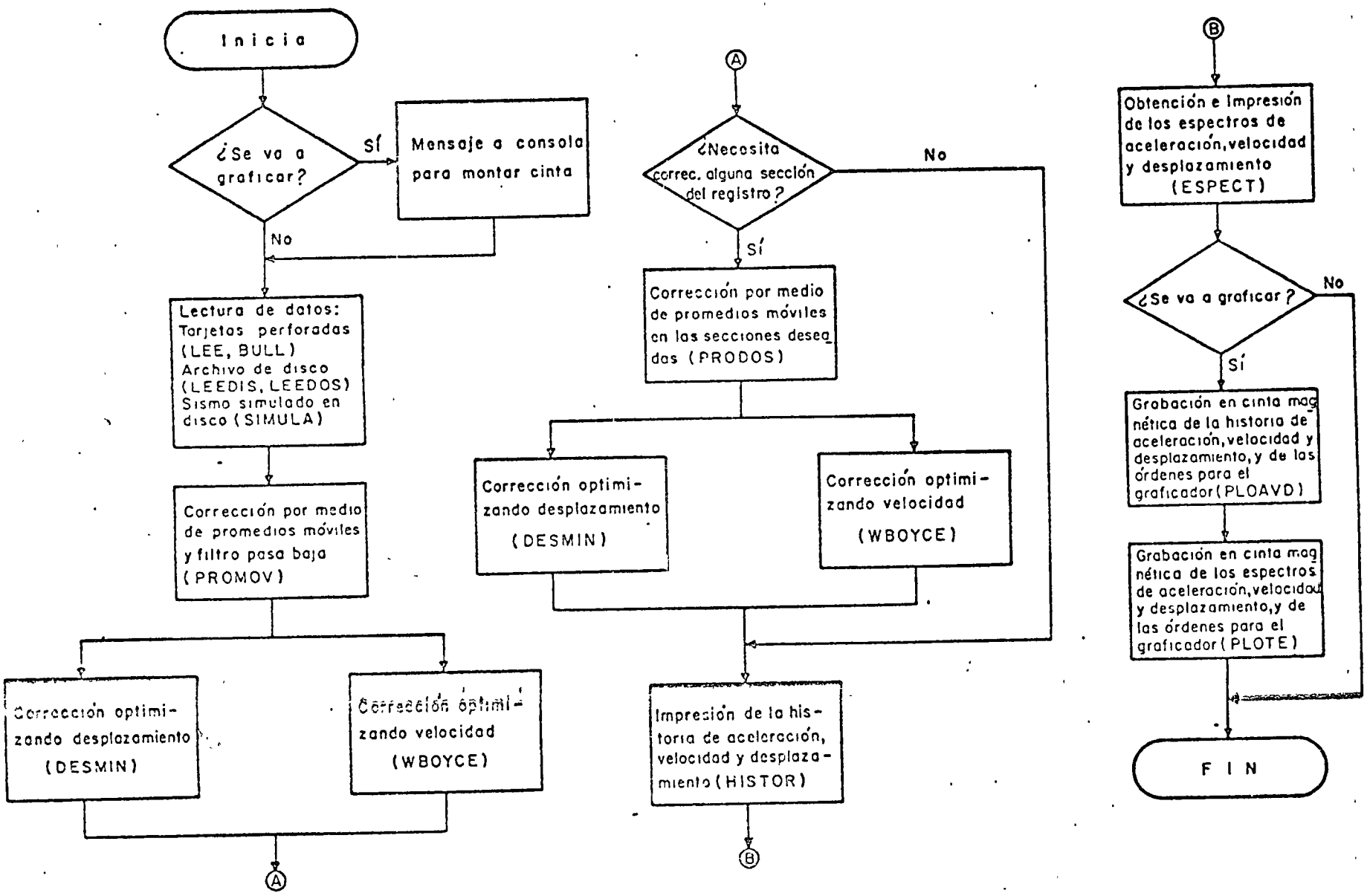

Fig 3 Diagrama de flujo del programa para computadora

Una explicación breve de los pasos del método es:

1. Interpolar el acelerograma a intervalos de tiempo constantes, Δt. Para registros en terreno duro se tomó $\Delta t=0.02$; para suelo blando, $\Delta t=0.04$ seg.

2. Trasladar la línea base original hasta situarla a la altura de la aceleración media nula, restándole a cada ordenada el promedio aritmético de todas las aceleraciones.

3. Diezmar el registro reteniendo 1 de cada N puntos con objeto de reducir el tiempo de computadora empleado para la corrección. El valor de N depende del contenido de frecuencias que visualmente se puedan detectar en el registro. Así, para los acelerogramas registrados en terreno duro se tomó N=5, y en blando, N=3, es decir los nuevos incrementos del tiempo fueron $\Delta t=0.1$ y 0.12 seg, respectivamente.

4. Obtener una línea base preliminar, $\ell_1(t_i)$, eliminando parcialmente las ondas de alta frecuencia del acelerograma mediante el empleo de promedios móviles de orden n (ref 13). En todos los casos se usó n=25, con lo cual se eliminó parte de las ondas de periodos menores de $25 \times 0.1 = 2.5$ seg en registros obtenidos en terreno duro, y $25 \times 0.12 \doteq 0.3$ seg, en terreno blando.

5. Obtener una nueva línea base, $\ell_2(t_i)$, pasando a $\ell_1(t_i)$ por el filtro digital de Ormsby (ref 14), con frecuencia de corte de 0.07 Hz, con el cual se eliminan casi por completo las ondas con periodos menores de 16 seg.

6. Interpolación de $\ell_2(t_i)$ a cada Δt original. La línea base resultante se denotará con $\ell_3(t_i)$.

7. Calcular el acelerograma corregido, restándole al obtenido en el punto 3 la línea base $\ell_3(t_i)$. Por lo tanto, este nuevo acelerograma casi no contendrá ondas con periodos mayores de 16 seg, que son las que se pretende eliminar, de acuerdo con lo descrito en capítulos anteriores.

8. Ajustar una nueva línea base al acelerograma mediante una parábola de segundo orden, tomando velocidad inicial diferente de cero, tal como se describe en la ref 12. El acelerograma resultante se denotará $a_5(t_i)$.

9. Obtener las velocidades y desplazamientos del terreno integrando el acelerograma una o dos veces, respectivamente, y el espectro de respuesta para amortiguamiento nulo.

10. Graficación automática de los acelerogramas y las funciones calculadas en el punto anterior.

11. Analizar las gráficas para juzgar si la corrección es adecuada. En caso de que la oscilación de las aceleraciones a todo lo largo del registro sea alrededor de la línea base, se puede considerar que la corrección es aceptable y pasar al punto 16. Si no sucede así, sino que aparece al principio o final un tramo que evidentemente no quedó bien corregido, como ocurre en la fig 2, entonces

...

hay que pasar al punto 12. Esto se puede confirmar observando también los tiempos en los cuales ocurrieron las aceleraciones espectrales correspondientes a periodos largos (mayores de 5 seg, por ejemplo).

12. Obtener promedios móviles de orden N' en los tramos que se juzga que la corrección no fue adecuada, en donde N' se escoge a criterio de la persona que procesa los datos, y se fija de manera de no eliminar ondas de periodos que obviamente no son espurios. En los casos aquí presentados, en que hubo necesidad de aplicar este paso, se usó N'=101 cuando se requirió esta corrección adicional en el tramo inicial del registro, o N'=251, cuando se requirió al final (se empleó Δt=0.04 seg). Este proceso conduce a una nueva línea base, $\ell_4(t_i)$.

13. Calcular el acelerograma nuevo, $a_6(t_i)$, restándole al anterior, $a_5(t_i)$, la línea base $\ell_4(t_i)$.

14. Ajuste parabólico igual al del punto 8; el acelerograma resultante se denota $a_7(t_i)$.

15. Cálculo y graficación de las nuevas velocidades y desplazamientos del terreno. Repetición del paso 11.

16. Cálculo y graficación de los espectros de respuesta para periodos, T, desde 0.1 hasta 10 seg, y fracciones de amortiguamiento 0, 0.02, 0.05, 0.10 y 0.20.

En la fig 3 se presenta el diagrama de flujo de este procedimiento.

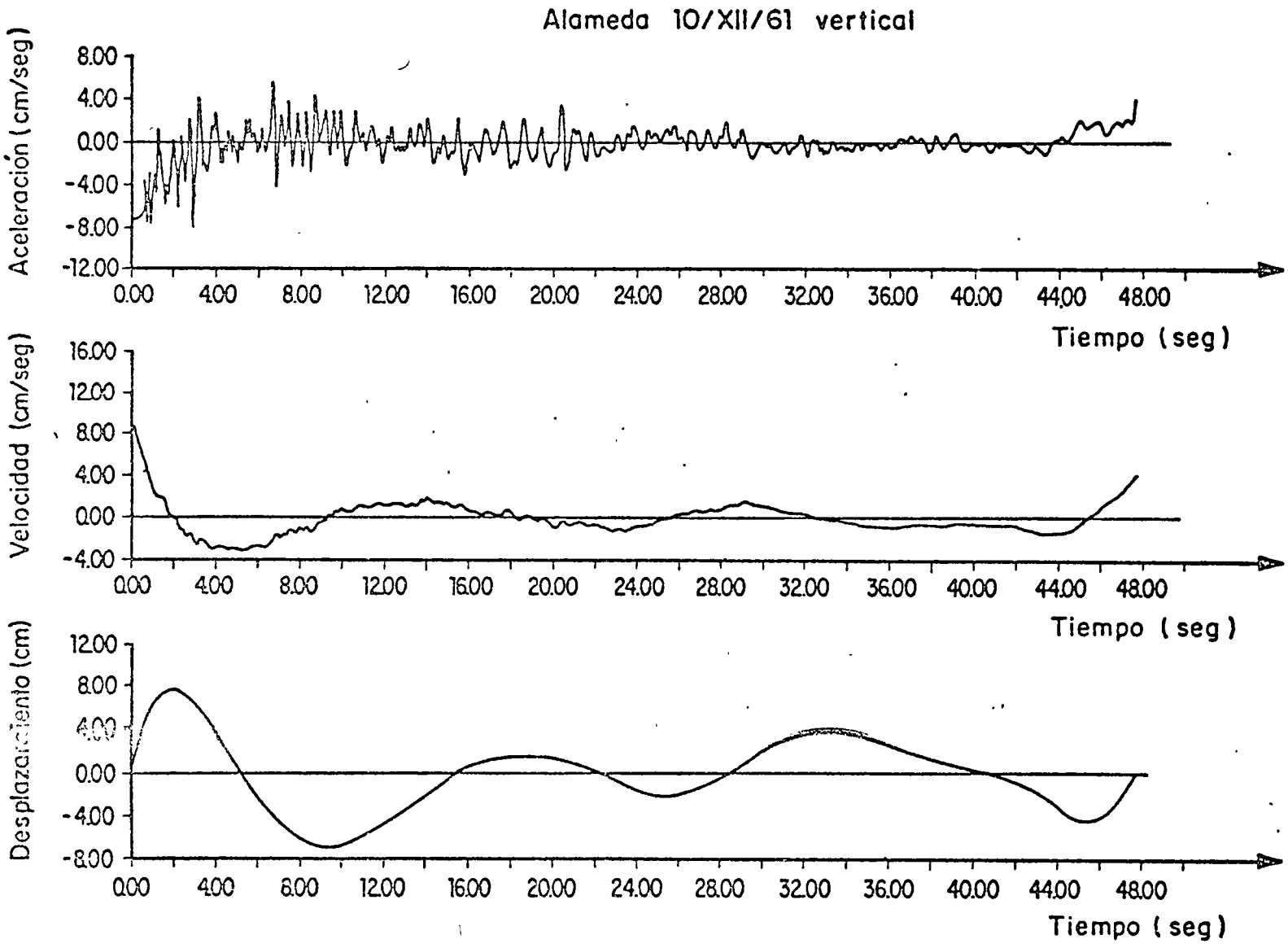

Fig 2 Acelerograma que requiere corrección adicional en sus extremos

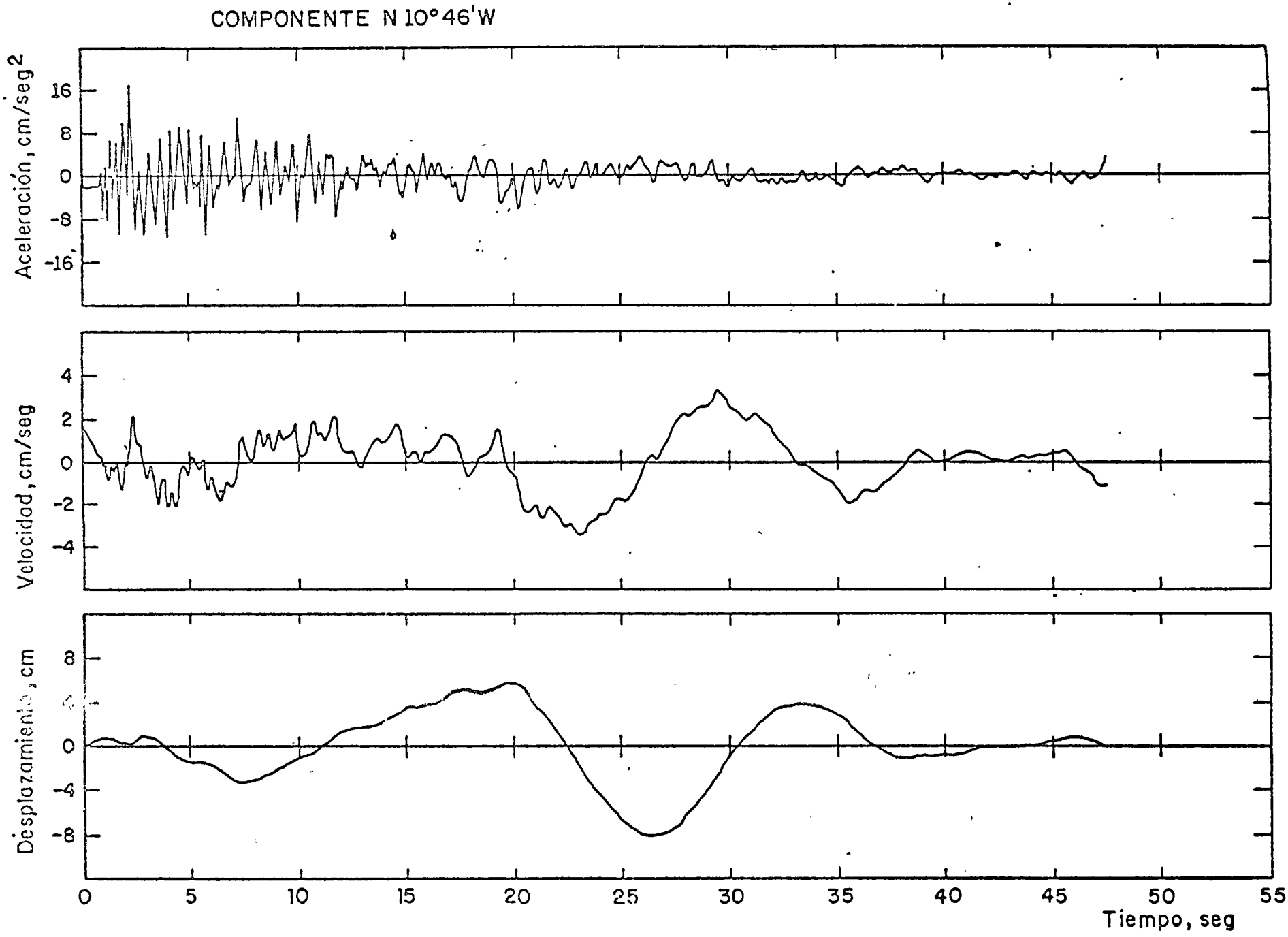

Fig 4 Movimiento del terreno. Alameda Central. 10 de diciembre de 1961

CLASIFICACION DE TEMBLORES:

1. REGISTRADOS EN TERRENO DURO Y DE PROFUNDIDAD FOCAL Y MAGNITUD PEQUEÑAS.

2. REGISTRADOS EN TERRENO DURO O ROCA, DE PROFUNDIDAD Y DISTANCIA FOCAL GRANDE Y DE MAGNITUD GRANDE.

3. REGISTRADOS EN TERRENO BLANDO Y DISTANCIA FOCAL Y MAGNITUD GRANDES.

4. REGISTRADOS EN SITIOS CON CONDICIONES DEL SUELO ALTAMENTE INELASTICAS (LICUACION DE ARENA, POR EJEMPLO)

1.3 Características de los temblores

Cualquiera que sea el origen de los temblores, se generan ondas que pueden clasificarse en dos grupos principales: ondas de cuerpo y ondas superficiales. Esta clasificación se basa en la forma de transmisión a través de la tierra: las ondas de cuerpo producen desplazamientos ya sea en la dirección de propagación (ondas P) o en dos direcciones mutuamente perpendiculares, normales a la dirección de propagación (ondas S); las ondas superficiales se transmiten a lo largo de los planos de frontera entre dos medios (Bullen, 1963).

Debido a que la velocidad de propagación de los diversos tipos de onda son diferentes, los sismogramas (gráficas de desplazamiento del terreno contra tiempo) muestran mas o menos definido el arribo de tres fases principales de ondas que dependen del mecanismo de generación y de su transmisión a través de medios estratificados con fronteras irregulares.

La contribución de las ondas superficiales a la aceleración del terreno es pequeña y, por tanto, el efecto principal sobre buena parte de las estructuras se debe a las ondas de cuerpo. Las ondas superficiales son, sin embargo, muy importantes en trabajos de sismología tales como el estudio de disipación de energía y de mecanismos de temblores.

Puede demostrarse que para una relación de Poisson del medio igual a 0.25, las ondas P viajan con una velocidad 1.7 veces la de las ondas S, la cual es del orden de 3.5 km/seg en la corteza terrestre (Housner, 1962).

Aun cuando la parte intensa de los temblores consiste en

movimientos muy irregulares, ha sido posible encontrar ciertas características comunes para algunos de ellos permitiendo una clasificación general en cuatro grupos (Newmark y Rosenblueth, 1968):

1. Temblores de corta duración
2. Movimientos extremadamente irregulares de duración moderada
3. Temblores de larga duración con periodos dominantes de vibración
4. Movimientos del terreno produciendo grandes deformaciones permanentes del suelo y/o grandes ondas de agua.

Esta clasificación no implica que no puedan ocurrir sismos con características intermedias o que condiciones locales no originen un movimiento con características diferentes a las esperadas.

A continuación nos referiremos a esos grupos como tipo 1, 2, 3, ó 4, respectivamente.

Tipo 1. Temblores de corta duración. Registros de este tipo son típicos de temblores poco profundos y de pequeña magnitud registrados sobre terreno duro a distancias epicentrales muy cortas (el término "terreno duro" tiene una interpretación bastante general y no necesariamente se refiere a rocas; la distinción se hace principalmente con respecto a suelos suaves estratificados, tales como el del Valle de México). Cuando esta condición no se cumple, las reflexiones múltiples de las ondas cambian la naturaleza del movimiento (Herrera, Rosenblueth y Rascón, 1965). Ejemplos son los temblores de Puerto Hueneme (1957), Agadir (1967), Libia (1963), Skopje (1963), San Salvador (1965) y el de Parkfield, California (1966). Todos ellos han tenido magnitudes de 4.7 a 6.2 y han mostrado mayor intensidad en una dirección. Para mayor información acerca de estos temblores ver Housner y Hudson (1958), Despeyroux (1960) Minami

(1965), Ambraseys (1964), Rosenblueth y Prince (1965), y Housner y Trifunac (1967).

En el temblor de Parkfield se observó mayor intensidad del movimiento del suelo en dirección casi perpendicular a la de la falla en las estaciones localizadas a distancias menores de 6.5 km. Esto puede explicarse en parte por la configuración espacial de las ondas S generadas por un mecanismo de doble par a los puntos cerca de los planos de falla (fig 1.1). Las figs 1.2 y 1.3 muestran el acelerograma y el registro de sismoscopio obtenidos en la estación situada a solo 60 m de la línea de falla. En este sitio la aceleración máxima del terreno fue del orden de la mitad de la aceleración de la gravedad, siendo la mayor que se haya medido durante un sismo. Este temblor fue registrado en doce estaciones situadas en una línea perpendicular a la línea de falla; la fig 1.4 muestra el acelerograma registrado en la estación situada a 16 km de la falla. Se observa que la naturaleza del movimiento cambió radicalmente y puede considerarse del tipo 2.

Newmark y Rosenblueth (1968) han calculado la respuesta de sistemas lineales a excitaciones de este tipo representadas por funciones prescritas del tiempo, especificadas por algunos parámetros tales como su máxima aceleración o velocidad.

Tipo 2. Movimientos extremadamente irregulares de duración moderada. Movimientos de esta clase se asocian con distancias focales moderadas y se registran sobre terreno duro; un ejemplo clásico es el temblor de El Centro, California, 1940, (fig 1.5). La parte intensa de las excitaciones es mayor que las del tipo 1. Sismos de esta clase ocurren con mayor frecuencia que los otros por lo cual existen mas re-

gistros disponibles y han sido mejor estudiados. Filtrando este tipo de perturbaciones a través de medios estratificados es posible obtener excitaciones del tipo 3.

Existen diferencias bien definidas entre las formas de los espectros suavizados obtenidos para diferentes distancias focales; estas diferencias dan idea del contenido relativo de ondas de diferentes frecuencias del movimiento. La fig 1.6 muestra los espectros suavizados para tres distancias focales diferentes; se observa que a distancias focales pequeñas las estructuras con periodos naturales cortos son mas afectadas que las de periodos naturales largos (Housner, 1965).

En la fig 1.7 se muestran los espectros medios suavizados calculados por Housner (1961). Los promedios se calcularon después de normalizar cada espectro en tal forma que los no amortiguados tuvieran la misma ordenada media. Estos espectros medios han sido utilizados por diferentes autores para ajustar los resultados obtenidos de modelos de simulación de sismos.

En el capítulo 4 se muestran algunas diferencias cualitativas entre los registros obtenidos en diferentes sitios y direcciones, relativos a la posición de la falla que origina el sismo.

El tipo 2 de movimiento del suelo ha sido el mas susceptible de idealizaciones como procesos estocásticos. En este trabajo se simularán registros de esta clase de excitación.

Tipo 3. Temblores de larga duración con periodos dominantes de vibración. Esta clase de movimientos resulta de filtrar temblores del tipo 2 a través de suelos suaves estratificados, con la concurrencia de las ondas múltiplemente reflejadas y refractadas (Kobagashi y Kagami,

1966); esta es la razón por la que se obtienen registros de mayor duración que los del tipo 2; como ejemplo se muestra en la fig 1.8 un registro obtenido en la zona de alta compresibilidad de la ciudad de México. Herrera y Rosenblueth (1965) y Herrera, Rosenblueth y Rascón (1965) han realizado estudios analíticos de este tipo de perturbación para suelos de comportamiento lineal o casi lineal.

La existencia de periodos dominantes largos puede verse en las densidades espectrales calculadas por Arias y Petit-Laurent (1964) para algunos temblores registrados en las ciudades de México, México y Seattle, Washington.

Tipo 4. Movimientos del terreno produciendo grandes deformaciones permanentes en el suelo y/o grandes ondas de agua. Grandes ondas de agua, deslizamientos del suelo y/o licuefacción del terreno son causadas por este tipo de exictación. Algunos ejemplos son los temblores ocurridos en Valdivia y Puerto Montt, Chile en 1967 (Rosenblueth, 1961), en Anchorage, Alaska en 1964 (Seed, 1966) y en Niigata, Japón en 1964 (Falconer, 1964). Es impráctico diseñar estructuras para soportar tales fenómenos; lo mejor que puede hacerse es construir donde la probabilidad de que ocurran es pequeña, o tratar el suelo antes de la construcción para evitar fallas locales.

1.4 Antecedentes sobre idealización y simulación de temblores

1.4.1 Procesos estocásticos. Antes de entrar a la revisión de trabajos previos sobre idealización y simulación de temblores intensos, es conveniente dar un breve resumen de los conceptos de teoría de probabilidades que serán utilizados posteriormente. La mayoría del material de esta sección fue obtenido de los trabajos de Crandall

y Mark (1963) y de Newmark y Rosenblueth (1968).

Muchos fenómenos se caracterizan por cambios imprevisibles con el tiempo, los cuales no pueden describirse antes de que ocurran. Sin embargo, si el mismo fenómeno ocurre varias veces, podría encontrarse una cierta regularidad estadística entre los resultados pudiéndose describir mediante un conjunto de distribuciones de probabilidad y/o estimarse las esperanzas de algunas características del proceso.

Sea X_i (t) una función real del tiempo t, e i un índice que identifica una función particular. El conjunto infinito de funciones X_i t) constituirá un proceso estocástico si no podemos predecir sus valores en ningún tiempo. Por tanto, un proceso estocástico es un conjunto infinito de funciones individuales descritas por un conjunto de distribuciones de probabilidades. El proceso define una variable aleatoria x (t), para cada tiempo fijo t_k. En particular, si para cualquier colección finita de tiempos t_k, las variables aleatorias $x(t_k)$ pertenecen a una distribución conjunta gausiana con valores medios iguales a cero, entonces se dice que el proceso estocástico es gausiano.

Esperanza. Sea $g(x_k)$ una función de la variable aleatoria $x_k = x(t_k)$. La esperanza (promedio a lo largo del conjunto infinito de funciones individuales) de $g(x_k)$ es, por definición,

$$E[g(x_k)] = \int_{-\infty}^{\infty} g(x_k)\,\phi(x_k)\,dx_k$$

donde $\phi(x_k)$ es la distribución de probabilidades de primer orden de x_k y $E[\cdot]$ denota esperanza.

En particular, si $g(x_k) = x_k$,

$$E[x_k] = \int_{-\infty}^{\infty} x_k \phi(x_k) dx_k$$

se llama esperanza o valor medio de x_k. Si $g(x_k) = x_k^2$,

$$E[x_k^2] = \int_{-\infty}^{\infty} x_k^2 \phi(x_k) dx_k$$

es el valor medio cuadrático de x_k. Si $g(x_k) = (x_k - E[x_k])^2$ se obtiene

$$E[(x_k - E[x_k])^2] = \int_{-\infty}^{\infty} (x_k - E[x_k])^2 \phi(x_k) dx_k$$

Esta cantidad es llamada variancia de x_k y suele designarse por $\sigma^2[x_k]$

Puede demostrarse que

$$\sigma^2[x_k] = E[x_k^2] - E^2[x_k]$$

A $\sigma[x_k]$ y al cociente $\sigma[x_k]/E[x_k]$ se les conoce como desviación estándar y coeficiente de variación respectivamente.

Sea $f(x_j)$ otra función de la variable aleatoria $x_j = x(t_j)$. Por definición,

$$E[g(x_k) f(x_j)] = \int_{-\infty}^{\infty} \int_{-\infty}^{\infty} g(x_k) f(x_j) \phi(x_k, x_j) dx_k dx_j$$

donde $\phi(x_k, x_j)$ es la distribución de probabilidades conjunta de segundo orden de x_k y x_j. En particular, si $g(x_k) = x_k$ y $f(x_j) = x_j$, la esperanza

$$E[x_k x_j] = \int_{-\infty}^{\infty} x_k x_j \phi(x_k, x_j)\, dx_k\, dx_j$$

se llama función de autocorrelación de x_k y x_j.

Si $g(x_k) = x_k - E[x_k]$ y $f(x_j) = x_j - E[x_j]$, resulta

$$E[(x_k - E[x_k])(x_j - E[x_j])] = \int_{-\infty}^{\infty}\int_{-\infty}^{\infty} (x_k - E[x_k])(x_j - E[x_j])\, \phi(x_k, x_j)\, dx_k\, dx_j$$

$$= E[x_k x_j] - E[x_k]E[x_j]$$

que se conoce como covariancia de x_k y x_j. Si $E[x_k] = E[x_j] = 0$ la covariancia es igual a la autocorrelación. Cuando $t_k = t_j$ la covariancia se reduce a la variancia y la autocorrelación se hace idéntica al valor medio cuadrático.

Estacionaridad y ergodicidad. Se dice que un proceso estocástico es estacionario si sus distribuciones de probabilidades son invariantes bajo una traslación de la escala del tiempo; de otra forma el proceso se llama no estacionario. En un proceso estacionario la distribución de probabilidades de primer orden $\phi(x)$ del proceso, es independiente del tiempo esto implica que la esperanza y la variancia son también constantes); la distribución de probabilidades de segundo orden, $\phi(x_k, x_j)$, es solo función del intervalo entre t_k y t_j y no de los valores individuales de t_k y t_j.

Nótese que un proceso estrictamente estacionario no tiene

principio ni fin, esto es, cada muestra va desde $t = -\infty$ hasta $t = \infty$. Los efectos de no estacionaridad asociados al comienzo y final de un proceso a menudo se desprecian en la práctica si la duración de la fase sensiblemente estacionaria es larga en comparación con los intervalos del comienzo y final.

Un proceso estacionario se llama ergódico si sus promedios temporales a lo largo de cualquier muestra representativa son iguales a los promedios a lo largo del conjunto infinito de funciones individuales. Cuando es difícil, costoso o imposible obtener un número grande de funciones muestra, es común suponer que el proceso es ergódico, ya que esto permite estimar promedios a lo largo del conjunto infinito de muestras tomando simplemente los promedios con el tiempo de una sola muestra.

Análisis armónico. Una herramienta muy útil en el análisis de procesos estocásticos es el llamado análisis armónico de un proceso estocástico. Por definición, la función de autocorrelación de un proceso estocástico (Parzen, 1962) está dada por

$$R(\tau) = \int_{-\infty}^{\infty} e^{i\omega\tau} dF(\omega) \quad ; \quad -\infty < \tau < \infty$$

donde $i = \sqrt{-1}$, $\tau = t_j - t_k$ $(t_j > t_k)$, ω = frecuencia circular y, para cualquier par de frecuencias, $\omega_1 < \omega_2$, $F(\omega_2) - F(\omega_1)$ puede interpretarse como una medida de la contribución de la banda de frecuencias, $\omega_2 - \omega_1$ al contenido del proceso estocástico. Si $F(\omega)$ es diferenciable, su derivada, $S(\omega)$, se llama densidad espectral del proceso estocástico. En tal caso puede escribirse

$$R(\tau) = \int_{-\infty}^{\infty} e^{i\omega\tau} S(\omega)\, d\omega$$

Se puede demostrar que la densidad espectral y la función de autocorrelación forman un par de Fourier, esto es

$$S(\omega) = \frac{1}{2\pi} \int_{-\infty}^{\infty} e^{-i\omega\tau} R(\tau)\, d\tau$$

Si $\tau = 0$, $(t_j = t_k)$,

$$R(0) = \int_{-\infty}^{\infty} S(\omega)\, d\omega$$

y, por tanto, el valor medio cuadrático del proceso es igual a la suma, sobre todas las frecuencias, de $S(\omega)d\omega$, así que $S(\omega)$ puede interpretarse como una densidad espectral para el valor medio cuadrático. Se puede demostrar que $F(\omega)$ es una función par no negativa de ω.

De las definiciones dadas se deducen las siguientes conclusiones (Crandall y Mark, 1963):

a. Si el proceso no contiene ninguna componente periódica, $F(\omega)$ es finita para toda ω.

b. Si el proceso tiene una componente armónica de frecuencias ω_0, la densidad espectral de potencia deberá ser infinita en $\omega = \omega_0$. En particular, si el valor medio del proceso es diferente de cero entonces hay una componente de frecuencia cero, y el espectro tendrá un pico en $\omega = 0$.

Ruido de escopeta. Un ruido de escopeta es una serie de pulsos instantáneos (Parzen, 1964, Newmark y Rosenblueth, 1968)

$$X_k(t) = \sum_j a_j \delta(t - t_j)$$

donde a_j y t_j son variables aleatorias independientes y δ es la función delta de Dirac. Si la probabilidad de que un tiempo t_j caiga dentro de un intervalo de tiempo dt, es independiente de los tiempos t_j previos, la familia de $X_k(t)$ constituye un proceso de Poisson (ver apéndice). Si $E[a_j] = 0$ y los intervalos $t_{j+1} - t_j$ tienden a cero cuando la duración del movimiento y la intensidad por unidad de tiempo $E[a_j^2]/E[t_{j+1} - t_j]$ permanecen finitos, el tiro de escopeta tiende a un proceso gausiano. Cuando la intensidad por unidad de tiempo es constante el proceso es estacionario y el ruido de escopeta se llama ruido blanco.

El ruido blanco puede también considerarse como una superposición de un número infinito de ondas senoidales de diferentes frecuencias distribuidas uniformemente entre cero e infinito (esta es la razón del nombre del proceso). Esto puede inferirse analizando su densidad espectral la cual es una constante S_0, para todas las frecuencias y, por tanto, su función de autocorrelación es

$$R(\tau) = 2\pi S_0 \delta(\tau)$$

1.4.2 Antecedentes sobre idealización y simulación de temblores. Reconociendo la importancia de tener una técnica confiable para simular temblores útiles para el diseño estructural, algunos investigadores han desarrollado un conjunto de modelos analíticos y experimentales. Estos pueden clasificarse en una o mas de las siguientes formas

a. Superposición de ondas o pulsos

b. Ruido blanco

c. Ruido blanco filtrado

d. Ruido blanco no estacionario

APENDICE

PROCESOS DE POISSON

En este apéndice se hará un resumen de los procesos estocásticos de Poisson, que se usaron en el capítulo 4. El material de esta sección se tomó del libro de Parzen (1962) y de la tesis doctoral de Cornell (1964). Se estudiará el proceso de Poisson simple, y sus derivados, tales como el compuesto, el múltiple, el no homogéneo y el filtrado.

A.1 El proceso simple de Poisson

El proceso simple de Poisson es un proceso que registra el número de ocurrencias de un fenómeno aleatorio específico, durante un intervalo de tiempo.

Sea $N(t)$ el número de eventos que han ocurrido hasta el tiempo t. Una muestra del proceso $N(t)$, $t > 0$ se muestra en la fig A.1. Este proceso está basado en cuatro axiomas:

a. $N(0) = 0$

b. El proceso tiene eventos estocásticamente independientes

c. El proceso tiene eventos estacionarios

d. La ocurrencia simultánea de dos o mas eventos no puede suceder.

Su distribución de probabilidades está dada por:

$$p(k) = \text{probab}\left\{N(t) = k\right\} = \frac{(\nu t)^k e^{-\nu t}}{k!} \quad ; \quad t > 0 \qquad (A.1)$$

donde ν es la intensidad del proceso (número medio de eventos que ocurren por unidad de tiempo).

La media, variancia, y covariancia quedan dados respecti-

vamente por

$$E\left[N(t)\right] = \nu t$$

$$\sigma^2\left[N(t)\right] = \nu t \qquad (A.2)$$

$$\mathrm{cov}\left\{N(t), N(s)\right\} = \nu s \quad ; \quad s \leq t$$

A.2 El proceso compuesto de Poisson

Si las magnitudes de cada evento que ocurre como un proceso simple de Poisson, son variables aleatorias, el proceso se llama proceso compuesto de Poisson.

Sea $\left\{Y_n,\ n = 1, 2, \ldots\right\}$ una familia de variables aleatorias independientes idénticamente distribuidos como una variable aleatoria Y. El proceso $X(t);\ t \geq 0$, la suma de las magnitudes de los eventos a través del tiempo, t, será:

$$X(t) = \sum_{n=1}^{N(t)} Y_n \quad ; \quad t \geq 0 \qquad (A.3)$$

donde $N(t)$ es el número de eventos de Poisson que han ocurrido en el intervalo de cero a t, el cual es independiente de las Y_n. Algunas de las esperanzas están dadas por:

$$E\left[X(t)\right] = \nu t\, E\left[Y\right]$$

$$\sigma^2\left[X(t)\right] = \nu t\, E\left[Y^2\right] \qquad (A.4)$$

$$\mathrm{cov}\left\{X(t), X(s)\right\} = \nu s\, E\left[Y^2\right] \quad ; \quad s \leq t$$

A.3 El proceso múltiple de Poisson

Sea M_1, M_2, M_3, ..., M_n, las magnitudes de los procesos simples de Poisson, $N_1(t)$, $N_2(t)$, $N_3(t)$ ....., $N_n(t)$, com intensidades ν_1, ν_2, ν_3, ..., ν_n tales que:

$$\sum_{j=1}^{n} \nu_j < \infty$$

el proceso múltiple de Poisson $\{X(t),\ t \geq 0\}$ es:

$$X(t) = \sum_{j=1}^{n} M_j N_j(t) \quad ; \quad t \geq 0 \tag{A.5}$$

la probabilidad que M_j ocurra está dada por:

$$p(j) = \nu_j / \nu \tag{A.6}$$

donde

$$\overline{\nu} = \sum_{j=1}^{n} \nu_j \tag{A.7}$$

A.4 El proceso no homogéneo de Poisson

Removiendo el axioma 2 del proceso simple de Poisson se obtiene el proceso no homogéneo de Poisson. Este proceso permite que la intensidad del proceso sea una función del tiempo.

El valor medio del proceso

$$m(t) = E\left[N(t)\right] \tag{A.8}$$

puede sustituirse en las ecs A.2 y A.4 en lugar de νt, para tener las esperanzas correspondientes del proceso no homogéneo.

Si se va a usar un proceso compuesto no homogéneo, la sustitución de $\nu_j(t)$ por ν_j y de $\bar{\nu}(t) = \sum_{j=1}^{n} \nu(t)$ en la ec A.6, conduce a los valores de las probabilidades, $p_j(t)$, de ocurrencia del j-ésimo evento al tiempo t_j, esto es

$$p_j(t) = \nu_j(t)/\bar{\nu}(t) \qquad (A.9)$$

A.5 El proceso filtrado de Poisson

El proceso filtrado de Poisson se define como

$$X(t) = \sum_{n=1}^{N(t)} \omega(t, \tau_n, Y_n) \quad ; \quad t \geq 0 \qquad (A.10)$$

donde $N(t)$ es un proceso simple de Poisson y $\omega(t, \tau_n, Y_n)$ es una función de influencia que depende del tiempo t, del tiempo de ocurrencia del enésimo evento, τ_n, y de la variable aleatoria Y_n. Las variables aleatorias Y_n están idénticamente distribuidas como una variable aleatoria Y y son independientes del proceso simple de Poisson.

La media, variancia y covariancia del proceso filtrado de Poisson están dadas por:

$$\begin{aligned} E[X(t)] &= \int_0^t \nu E_Y[\omega(t,\tau,Y)]\, d\tau \quad ; \quad t \geq 0 \\ \sigma^2[X(t)] &= \int_0^t \nu E_Y[\omega^2(t,\tau,Y)]\, d\tau \quad ; \quad t \geq 0 \\ \operatorname{cov}\{X(t), X(s)\} &= \int_0^s \nu E_Y[\omega(t,\tau,Y)\,\omega(s,\tau,Y)]\, d\tau \quad ; \quad t \geq s \geq 0 \end{aligned} \qquad (A.11)$$

donde $E_y[\cdot]$ indica la esperanza con respecto a la variable aleatoria Y.

Si $N(t)$ es un proceso no homogéneo de Poisson, será sufi-

ciente sustituir $\nu(t)$ por ν en las ecs A.11 para obtener las esperanzas correspondientes. Si la función de influencia tiene valores finitos solo en un intervalo de tiempo T (como en el caso de un pulso), el límite inferior de las integrales en las dos primeras ecs A.11, debe ser cambiado a t - T y el límite superior permanece igual; para la última ecuación el cambio sería s - T.

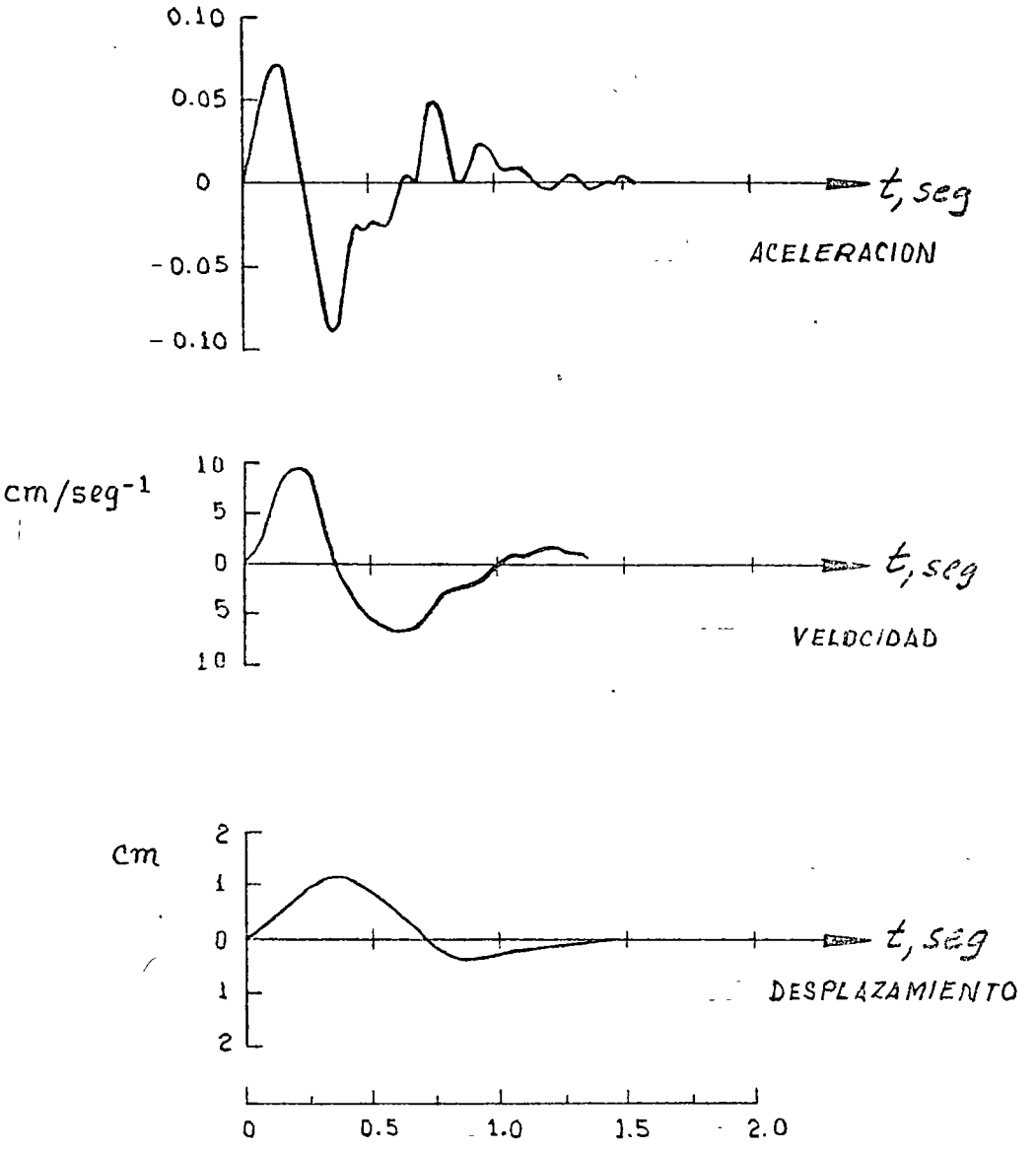

TEMBLOR DE PORT HUENENE DEL 18 DE MARZO DE 1957 , COMPONENTE EW

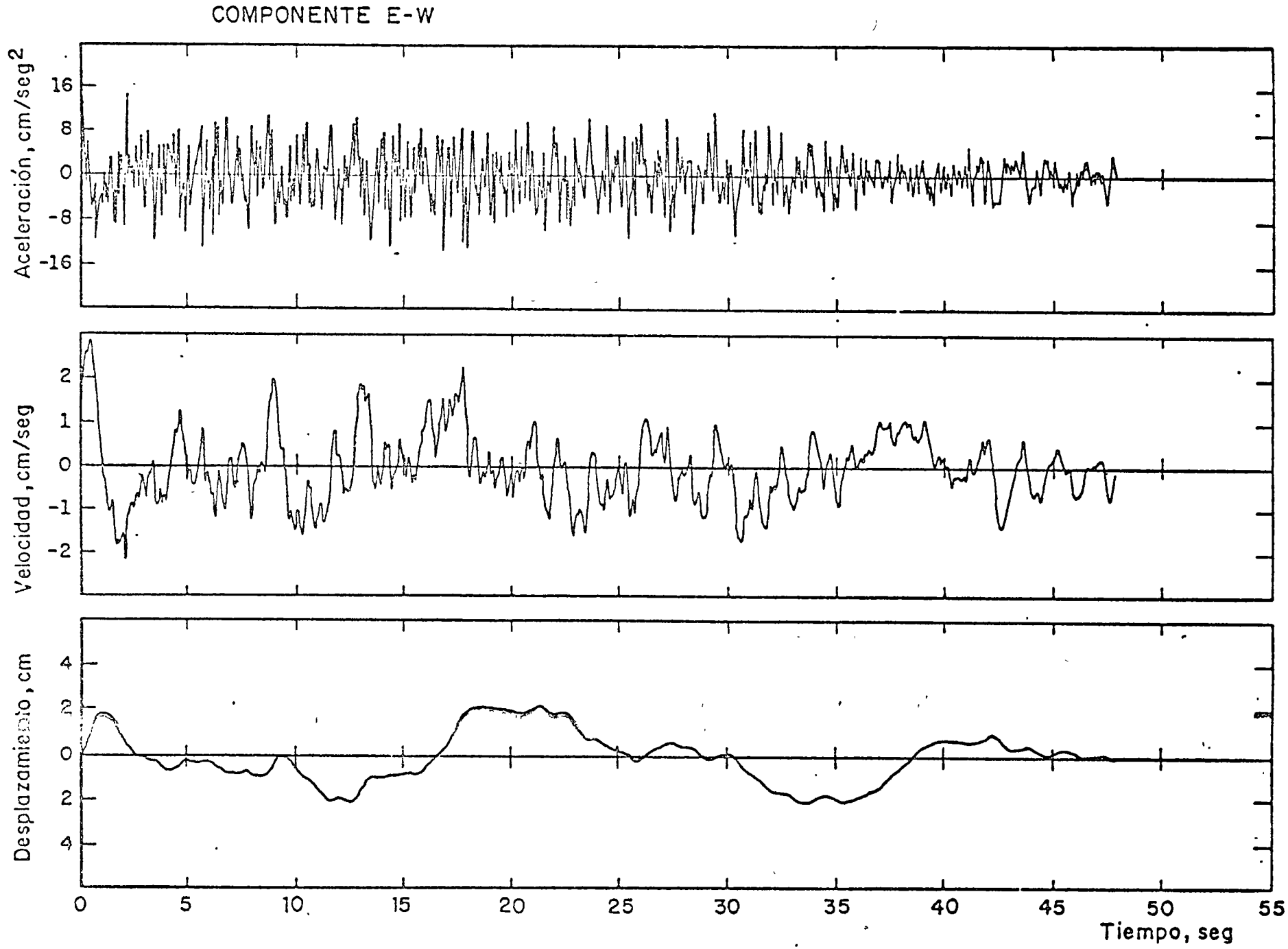

Fig 42 Movimiento del terreno. Ciudad Universitaria, 6 de julio de 1964

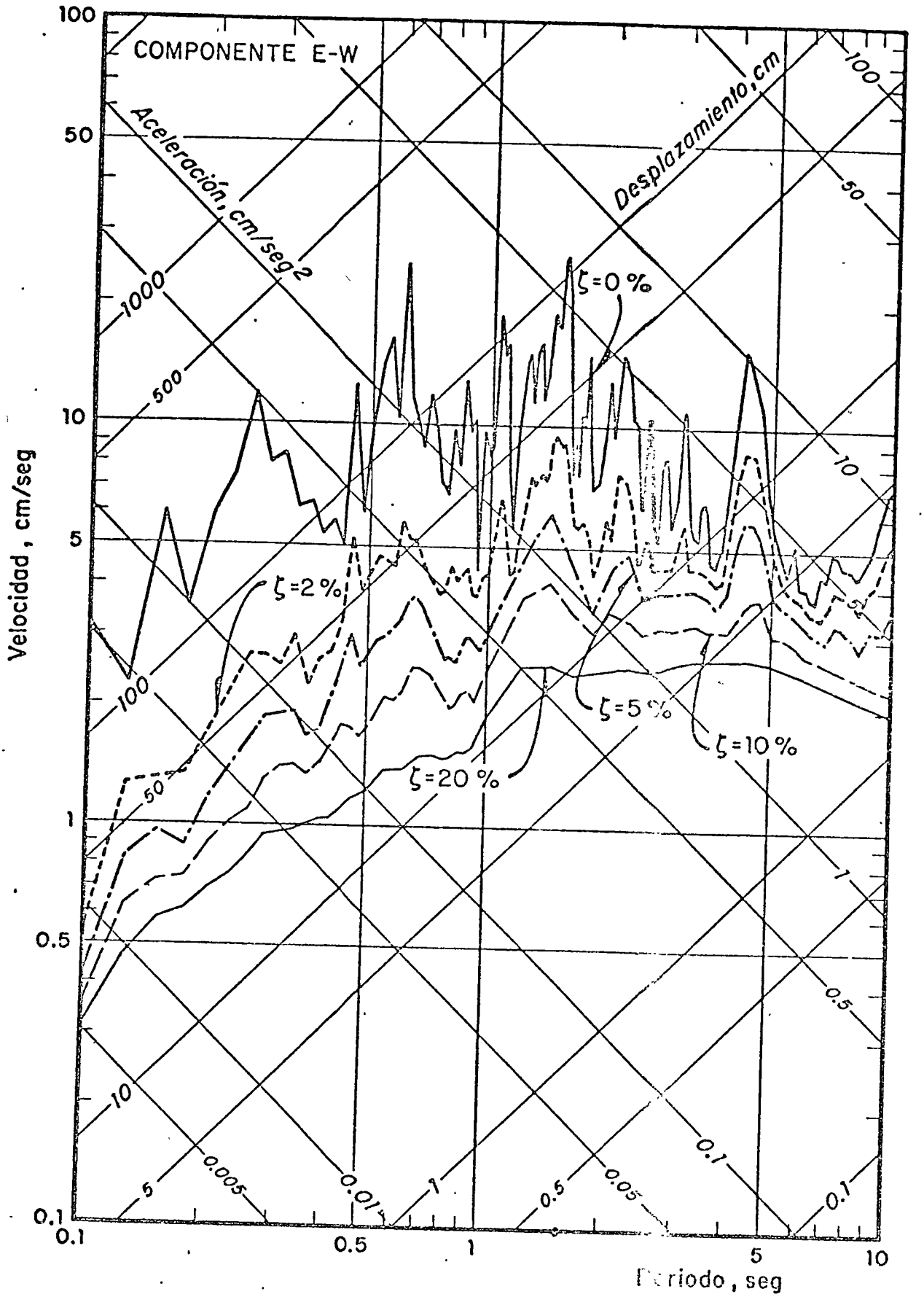

Fig 116 Espectros de respuesta. Ciudad Universitaria, 6 de julio de 1964

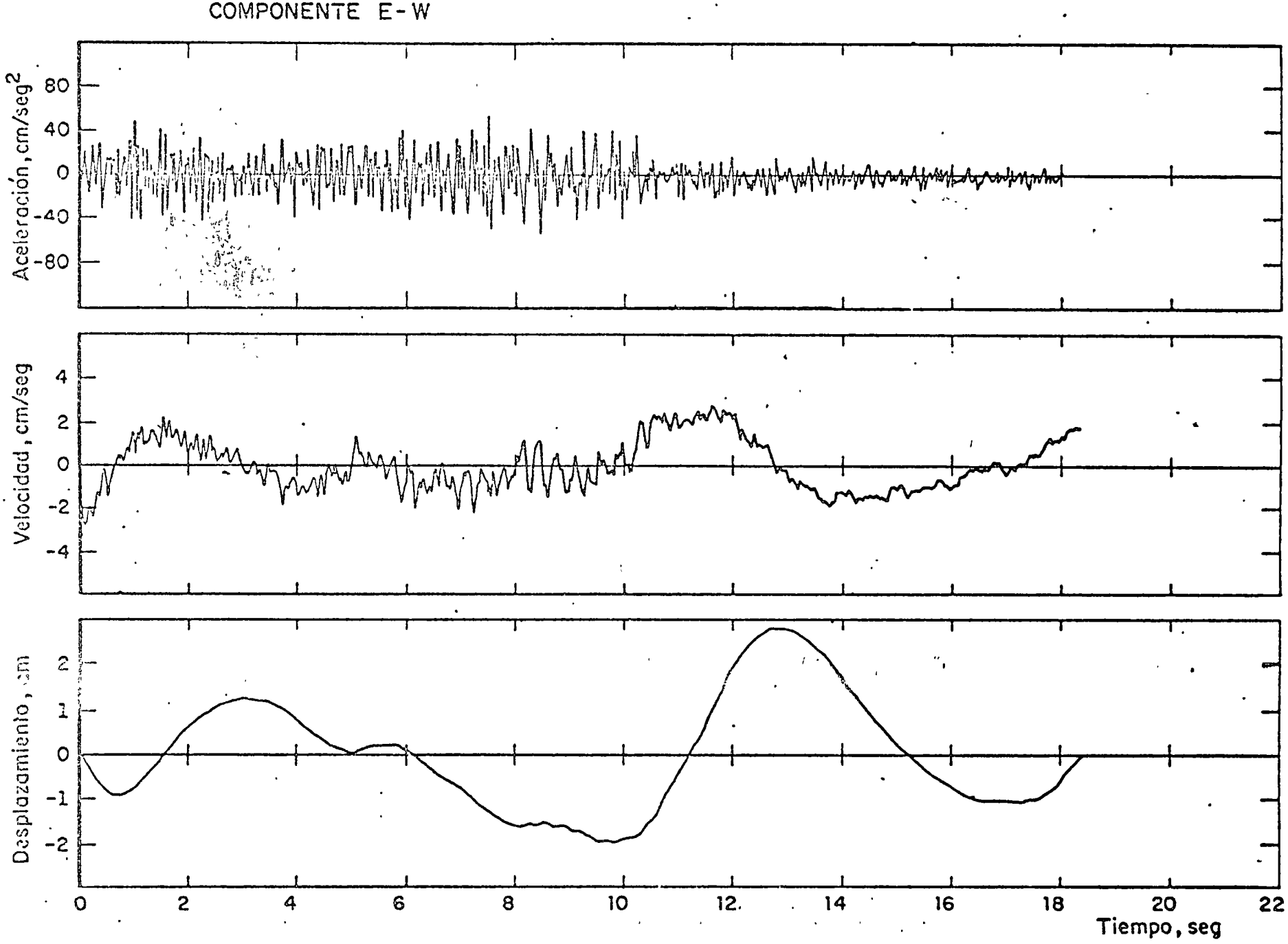

Fig 39 Movimiento del terreno. Acapulco, 1o julio de 1968

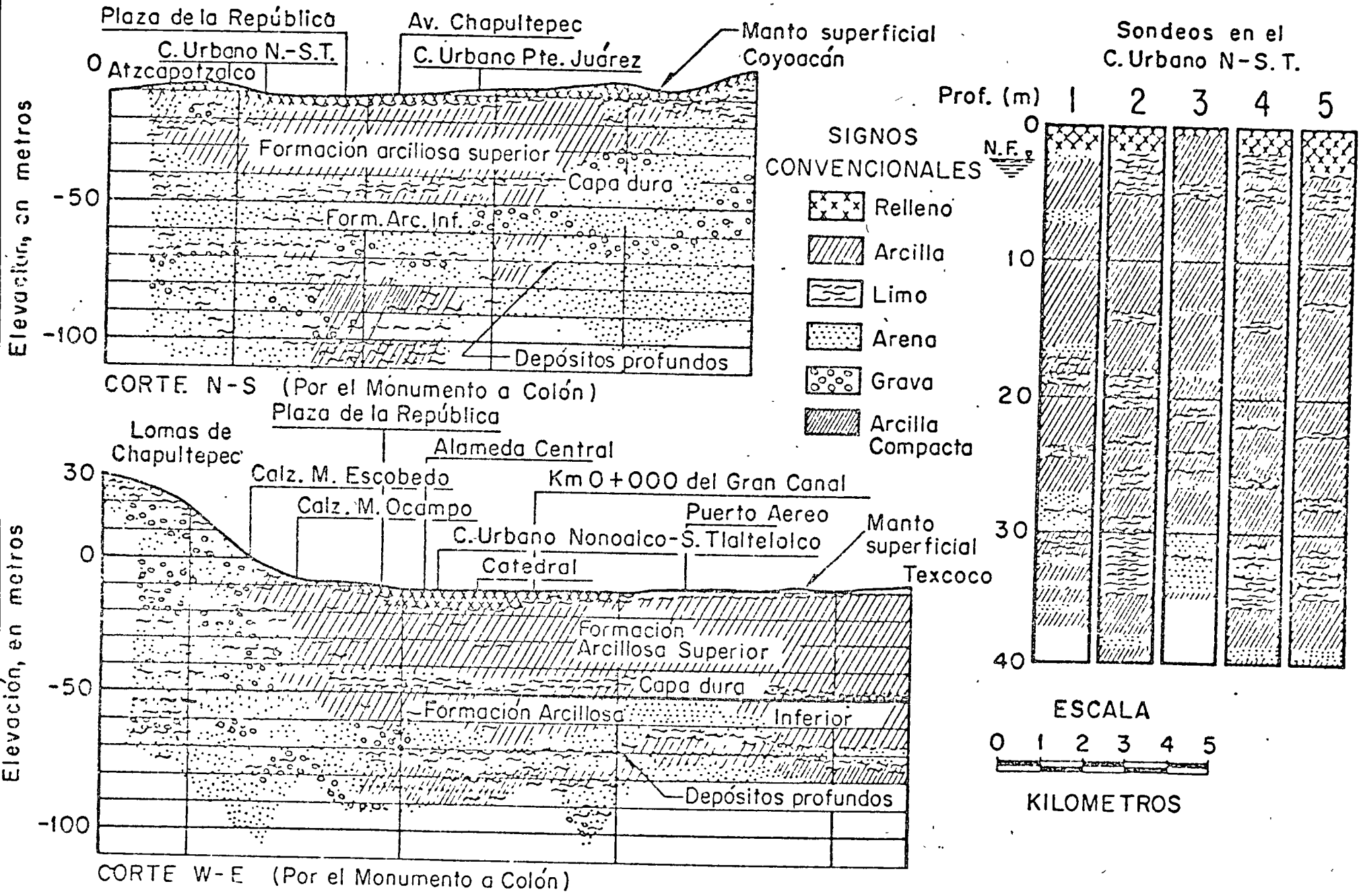

Fig 7 Cortes estratigráficos. Nonoalco-S. Tl[illegible]lolco

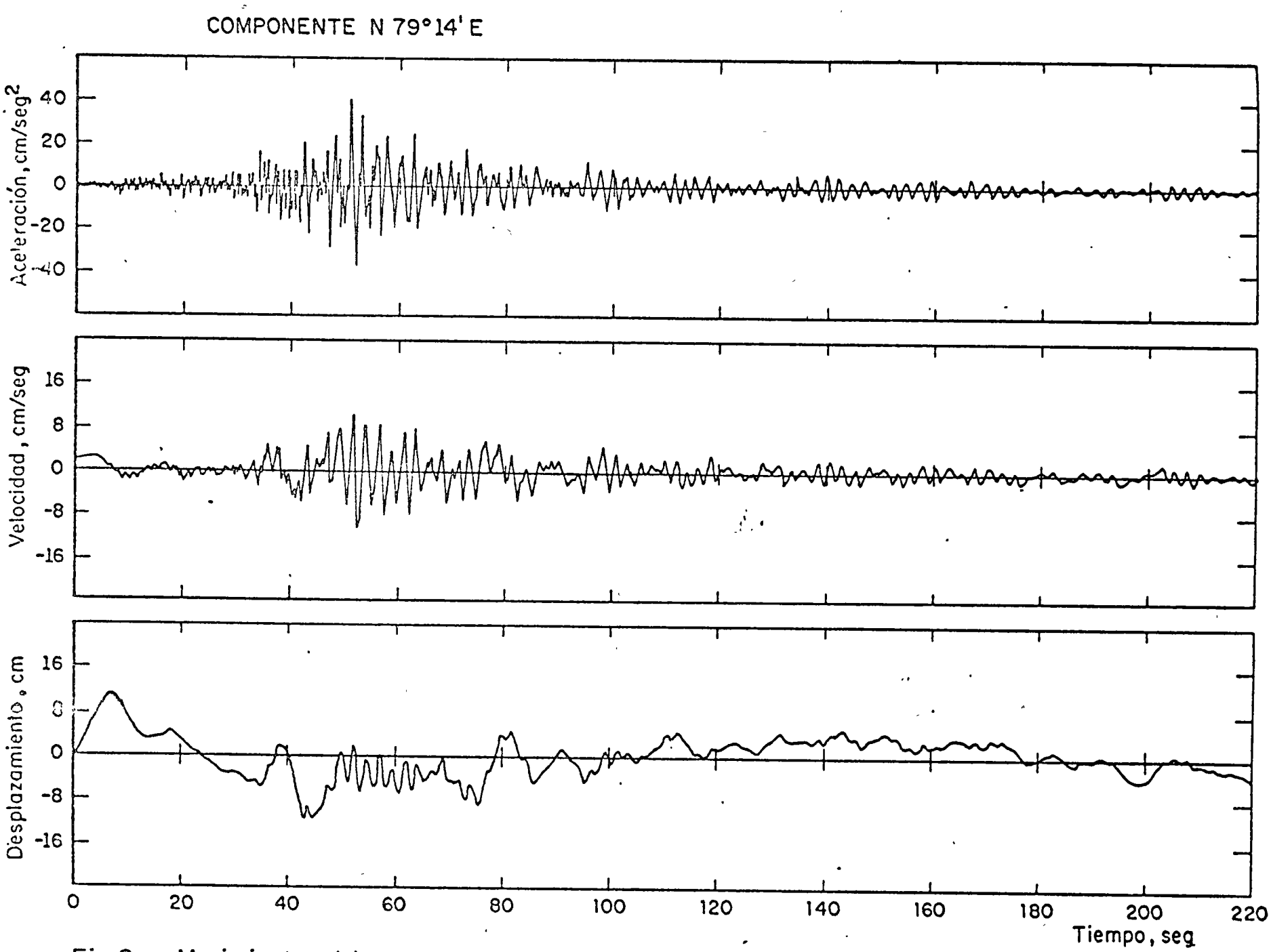

Fig 8 Movimiento del terreno. Alameda Central, 11 de mayo de 1962

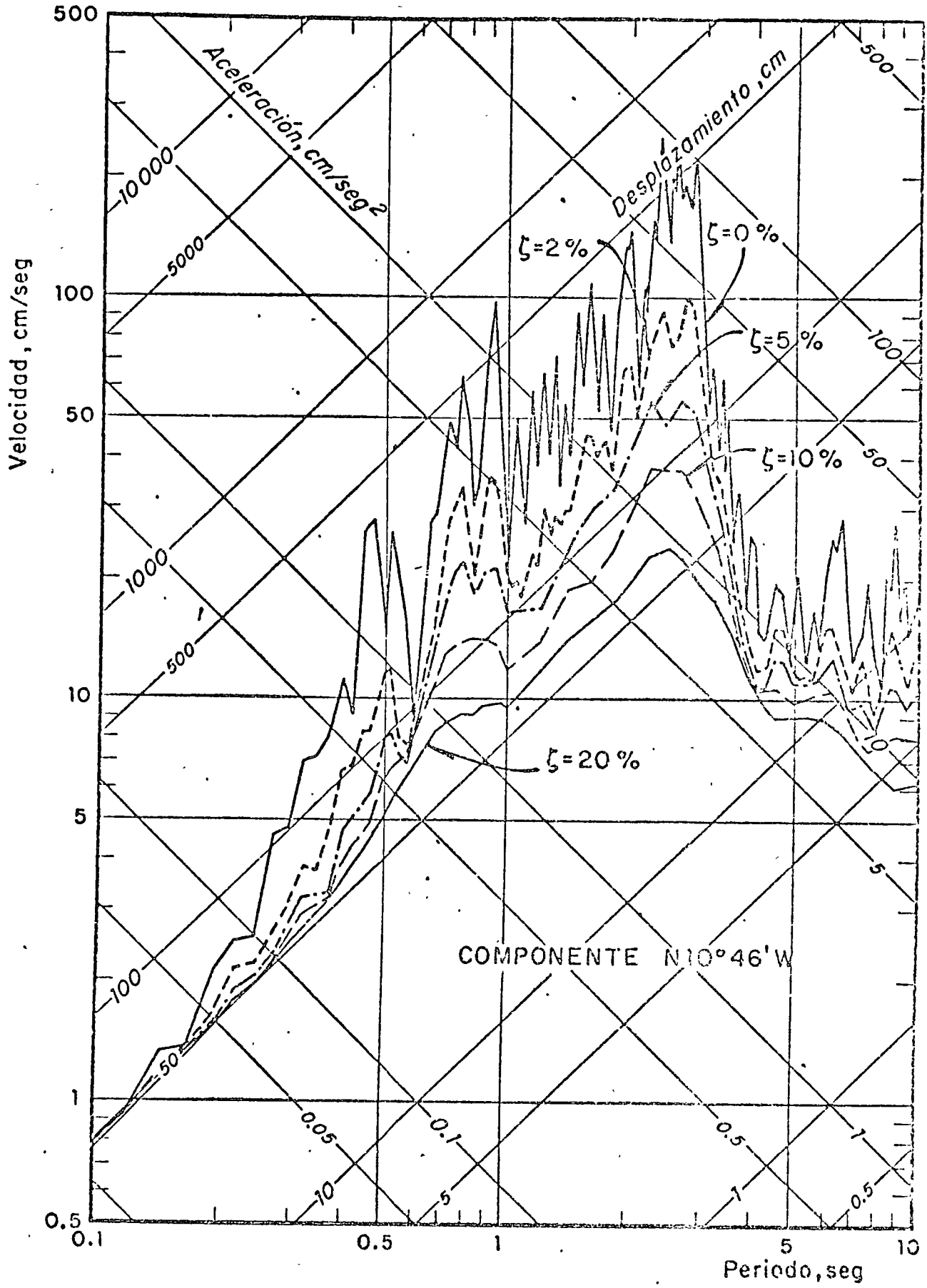

Fig 80 Espectros de respuesta. Alameda Central, 11 de mayo de 1962

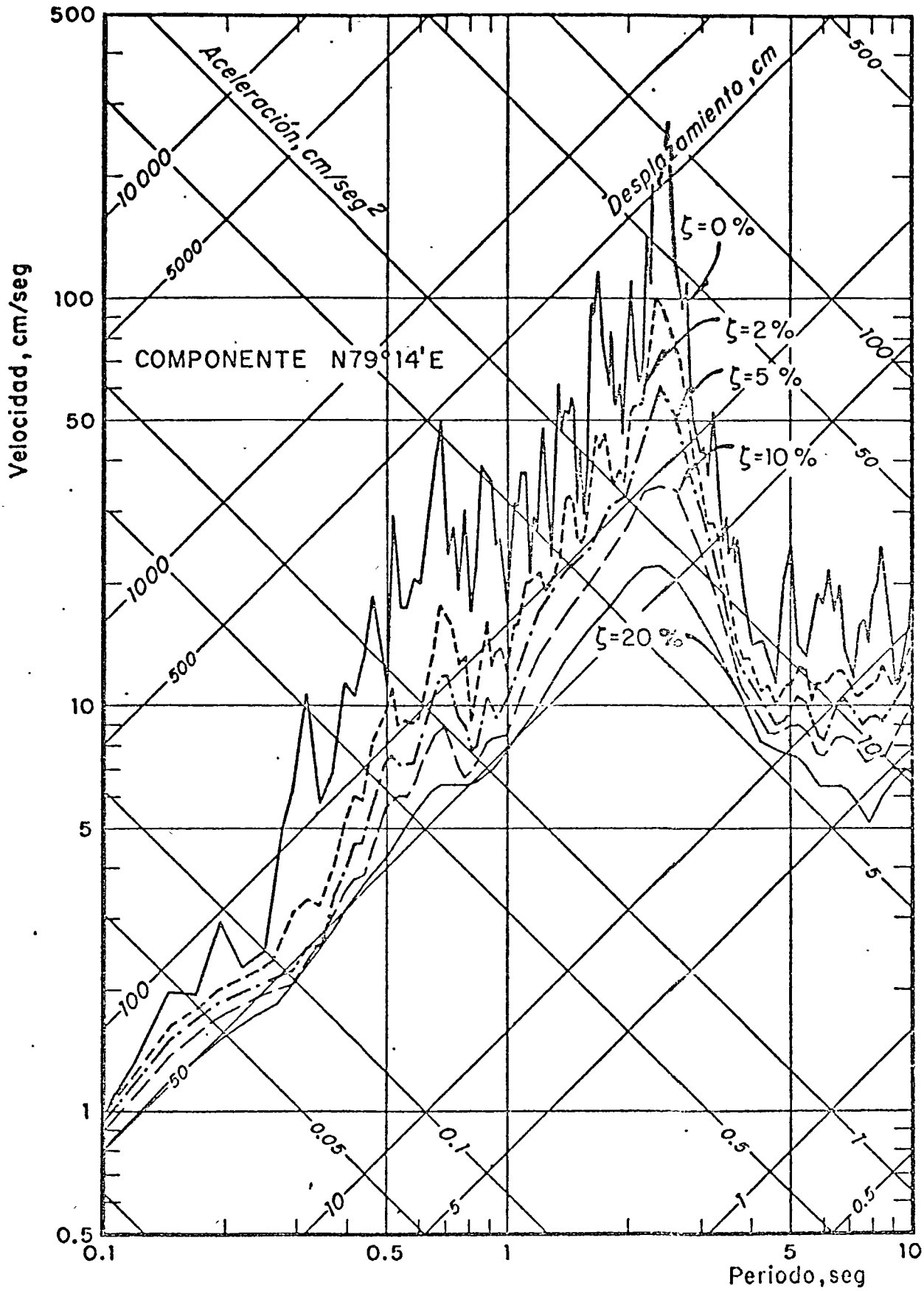

Fig 81 Espectros de respuesta. Alameda Central, 11 de mayo de 1962

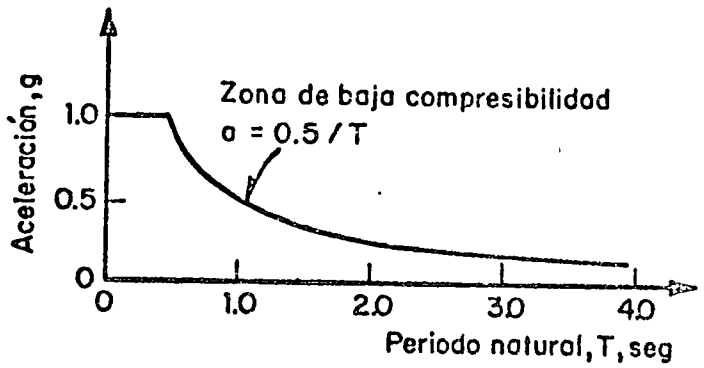

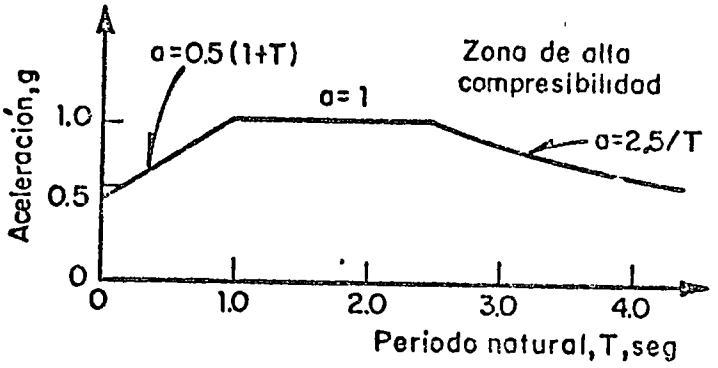

Espectros de aceleraciones de diseño.
Reglamento del D. F.

III CURSO INTERNACIONAL DE INGENIERIA SISMICA

BIBLIOGRAFIA

1. Newmark, N. y Rosenblueth, E., "Fundamentals of Earthquake Engineering", Prentice-Hall o "Fundamentos de Ingeniería Sísmica" (en español) Limusa-Wiley (México)

2. Clough, R.W. y Penzien, J., "Dynamics of structures", McGraw-Hill.

3. "Elements of Earthquake Engineering", J.Krishna y A.R. Chandrasekaran, editores. Edit. Sarita Prakashan, Meerut, India.

4. Esteva, L. "Geology and Probability in the Assessment of Seismic Risk", Informe E13 (enero, 1975) del Instituto de Ingeniería, UNAM.

5. Faccioli, E., "Site-Dependent Probability Distributions for Peak Ground motion Parameters in Strong Earthquakes", Informe E24 (feb, 1977) del Instituto de Ingeniería, UNAM.

6. "Seismic Risk", C.Lomnitz y E. Rosenblueth, editores, Elsevier Co.

7. O.Rascón, M.Chávez, L.Alonso y V.Palencia, "Registros y Espectros de Temblores en las ciudades de México y Acapulco, 1961-1968", Informe 385 (feb, 1977), Instituto de Ingeniería, UNAM.

8. O.Rascón, "Modelo estocástico para simular registros de temblores en terreno duro", Informe 169 (abril, 1968), Instituto de Ingeniería, UNAM.

9. E.Rosenblueth, "Predicción e Ingeniería Sísmicas en China", Sociedad Mexicana de Ingeniería Sísmica (dic, 1976)

10. "El capítulo de Diseño por Sismo de la Propuesta del Nuevo Reglamento para las Construcciones del Distrito Federal", Revista Ingeniería Sísmica, No. 15 (mayo-agosto, 1976) Soc. Mex. de Ing. Sísmica, México.

REVISTAS E INFORMES

1. Bulletin of the Seismological Soc. of America

2. Journals of the American Society of Civil Engineers

3. Memorias de los congresos mundiales de Ingeniería Sísmica y de los congresos nacionales de México, India, Europa, Japón, etc.

4. Reportes de las universidades, Berkely, M.I.T., Stanford, Caltec, etc.

5. Journal of the Earthquake Research Institute, Japón.

6. Earthquake Engrg. and Structural Dynamics. The Journal of the International Assoc. of Earthq. Engrg. (editada por J.Wiley)

Dr. OCTAVIO A. RASCON Ch.

1. ECUACION DIFERENCIAL DE MOVIMIENTO DE UNA VIGA QUE SE DEFORMA EXCLUSIVAMENTE POR CORTE

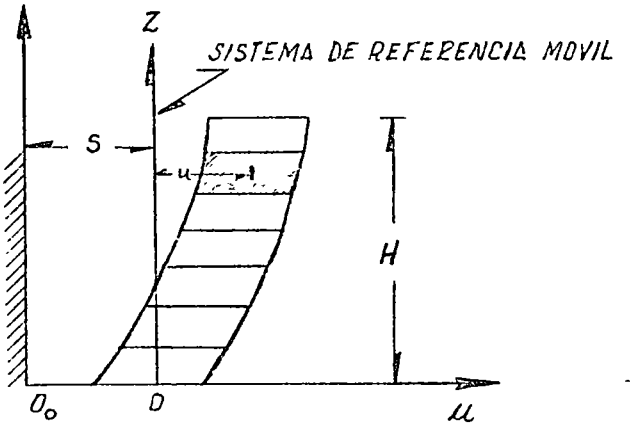

FIG 1a

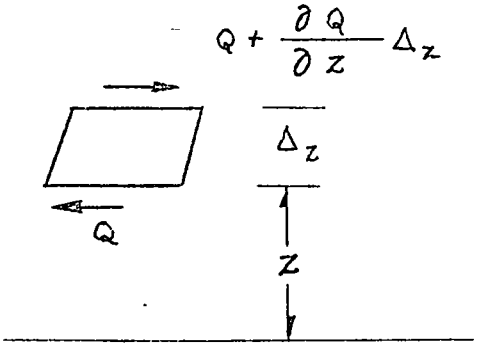

FIG 1b

Consideraremos el problema del movimiento de una viga en voladizo, empotrada en un extremo y libre en el otro, que tiene la propiedad de deformarse exclusivamente por efecto de las fuerzas cortantes. Este sistema puede servir de modelo sencillo para estudiar, al menos cualitativamente, el comportamiento de edificios altos estructurados a base de marcos rígidos así como la transmisión de ondas planas de corte que se propagan verticalmente en un estrato de suelo horizontal. No obstante lo dicho, la ecuación diferencial se establecerá con alguna generalidad algo mayor de manera que sea aplicable a otros casos.

Consideremos la viga de Fig. 1a, empotrada en O y libre en su otro extremo. El movimiento lo referiremos a un sistema de referencia absoluta (sistema inercial); elegiremos además un sistema de referencia móvil, solidario con la base de la estructura y animado de un movimiento de traslación horizontal y rectilíneo.

De manera que si O_o y O son, respectivamente, los orígenes de los

dos sistemas de referencia mencionados

$$\overline{O_o O} = S(t) \qquad (1)$$

es una función conocida del tiempo t, que representa el movimiento del suelo en la dirección Ox. Supondremos que el movimiento de la base es inexorable; es decir, la base tiene un movimiento impuesto por el suelo, no hay desplazamiento de la base respecto del suelo circundante, ni tampoco la base gira. Dicho de otro modo, ignoramos o no tenemos en cuenta la interacción dinámica entre el suelo y la estructura. Tendremos, entonces, que

$$\ddot{S}(t) = a(t) \qquad (2)$$

es la componente horizontal de la aceleración del suelo en la dirección Ox.

Llamaremos, x(z,t) el desplazamiento horizontal de la estructura en el punto de cota z, referido a su base O; z la cota de un punto cualquiera de la viga; A el área de la sección transversal de la viga, G el módulo de elasticidad transversal del material de la viga, K un factor que depende la forma de la sección transversal (adimensional) y H el largo de la viga, que representa la altura total del edificio que pretendemos modelar, o el espesor de la capa de suelo, si es eso lo que pretendemos representar. Finalmente, llamaremos m la masa por unidad de largo de la viga y Q el esfuerzo cortante en la sección a cota z.

Del segundo principio de Newton aplicado a un segmento de viga (ver Fig 1b) obtenemos la ecuación diferencial

$$m\ \Delta z \frac{\partial^2}{\partial t^2}(x + s) = -Q + Q + \frac{\partial Q}{\partial Z}\ \Delta Z$$

O BIEN

$$m \frac{\partial^2 x}{\partial t^2} + ma(t) = \frac{\partial Q}{\partial z} \tag{3}$$

La ecuación constitutiva de la viga de corte es

$$Q = KAG \frac{\partial x}{\partial z} \tag{4}$$

eliminando Q entre las ecuaciones (3) y (4), obtenemos

$$m\frac{\partial^2 x}{\partial t^2} + ma(t) = \frac{\partial}{\partial z}\left[KAG\frac{\partial x}{\partial z}\right] \tag{5}$$

En general, m y KAG son funciones de z (viga de sección variable y con distribución variable, mejor dicho no uniforme, de la masa). En el caso general tendremos, entonces, poniendo explícitamente esta dependencia funcional

$$\left.\begin{aligned} m &= m(z) \\ KAG &= k(z) \end{aligned}\right\} \tag{6}$$

en que m(z) y k(z) representan la masa local y la rigidez de corte local de la viga.

En el caso particular de una viga uniforme, que será el que trataremos en detalle, m(z) y k(z) son costantes y la ecuación (5) toma la forma

$$\frac{\partial^2 x}{\partial t^2} = \frac{KAG}{m} \frac{\partial^2 x}{\partial z^2} - a(t) \tag{7}$$

Pondremos

$$c^2 = \frac{KAG}{m} \tag{8}$$

con lo cual la ecuacion (7) se transforma en

$$\frac{\partial^2 x}{\partial t^2} = c^2 \frac{\partial^2 x}{\partial z^2} - a(t) \tag{9}$$

que es la forma más cimple de la *ecuación de ondas*.

El parámetro c tiene dimensiones $|LT^{-1}|$ y, según veremos, representa la velocidad de propagación de las ondas a lo largo de la viga.

Para resolver cualquiera de las dos ecuaciones (5) o (9) necesitamos conocer las condiciones iniciales y las condiciones en los extremos o condiciones de borde. Las primeras se refieren al estado en que se encuentra la viga en un instante determinado, t=o, por ejemplo. Las segundas describen las condiciones de vínculo.

Las condiciones iníciales se pueden dar especificando, por ejemplo, la posición y la velocidad de todos los puntos de la viga en el instante t=o:

$$x(z,0) = f_i(z) \tag{10}$$

$$x_H(z,0) = f_2(z) \tag{11}$$

Las condiciones de borde pueden ser muy variadas. En nuestro caso se tiene

$$x(o,t) = 0 \tag{12}$$

$$x'_H = (H,t) = 0 \tag{13}$$

La primera de estas ecuaciones dice que el extremo inferior de la viga se mueve junto con la base. La última expresa que el esfuerzo

de corte es nulo en el extremo superior.

Observemos, aunque sea trivial, que la ecuación diferencial |ec (5) o ec ($\bar{9}$), según el caso| es independiente de las condiciones iniciales y de borde; por lo tanto, su validez es general. Esto fluye indistintamente del borde de dichas condiciones no han tenido para que ser tomadas en cuenta en la deducción de la ecuación diferencial y que la consideración del caso particular de la viga en voladizo no ha tenido otro fin que fijar la atención sobre un caso concreto.

2. *MODOS NORMALES DE LA VIGA DE CORTE EN VOLADIZO*

Consideramos el caso particular de una viga uniforme en voladizo que se deforma por corte exclusivamente, suponiendo que la base se encuentra en reposo (S(t) = constante). Trataremos de determinar movimientos en que x(z,t) pueda expresarse como el producto de dos funciones, una que depende exclusivamente de z, y otra que es función de t solamente. Veremos que esto es posible siempre que la función de t sea una función sinusidal cuya frecuencia sea igual a uno de un conjunto de valores discretos. Resultará así que todos los puntos de la viga se moverán con movimiento armónico simple, con la misma frecuencia y en fase o en oposición. Las funciones de z quedarán completamente determinadas, salvo un factor de amplitud arbitrario. A estos movimientos tan especiales los llamaremos *modos normales o modos principales* de oscilar.

Pongamos entonces

$$x(z,t) = \emptyset(z)f(t) \qquad \ldots (1)$$

La ecuación diferencial para la viga uniforme con base fija ($s(t)$ = constante) se obtiene de la ecuación (1.9) poniendo en ella $a(t) = 0$. Resulta

$$\frac{\partial^2 x}{\partial t^2} = c^2 \frac{\partial^2 x}{\partial z^2} \tag{2}$$

Sustituyendo la expresión (1) obtenemos

$$\phi(z) \frac{d^2 f}{dt^2} = c^2 \frac{d^2 \phi}{dz^2} f(t)$$

o bien

$$\frac{\frac{d^2 f}{dt^2}}{f(t)} = c^2 \frac{\frac{d^2 \phi}{dz^2}}{\phi(z)} \tag{3}$$

Ahora bien, el primer miembro de (3) es función de t solamente, mientras que el segundo miembro depende sólo de z. Pero t y z son variables independientes; luego, para que se pueda cumplir (3) es preciso que ambos miembros sean iguales a una misma constante.

Llamemos $-\omega^2$ dicha constante. Obtenemos así las dos ecuaciones diferenciales ordinarias siguientes

$$\frac{d^2 f}{dt_2} + \omega^2 f = 0 \tag{4}$$

$$\frac{d^2 \phi}{dz^2} + \frac{\omega^2}{c^2} \phi = 0 \tag{5}$$

Decimos que hemos logrado *separar* las variables de la ecuación en derivadas parciales (2), o que hemos *separado* dicha ecuación en dos ecuaciones diferenciales ordinarias. La constante ω recibe por ello el nombre de *constante de separación*.

La solución general de (4) se puede escribir en la forma

$$f(t) = R\cos(\omega t+\varepsilon) \tag{6}$$

que representa una oscilación armónica simple de frecuencia circular ω y fase inicial ε.

La solución general de (5) es

$$\phi(z) = A\,\mathrm{sen}\left(\frac{\omega z}{c}\right) + B\cos\left(\frac{\omega z}{c}\right) \tag{7}$$

Recurrimos ahora a las condiciones de borde (1.12) y (1.13) que se pueden expresar en la forma

$$\left.\begin{aligned}\phi(o) &= 0\\ \phi'(H) &= 0\end{aligned}\right\} \tag{8}$$

Sustituyendo la expresión de $\phi(z)$ encontrada en (7) obtenemos

$$\left.\begin{aligned}B &= 0\\ \frac{\omega}{c}A\cos\left(\frac{\omega H}{c}\right) &= 0\end{aligned}\right\} \tag{9}$$

Este sistema admite la solución trivial $\frac{\omega A}{c}=0$, $B=0$, que corresponde al reposo en la posición de equilibrio y no nos interesa. Por lo tanto, suponemos $\frac{\omega A}{c} \neq 0$, con lo cual nos vemos obligados a concluir que un movimiento del tipo postulado sólo es posible si ω es raíz de la ecuación trascendente

$$\cos\left(\frac{\omega H}{c}\right) = 0 \tag{10}$$

cuyas soluciones son

$$\omega_n = (2n-1)\frac{\pi c}{2H} \qquad (n = 1,2,3,\ldots) \tag{11}$$

Las frecuencias ω_n reciben el nombre de *frecuencias normales o frecuencias naturales* de la viga. La ec (10) es la *ecuación de frecuencias*.

Observemos que

$$\omega_1 : \omega_2 : \omega_3 : \ldots = 1 : 3 : 5 : \ldots \qquad (12)$$

Las frecuencias naturales, ordenadas de menor a mayor, son entre sí como la sucesión de los números impares. Los períodos correspondientes valen

$$T_n = \frac{4H}{c} \cdot \frac{1}{(2n-1)} \qquad (13)$$

y forman, por consiguiente, una *progresión armónica*.

Finalmente el conocimiento transversal de la sección de la viga situada a la cota z, para un instante t cualquiera, está dado por

$$x_n(z,t) = A_n \operatorname{sen}\left(\frac{(2n-1)\pi z}{2H}\right) \cos(\omega_n t + \varepsilon_n) \quad (n = 1,2,3,\ldots) \qquad (14)$$

Cada uno de estos movimientos recibe el nombre de *modo normal o modo principal* de oscilar. Nótese que las constantes A_n y ε_n han quedado sin determinar. Esto es así porque no hemos hecho uso de las condiciones inciales. A_n es la *amplitud* del modo de orden n; ε_n es su *fase inicial* o simplemente *fase*. Al modo de menor frecuencia se le da el nombre de *modo fundamental*. Los demás se designan como 2o., 3er...modo, o, genéricamente, como *modos superiores*. En el caso particular que nos ocupa, dada la relación armónica de los períodos, establecida anteriormente, se habla de *armónicas superiores*.

Las frecuencias ω_n y las funciones $\phi_n(z)$ reciben el nombre de *frecuencias modales y funciones modales*, respectivamente. También se usan los apelativos de *frecuencia característica, valor característico, frecuencia propia, valor propio, eigenvalue* y los correspondientes *función característica*, etc.

Convendremos en normalizar o estandarizar las funciones modales, elijiendo su amplitud igual a la unidad. Con esta convención tendremos

$$\phi_n(z) = \operatorname{sen}\frac{(2n-1)\pi z}{2H} \qquad (n = 1,2,3,\ldots) \qquad (15)$$

Las fuerzas cortantes del modo de orden n quedan dados (para $A_n=1$) por

$$Q_n(z,t) = kAG\,\frac{\partial x_n(z,t)}{\partial z} = kAG\,\frac{(2n-1)\pi}{2H}\cos\frac{(2n-1)\pi z}{2H}\cos(\omega_n t + \varepsilon_n)$$

El corte en la base es (para $A_n=1$)

$$Q_n(0,t) = kAG\,\frac{(2n-1)\pi}{2H}\cos(\omega_n t + \varepsilon_n) \qquad (16)$$

Luego, el corte en la sección situada en la cota z referido al corte basal valdrá

$$\frac{Q_n(z,t)}{Q_n(o,t)} = \cos\frac{(2n-1)\pi z}{2H} \qquad (n = 1, 2, 3,\ldots) \qquad (17)$$

El momento de volteo (positivo en el sentido trigonométrico positivo 7) está dado por (para $A_n=1$)

$$M_n(z,t) = kAG\left[(-1)^n + \text{sen}\frac{(2n-1)\pi z}{2H}\right]\cos(\omega_n t + \varepsilon_n)$$

Luego

$$M_n(o,t) = (-1)^n\, kAG\cos(\omega_n t + \varepsilon_n) \qquad (18)$$

Por lo tanto el momento de volteo referido al momento de volteo local es

$$\frac{M_n(z,t)}{M_n(o,t)} = 1 + (-1)^n \text{ sen } \frac{(2n-1)\pi z}{2H} \qquad (19)$$

Finalmente, llamemos k_n la altura a la cual habría que aplicar el corte basal para obtener en la base un momento estático igual (numéricamente, o sea, en valor absoluto) al momento de volteo basal. Tendremos

$$|Q_n(o,t)|h_n = |M_n(o,t)|$$

de donde

$$\frac{h_n}{H} = \frac{2}{(2n-1)\pi} \qquad (n = 1, 2, 3,\ldots) \qquad (20)$$

expresión que se ha tabulado a continuación.

n	$\frac{h_n}{H}$
1	0.6366
2	0.2122
3	0.1273
4	0.0909
5	0.0707

La tabla anterior da los valores de $\frac{h_n}{H}$ para los cinco primeros modos. Así, si se aplica el corte basal correspondiente al primer modo como una fuerza estática horizontal a la cota 0,6366 H, el momento de dicha fuerza respecto de la base es igual al momento de volteo basal en el modo fundamental. El resultado de ec (20) y la tabla muestran que, a igualdad de corte basal, el modo fundamental es el que tiene importancia predominante en el momento de volteo basal.

A una conclusión análoga llegamos examinando las ecuaciones (16) y (18). A igualdad de amplitud de oscilación, mientras los cortes basales máximos crecen con el número de orden del modo, según la serie de los números impares (1, 3, 5,...), el momento de volteo basal máximo permanece el mismo (en valor absoluto) para todos los modos.

En la Fig 2 hemos representado esquemáticamente las funciones modales y las razones $\frac{Q_n(z,t)}{Q_n(o,t)}$, $\frac{M_n(z,t)}{M_n(o,t)}$ para n = 1, 2, 3

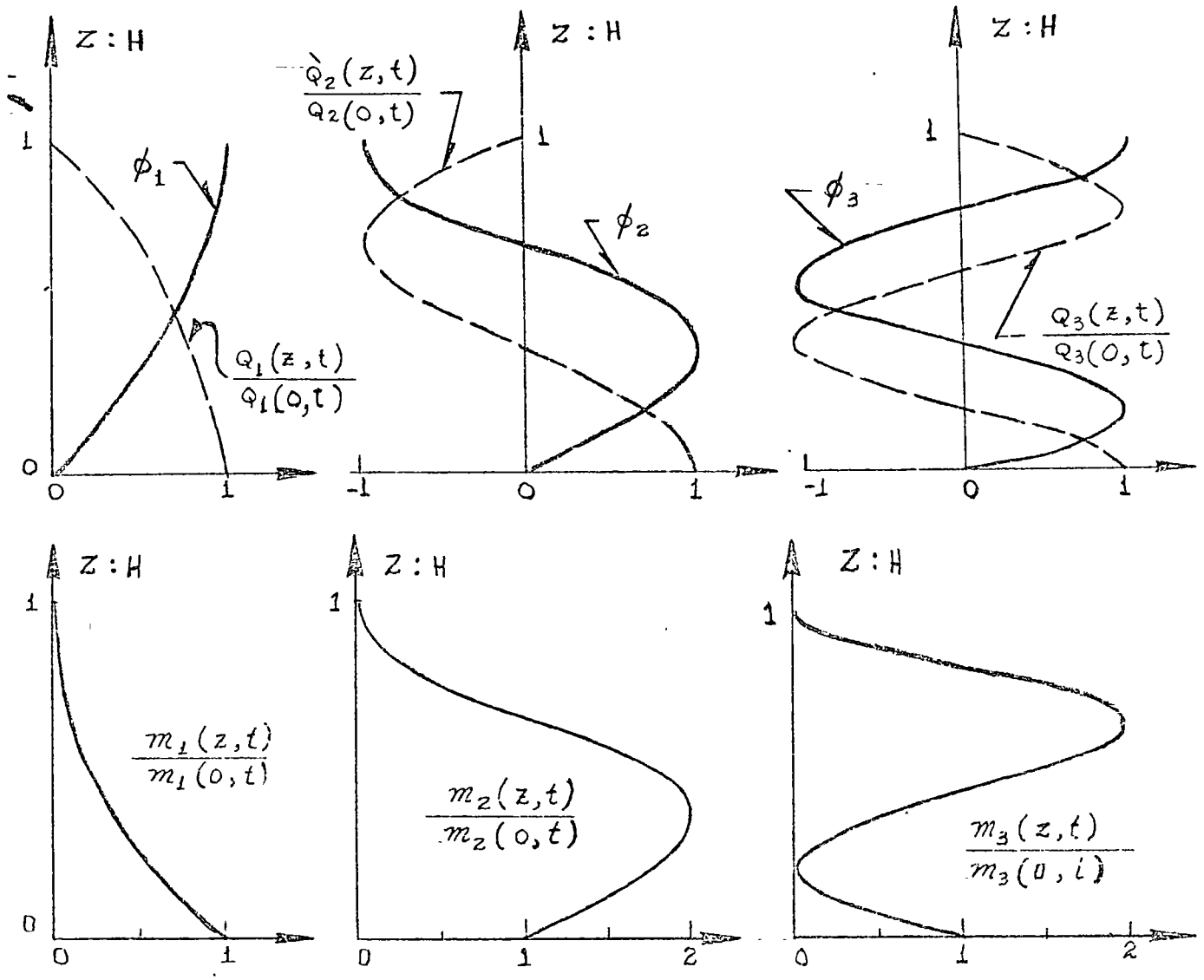

FIGURA 2

Los puntos para los cuales $\phi_n(2)$ se anula se llaman *nodos*; aquéllos para los cuales $\phi_n(2)$ es extremo (máximo o mínimo) se llaman *vientres*. Podemos observar que $\phi_n(z)$ presenta exactamente n vientres y n nodos (si se cuenta con tal el punto z=o).

Observemos también que, salvo para x=1, en que el mayor momento de volteo ocurre en la base, en los modos superiores el momento de volteo máximo no ocurre en la base y es numéricamente igual al doble del momento de volteo máximo basal.

3.- ORTOGONALIDAD DE LOS MODOS NORMALES, VIBRACIONES LIBRES

Las funciones modales encontradas en la Sección 2 satisfacen la relación de ortogonalidad

$$\int_0^H m\phi_i(z)\ \phi_j(z)\ dz = 0 \qquad \text{para } i \neq j \qquad (1)$$

En efecto

$$\int_0^H \operatorname{sen}\frac{(2i-1)\pi z}{2H}\ \operatorname{sen}\frac{(2j-1)\pi z}{2H}\ dz = \frac{1}{2}\int_0^H \left[\cos\frac{(i-j)\pi z}{H} - \cos\frac{(i+j-1)\pi z}{H}\right] dz$$

$$= 0 \qquad (i \neq j)$$

Esta propiedad tiene extraordinaria importancia para el desarrollo de la teoría de las vibraciones libres y de las vibraciones forzadas.

Las funciones $\phi_i(z)$ forman una base ortogonal (completa) en el intervalo (0,H) y, con algunas restricciones que no tienen importancia en las aplicaciones prácticas, cualquiera función se puede representar en dicho intervalo como una combinación lineal de las $\phi_i(z)$. No entraremos aquí a establecer la posibilidad de tal representación ni su unicidad. Nos limitaremos a establecer cómo se pueden calcular los coeficientes de la combinación lineal.

Sea

$$f(z) \qquad 0 < z < H$$

una función cualquiera de z, y admitamos que es posible representarla en la forma

$$f(z) = \sum_{i=1}^{\infty} \alpha_i\ \phi_i(z) \qquad (2)$$

Para determinar los coeficientes α_j multiplicamos ambos miembros de (2) por $\phi_j(z)$ e integramos entre 0 y H, teniendo en cuenta las relaciones de ortogonalidad. Obtenemos

$$\alpha_j = \frac{\int_0^H f(z)\ \phi_j(z)\ dz}{\int_0^H \phi_i^2(z)\ dz} \qquad (3)$$

Que la representación (2) es única es una consecuencia directa del hecho que las funciones $\phi_i(z)$ son linealmente independientes.

El resultado recién encontrado nos permite resolver de inmediato el problema de las vibraciones libres. Se trata de resolver el sistema diferencial

$$\left.\begin{aligned} &\frac{\partial^2 x}{\partial t^2} = c^2\ \frac{\partial^2 x}{\partial z^2} \\ &x(0,t) = 0 \qquad ,\ x_z(H,t) = 0 \\ &x(z,0) = f_1(z) \quad ,\ x_t(z,0) = f_2(z) \end{aligned}\right\} \qquad (4)$$

correspondiente a las vibraciones libres de una viga uniforme que se deforma exclusivamente por corte, empotrada en z=0 y libre en z=H, sujeta a las condiciones iniciales expresadas en la última línea de (4).

La función

$$x(z,t) = \sum_{i=1}^{\infty} \left[\alpha_i \cos \omega_i t + \beta_i \operatorname{sen} \omega_i t\right] \phi_i(z) \qquad (5)$$

satisface la ecuación diferencial y las condiciones de borde. Determinaremos los coeficientes α_i, β_i de manera que las condiciones iniciales queden también cumplidas.

Derivando (5) respecto del tiempo obtenemos

$$x_t(z,t) = \sum_{i=1}^{\infty} \left[- \omega_i \alpha_i \text{ sen } \omega_i t + \omega_i \beta_i \cos \omega_i t \right] \phi_i(z) \quad (6)$$

Haciendo t=0 en (5) y (6) y tomando en cuenta las condiciones iniciales, obtenemos

$$x(z,0) = \sum_{i=1}^{\infty} \alpha_i \phi_i(z) = f_1(z) \quad (7)$$

y

$$x_t(z,0) = \sum_{i=1}^{\infty} \omega_i \beta_i \phi_i(z) = f_2(z) \quad (8)$$

Por lo tanto

$$\alpha_i = \frac{\int_0^H f_1(z) \phi_i(z) \, dz}{\int_0^H \phi_i^2(z) \, dz} \quad (9)$$

$$\omega_i \beta_i = \frac{\int_0^H f_2(z) \phi_i(z) \, dz}{\int_0^H \phi_i^2(z) \, dz} \quad (10)$$

y el problema queda resuelto. La vibración libre consiste en una superposición de movimientos armónicos simples de frecuencias iguales a las frecuencias modales, cuyas amplitudes y fases quedan determinadas por las condiciones iniciales.

Pongamos

$$\xi_i(t) = \alpha_i \cos \omega_i t + \beta_i \text{ sen } \omega_i t \quad , \quad (11)$$

entonces

$$x(z,t) = \sum_{i=1}^{\infty} \xi_i(t) \phi_i(z) \quad (12)$$

Los variables $\xi_i(t)$ las llamaremos coordenadas normales del sistema.

4.- SIGNIFICADO FISICO DE LAS RELACIONES DE ORTOGONALIDAD, OSCILADORES MODALES

En la Sección 3 hemos establecido las relaciones de ortogonalidad para las funciones modales de la viga de corte en voladizo como una propiedad matemática de dichas funciones. Queremos ahora darle a dichas relaciones un significado o interpretación física.

Empezaremos por establecer expresiones para la energía cinética y la energía potencial de la viga cuando ésta se encuentra animada de un movimiento libre arbitrario que como hemos visto recién se puede representar por la expresión (3.12).

Por definición la energía cinética del sistema es

$$T = \frac{1}{2}\int_0^H m\left(\frac{\partial x}{\partial t}\right)^2 dz = \frac{m}{2}\int_0^H \left[\sum_{i=1}^{\infty} \dot{\xi}_i \phi_i(z) \sum_{j=1}^{\infty} \xi_j \phi_j(z)\right] dz \quad (1)$$

Invirtiendo el orden de integración y de suma y teniendo en cuenta las relaciones de ortogonalidad obtenemos

$$T = \frac{m}{2} \sum_{i=1}^{\infty} \dot{\xi}_i^2(t) \int_0^H \phi_i^2(z)\, dz \quad (2)$$

Para obtener la energía potencial observamos que ésta es simplemente el trabajo acumulado por las fuerzas internas (esfuerzos de corte) desde la posición de equilibrio en reposo (configuración no deformada) basta la configuración definida por (3.12). En un elemento de viga como el de fig 1a se ha acumulado la energía

$$\delta V = \frac{1}{2} Q\gamma\delta z \quad (3)$$

en que Q es el corte y γ la distorsión. Pero según (1.4)

$$Q = kAG\frac{\partial x}{\partial z}$$

y para pequeñas amplitudes

$$\gamma = \frac{\partial x}{\partial z}$$

Luego,

$$\delta V = \frac{1}{2}\, kAG\left(\frac{\partial x}{\partial z}\right)^2 \delta z \qquad (4)$$

y por lo tanto

$$V = \frac{1}{2}\, kAG \int_0^H \left[\sum_{i=1}^{\infty} \xi_i \phi_i'(z) \sum_{j=1}^{\infty} \xi_j \phi_j'(z)\right] dz \qquad (5)$$

Una integración por partes nos da

$$\int_0^H \phi_i'(z)\ \phi_j'(z)\ dz = \left[\phi_i'\ \phi_j\right]_0^H - \int_0^H \phi_i''(z)\ \phi_j(z)\ dz \qquad (6)$$

Pero, según las condiciones de borde $\phi_j(0) = 0$, $\phi_i'(H) = 0$; luego, el primer término del segundo miembro es nulo para toda combinación de i y de j. Por otro lado según la ec (2.5)

$$\phi_i''(z) = -\frac{\omega_i^2}{c^2}\, \phi_i(z) \qquad (7)$$

Luego, la integral

$$\int_0^H \phi_i'(z)\ \phi_j'(z)\ dz \qquad (6\ bis)$$

es nula si $i \neq j$, en virtud de las relaciones de ortogonalidad. Cuando i = j tenemos

$$\int_0^H \phi_i'(z)\ \phi_i'(z)\ dz = \int_0^H \left[\phi_i'(z)\right]^2 dz = \frac{\omega_i^2}{c^2} \int_0^H \left[\phi_i(z)\right]^2 dz \qquad (8)$$

En consecuencia, invirtiendo en (5) el orden de integración y suma:

$$V = \frac{1}{2}\frac{kAG}{c^2}\sum_{i=1}^{\infty}\xi_i^2(t)\ \omega_i^2\int_0^H \phi_i^2(z)\ dz \qquad (9)$$

Pero

$$c^2 = \frac{kAG}{m}$$

Luego, finalmente

$$V = \frac{1}{2}\,m\sum_{i=1}^{\infty}\xi_i^2(t)\ \omega_i^2\int_0^H \phi_i^2(z)\ dz = \frac{1}{2}\,kAG\sum_{i=1}^{\infty}\xi_i^2\int\left[\phi_i'(z)\right]^2 dt \qquad (10)$$

Lo interesante de los resultados (2) y (10) es que en las expresiones de V y de T solamente aparecen cuadrados de las coordenadas normales ξ_i (en la expresión de V) o cuadrados de los derivadas temporales $\dot{\xi}_i$ de dichas coordenadas (en la expresión de T). No aparecen productos de la forma $\xi_i\xi_j$ o $\dot{\xi}_i\dot{\xi}_j$ con $i \neq j$.

Este resultado lo expresamos diciendo que hemos diagonalizado simultáneamente las expresiones de la energía cinética y de la energía potencial. La consecuencia inmediata es que la ecuación del movimiento (2.2). que es una ecuación a derivadas parciales, se puede representar por una infinidad numerable de ecuaciones diferenciales ordinarias no acopladas; es decir, en cada una de las cuales aparece una y sólo una de las coordenadas ξ_i. Esto facilita enormemente el problema de integrar las ecuaciones del movimiento.

Empleando las ecuaciones de Lagrange

$$\frac{d}{dt}\frac{\partial T}{\partial \dot{q}_i} - \frac{\partial T}{\partial q_i} = -\frac{\partial V}{\partial q_i}\ (i=1,2\ .\ .\ .) \qquad (11)$$

encontramos inmediatamente que las coordenadas normales satisfacen las ecuaciones

$$\ddot{\xi}_i + \omega_i^2 \xi_i = o \qquad (i = 1, 2, 3, \ldots) \quad (12)$$

Como era de esperar, si se tiene en cuenta la relación (3.11). Cada modo normal se comporta, entonces, como un oscilador armónico simple, independiente de los demás. Si M_i y K_i son, respectivamente, la masa y la constante elástica del oscilador que corresponde al modo i, debemos tener necesariamente

$$\frac{K_i}{M_i} = \omega_i^2 \qquad (i = 1, 2, 3, \ldots) \quad (13)$$

Por lo tanto, para determinar completamente el oscilador que representa al $i^{ésimo}$ modo nos bastará determinar su masa M_i. La ecuación de frecuencias y ecs. (13) nos dan los K_i.

Llamaremos <u>oscilador modal equivalente</u> o simplemente <u>oscilador modal</u>, a un oscilador armónico simple cuya masa y rigidez (o constante elástica) son tales, que es capaz de oscilar de manera que, en cada constante, su energía cinética, su energía potencial y su cantidad de movimiento sean iguales a los del sistema estudiado oscilando en un modo normal.

Si M_i y K_i son respectivamente, la masa y la constante elástica del oscilador modal equivalente al $i^{ésimo}$ modo debemos tener

$$\frac{1}{2} M_i R_i^2 \xi_i^2 = \frac{m}{2} \dot{\xi}_i^2 \int_C^H \phi_i^2(z)\,dz \quad (14)$$

$$\frac{1}{2} K_i R_i^2 \xi_i^2 = \frac{m}{2} \xi_i^2 \omega_i^2 \int_o^H \phi_i^2(z)dz \qquad (15)$$

$$M_i R_i \dot{\xi}_i = m\dot{\xi}_i \int_0^H \phi_i(z)dz \qquad (16)$$

en que R_i es un factor de escala.

De (14) y (15) obtenemos inmediatamente (13), dividiendo miembro a miembro. Elevando al cuadrado (16) y dividiendo por (14) resulta

$$M_i = m \frac{\left[\int_o^H \phi_i(z)dz\right]^2}{\int_o^H \phi_i^2(z)dz} = \frac{\left[\int_o^H m\phi_i(z)dz\right]^2}{\int_o^H m\phi_i^2(z)dz} \qquad (17)$$

Sustituyendo en (17) las expresiones de las funciones modales encontradas en (2.15), concluimos que las masas de los osciladores modales para una viga uniforme en voladizo que se deforma exclusivamente por corte están dadas por la expresión

$$M_i = \frac{8M}{(2i-1)^2\pi^2} \qquad (i = 1, 2, 3,...) \qquad (18)$$

en que M es la masa total de la viga.

La tabla siguiente da los valores de M_i/M para los cinco primeros modos.

i	$\frac{M_i}{M}$
1	0.81057
2	0.09006
3	0.03242
4	0.01654
5	0.01001

Observemos que los osciladores modales de los tres primeros modos contienen, en conjunto, poco más del 93% de la masa total de la viga, y que entre los cinco primeros completan alrededor del 96%.

Se demuestra en los libros de teoría de las series de Fourier que

$$\sum_{n=1}^{\infty} \frac{1}{(2n-1)^2} = \frac{\pi^2}{8} \qquad (19)$$

Concluímos, entonces, que

$$\sum_{i=1}^{\infty} M_i = M \qquad (20)$$

La suma de las masas de los osciladores modales, definidos en la forma que se ha hecho más arriba, es igual a la masa total de la estructura. Podemos establecer este resultado sin necesidad de recurrir a la relación (19). Concibamos un movimiento impulsivo de la viga a partir de su configuración de equilibrio

con reposo, por el cual damos a cada punto de la viga una velocidad igual a la unidad. Evidentemente la cantidad de movimiento inicial de la viga será igual a su masa total M.

Ahora bien, para este movimiento tan especial tenemos las condiciones iniciales

$$x(z,0) = 0 = f_1(z) \tag{21}$$

$$x_t(z,0) = 1 = f_2(z) \tag{22}$$

Luego, las ecuaciones (3.9) y (3.10) nos dan

$$\alpha_i = 0 \tag{23}$$

$$\omega_i \beta_i = \frac{\int_0^H \phi_i(z)dz}{\int_0^H \phi_i^2(z)dz} \tag{24}$$

y la cantidad de movimiento inicial será, de acuerdo con (3.8),

$$\int_0^H m x_t(z,0)dz = \int_0^H \sum_{i=1}^{\infty} m\omega_i\beta_i\phi_i(z)dz = \sum_{i=1}^{\infty} m \frac{\left[\int_0^H \phi_i(z)dz\right]^2}{\int_0^H \phi_i^2(z)dz} =$$

$$= \sum_{i=1}^{\infty} M_i \tag{25}$$

por (17). Luego, $\sum_{i=1}^{\infty} M_i = M$.

Profundizando en el significado físico de las relaciones de ortogonalidad, demostraremos que: el trabajo virtual de las fuerzas de inercia desarrolladas en un modo para un desplazamiento virtual correspondiente a un modo distinto es idénticamente nu-

lo. Análogamente, el trabajo virtual de las fuerzas elásticas internas (esfuerzos de corte) desarrollado en un modo para un desplazamiento correspondiente a un modo distinto e idénticamente nulo.

En efecto, las fuerzas de inercia correspondientes al modo están dadas por (ver ec. 3.12)

$$- m \ddot{\xi}_i(t) p_i(z) dz \tag{26}$$

y un desplazamiento virtual correspondiente al modo j está dado por

$$\dot{\xi}_j(t) \phi_j(z) \delta t \tag{27}$$

Llamemos δW_{ij} el trabajo virtual; tendremos

$$\delta W_{ij} = -m \ddot{\xi}_i(t) \dot{\xi}_j(t) \delta t \int_0^H \phi_i(z) \phi_j(z) dz \tag{28}$$

Si $i \neq j$ $\qquad \delta W_{ij} = 0 \qquad (i \neq j)$ (29)

en virtud de las relaciones de ortogonalidad

Para $i=j$, la ec. (28) dá

$$\delta W_{ii} = -m \ddot{\xi}_i \dot{\xi}_i \delta t \int_0^H \phi_i^2(z) dz$$

o sea

$$\delta W_{ii} = - \frac{d}{dt} \left[\frac{1}{2} m \dot{\xi}_i^2 \int_0^H \phi_i^2(z) dz \right] \delta t = -\delta T_i \tag{30}$$

El trabajo de las fuerzas de inercia desarrolladas en el modo i para un desplazamiento correspondiente al mismo modo es igual al decremento de la energía cinética de dicho modo.

Analizando ahora el trabajo virtual de las fuerzas elásticas internas, encontramos, llamando δU_{ij} el trabajo realizado por las fuerzas elásticas del modo i para un desplazamiento correspondiente al modo j

$$\delta U_{ij} = \int_o^H Q_i \frac{\partial \dot{x}_j}{\partial z} \delta t dz \qquad (31)$$

pero $$Q_i = KAG \frac{\partial x_i}{\partial z} = KAG\ \xi_i(t) \phi_i'(z) \qquad (32)$$

y $$\frac{\partial \dot{x}_j}{\partial z} = \dot{\xi}_j(t) \phi_j'(z) \qquad (33)$$

Luego $$\delta U_{ij} = \delta t\ KAG \dot{\xi}_j(t) \xi_j(t) \int_o^H \phi_i^1(z) \phi_j^1(z) dz \qquad (34)$$

que según hemos demostrado en (6 bis) es igual a cero para $i \neq j$.

Ahora bien, para i=j, tenemos

$$\delta U_{ii} = \delta t\ KAG\ \xi_i(t)\ \dot{\xi}_i(t) \int_o^H [\phi_i'(z)]^2 dz$$

o sea

$$\delta U_{ii} = \frac{d}{dt} \left[\frac{1}{2} KAG\ \xi_i^2(t) \int_o^H [\phi_i'(z)]^2 dz\right] \delta t = \delta V_i \qquad (35)$$

en que V_i es la energía elástica del modo i. Tenemos en concecuencia que el trabajo de las fuerzas elásticas desarrolladas en el modo i para un desplazamiento correspondiente a ese mismo modo es igual a la variacion de la energía potencial del modo en cuestión.

Con esto terminamos la demostración de que no hay interacción entre los modos de vibrar durante una oscilación libre. Cada modo se comporta como si los demás no existieran. Resulta, entonces, que no sólo el sistema como un todo es conservativo, sino que, además, la energía se conserva dentro de cada modo.

5. RESPUESTA DE LA VIGA DE CORTE EN VOLADIZO PARA UN MOVIMIENTO ARBITRARIO DE SU BASE.

Supongamos cumplidas las hipótesis sobre el movimiento del suelo enunciadas al comienzo de la sección 1. Las expresiones de la energía cinética y potencial en términos de las coordenadas normales, serán (nótese que T es la energía cinética absoluta; es decir, la del movimiento referido a un sistema inicial):

$$T = \sum_{i=1}^{\infty} \frac{1}{2} M_i (R_i \dot{\xi}_i + \dot{S})^2 \tag{1}$$

$$V = \sum_{i=1}^{\infty} \frac{1}{2} K_i R_i^2 \xi_i^2 \tag{2}$$

Las ecuaciones de Lagrange

$$\frac{\delta}{\delta t}\left(\frac{\partial T}{\partial \dot{\xi}_i}\right) - \frac{\partial T}{\partial \xi_i} = - \frac{\partial V}{\partial \xi_i} \qquad (i=1,2,3,\ldots) \tag{3}$$

nos dan

$$M_i R_i^2 \ddot{\xi}_i + M_i R_i \ddot{S}(t) = - K_i R_i^2 \xi_i$$

o bien

$$\ddot{\xi}_i + \omega_i^2 \xi_i = - \frac{a(t)}{R_i} \qquad (i=1,2,3\ldots) \tag{4}$$

La solución de estas ecuaciones esta dada por la conocida integral de Duhamel

$$\xi_i = - \frac{1}{\omega_i R_i} \int_{-\infty}^{t} a(\tau) \operatorname{sen} \omega_i (t-\tau) d\tau \qquad (i=1,2,3\ldots) \tag{5}$$

Recurriendo a la ecuación (3.12) obtenemos inmediatamente para el corrimiento lateral de la sección de la viga a la cota z en

el instante t:

$$x(z,t) = -\sum_{i=1}^{\infty} \frac{\phi_i(z)}{\omega_i R_i} \int_{-\infty}^{t} a(\tau)\,\text{sen}\,\omega_i(t-\tau)\,d\tau \qquad (6)$$

De la ec (4.16 se tiene, tomando en cuenta (4.17),

$$\frac{1}{R_i} = \frac{M_i}{m\int_0^H \phi_i(z)\,dz} = \frac{\int_0^H \phi_i(z)\,dz}{\int_0^H \phi_i^2(z)\,dz} \qquad (7)$$

Luego, finalmente,

$$x(z,t) = -\sum_{i=1}^{\infty} \phi_i(z) \frac{\int_0^H \phi_i(z)\,dz}{\int_0^H \phi_i^2(z)\,dz} \frac{1}{\omega_i} \int_{-\infty}^{t} a(\tau)\,\text{sen}\,\omega_i(t-\tau)\,d\tau \qquad (8)$$

La respuesta queda así expresada como una superposición de las funciones, modales multiplicada cada una por una función del tiempo que no es otra cosa que la respuesta del oscilador modal correspondiente y que un factor constante, característico de cada modo, que se ha dado en llamar <u>factor de participación.</u> Para nuestro caso dicho factor vale

$$\frac{1}{R_i} = \frac{\int_0^H \phi_i(z)\,dz}{\int_0^H \phi_i^2(z)\,dz} \qquad (i=1,2,3\ldots)$$

Sustituyendo las expresiones de $\phi_i(z)$, encontramos

$$\frac{1}{R_i} = \frac{4}{(Zi-1)\pi} \qquad (9)$$

En la tabla siguiente se dan los valores de $\frac{1}{R_i}$ para los cinco primeros modos de la viga de corte uniforme en voladizo

i	$\frac{1}{R_i}$
1	1.2732
2	0.4244
3	0.2546
4	0.1819
5	0.1415

Para el esfuerzo cortante tenemos la expresión

$$Q(z,t) = KAG \frac{\partial_{Xe}(z_1 t)}{\partial z} = - KAG \sum_{i=1}^{\infty} \frac{\phi'_i(z)}{\omega_i R_i} \int_{-\infty}^{t} a(\tau) \operatorname{sen} \omega_i (t-\tau) d\tau \qquad (10)$$

y para el momento volcante

$$\mathcal{M}(z,t) = - KAG \sum_{i=1}^{\infty} \frac{(-1)^i + \phi_i(z)}{\omega_i R_i} \int_{-\infty}^{t} a(z) \operatorname{sen} \omega_i (t-\tau) d\tau \qquad (11)$$

6. EJEMPLO.

Calcular las respuestas modales máximas de una viga de corte uniforme, en voladizo, cuyo período fundamental es 3 seg, sometido a un "temblor" cuyo espectro de aceleraciones absolutas $S_a(T_o)$ es el dado por la Fig. 3.

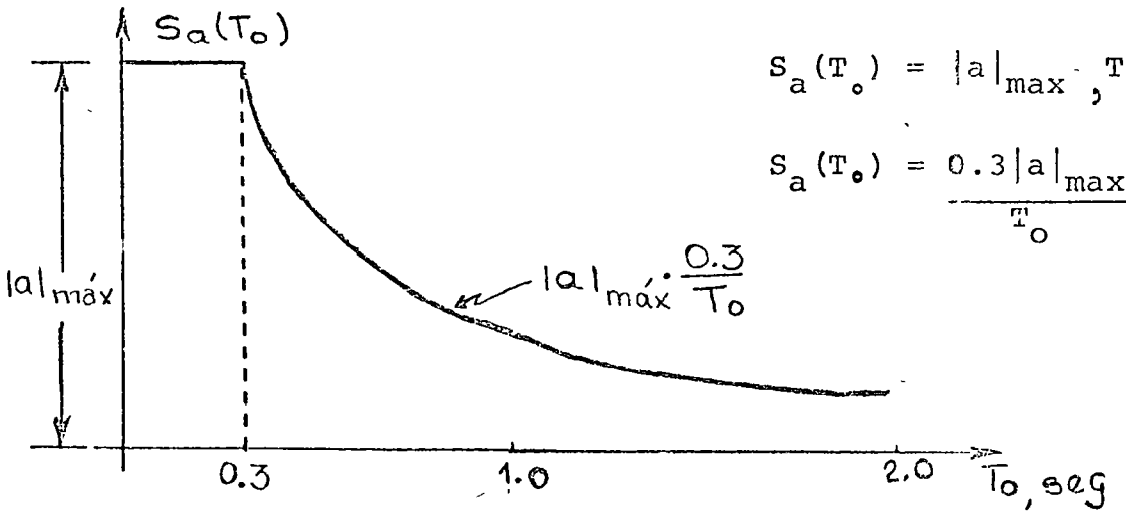

$$S_a(T_o) = |a|_{max}, \quad T_o \leq 0.3 \text{ seg}$$

$$S_a(T_o) = \frac{0.3|a|_{max}}{T_o}, \quad T_o \geq 3 \text{ seg}$$

Fig. 3

El espectro dado corresponde al que se puede obtener en un terreno relativamente duro. En ese tipo de terreno y para una estructura de período fundamental igual a 3 seg, la interacción entre el nulo y la estructura puede no tenerse en cuenta, aunque esta asección debe tomarse con alguna precaución.

La estructura misma podría ser el modelo ultra-simplificado de un edificio en forma de torre, estructurado a base de marcos rígidos de acero, de unos 30 a 35 pisos de altura.

No nos va a interesar el valor mínimo de cada una de las respuestas modales, sino más bien comparar la influencia relativa de las diferentes modos. No interesa, por lo tanto, el valor absoluto de las ordenadas espectrales, sino su forma en relación con los períodos de la estructura.

El espectro de desplazamientos relativos $S_d(T_o)$ (para amortiguamiento nulo) está relacionado con el de aceleraciones absolutas a través de la ecuación.

$$S_d(T_o) = \frac{1}{\omega_o^2} \quad S_a(T_o) = \frac{T_o^2 \, S_a(T_o)}{4\pi^2} \qquad (1)$$

Entonces

$$S_d(T_o) = \frac{T_o^2}{4\pi^2} \, |a|_{max} \quad \text{para } T_o \leq 0.3 \text{ seg} \qquad (2)$$

$$S_d(T_o) = \frac{0.3T_o}{4\pi^2} \, |a|_{max} \quad \text{para } T_o \geq 0.3 \text{ seg} \qquad (3)$$

Los períodos naturales cumplen la relación

$$T_1 : T_2 : T_3 : \ldots = 1 : \frac{1}{3} : \frac{1}{5} : \ldots$$

Luego, con $T_1 = 3$ seg, tendremos $T_2 = 1$ seg, $T_3 = 0.6$ seg, ...
El corte basal máximo para el modo $i^{ésimo}$ se puede expresar en la forma siguiente

$$|Q_i(o,t)|_{Máx} = M_i \; S_a(T_i)$$

en que M_i es la masa del oscilador modal correspondiente al modo i
Llamando W el peso total de la viga obtenemos los cortes barales máximos por modo que se tabulan a continuación

i	$\frac{W_i}{W} = \frac{M_i}{M}$	T_i(seg)	$\frac{S_a(T_i)}{g}$	$\lvert Q_{ibasal}\rvert_{máx}$
1	0.81057	3.000	0.1 $\frac{\lvert a\rvert máx}{g}$	0.081057 W|a|máx:g
2	0.09006	1.000	0.3 "	0.027018 W|a|máx:g
3	0.03242	0.600	0.5 "	0.016210 W|a|máx:g
4	0.01654	0.429	0.7 "	0.011578 W|a|máx:g
5	0.01001	0.333	0.9 "	0.009009 W|a|máx:g
6	0.00670	0.273	1.0 "	0.006700 W|a|máx:g

La suma de los cortes basales modales máximos, tomados en valor absoluto, representa una cota superior para el corte basal total, ya que los máximos de cada modo no ocurren simultáneamente. A partir del sexto modo $T_i \leq 0.3$ seg; luego, a partir de dicho modo, las ordenadas del espectro de aceleraciones son cortantes, e iguales, a $|a|máx$. Luego,

$$|Q|_{base} < \sum_{i=1}^{\infty} |Q_i|_{base,máx} = \left[0.144872 + \sum_{n=6}^{\infty} \frac{1}{(2n-1)^2} \cdot \frac{8}{\pi^2}\right] \frac{W|a|máx}{g}$$

La serie que aparece en esta expresión es convergente y sus valores

$$\sum_{n=1}^{\infty} \frac{1}{(2n-1)^2} \frac{8}{\pi^2} - \frac{8}{\pi^2} \sum_{n=1}^{S} \frac{1}{(2n-1)^2} = 1 - \sum_{i=1}^{S} \frac{Mi}{M} = 1-0.45960=0.04040$$

Luego

$$\Sigma |Q_i|_{base,máx} = 0.185272 \frac{W|a|máx}{g} \; ; \; |Q|_{base} < 0.185272 \frac{W|a|máx}{g}$$

Por otro lado, la expresión

$$\sqrt{\sum_{i=1}^{\omega} Q_i^2 \, base,máx}$$

llamada superposición cuadrática representa el valor más probable de $|Q|_{basal}$, en la hipótesis de que las respuestas modales no están correlacionadas entre sí. Esta expresión dá una estimación por defecto, ya que la hipótesis de partida es falsa. Efectuado el cálculo obtenemos

$$\sqrt{\sum_{i=1}^{\infty} Q_i^2 \, base,máx} = 0.08877 \frac{W|a|máx}{g}$$

Entonces

$$0.08877 \frac{W|a|máx}{g} < |Q_{base}|_{máx} < 0.185272 \frac{W|a|máx}{g}$$

Desgraciadamente no disponemos de una teoría realmente confiable para tener estimaciones más estrechas y realistas de $|Q_{base}|_{máx}$ basados en un análisis modal. La norma chilena para el diseño sísmico de edificios permite emplear el promedio de los resultados

obtenidos superponiendo los valores modales en valor absoluto y en forma cuadrática y exije emplear, por lo menos, los tres primeros modos. Procediendo de esta manera resulta

$$|Q_{base}|_{máx} = 0.106\ \dot{W}\frac{|a|máx}{g}$$

si se consideran los tres primeros modos

$$|Q_{base}|_{máx} = 0.137\ W\frac{|a|máx}{g}$$

si se consideran todos los modos.

En la Fig 4, hemos representado los cortes (en valor absoluto) como función de $\frac{Z}{H}$ para los tres primeros modos, a una misma escala. La Fig 5, muestra los cortes de los tres primeros modos superpuestos en valor absoluto.

Se puede apreciar que la influencia de los modos 2o. y 3o. es muy importante en el tercio superior de la estructura. En los que en lenguaje vulgar se describe con los nombres de efecto de "chicoteo" o de "coleo".

Consideremos ahora el caso de una viga más rígida, con un período fundamental de 0.3 seg, que podría corresponder a un edificio de hormigón armado de unos cuatro o cinco pisos.

Repitiendo los cálculos tenemos

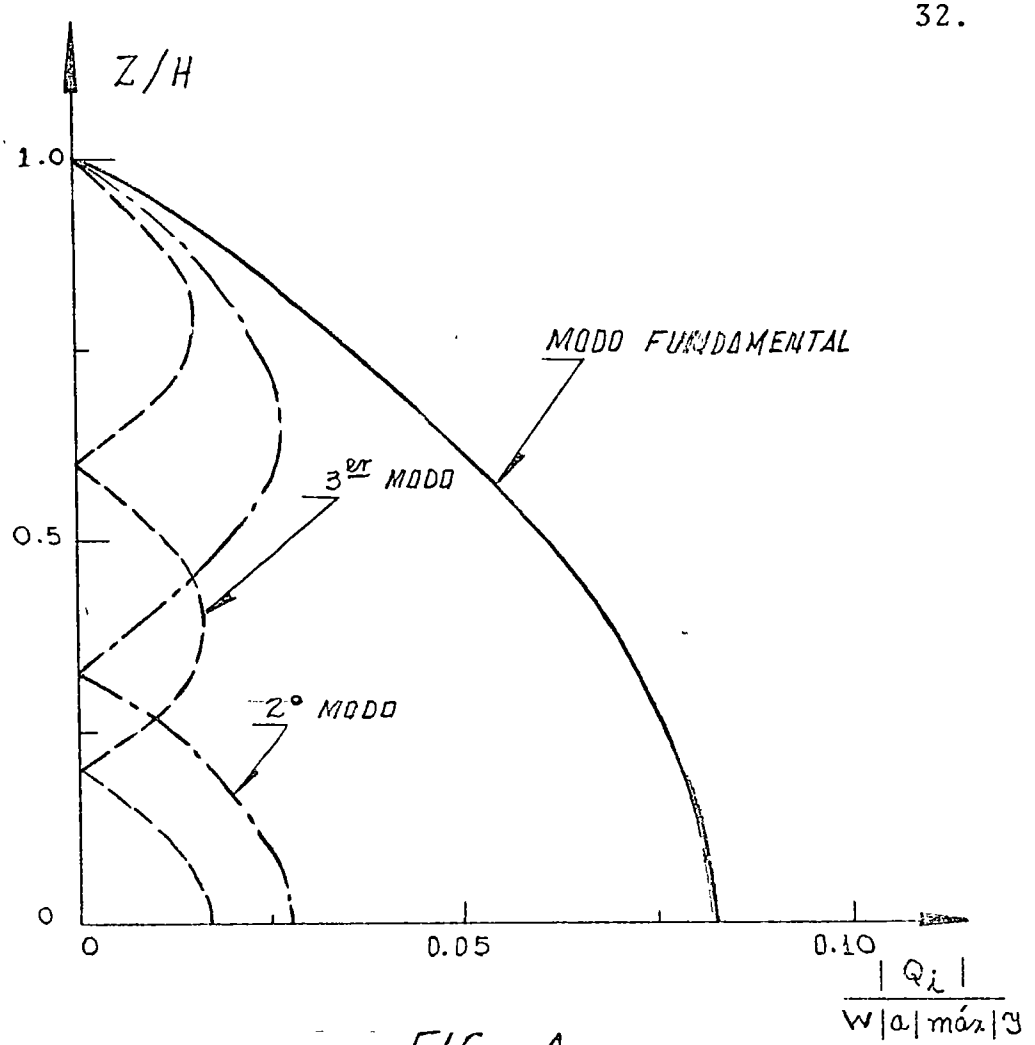
Z/H
1.0
0.5
0
0
0.05
0.10
MODO FUNDAMENTAL
3er MODO
2° MODO
| Qi |
W |a| máx |y

FIG 4

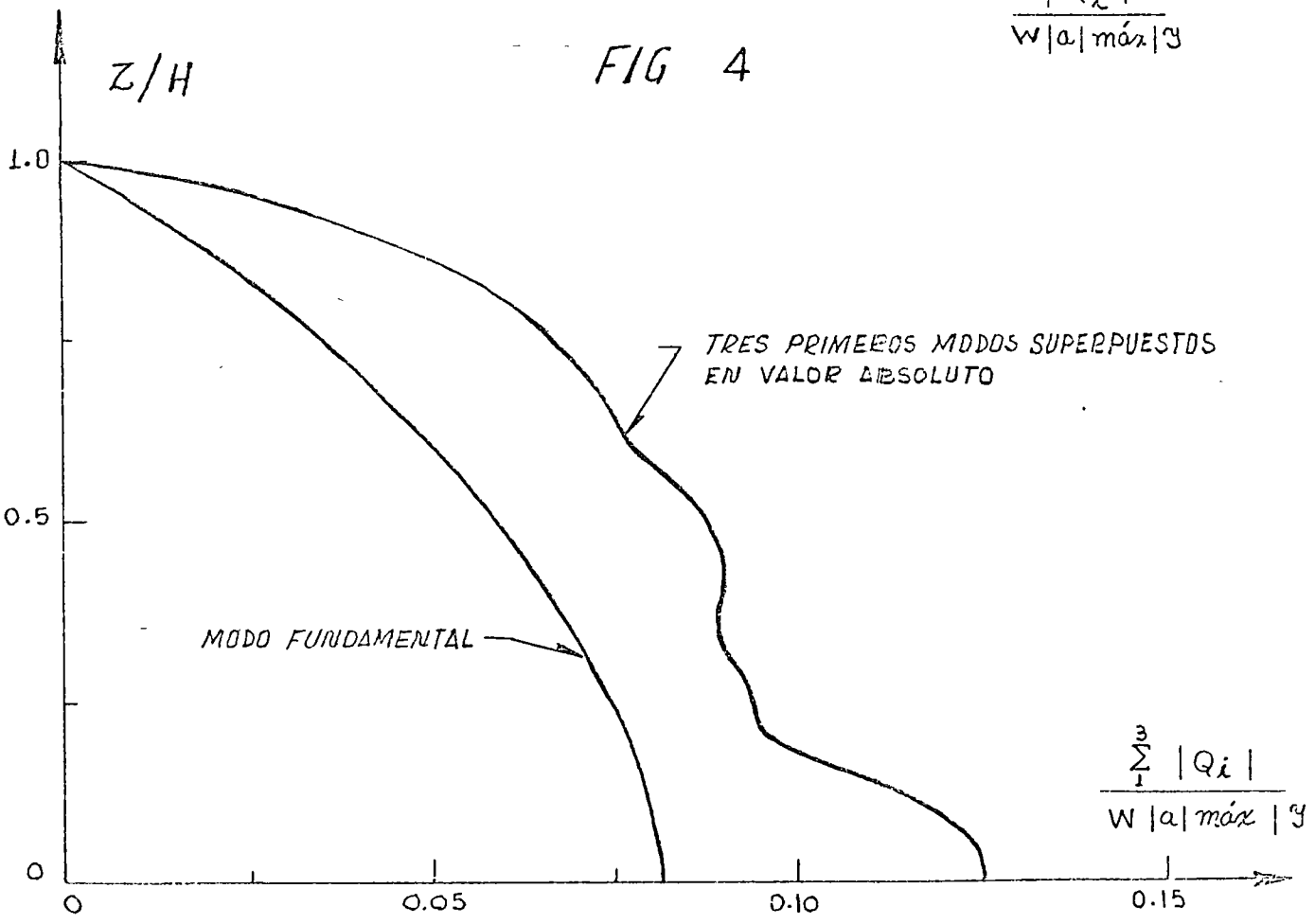
Z/H
1.0
0.5
0
0
0.05
0.10
0.15
TRES PRIMEROS MODOS SUPERPUESTOS
EN VALOR ABSOLUTO
MODO FUNDAMENTAL
Σ 3 1 |Qi|
W |a| máx |y

FIG 5

i	$\frac{W_i}{W} = \frac{M_i}{M}$	T_i(seg)	$\frac{S_a(T_i)}{g}$	$\lvert Q_{i\ base}\rvert_{máx}$
1	0.81057	0.3	$\lvert a\rvert_{máx}:g$	0.81057 $W\lvert a\rvert_{máx}/g$
2	0.09006	0.1	"	0.09006 "
3	0.03242	0.06	"	0.03242 "
4	0.01654	0.0429	"	0.01654 "
5	0.01001	0.0333	"	0.01001 "
Σ				$W\lvert a\rvert_{máx}/g$

La superposición en valor absoluto dá simplemente

$$\Sigma\lvert Q_{i\ base}\rvert = W\lvert a\rvert_{máx}/g$$

Mientras que la superposición cuadrática dá:

$$\sqrt{\Sigma\ Q^2_{i\ base,máx}} = 0.816\ W\lvert a\rvert_{máx}/g$$

Ahora las dos estimaciones son más parecidas y podemos encerrar $\lvert Q_{base,máx}\rvert$ entre límites más estrechos

$$0.816\ W\lvert a\rvert_{máx}/g < \lvert Q_{base,máx}\rvert < W\lvert a\rvert_{máx}/g$$

La Fig 6 muestra que en las estructuras de período relativamente corto (para el espectro de respuesta que hemos supuesto), la influencia de los modos superiores es menor importante que en la del período fundamental largo. También resulta menos importante el efecto de "chicoteo"

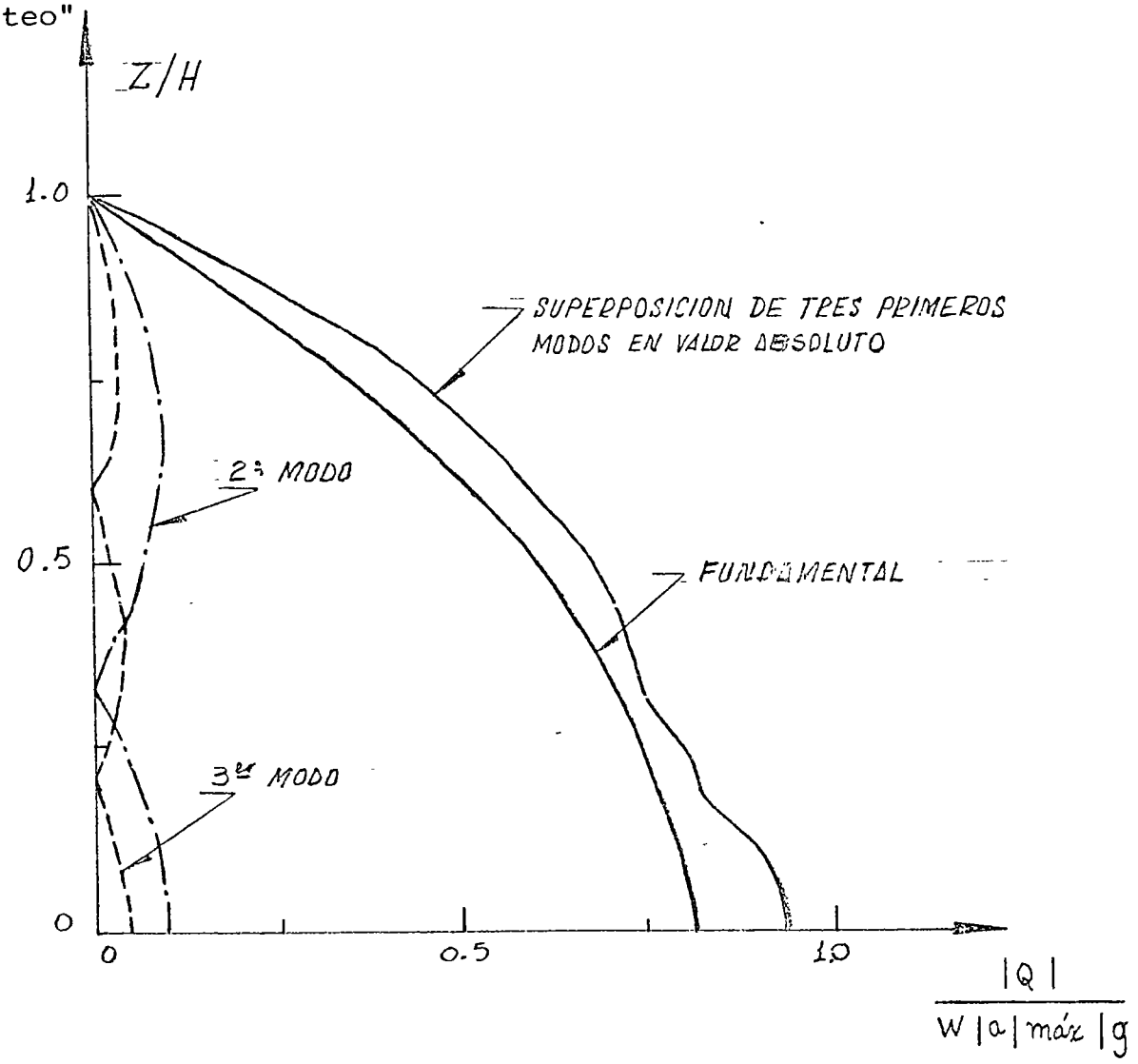

FIG 6

Examinemos ahora los momentos de volteo. Para ello aprovechamos el resultado encontrado en (2.20) que determina el momento de volteo basal en función del corte basal para cada modo. Encontramos para la viga cuyo período fundamental es 3 seg, los valores que se anotan en la tabla que va a continuación.

i	$\frac{\lvert M_{i\ máx}\rvert_{base}}{WH\lvert a\rvert_{máx/g}}$
1	0.05160
2	0.00573
3	0.00206
4	0.00105
5	0.00064

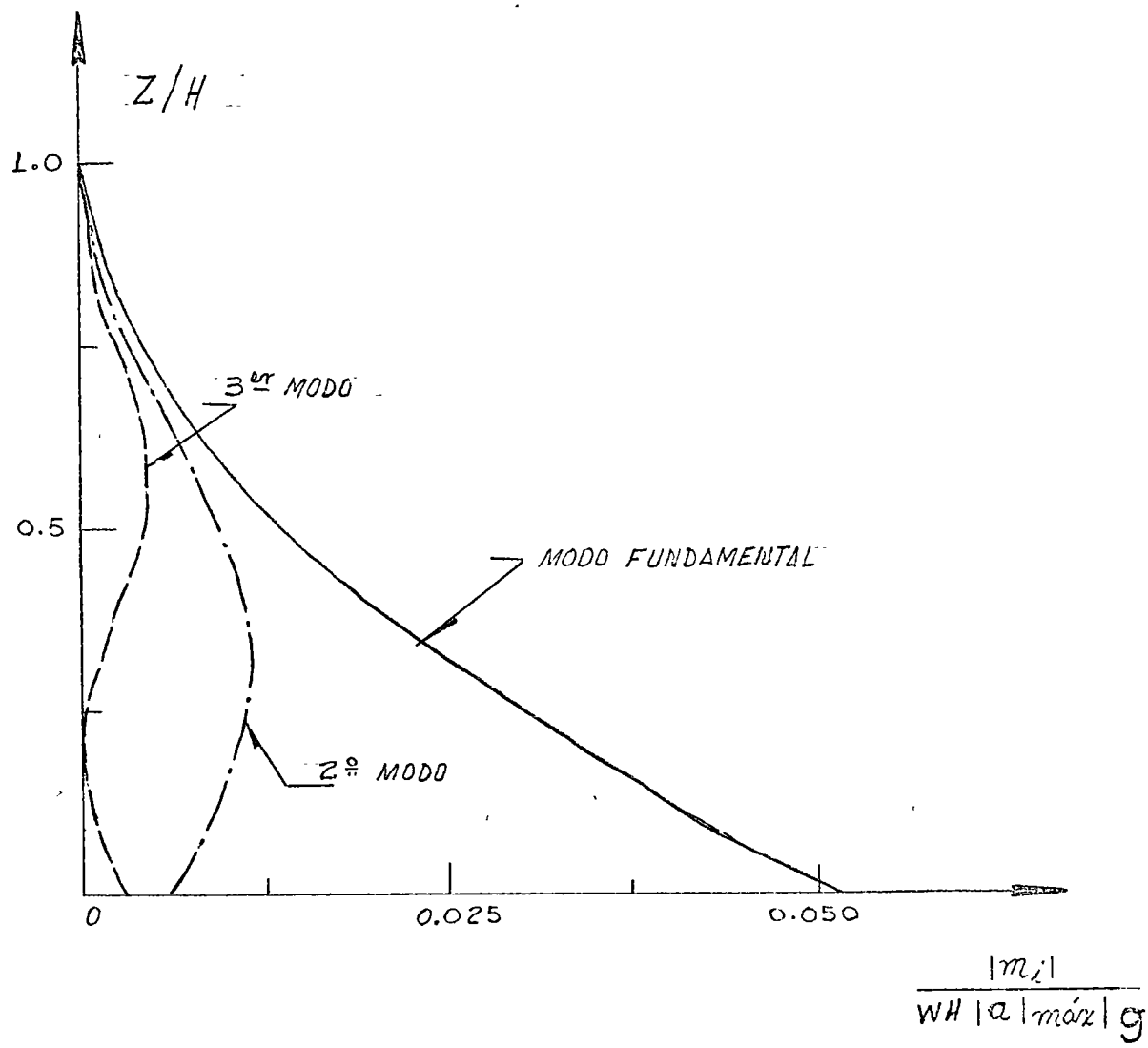

FIG 7

MICROZONING: MODELS AND REALITY

Contribution to a panel session on Ground Motion Characteristics

6WCEE, Delhi, 1977

by

Luis Esteva[1]

INTRODUCTION

Nobody doubts that local conditions usually have a significant influence on the characteristics of earthquake ground motion. What is not agreed upon, however, is the manner in which that influence must be evaluated. When one talks about microzoning, attention is usually focused on shear-beam models of stratified soil formations and in unidimensional, vertically traveling shear waves. But strong-motion and seismological records have shown that those models can only be applied to a much narrower range of conditions than is usually believed, and that many other geologic or topographic features can have a more pronounced influence on ground motion than the presence of sediments. More general analytical models have been developed in order to account for two-dimensional and three-dimensional response and various types of arriving waves, but their validity and range of applicability have not been determined yet. Because of this, and because of the greater complexity of these models as compared with shear-beam amplification models, they have not gained wide acceptance in the solution of actual engineering problems.

Not only is the shear-beam amplification model the object of strong controversy with respect to the types of waves that significantly contribute to the earthquake motion at a site, but also with respect to the lack of consistent criteria intended to define base rock level, i.e., the level at which usual intensity-attenuation laws are supposed to be valid, and above which local soil contributes to modify intensity and frequency content of seismic motions. In other words, it cannot be uniquely defined what constitutes local conditions and what is a portion of the path. Those criteria can be objected also on the grounds that the influence of local soil conditions is often accounted for twice when making estimates of seismic risk: as a random factor associated with the path when establishing empirical attenuation laws and as a systematic correction associated with local conditions when studying amplification.

But microzoning is not only a matter of ground-motion amplification; it also implies formulation of consistent criteria to define design spectra at different sites, and evaluation of liquefaction potential. The former point requires consideration of the different laws that govern amplification of different types of waves and different directions of arrival, as well as their corresponding probabilities; the latter is not covered by this discussion, as it will be included in another panel session. Thus, the paper deals with the problems of ground motion characteristics, under the framework of conceptual models, analytic results and observed facts. The paper is not intended to be a state-of-the-art report although it is based on one

[1] Institute of Engineering, National University of Mexico

(Ruiz, 1976) The intention of the author is mainly to point out some basic questions pertinent to the topic, aiming at the generation of vivid and fruitful discussion.

SEISMIC WAVES

The results of some analytical studies show that the influence of local soil on the ground motion is strongly dependent on the nature of the incoming seismic waves. Hence, analytical prediction of the amplitudes of ground motion at a site characterized by given local conditions as compared with those that would occur under standard conditions requires both the decomposition of the motion into various types of incoming waves, and the formulation of models adequate for the study of amplification and transformation of those types of waves. Despite the very significant effort devoted by seismologists to the formulation of analytical models for the study of wave amplification and transformation, very little of their contributions is either available or of use to engineers, as those models deal in general with the types of waves that are recorded at large epicentral distances (far field), or consider highly idealized topographical features. These results should not be overlooked, however, as they can provide a qualitative insight to many engineering problems.

If a reasonable degree of success is to be attained in the prediction of the influence of local conditions for a sufficiently wide range of cases, a lot of understanding has to be previously achieved about the decomposition of ground motion into different types of seismic waves in the near and intermediate fields. Obviously, the detailed source mechanism and the propagation path can be decisive in the directions and relative amplitudes of the most significant incoming waves, and hence on the laws governing ground motion amplification.

MECHANISM, PATH AND LOCAL CONDITIONS

The profusion of heterogeneities, irregularities and discontinuites in the earth's crust (Fig. 1) is responsible for the complex patterns of reflection, refraction, and scattering that seismic waves suffer in their path from source to site. Hence, it is not surprising that the influence of mechanism and path on ground motion characteristics is in some instances more pronounced than that of local conditions. This influence stems both from the modification of the surface ground motion itself, independent of local conditions, and from the fact that the different types of seismic waves resulting from mechanism and path effects are modified by local soil in different manners.

Fig 2 shows the two main paths followed by seismic energy form the source to a site of interest: through the interior of the crust, in the form of body waves, and along the surface, in the form of surface waves. But this picture still displays an oversimplified conception of the process: the source is not a point, but a large volume, and the influence of path is much more pronounced and complex than is implied by Fig. 2.

The general type of source mechanism, and not only the detailed history of relative displacement along a fault, has a strong influence on the types of seismic waves generated, and hence on the motion characteristics for standard ground conditions, and in the manner in which local conditions modify them. Thus, strike-slip motion tends to produce a relative higher proportion of SH and Love waves, while subduction faults tend to produce higher proportions of P, SV and Rayleigh waves. The fact that seismic waves are generated from a large volume that may extend as far as the ground surface or its close proximity means that a significant portion of the motion at the near field should be made up of the contribution

of body waves that travel at very low angles with respect to the horizontal (Fig 3). These waves are probably guided along stratified formations and then modified by local conditions according to patterns similar to those affecting surface waves. Besides, it is likely that they give place to conventional surface waves that significantly contribute to ground motion at short epicentral distances and in the range of small and moderate frequencies. This pattern of energy travel seems plausible, and provides an explanation to the failure of conventional amplification theory to adequately predict the influence of local conditions.

The complexity of the path followed by waves is another reason for stating that surface ground motion at the near field is not the result of the superposition of a short number of wave trains: every wave impinging on a crust heterogeneity, subsurface discontinuity or topographic feature, gives place to a number of secondary trains of all types of waves (Fig 4).

Whatever the mechanism and the path of the waves for a given shock, it is of interest to assess the influence of local conditions; but, as Fig 5 shows, that influence cannot in general be made to depend only on the stratified soil formations underlying the site of interest: as an important portion of the energy may be traveling in the horizontal direction, the meaning of the term *local conditions* should be extended to include geologic and topographic features in the immediate vicinity of the site. Local amplification would hence be sensitive to the direction of wave arrival.

Even in the case that adequate tools were available for estimating the influence of local conditions on the amplification functions for the various significant types of seismic waves, the problem would remain of determining the trains of waves of different types that would arrive from a given direction. This is probably not feasible when dealing with near-field problems, first because of the possible occurrence of a large number of significant wave trains of different types incoming from different directions, and second because it is not always clear whether a given geologic or topographic accident should be taken as portion of the path –the influence of which would be included as a random factor in the experimental error of an *intensity attenuation expression* (expression relating intensity with magnitude and distance)– or of the local conditions –the influence of which should be included as a systematic correction– when trying to predict ground motion produced by seismic waves arriving from a given direction. For instance, coming back to Fig 5, a promontory such as *B* could be taken as a part of the path or of the local conditions for the purpose of assessing the contribution of surface waves coming from the left to ground motion at *A*, depending on whether the local zone is assumed to be bounded by line 1 or 2, respectively. Because the absence or presence of features such as these has not been explicity included in empirical attenuation expressions, a unique criterion cannot be easily established. For the purpose of microzoning, however, a great deal of information is provided by ratios of surface wave amplitudes at *A* and *B* –and not necessarily their absolute values– for earthquakes originated at the left of the figure.

OBSERVED FACTS

Before the San Fernando earthquake of 1971, conceptual models of soil-related intensity amplification had gained their main support from nearly qualitative comparisons of observed differences between intensities on firm ground and on sedimentary deposits at a number of sites, notably Tokyo, San Francisco, Mexico City and Caracas. A more quantitative support to models based on the concept of vertically traveling SV waves had been provided by the comparison of predicted and observed response of the soft clay

deposits underlying Mexico City (Herrera I. *et al,* 1965); but conclusions valid for very peculiar conditions –existence of a very pronounced contrast between shear wave velocities of soil and underlying material– were being indiscriminately extrapolated, in spite of the fact that, in order to apply the same criterion, arbitrary decisions had often to be made concerning the portion of the ground profile that should be considered as a filter that would amplify standard-conditions-ground-motion. But records obtained during San Fernando earthquake disclosed the limitations of the mentioned criterion. Although a large portion of the area affected by that earthquake is known to be underlain by deep sedimentary formations (Fig 6), no pronounced contrast between shear wave velocities is apparent. Fig 7 (from Hudson, 1972) shows a sampling of peak accelerations measured at different sites. Included are all sites for which a clear distinction could be made between rock and alluvium as the basic site condition. It is evident that many factors other than distance and local site characteristics must be important.

Influence on ground motion of fault mechanism and propagation path has been disclosed by recordings obtained at a number of sites during several events. Thus, Udwadia and Trifunac (1973) analyzed a group of 15 events recorded at El Centro, California, characterized by short epicentral distances and magnitudes ranging from 3 to 6.8; the same authors (Trifunac and Udwadia, 1974) studied the records obtained at 6 stations located in the metropolitan area of Los Angeles during three different earthquakes, and Hudson (1972) analyzed the records of a number of seismoscopes and accelerographs obtained within an area of 40 square miles during San Fernando earthquake.

The 15 events recorded at El Centro were classified into four sub-groups, according to source azimuth with respect to the station, and Fourier spectra of records within each sub-group were compared. Group I included four events, three of them having the same epicenter, but different magnitudes. Spectral shapes of the components corresponding to the various events differ considerably among themselves. As propagation path and local conditions are the same, differences can only be ascribed to differences in fault mechanism and perhaps to nonlinear effects. Group II includes four events with different magnitudes and origins and, again, no similarity attributable to path or local conditions can be detected in the records. For one event in particular, predominant frequencies are very low, which can be explained in terms of predominance of surface waves. Group III includes the Imperial Valley earthquake of 1940, the record of which has been analyzed (Trifunac, 1971a) leading to the conclusion that it actually consisted of the superposition of several events, each starting a few seconds after the previous one. Horizontal components are similar, but the vertical component of the Imperial Valley earthquake shows significantly higher ordinates for high frequencies. This is probably a consequence of the short epicentral distance, that implies low attenuation of body waves, and of the peculiar source mechanism. Finally, the last group included events with large epicentral distances –about 150 km– and records were characterized by the low frequencies typical of surface waves. Despite very clear similarities between magnitude and origin of events in this group, their spectral shapes are significantly different, thus suggesting predominance of source effects over path and local conditions.

Similar conclusions are obtained from Trifunac and Udwadia's study concerning the records obtained at six stations during Borrego Mountain (1968), Lytle Creek (1970) and San Fernando (1971) earthquakes: source mechanism and epicentral distance significantly affected the records, while local conditions played only a secondary role. Of the six stations, four lie within Los Angeles Metropolitan area, two of them less than 1 km apart; two are located on base-rock and the other four –those within Los Angeles– on deep sediments of intermediate stiffness. In no case are dominant ground periods evident. An analysis of

records obtained at the four sites on sediments makes apparent the influence of source mechanism. For the Borrego Mountain shock, for instance, transverse displacements are systematically larger than radial ones, thus suggesting significant contribution of Love waves; the shapes of the displacement and velocity records are the same at all four sites, but their amplitudes differ, probably as a consequence of variations in the depth of alluvium from station to station, within a distance of 12 km. Records and spectra corresponding to the San Fernando earthquake are also very similar among themselves, but they differ in shape and in relative frequency content from those obtained during the other shocks. Large amplitudes of radial and transverse displacements have been ascribed (Hanks, 1975) to Rayleigh and Love waves, respectively. Fourier spectra of Borrego Mountain records at the four Los Angeles stations shown are very similar in the range of frequencies smaller than 1 hz; the similarity should not be ascribed to dominant group periods, but to the predominance of surface waves, given the long epicentral distance –about 200 km. For San Fernando earthquake, instead, the contribution of high frequencies is rather important, as could be expected, given the proximity of the source—40 km.

Hudson's observations during San Fernando earthquake covered a wide range of ground conditions, from crystalline rock to alluvial deposits 300 m deep. Notorious discrepancies were observed in seismoscope traces even for sites with very similar ground conditions, stressing the importance of other factors, such as topography or subsurface irregularities, pointed out, for instance, by Jackson (1971) and Boore (1972). A comparison of response spectra corresponding to rock and alluvium sites fails to show any systematic influence of local soil. The author concludes that the properties of response spectra at the same sites during another earthquake would probably show quite different relative variations. This implies that formulation of microzoning maps must be based on the analysis of records obtained during a sufficiently large number of intense earthquakes.

Some interesting cases have been presented in the literature, describing the overall response of some soil formations during strong earthquakes. Although the influence of local conditions was shown to be clear in those cases, it was also clear that it may not suffice to study the influence of the soil directly underneath the structure of interest, but that an analysis of the response of a wider area can explain observed facts. Two instances will be described in this respect: one corresponds to the Skopje earthquake of 1963, and the other to two records obtained at Hutt Valley, New Zealand.

Poceski (1969) describes the geological setting of Skopje: the city is located in a long valley along which flows the Vardar river. A cross section of the valley shows a large discontinuity of the sediment thickness along a line that follows the river course (Fig 8). The greatest intensity of damage on constructions was observed directly above the discontinuity, and was ascribed to the hypothetical occurrence of large rotational components of the ground motion with respect to a vertical axis, motivated by the also hypothetical difference in the horizontal response of the alluvial deposits at each side of the discontinuity.

The rotational response of a large volume of alluvium was actually detected by Stephenson (1974), when he analyzed the records obtained at two sites near Hutt Valley. The sites are 900 m apart, and are underlain by saturated recent alluvial deposits with shear wave velocities of about 100 m/sec. Spectral densities of acceleration at both sites show each a predominant direction of response, with a high statistical correlation between the corresponding predominant components, thus suggesting the torsional oscillation of a large mass of alluvium.

How should microzoning be influenced by effects such as those described in this section? .

EFFECTS OF TOPOGRAPHY

The largest acceleration ever recorded occurred at one of the abutments of Pacoima dam during the San Fernando earthquake and implied, according to Reimer *et al* (1973) a three-fold amplification of its peak value. Ratios of up to 30 between the peak ordinates of the Fourier spectrum of the velocity record obtained at the top and at the base of Kagel mountain were computed for several aftershocks of the mentioned event, while the corresponding ratios of peak ground velocities "only" reached 3.95. This implies a resonant effect of the mountain, which was explained by Davis and West (1973) in terms of the ratio of its average width and the length of shear waves. The values indicated are not necessarily amplifications with respect to standard conditions (whatever they are), as analytical studies show (see Fig. 9) that at some frequencies wave amplitudes tend to be amplified at the top of promontories and reduced at their base (Bouchon, 1973; Aki & Larner, 1970; Boore, 1972), but the fact remains that the effects of surface topography cannot be overlooked. Similar considerations can be made regarding the significance of subsurface topography: the distribution of structural damage in Skopje in 1963 was ascribed to excessive torsional oscillations in the region directly above a sharp discontinuity of soft layer thickness (Fig. 8) for incident waves that possessed significant horizontal components parallel to the discontinuity; and analytical studies predict focusing of waves in the vicinity of subsurface irregularities (Jackson, 1971). The interaction of subsurface topography and direction of wave arrival is illustrated in Fig 10 (Trifunac, 1971b), which shows relative amplitudes of the motion produced at the surface by SH waves arriving at a semicylindrical valley. Amplitudes vary with site location and with incidence angle at a fast rate, thus suggesting that detailed knowledge of subsurface topography and of directions and types of incoming waves would be required for the deterministic prediction of the influence of topographic features. As this knowledge is not easy to achieve at present, careful judgement must be exercised when trying to employ analytical results as those shown here in the predictions of seismic risk.

A further question stemming from the significance of surface and subsurface irregularities is that related to the homogeneity of the data set that has been used by different investigators in the derivations of empirical attenuation expressions: unless those sites for which the topographic conditions are suspected to have a significant systematic influence on ground motion are eliminated from the data set used to derive those attenuation expressions, we face the danger of accounting for the mentioned conditions twice: as random effects in one step and as systematic effects in another.

MODELS AND REALITY

Theoretical considerations and observed facts concerning mechanism, path and local conditions, point at the complexities involved in the formulation of mathematical models intended to predict the influence of local conditions on ground motion.

Hence, the question arises of whether the role of those models is too limited to be of practical significance. This is probably too pessimistic an outlook although detailed simulations of near-field motions based on physical models that account for source, path and local conditions are probably beyond reach of present engineering practice, the writer believes that a fair degree of understanding of the parameters and mechanisms that affect ground motion amplification and attenuation can be gained by means of simplified analytical models that consider alternate patterns of energy liberation and propagation.

The significance of models as related to reality and to decision making in engineering is dramatically illustrated by the applicability of the vertically-traveling-shear wave model to the study of ground motion amplification in the valley of Mexico: this is the site on earth where that model has been most beautifully supported by instrumental evidence, and however, the shallow depths and large epicentral distances of earthquakes usually observed there imply that practically all energy must arrive in the form of surface waves. It is easy to understand that the apparent confirmation of the unidimensional-shear-wave model in this case stems from the fact that the large lengths of the incoming surface waves lead to the response of the soft soil formation far away from the borders of the valley according to a pattern very similar to that of the shear beam model. The agreement is accentuated because very little energy is radiated back to the base, and because a significant portion of it is radiated in accordance with the shear beam model. This form of soil response and the small ratio of energy radiation are responsible for the occurrence of dominant ground periods. For the same reasons, dominant ground periods determined by means of excitation applied at the surface coincide with those resulting from earthquake excitation. But the conditions that favor the practical applicability of the mentioned model in the case where a pronounced contrast exists between the soft formations and the base do not appear in the absence of that contrast, and conditions other than sediment properties may dominate the local pattern of intensity variations.

In an attempt at developing a unified approach to the combined intensity-attenuation and local-amplification effects for site underlain by stratified soil formations, Sanchez and Esteva (1977) made use of available data for the derivation of attenuation expressions that directly account for the systematic influence of local soil, while random deviations were dealt with as equation errors. Data of earthquakes recently recorded at sites where detailed information was available about local soil conditions (this means 50 horizontal components at 10 different sites) provided the basis for semiempirical attenuation expressions for Fourier spectra at the ground surface. These expressions are of the form $F(\omega) = G(\omega; R, M)\, g(\omega, s)$, where $F(\omega)$ is the ordinate of Fourier spectrum for frequency ω, G accounts for source (M) and path (R) effects, and g is a function that accounts for amplification effects in terms of local soil properties (s). G was assumed of the form $b_1(R + c)^{-b_3} \exp(b_2 M)$, and g was taken as the amplification function of an equivalent single-degree-of-freedom model of a linear shear beam assumed to represent the soil layers above firm ground. A number of expressions were derived for seven values of ω, in accordance with three alternate definitions of firm ground: the surface material itself, or those with shear wave velocities of 400 and 800 m/sec, respectively. The results were disappointing: the ratio of observed to predicted ordinates of Fourier spectra was systematically greater than unity for the components recorded at the particular site where the computed values of g were highest (i.e., where a thick layer of very soft materials existed), and the standard deviation of that ratio for the whole ensemble of sites and records was very high and independent of the definition of firm ground. But Mohraz (1976) obtained significantly different intensity attenuation expressions for different alluvium thickness. A similar study was carried out by Faccioli (1976), who classified ground properties into four categories: crystalline rock, sedimentary rock (including stiff conglomerates and very compact sands), typical alluvial deposits with intermediate stiffness and soft deposits (loose sands and soft clays). He succeeded in obtaining empirical attenuation expressions for each of these categories, for which the standard deviation of error is lower than that associated with previous expressions that neglected the influence of local conditions (Esteva and Villaverde, 1973; Mc Guire, 1974). The systematic influence of such conditions is thus confirmed, as well as the inadequacy of the shear beam model to predict them.

Two-dimensional models as shown in Fig 11 can perhaps suffice for the qualitative study of

the overall patterns of wave generation and transformation. They should also prove useful for the understanding of the possible influence of irregularities and discontinuites found by different types of waves along their path, and for the assessment of local variability of intensities in the neighborhood of some geological or topographical accidents. Probably, they can even help at gaining some insight into the general patterns of waves arriving at a site, thus permitting the formulation of adequate amplification models. There are instances, however, where three-dimensional models may be required. One such case is the study of the amplified motion recorded at one of the abutments of Pacoima Dam during San Fernando earthquake; another would be the study of the response of an alluvial formation where torsional oscillations might be of importance.

Given a train of incoming waves, predictions of the resulting motion at a site with heterogeneous properties or irregular topography can be dealt with as a diffraction problem. However, standard analytical formulation (Morse & Feshbach, 1953) can only be applied in practice to simplified idealizations of actual conditions (see, for instance, Aki and Larner, 1970; Bouchon, 1973; Trifunac, 1971b). For more general applications, finite difference solutions of the wave equation (Boore, 1972), finite element wave-propagation investigations (Smith, 1974) and dynamic response studies of finite-element models of small local regions (Lysmer & Drake, 1971; Ayala & Aranda, 1977) have been undertaken. The latter formulation is very attractive to engineers, because it permits direct application of standard programs of frequency-domain or time-response dynamic analysis. But adequate boundary conditions have to be defined at the edges of the region under study in order to allow transmittal of incoming and outgoing waves without excessive energy losses or reflections. When incoming and outgoing waves are of the same type and have the same direction, theoretically exact boundary conditions can be established, expressed in terms of equivalent damping units (Lysmer & Drake, 1971; Tsai, 1969). Aproximate solutions have also been formulated for the case of outgoing body waves of known type and unknown direction (Lysmer & Kuhlenmeyer, 1969) and these solutions have been extended to the combination of incoming and outgoing waves (Ayala & Aranda, 1977), but the general case of known incoming waves and unknown outgoing wave types and directions has not been sufficiently studied.

Despite these problems, criteria based on the time-history analysis of finite element models will probably gain wide acceptance in view of their ability to account for nonlinear soil behavior. But despite the importance usually ascribed to nonlinearities when trying to explain discrepancies between observed and predicted local amplification effects, it must be recognized that their influence is often overshadowed by the overall patterns of shock generation and propagation. It is this consideration that supports the usefulness of frequency-domain studies as advocated above.

CONCLUDING REMARKS

Microzonation implies much more than influence of stratified soil formations. It implies a better knowledge of the fault mechanisms of earthquakes that significantly contribute to seismic risk at a site, study of the possible influence of path characteristics on the types of arriving seismic waves and hence on the manner in which local conditions will affect them. More general analytical models for the study of all factors affecting seismic waves from their source will have to be developed, adapted and implemented by engineers. But, as a consequence of the complexities inherent in the phenomena under study, those models should only play a role complementary to instrumental observations. Because path and

mechanism effects have been shown to affect local variations of ground motion, a large number of events will have to be recorded at every site of interest and its neighborhood before reliable conclusions can be drawn concerning those variations. Hence, small magnitude shocks should be given increased attention, as they will probably constitute the main source of information at some sites, in spite of their inability to provide information about the influence of nonlinear soil behavior associated with severe shocks. Deployment, operation and interpretation of the records of local instrumental networks should aim at the description of earthquake motion variability throughout small regions, and at the understanding of the patterns of seismic waves giving place to that variability.

ACKNOWLEDGEMENTS

The author wishes to express his gratitude to S. E. Ruiz for her assistance in the revision and interpretation of the literature, through the preparation of a state-of-the-art report. Critical reading of the manuscript by G. Ayala and J. Bielak is also gratefully acknowledged.

REFERENCES

Aki, K. & Larner K., 1970, "Surface motion of a layered medium having an irregular interface due to incident plane SH waves", J. Geophys Res., 75, pp. 933-954

Ayala, G. & Aranda R., 1977 "Boundary conditions in soil amplification studies", 6WCEE, Delhi

Boore D. M., 1972, "A note on the effect of simple topography on seismic SH waves", Bull, Seism. Soc. Am., Vol 62, No. 1, pp. 275-284

Bouchon, M., 1973, "Effect of topography on surface motion", Bull. Seism. Soc. Am., Vol 63, No. 3, pp.615-632

Davis, L. L. & West, L. R., 1973, "Observed effects of topography on ground motion", Bull. Seism. Soc. Am., Vol 63, No. 1, pp. 283-298

Esteva, L. & Villaverde, L., 1973, "Seismic risk, design spectra and structural reliability", Proc. 5WCEE, Rome

Faccioli, 1976, personal communication

Hanks, T. C., 1975, "Strong ground motion following the San Fernando, California, earthquake. 1. Ground displacements", mentioned by Trifunac and Udwadia, 1974

Herrera, I., Rosenblueth, E. & Rascón, O. A., 1965, "Earthquake spectrum prediction for the valley of Mexico", Proc. 3WCEE, Vol 1, pp 161-174

Hudson, D. E., 1972, "Local distribution of strong earthquake ground motions", Bull of the Seismological Soc. of America, Vol 62, No. 6, pp. 1765-1786

Jackson, P. S., 1971, "The focusing of earthquakes", Bull. Seism. Soc. Am., Vol 61, No. 3, pp. 685-695

Lysmer, J. & Drake, L. A., 1971, "A finite element method for seismology", Methods in Computational Physics, Cap. VI, University of California, Berkeley

Lysmer, J. & Kuhlemeyer, R. L., 1969, "Finite dynamic model for infinite media", Journ. Eng. Mech. Div. ASCE, Vol 95, No. EM4, pp. 859-877

Mohraz, B., "A study of earthquake response spectra for different geologic conditions", Bull. Seism. Soc. Am., Vol 66, No. 3, pp. 915-936

Morse, & Feshbach, 1953, "Methods of Theoretical Physics", McGraw-Hill, Kogakusha, Tokyo

Poceski, A., 1969, "The ground effects of the Skopje July 26, 1963 earthquake", Bull. Seism. Soc. Am., Vol 59, No. 1, pp. 1-29

Reimer, R. B., Clough, R. W. and Raphael, J. M., 1974, "Evaluation of the Pacoima Dam accelerogram", 5WCEE, Vol 2, pp. 2328-2337

Ruiz, S. E., 1976, "Influencia de las condiciones locales en las características de los sismos", M S Thesis, Faculty of Engineering, National University of Mexico

Sánchez-Sesma, F. J. & Esteva, L., 1977, "Intensity attenuation and local amplification: a unified approach", Institute of Engineering, National University of Mexico

Smith, W. D., 1974, "A non reflecting plane boundary for wave propagation problems", Journal of Computational Physics, Vol 15, No. 4, pp. 492-503

Stephenson, W. R., 1974, "Earthquake induced resonant motion of alluvium", Bull. New Zealand Nat. Soc. for Earthquake Engng, Vol 7, No. 3

Trifunac, M. D., 1971a, "Response envelope spectrum and interpretation of strong earthquake ground motion", Bull. Seism. Soc. Am., Vol 61, No. 2, pp. 343-356

Trifunac, M. D., 1971b, "Surface motion of a semi-cylindrical alluvial valley for incident plane SH waves", Bull. Seism. Soc. Am., Vol 61, pp. 1755-1770

Trifunac, M. D. & Udwadia, F. E., 1974, "Variations of strong earthquake ground shaking in the Los Angeles area", Bull. Seism. Soc. Am., Vol. 64, No. 5, pp. 1429-1454

Tsai, N., 1969, "Influence of local geology on earthquake motion", Ph. D. Thesis, California Institute of Technology, Pasadena, Calif

Udwadia, F. E. & Trifunac, M. D., 1973, "Comparison of earthquake and microtremor ground motions in El Centro California", Bull. of the Seismological Soc. of America, Vol 63, No. 4, pp. 1227-1253

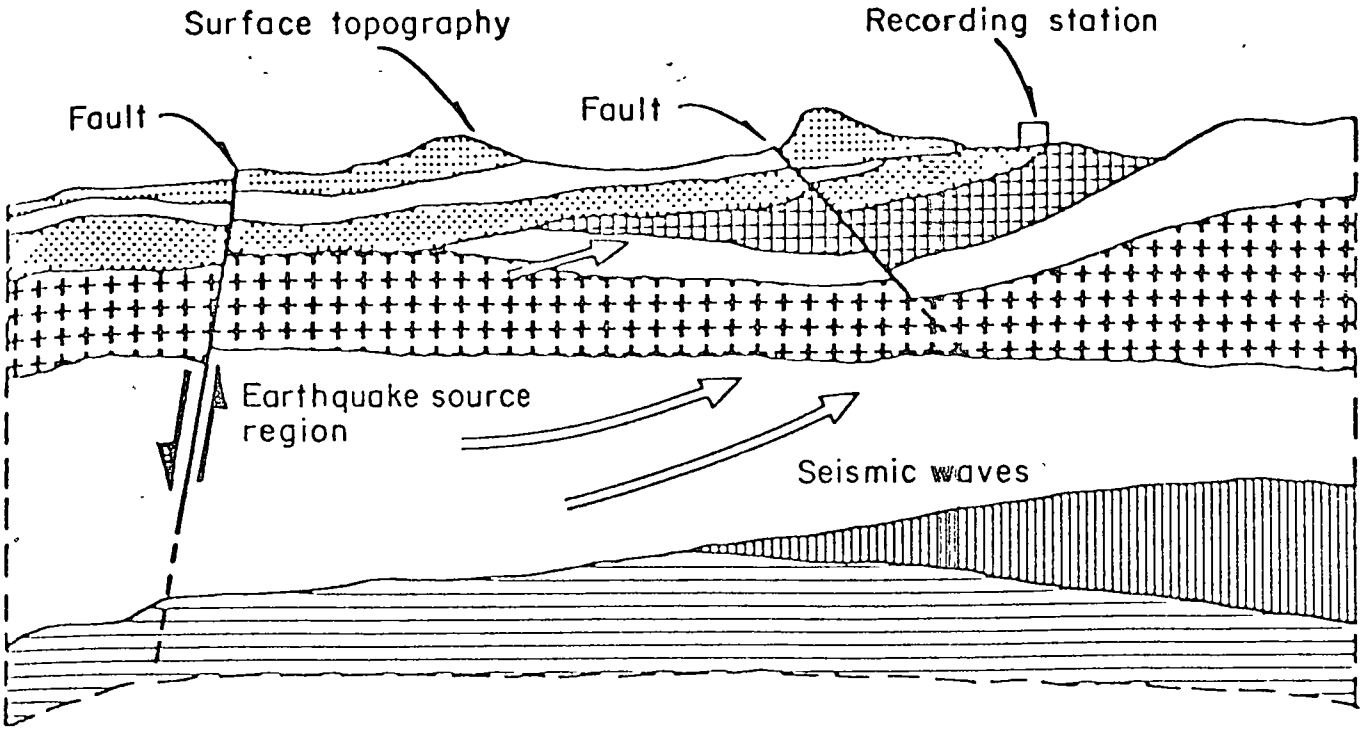

Fig. 1 Source, path and local conditions (Hudson, 1972)

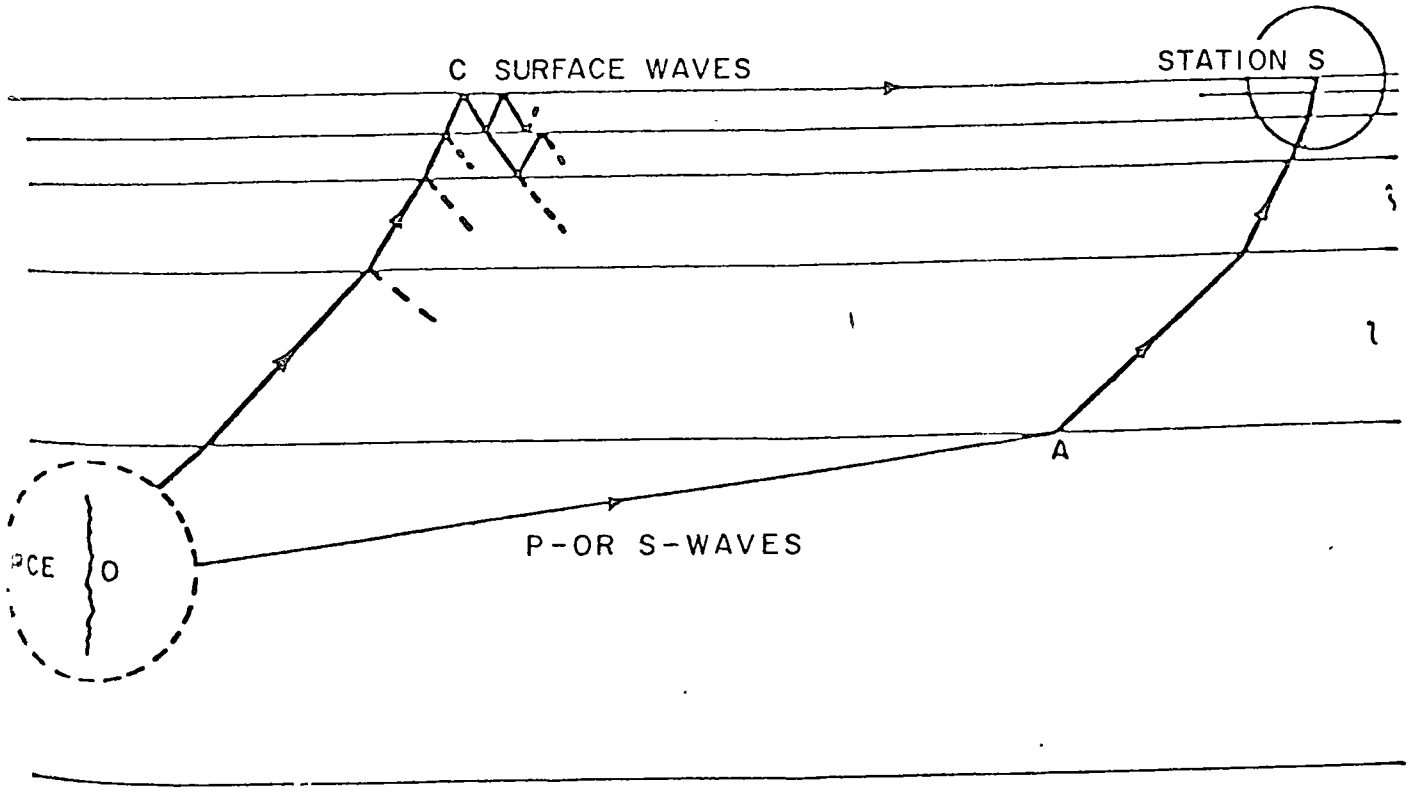

Fig. 2 Seismic waves (Tsai, 1969)

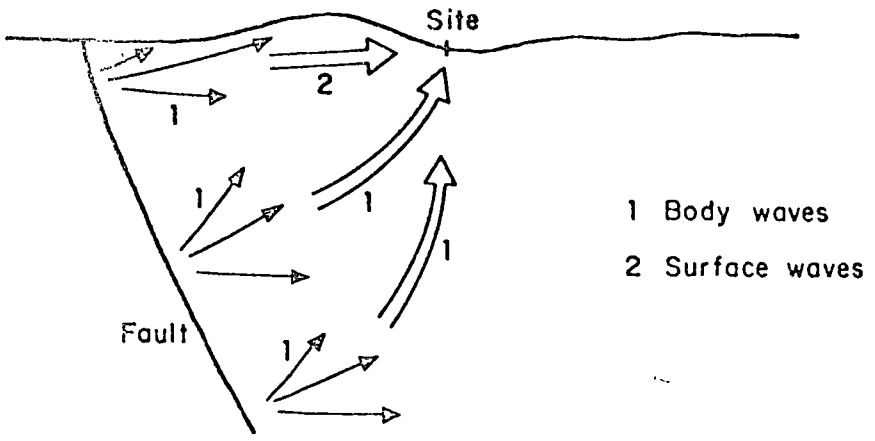

Fig. 3 Seismic waves in the near field

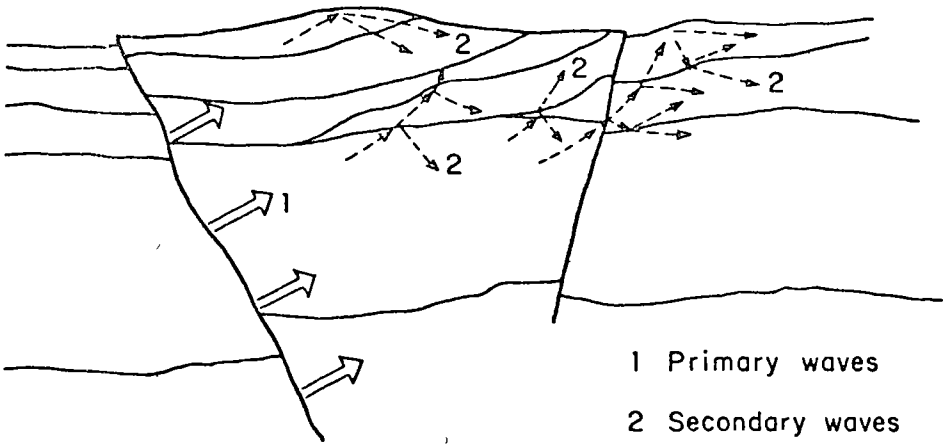

Fig. 4 Secondary wave trains

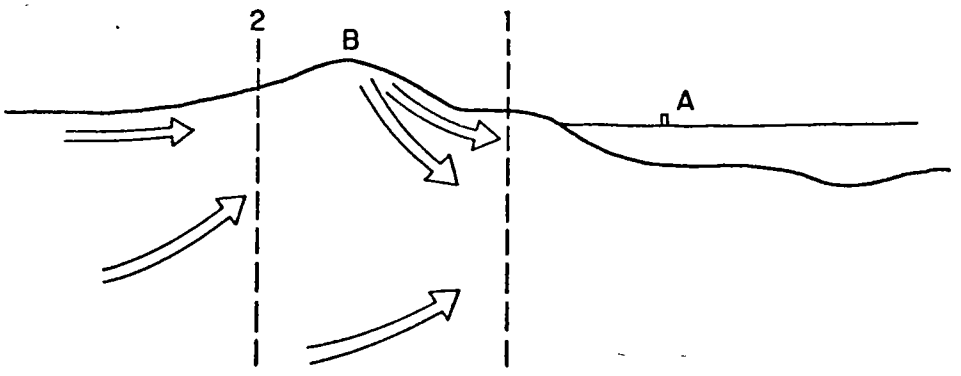

Fig. 5 Path and local conditions

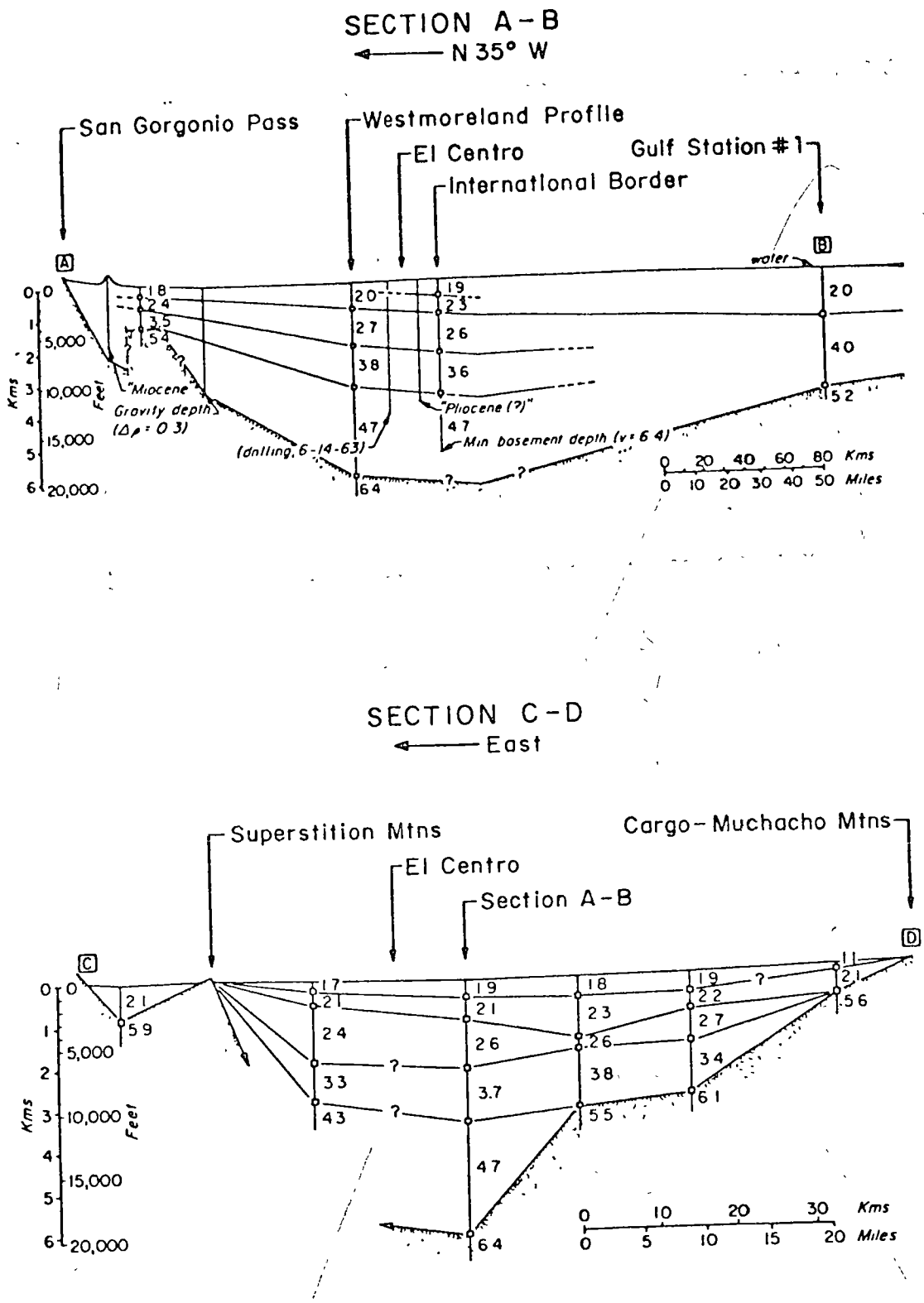

Fig. 6 Geologic cross section, Los Angeles area (Udwadia and Trifunac, 1973)

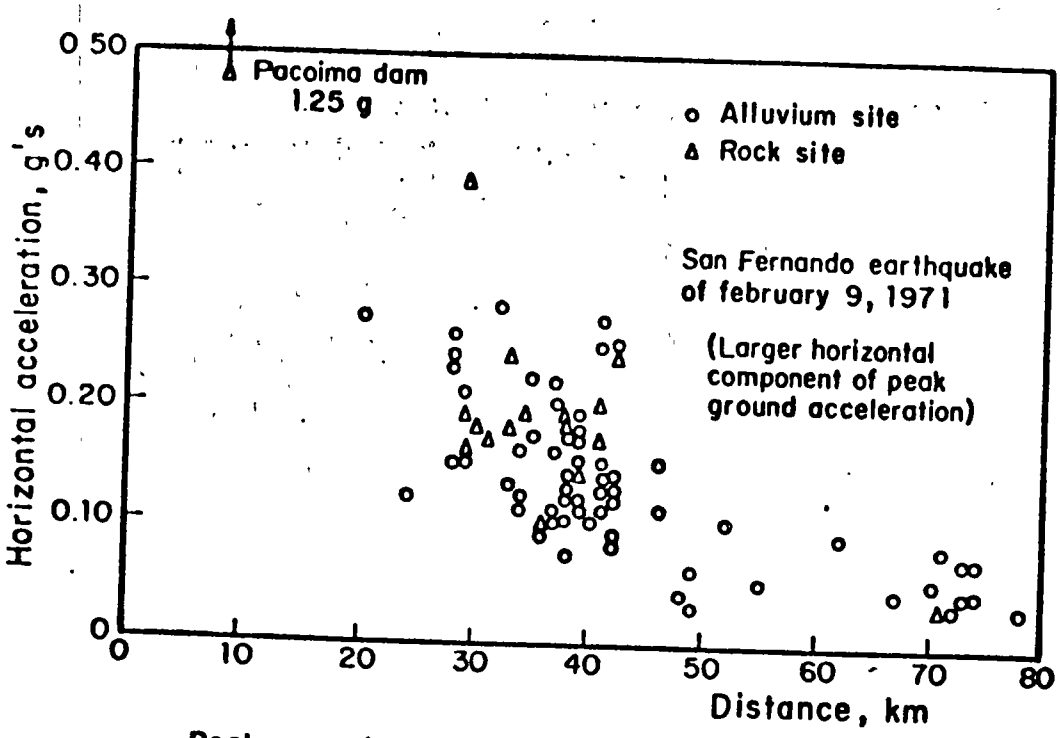

Peak ground acceleration versus distance

Fig. 7 Peak accelerations and ground conditions (Hudson, 1972)

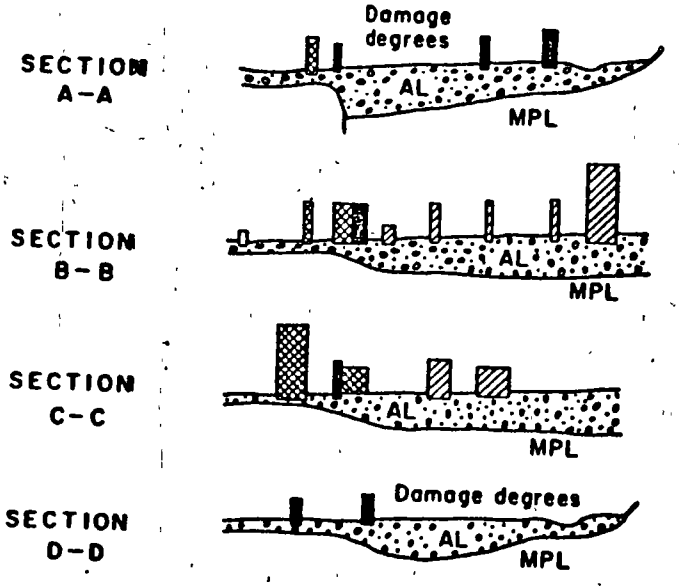

Fig. 8 Geologic cross section at Skopje (Poceski, 1969)

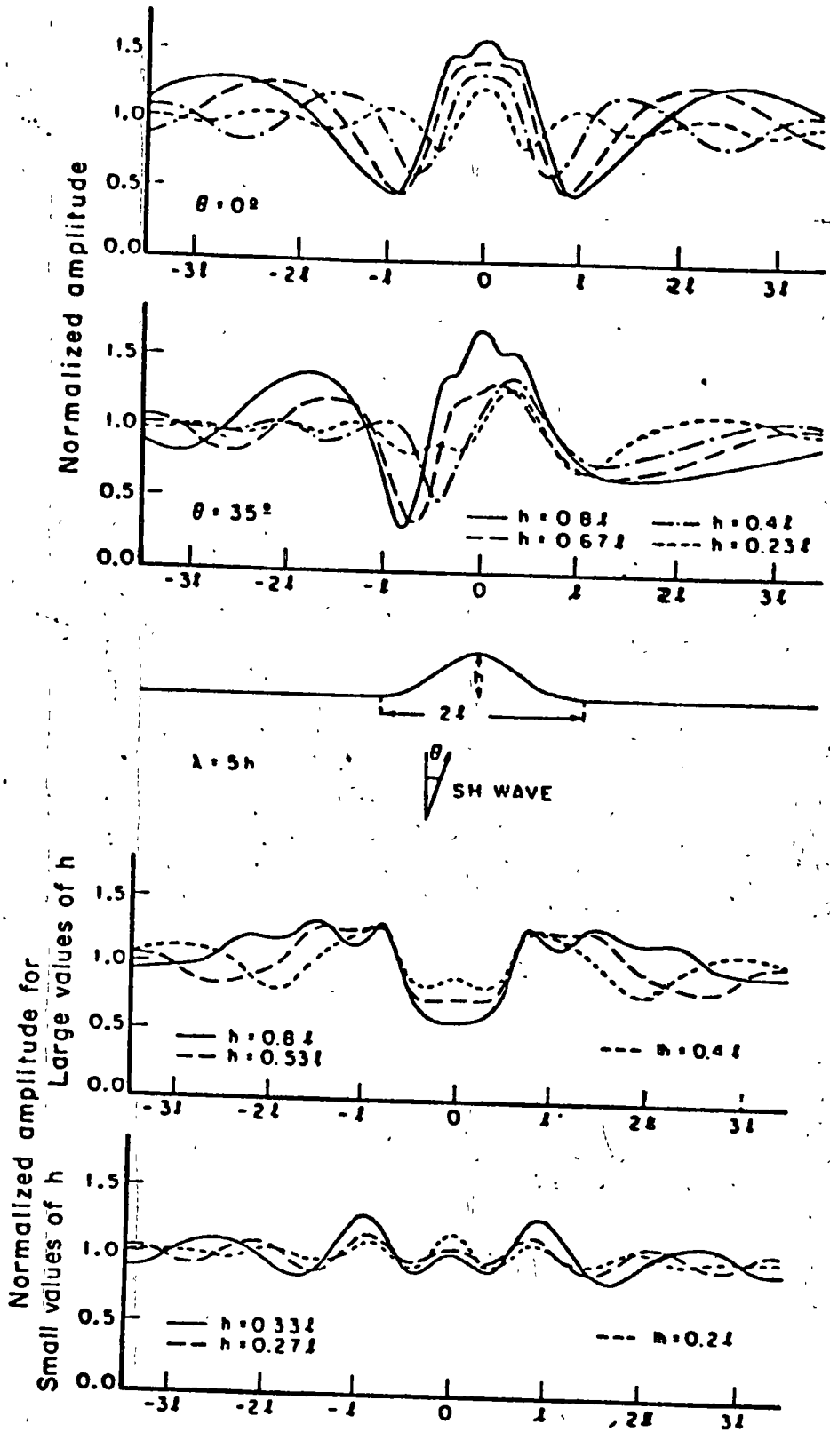

Fig. 9 Normalized amplitudes of motion produced by SH waves (Bouchon, 1973)

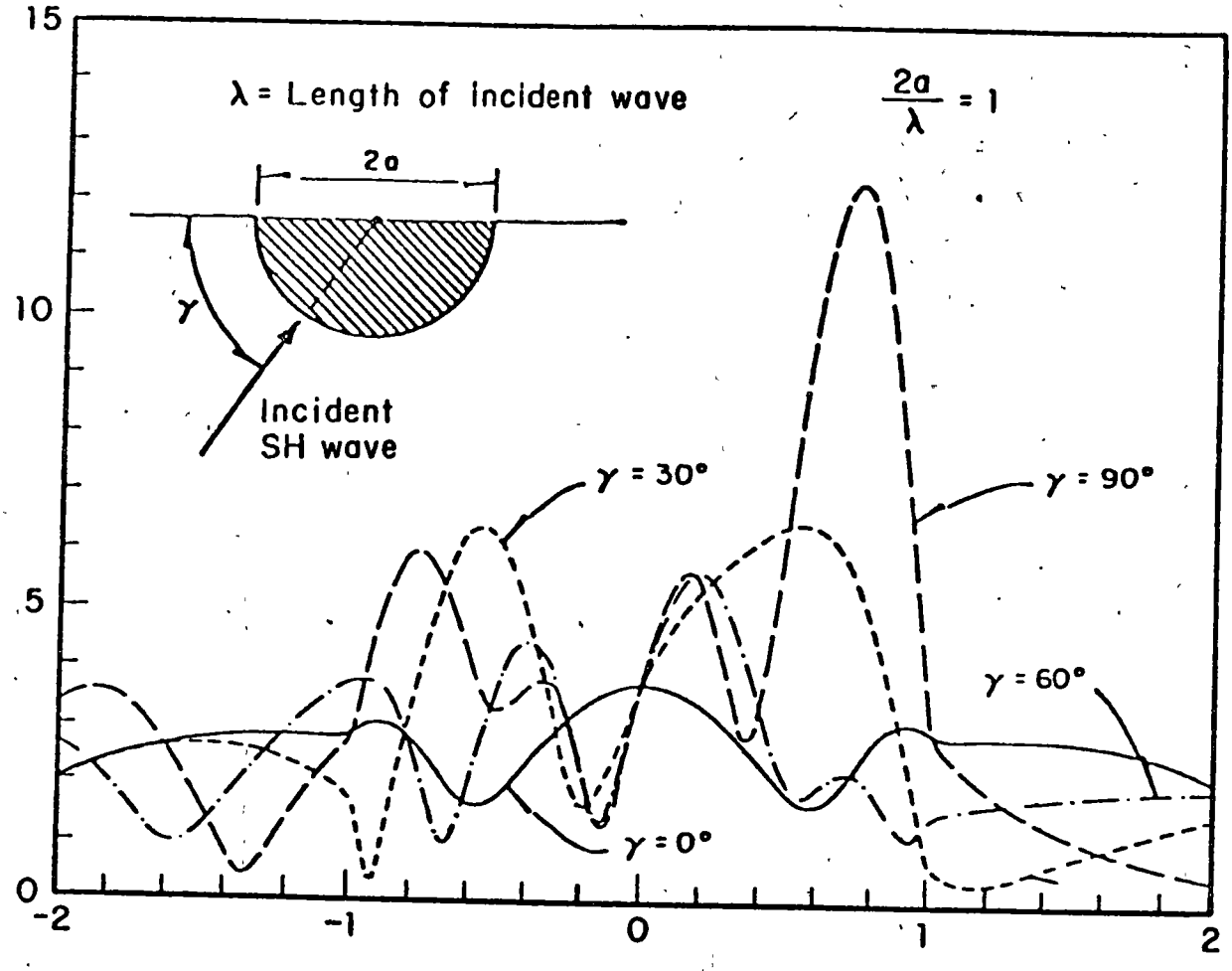

Fig. 10 Displacement amplitudes at the surface of a semicylindrical valley (Trifunac, 1971b)

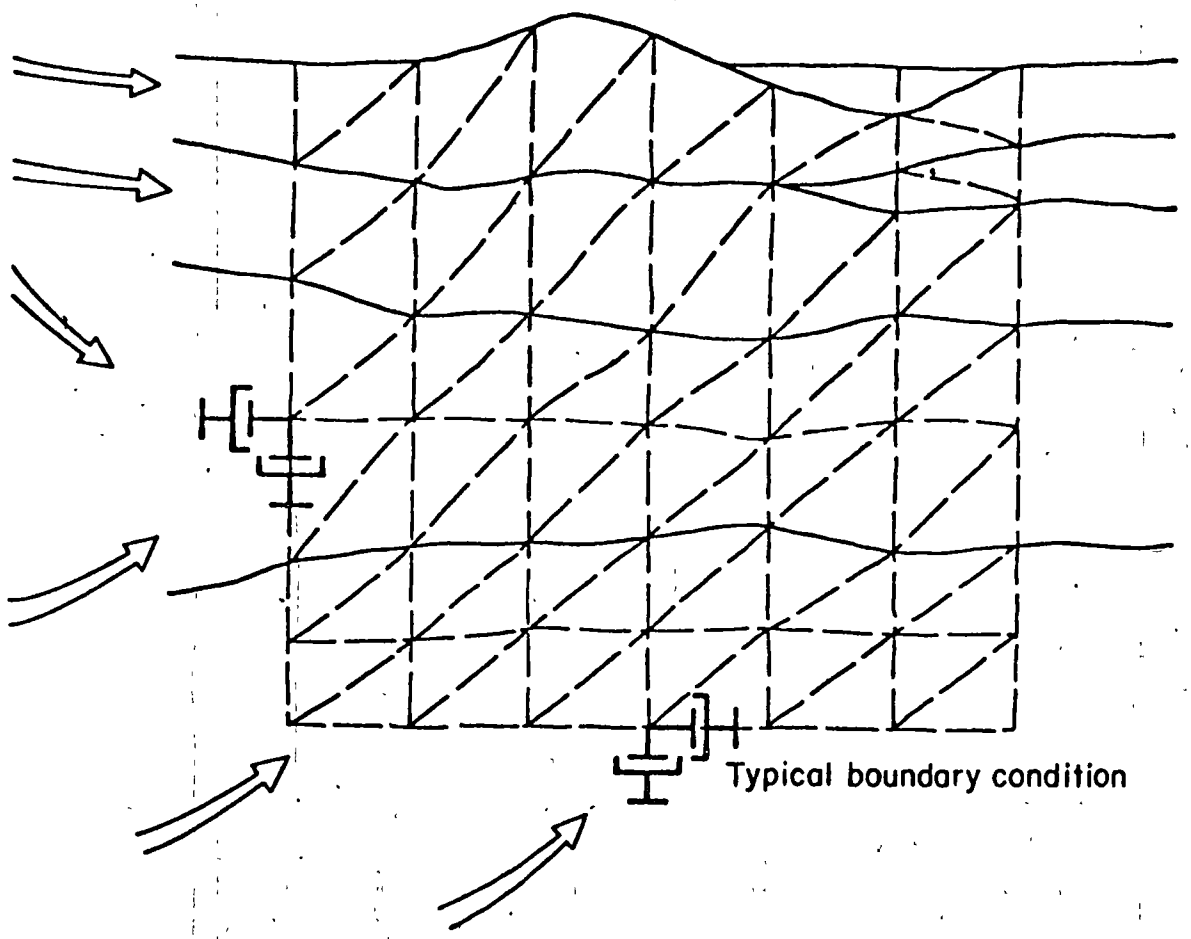

Fig. 11 Two-dimensional finite element models

centro de educación continua
división de estudios superiores
facultad de ingeniería, unam

III CURSO INTERNACIONAL DE

INGENIERIA SISMICA

SISMOLOGIA Y SISMICIDAD

JULIO 12, 1977

Palacio de Minería Calle de Tacuba 5, primer piso. México 1, D. F.

Chapter 6

SEISMICITY

LUIS ESTEVA

Instituto de Ingeniería, Universidad Nacional Autónoma de México, México

6.1 ON SEISMICITY MODELS

Rational formulation of engineering decisions in seismic areas requires quantitative descriptions of seismicity. These descriptions should conform with their intended applications: in some instances, simultaneous intensities during each earthquake have to be predicted at several locations, while in others it suffices to make independent evaluations of the probable effects of earthquakes at each of those locations.

The second model is adequate for the selection of design parameters of individual components of a regional system (the structures in a region or country) when no significant interaction exists between response or damage of several such individual components, or between any of them and the system as a whole. In other words, it applies when the damage — or negative utility — inflicted upon the system by an earthquake can be taken simply as the addition of the losses in the individual components.

The linearity between monetary values and utilities implied in the second model is not always applicable. Such is the case, for instance, when a significant portion of the national wealth or of the production system is concentrated in a relatively narrow area, or when failure of life-line components may disrupt emergency and relief actions just after an earthquake. Evaluation of risk for the whole regional system has then to be based on seismicity models of the first type, that is, models that predict simultaneous intensities at several locations during each event; for the purpose of decision making, nonlinearity between monetary values and utilities can be accounted for by means of adequate scale transformations. These models are also of interest to insurance companies, when the probability distribution of the maximum loss in a given region during a given time interval is to be estimated.

Whatever the category to which a seismic risk problem belongs, it requires the prediction of probability distributions of certain ground motion characteristics (such as peak ground acceleration or velocity, spectral density, response or Fourier spectra, duration) at a given site during a single shock or of maximum values of some of those characteristics in earthquakes occurring during given time intervals. When the reference interval tends to infinity, the probability distribution of the maximum value of a given characteristic ap-

proaches that of its maximum *possible* value. Because different systems or subsystems are sensitive to different ground motion characteristics, the term *intensity characteristic* will be used throughout this chapter to mean a particular parameter or set of parameters of an earthquake motion, in terms of which the response is to be predicted. Thus, when dealing with the failure probability of a structure, intensity can be alternatively measured — with different degrees of correlation with structural response — by the ordinate of the response spectrum for the corresponding period and damping, the peak ground acceleration, or the peak ground velocity.

In general, local instrumental information does not suffice for estimating the probability distributions of maximum intensity characteristics, and use has to be made of data on subjective measures of intensities of past earthquakes, of models of *local seismicity*, and of expressions relating characteristics with magnitude and site-to-source distance. Models of local seismicity consist, at least, of expressions relating magnitudes of earthquakes generated in given volumes of the earth's crust with their return periods. More often than not, a more detailed description of local seismicity is required, including estimates of the maximum magnitude that can be generated in these volumes, as well as probabilistic (stochastic process) models of the possible histories of seismic events (defined by magnitudes and coordinates).

This chapter deals with the various steps to be followed in the evaluation of seismic risk at sites where information other than direct instrumental records of intensities has to be used: identifying potential sources of activity near the site, formulating mathematical models of local seismicity for each source, obtaining the contribution of each source to seismic risk at the site and adding up contributions of the various sources and combining information obtained from local seismicity of sources near the site with data on instrumental or subjective intensities observed at the site.

The foregoing steps consider use of information stemming from sources of different nature. Quantitative values derived therefrom are ordinarily tied to wide uncertainty margins. Hence they demand probabilistic evaluation, even though they cannot always be interpreted in terms of relative frequencies of outcomes of given experiments. Thus, geologists talk of the maximum magnitude that can be generated in a given area, assessed by looking at the dimensions of the geological accidents and by extrapolating the observations of other regions which available evidence allows to brand as similar to the one of interest; the estimates produced are obviously uncertain, and the degree of uncertainty should be expressed together with the most probable value. Following nearly parallel lines, some geophysicists estimate the energy that can be liberated by a single shock in a given area by making quantitative assumptions about source dimensions, dislocation amplitude and stress drop, consistent with tectonic models of the region and, again, with comparisons with areas of similar tectonic characteristics.

Uncertainties attached to estimates of the type just described are in general extremely large: some studies relating fault rupture area, stress drop, and magnitude (Brune, 1968) show that, considering not unusually high stress drops, it does not take very large source dimensions to get magnitudes 8.0 and greater, and those studies are practically restricted to the simplest types of fault displacement. It is not clear, therefore, that realistic bounds can always be assigned to potential magnitudes in given areas or that, when this is feasible, those bounds are sufficiently low, so that designing structures to withstand the corresponding intensities is economically sound, particularly when occurrence of those intensities is not very likely in the near future. Because uncertainties in maximum feasible magnitudes and in other parameters defining magnitude-recurrence laws can be as significant as their mean values when trying to make rational seismic design decisions, those uncertainties have to be explicitly recognized and accounted for by means of adequate probabilistic criteria. A corollary is that geophysically based estimates of seismicity parameters should be accompanied with corresponding uncertainty measures.

Seismic risk estimates are often based only on statistical information (observed magnitudes and hypocentral coordinates). When this is done, a wealth of relevant geophysical information is neglected, while the probabilistic prediction of the future is made to rely on a sample that is often small and of little value, particularly if the sampling period is short as compared with the desirable return period of the events capable of severely damaging a given system.

The criterion advocated here intends to unify the foregoing approaches and rationally to assimilate the corresponding pieces of information. Its philosophy consists in using the geological, geophysical, and all other available non-statistical evidence for producing a set of alternate assumptions concerning a mathematical (stochastic process) model of seismicity in a given source area. An initial probability distribution is assigned to the set of hypotheses, and the statistical information is then used to improve that probability assignment. The criterion is based on application of *Bayes theorem*, also called the *theorem of the probabilities of hypotheses*. Since estimates of risk depend largely on conceptual models of the geophysical processes involved, and these are known with different degrees of uncertainty in different zones of the earth's crust, those estimates will be derived from stochastic process models with uncertain forms or parameters. The degree to which these uncertainties can be reduced depends on the limitations of the state of the art of geophysical sciences and on the effort that can be put into compilation and interpretation of geophysical and statistical information. This is an economical problem that should be handled, formally or informally, by the criteria of decision making under uncertainty.

6 2 INTENSITY ATTENUATION

Available criteria for the evaluation of the contribution of potential seismic sources to the risk at a site make use of *intensity attenuation* expressions that relate intensity characteristics with magnitude and distance from site to source. Depending on the application envisaged, the intensity characteristic to be predicted can be expressed in a number of manners, ranging from a subjective index, such as the *Modified Mercalli intensity*, to a combination of one or more quantitative measures of ground shaking (see Chapter 1).

A number of expressions for attenuation of various intensity characteristics with distance have been developed, but there is little agreement among most of them (Ambraseys, 1973). This is due in part to discrepancies in the definitions of some parameters, in the ranges of values analyzed, in the actual wave propagation properties of the geological formations lying between source and site, in the dominating shock mechanisms, and in the forms of the analytical expressions adopted a priori.

Most intensity-attenuation studies concern the prediction of earthquake characteristics on rock or firm ground, and assume that these characteristics, properly modified in terms of frequency-dependent soil amplification factors, should constitute the basis for estimating their counterparts on soft ground. Observations about the influence of soil properties on earthquake damage support the assumption of a strong correlation between type of local ground and intensity in a given shock. Attempts to analytically predict the characteristics of motions on soil given those on firm ground or on bedrock have not been too successful, however (Crouse, 1973; Hudson and Udwadia, 1973; Salt, 1974), with the exception of some peculiar cases, like Mexico City (Herrera et al., 1965), where local conditions favor the fulfillment of the assumptions implied by usual analytical models. The following paragraphs concentrate on prediction on intensities on firm ground; the influence of local soil is discussed in Chapter 4.

6.2.1 Intensity attenuation on firm ground

When isoseismals (lines joining sites showing equal intensity) of a given shock are based only on intensities observed on homogeneous ground conditions, such as *firm ground* (compact soils) or bedrock, they are roughly elliptical and the orientations of the corresponding axes are often correlated with local or regional geological trends (Figs. 6.1—6.3). In some regions — for instance near major faults in the western United States — those trends are well defined and the correlations are clear enough as to permit prediction of intensity in the near and far fields in terms of magnitude and distance to the generating fault or to the centroid of the energy liberating volume. In other regions, such as the eastern United States and most of Mexico, isoseismals seem to elongate systematically in a direction that is a function of the epicentral coordinates (Bollinger, 1973, Figueroa, 1963). In that case, intensity should be expressed as a function of magnitude and coordinates of source and site. For most areas in the world, intensity has to be predicted in terms of simple — and cruder — expressions that depend only on magnitude and distance from site to instrumental hypocenter. This stems from inadequate knowledge of geotectonic conditions and from limited information concerning the volume where energy is liberated in each shock.

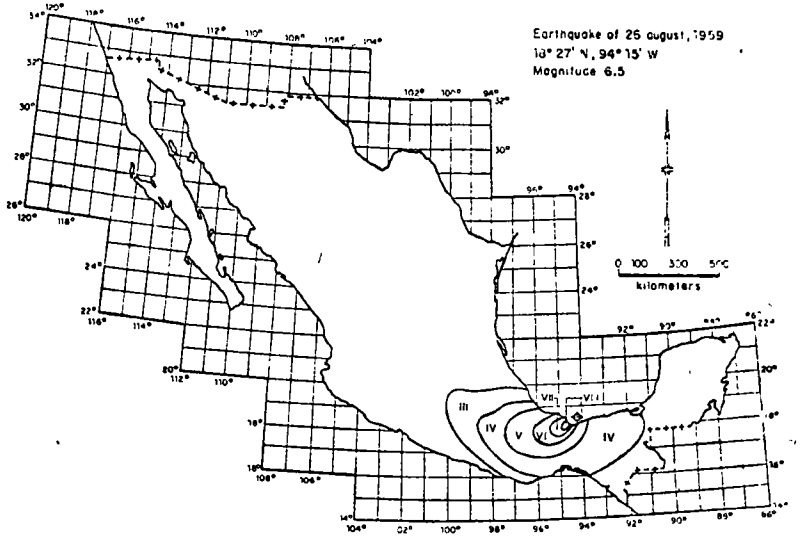

Fig. 6 1. Isoseismals of an earthquake in Mexico. (After Figueroa, 1963.)

A comparison of the rates of attenuation of intensities on firm ground for shocks on western and eastern North America has disclosed systematic differences between those rates (Milne and Davenport, 1969). This is the source of a basic, but often unavoidable, weakness of most intensity-attenuation expressions, because they are based on heterogeneous data, recorded in different zones, and the very nature of their applications implies that the less is known about possible systematic deviations in a given zone, as a consequence of the meagerness of local information, the greater weight is given to predictions with respect to observations.

6.2.1.1 Modified Mercalli intensities

An analysis of the Modified Mercalli intensities on firm ground reported for earthquakes occurring in Mexico in the last few decades leads to the fol-

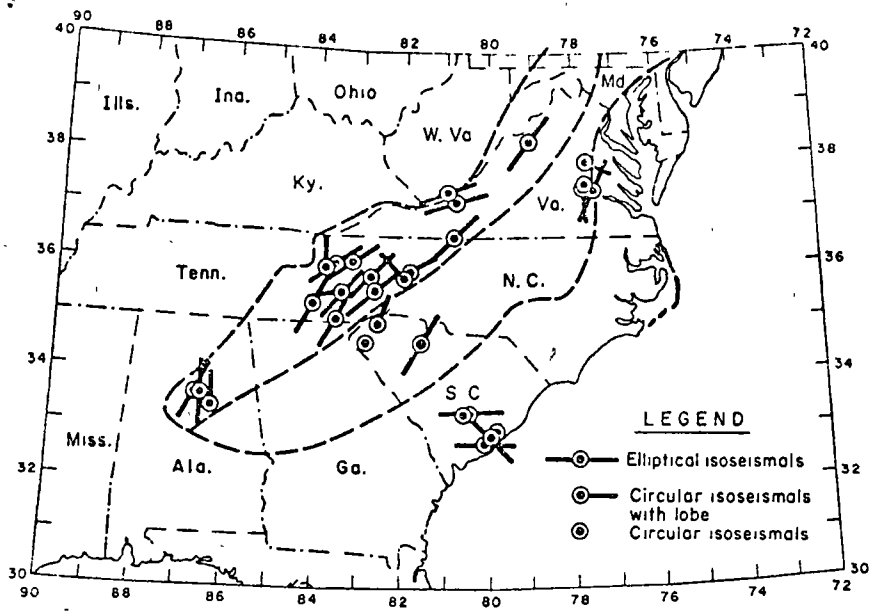

Fig 6 2 Elongation of isoseismals in the southeastern United States. (After Bollinger, 1973.)

lowing expression relating magnitude M, hypocentral distance R (in kilometers) and intensity I (Esteva, 1968):

$$I = 1.45\,M - 5.7\,\log_{10} R + 7.9 \qquad (6.1)$$

The prediction error, defined as the difference between observed and computed intensity, is roughly normally distributed, with a standard deviation of 2.04, which means that there is a probability of 60% that an observed intensity is more than one degree greater or smaller than its predicted value.

6.2 1 2 Peak ground accelerations and velocities

A few of the available expressions will be described. Their comparison will show how cautiously a designer intending to use them should proceed.

Housner studied the attenuation of peak ground accelerations in several regions of the United States and presented his results graphically (1969) in terms of fault length (in turn a function of magnitude), shapes of isoseismals and areas experiencing intensities greater than given values (Fig. 6.4 and 6.5).

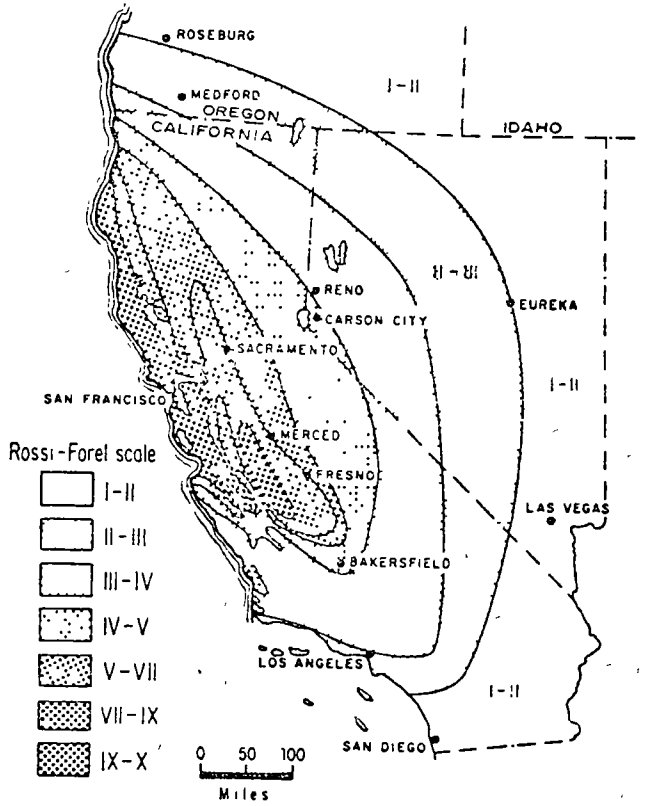

Fig. 6.3 Isoseismals in California. (After Bolt, 1970.)

He showed that intensities attenuate faster with distance on the west coast than in the rest of the country. This comparison is in agreement with Milne and Davenport (1969), who performed a similar analysis for Canada From observations of strong earthquakes in California and in British Columbia, they developed the following expression for a, the peak ground acceleration, as a fraction of gravity:

$$a/g = 0.0069\,e^{1.6M}/(1.1\,e^{1.1M} + R^2) \qquad (6.2)$$

Here, R is epicentral distance in kilometers. The acceleration varies roughly as $e^{1.64M}R^{-2}$ for large R, and as $e^{0.54M}$ where R approaches zero. This reflects to some extent the fact that energy is released not at a single point but from a finite volume. A later study by Davenport (1972) led him

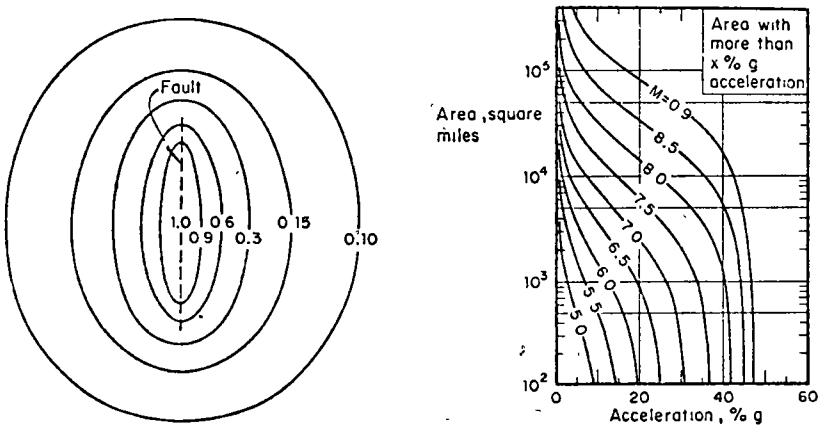

Fig. 6.4. Idealized contour lines of intensity of ground shaking (After Housner, 1969.)

Fig 6 5 Area in square miles experiencing shaking of x %g or greater for shocks of different magnitudes. (After Housner, 1969.)

to propose the expression:

$$a/g = 0.279\ e^{0.8M}/R^{1.64} \qquad (6.3)$$

The statistical error of this equation was studied by fitting a lognormal probability distribution to the ratios of observed to computed accelerations. A standard deviation of 0.74 was found in the natural logarithms of those ratios.

Esteva and Villaverde (1973), on the basis of accelerations reported by Hudson (1971, 1972a,b), derived expressions for peak ground accelerations and velocities, as follows:

$$a/g = 5.7\ e^{0.8M}/(R + 40)^2 \qquad (6.4)$$

$$v = 32\ e^{M}/(R + 25)^{1.7} \qquad (6.5)$$

Here v is peak ground velocity in cm/sec and the other symbols mean the same as above. The standard deviation of the natural logarithm of the ratio of observed to predicted intensity is 0.64 for accelerations and 0.74 for velocities. If judged by this parameter, eqs. 6.3 and 6.4 seem equally reliable. However, as shown by Fig. 6.6, their mean values differ significantly in some ranges.

With the exception of eq. 6.2, all the foregoing attenuation expressions are products of a function of R and a function of M. This form, which is acceptable when the dimensions of the energy-liberating source are small com-

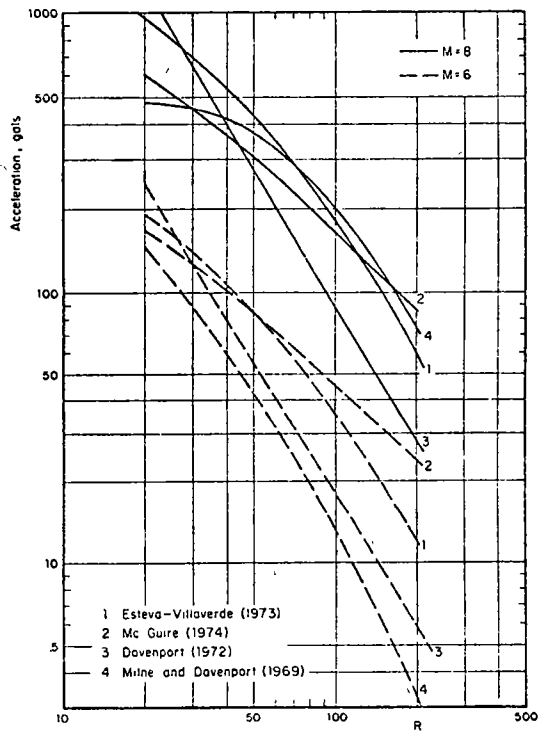

Fig 6.6. Comparison of several attenuation expressions.

pared with R, is inadequate when dealing with earthquake sources whose dimensions are of the order of moderate hypocentral distances, and often greater than them. Although equation errors (probability distributions of the ratio of observed to predicted intensities) have been evaluated by Davenport (1972) and Esteva and Villaverde (1973), their dependence on M and R has not been analyzed Because seismic risk estimates are very sensitive to the attenuation expressions in the range of large magnitudes and short distances more detailed studies should be undertaken, aiming at improving those expressions in the mentioned range, and at evaluating the influence of M and R on equation error. Information on strong-motion records will probably be scanty for those studies, and hence they will have to be largely based on analytical or physical models of the generation and propagation of seismic waves. Although significant progress has been lately attained in this direction (Trifunac, 1973) the results from such models have hardly influenced the

practice of seismic risk estimation because they have remained either unknown to or imperfectly appreciated by engineers in charge of the corresponding decisions.

6 2 1.3 Response spectra

Peak ground acceleration and displacement are fairly good indicators of the response of structures possessing respectively very high and very small natural frequencies. Peak velocity is correlated with the response of intermediate-period systems, but the correlation is less precise than that tying the former parameters, hence, it is natural to formulate seismic risk evaluation and engineering design criteria in terms of spectral ordinates.

Response spectrum prediction for given magnitude and hypocentral or site-to-fault distance usually entails a two-step process, according to which peak ground acceleration, velocity and displacement are initially estimated and then used as reference values for prediction of the ordinates of the response spectrum. Let the second step in the process be represented by the operation $y_s = \alpha y_g$, where y_s is an ordinate of the response spectrum for a given natural period and damping ratio, and y_g is a parameter (such as peak ground acceleration or velocity) that can be directly obtained from the time-history record of a given shock regardless of the dynamic properties of the systems whose response is to be predicted. For given M and R, y_g is random and so is $y_s/y_g = \alpha$; the mean and standard deviation of y_s depend on those of y_g and α and on the coefficient of correlation of the latter variables. As shown above, y_g can only be predicted within wide uncertainty limits, often wider than those tied to y_s (Esteva and Villaverde, 1973). The coefficient of variation of y_s given M and R can be smaller than that of y_g only if α and y_g are negatively correlated, which is often the case: the greater the deviation of an observed value of y_g with respect to its expectation for given M and R, the lower is likely to be α. In other words, it seems that in the intermediate range of natural periods the expected values of spectral ordinates for given damping ratios can be predicted directly in terms of magnitude and focal distance with narrower (or at most equal) margins of uncertainty than those tied to predicted peak ground velocities. For the ranges of very short or very long natural periods, peak amplitudes of ground motion and spectral ordinates approach each other and their standard errors are therefore nearly equal.

McGuire (1974) has derived attenuation expressions for the conditional values (given M and R) of the mean and of various percentiles of the probability distributions of the ordinates of the response spectra for given natural periods and damping ratios. Those expressions have the same form as eqs. 6.4 and 6.5, but their parameters show that the rates of attenuation of spectral ordinates differ significantly from those of peak ground accelerations or velocities. For instance, McGuire finds that peak ground velocity attenuates in proportion to $(R + 25)^{-1\ 20}$, while the mean of the pseudovelocity for a

TABLE 6.I

McGuire's attenuation expressions $y = b_1\ 10^{b_2 M}(R + 25)^{-b_3}$

y	b_1	b_2	b_3	$V(y)$ = coeff of var of y
a gals	472.3	0.278	1.301	0 548
v cm/sec	5 64	0 401	1.202	0 696
d cm	0 393	0 434	0.885	0 883
Undamped spectral pseudovelocities				
T = 0.1 sec	11.0	0.278	1.346	0 941
0 5	3 05	0.391	1.001	0 636
1.0	0 631	0.378	0 549	0.768
2.0	0 0768	0.469	0 419	0 989
5 0	0.0834	0.564	0.897	1.344
5% damped spectral pseudovelocities				
T = 0 1 sec	10.09	0 233	1.341	0 651
0 5	5 74	0 356	1 197	0 591
1.0	0.432	0.399	0.704	0.703
2.0	0.122	0.466	0.675	0 941
5.0	0 0706	0.557	0 938	1.193

natural period of 1 sec and a damping ratio of 2% attenuates in proportion to $(R + 25)^{-0\ 59}$. These results stem from the way that frequency content changes with R and lead to the conclusion that the ratio of spectral velocity should be taken as a function of M and R.

Table 6.I summarizes McGuire's attenuation expressions and their coefficients of variation for ordinates of the pseudovelocity spectra and for peak ground acceleration, velocity and displacement. Similar expressions were derived by Esteva and Villaverde (1973), but they are intended to predict only the maxima of the expected acceleration and velocity spectra, regardless of the periods associated with those maxima. No analysis has been performed of the relative validity of McGuire's and Esteva and Villaverde's expressions for various ranges of M and R.

6.3 LOCAL SEISMICITY

The term *local seismicity* will be used here to designate the degree of seismic activity in a given volume of the earth's crust; it can be quantitatively described according to various criteria, each providing a different amount of information. Most usual criteria are based on upper bounds to the magnitudes of earthquakes that can originate in a given seismic source, on the

amount of energy liberated by shocks per unit volume and per unit time or on more detailed statistical descriptions of the process.

6.3.1 Magnitude-recurrence expressions

Gutenberg and Richter (1954) obtained expressions relating earthquake magnitudes with their rates of occurrence for several zones of the earth. Their results can be put in the form:

$$\lambda = \alpha e^{-\beta M} \tag{6.6}$$

where λ is the mean number of earthquakes per unit volume and per unit time having magnitude greater than M and α and β are zone-dependent constants; α varies widely from point to point, as evidenced by the map of epicenters shown in Fig. 6.7, while β remains within a relatively narrow range, as shown in Fig. 6.8. Equation 6.6 implies a distribution of the energy liberated per shock which is very similar to that observed in the process of microfracturing of laboratory specimens of several types of rock subjected to gradually increasing compressive or bending strain (Mogi, 1962; Scholz, 1968). The values of β determined in the laboratory are of the same order as those obtained from seismic events, and have been shown to depend on the heterogeneity of the specimens and on their ability to yield locally. Thus, in heterogeneous specimens made of brittle materials many small shocks precede a major fracture, while in homogeneous or plastic materials the number of small shocks is relatively small. These cases correspond to large and small β-values, respectively. No general relationship is known to the writer between β and geotectonic features of seismic provinces: complexity of crustal structure and of stress gradients precludes extrapolation of laboratory results, and statistical records for relatively small zones of the earth are not, as a rule, adequate for establishing local values of β. Figure 6.8 shows that for very high magnitudes the observed frequency of events is lower than predicted by eq. 6.6. In addition, Rosenblueth (1969) has shown that β cannot be smaller than 3.46, since that would imply an infinite amount of energy liberated per unit time. However, Fig. 6.8 shows that the values of β which result from fitting expressions of the form 6.6 to observed data are smaller than 3.46; hence, for very high values of M (above 7, approximately) the curve should bend down, in accordance with statistical evidence.

Expressions alternative to eq. 6.6 have been proposed, attempting to represent more adequately the observed magnitude-recurrence data (Rosenblueth, 1964; Merz and Cornell, 1973). Most of these expressions also fail to recognize the existence of an upper bound to the magnitude that can be generated in a given source. Although no precise estimates of this upper bound can yet be obtained, recognition of its existence and of its dependence on the geotectonic characteristics of the source is inescapable. Indeed, the prac-

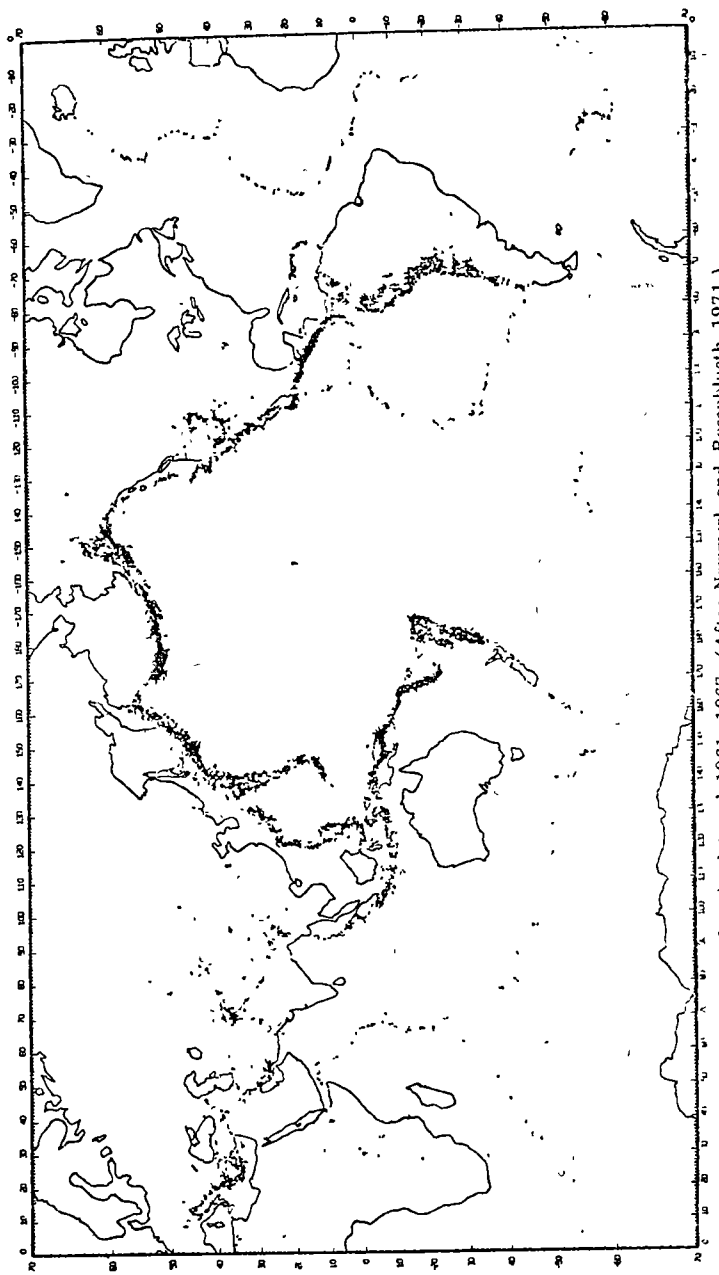

Fig. 6.7 Map showing epicenters for the interval 1961–1967 (After Newmark and Rosenblueth, 1971.)

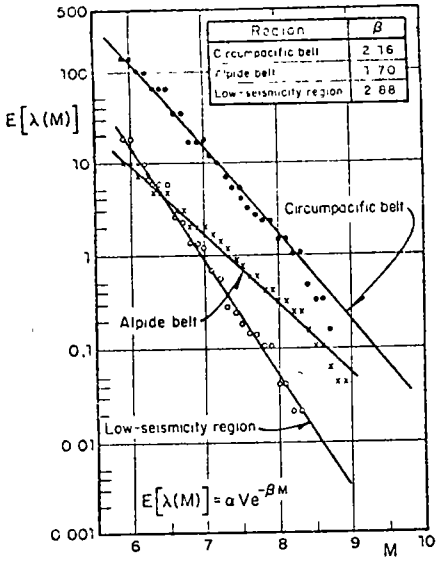

Fig. 6.8. Seismicity of macrozones. (After Esteva, 1968.)

tice of seismic zoning in the Soviet Union has been based on this concept (Gzovsky, 1962. Ananin et al., 1968) and in many countries design spectra for very important structures, such as nuclear reactors or large dams, are usually derived from the assumption of a maximum credible intensity at a site; that intensity is ordinarily obtained by taking the maximum of the intensities that result at the site when at each of the potential sources an earthquake with magnitude equal to the maximum feasible value for that source is generated at the most unfavourable location within the same source. When this criterion is applied no attention is usually paid to the uncertainty in the maximum feasible magnitude nor to the probability that an earthquake with that magnitude will occur during a given time period. The need to formulate seismic-risk-related decisions that account both for upper bounds to magnitudes and for their probabilities of occurrence suggests adoption of magnitude recurrence expressions of the form:

$$\begin{aligned} \lambda &= \lambda_L G^*(M) \qquad \text{for } M_L \leq M \leq M_U \\ &= \lambda_L \qquad \text{for } M < M_L \\ &= 0 \qquad \text{for } M > M_U \end{aligned} \tag{6.7}$$

where M_L = lowest magnitude whose contribution to risk is significant, M_U = maximum feasible magnitude, and $G^*(M)$ = complementary cumulative probability distribution of magnitudes every time that an event ($M \geq M_L$) occurs. A particular form of $G^*(M)$ that lends itself to analytical derivations is:

$$G^*(M) = A_0 + A_1 \exp(-\beta M) - A_2 \exp[-(\beta - \beta_1)M] \tag{6.8}$$

where:

$$A_0 = A\beta_1 \exp[-\beta(M_U - M_L)]$$

$$A_1 = A(\beta - \beta_1)\exp(\beta M_L)$$

$$A_2 = A_\beta \exp(-\beta_1 M_U + \beta M_L)$$

$$A = [\beta\{1 - \exp[-\beta_1(M_U - M_L)]\} - \beta_1\{1 - \exp[-\beta(M_U - M_L)]\}]^{-1}$$

As M tends to M_L from above, eq. 6.7 approaches eq. 6.6. Adoption of adequate values of M_U and β_1 permits satisfying two additional conditions: the maximum feasible magnitude and the rate of variation of λ in its vicinity. When $\beta_1 \to \infty$, eq. 6.8 tends to an expression proposed by Cornell and Vanmarcke (1969).

Yegulalp and Kuo (1974) have applied the theory of extreme values to estimating the probabilities that given magnitudes are exceeded in given time intervals. They assume those probabilities to fit an extreme type-III distribution given by:

$$\begin{aligned} F_{M_{max}}(M|t) &= \exp[-C(M_U - M)^K t] \qquad \text{for } M \leq M_U \\ &= 0 \qquad \text{for } M > M_U \end{aligned} \tag{6.9}$$

Here $F_{M_{max}}(M|t)$ indicates the probability that the maximum magnitude observed in t years is smaller than M, M_U has the same meaning as above, and C and K are zone-dependent parameters. This distribution is consistent with the assumption that earthquakes with magnitudes greater than M take place in accordance with a Poisson process with mean rate λ equal to $C(M_U - M)^K$. Equation 6.9 produces magnitude recurrence curves that fit closely the statistical data on which they are based for magnitudes above 5.2 and return periods from 1 to 50 years, even though the values of M_U that result from pure statistical analysis are not reliable measures of the upper bound to magnitudes, since in many cases they turn out inadmissibly high.

For low magnitudes, only a fraction of the number of shocks that take place is detected. As a consequence, λ-values based on statistical information lie below those computed according to eqs. 6.6 and 6.8 for M smaller than about 5.5. In addition, Fig. 6.9, taken from Yegulalp and Kuo (1974), shows that the numbers of detected shocks fit the extreme type III in eq. 6.9 better than the extreme type-I distribution implied by eq. 6.6., coupled with the assumption of Poisson distribution of the number of events. It is not

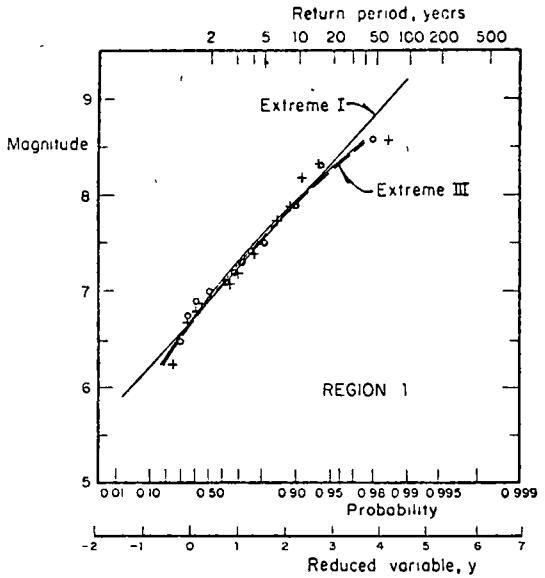

Fig. 6.9 Magnitude statistics in the Aleutian Islands region. (After Yegulalp and Kuo, 1974.)

clear what portion of the deviation from the extreme type-I distribution is due to the low values of the detectability levels and what portion comes from differences between the actual form of variation of λ with M and that given by eq. 6.6. The problem deserves attention because estimates of expected losses due to nonstructural damage may be sensitive to the values of λ for small magnitudes (say below 5.5) and because the evaluation of the level of seismic activity in a region is often made to depend on the recorded numbers of small magnitude shocks and on assumed detectability levels, i.e. of ratios of numbers of detected and occurred earthquakes (Kaila and Narain 1971; Kaila et al., 1972, 1974).

None of the expressions for λ presented in this chapter possess the desirable property that its applicability over a number of non-overlapping regions of the earth's crust implies the validity of an expression of the same form over the addition of those regions, unless some restrictions are imposed on the parameters of each λ. For instance, the addition of expressions like 6.6 gives place to an expression of the same form only if β is the same for all terms in the sum. Similar objections can be made to eq. 6.8. In what follows these forms will be preserved, however, as their accuracy is consistent with

the amount of available information and their adoption offers significant advantages in the evaluation of regional seismicity, as shown later.

6.3.2 Variation with depth

Depth of prevailing seismic activity in a region depends on its tectonic structure. For instance, most of the activity in the western coast of the United States and Canada consists of shocks with hypocentral depths in the range of 20—30 km. In other areas, such as the southern coast of Mexico, seismic events can be grouped into two ensembles: one of small shallow shocks and one of earthquakes with magnitudes comprised in a wide range, and with depths whose mean value increases with distance from the shoreline (Fig. 6.10). Figure 6.11 shows the depth distribution of earthquakes with magnitude above 5.9 for the whole circum-Pacific belt.

6.3.3 Stochastic models of earthquake occurrence

Mean exceedance rates of given magnitudes are expected averages during long time intervals. For decision-making purposes the times of earthquake occurrence are also significant. At present those times can only be predicted within a probabilistic context.

Let t_i ($i = 1, \ldots, n$) be the unknown times of occurrence of earthquakes generated in a given volume of the earth's crust during a given time interval, and let M_i be the corresponding magnitudes. For the moment it will be assumed that the risk is uniformly distributed throughout the given volume, and hence no attention will be paid to the focal coordinates of each shock.

Classical methods of time-series analysis have been applied by different researchers attempting to devise analytical models for random earthquake sequences. The following approaches are often found in the literature:

(a) Plotting of histograms of waiting times between shocks (Knopoff, 1964, Aki, 1963).

(b) Evaluation of Poisson's index of dispersion, that is of the ratio of the sample variance of the number of shocks to its expected value (Vere-Jones, 1970; Shlien and Toksoz, 1970). This index equals unity for Poisson processes, is smaller for nearly periodic sequences, and is greater than one when events tend to cluster.

(c) Determination of autocovariance functions, that is, of functions representing the covariance of the numbers of events observed in given time intervals, expressed in terms of the time elapsed between those intervals (Vere-Jones, 1970; Shlien and Toksöz, 1970). The autocovariance function of a Poisson process is a Dirac delta function. This feature is characteristic for the Poisson model since it does not hold for any other stochastic process.

(d) The hazard function $h(t)$, defined so that $h(t)\,dt$ is the conditional probability that an event will take place in the interval $(t, t + dt)$ given that

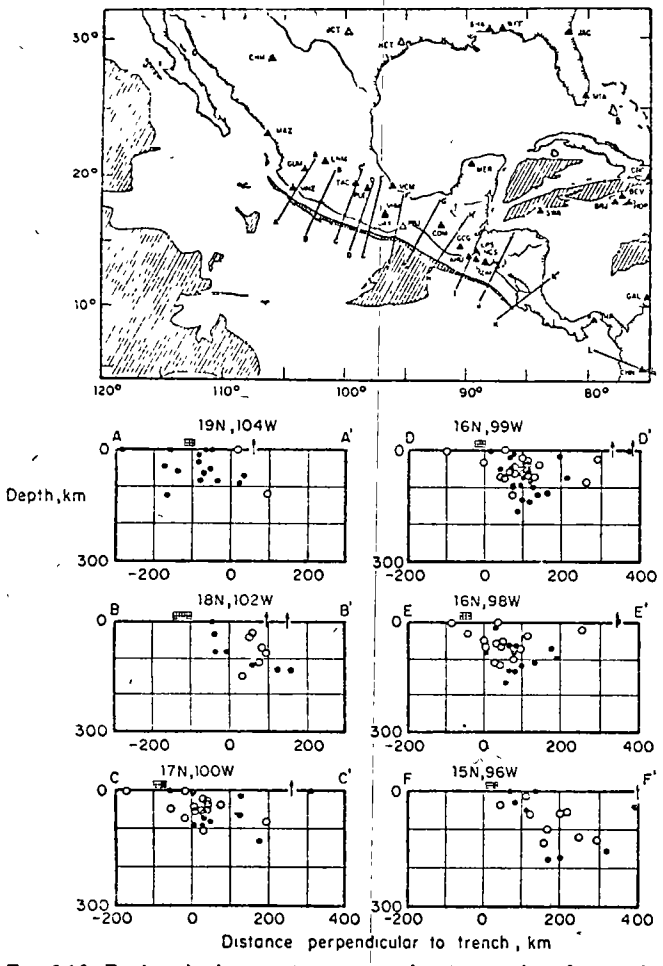

Fig. 6.10 Earthquake hypocenters projected onto a series of vertical sections through Mexico (After Molnar and Sykes, 1969)

no events have occurred before t. If $F(t)$ is the cumulative probability distribution of the time between events:

$$h(t) = f(t)/[1 - F(t)] \tag{6.10}$$

where $f(t) = \partial F(t)/\partial t$.

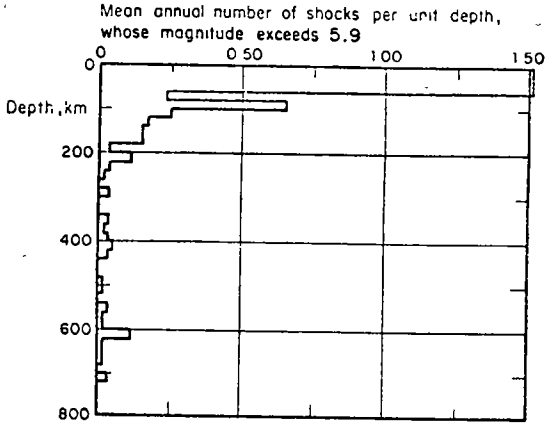

Fig. 6.11. Variation of seismicity with depth. Circum-Pacific Belt, (After Newmark and Rosenblueth, 1971.)

For the Poisson model, $h(t)$ is a constant equal to the mean rate of the process.

6.3.3.1 Poisson model

Most commonly applied stochastic models of seismicity assume that the events of earthquake occurrence constitute a Poisson process and that the M_i's are independent and identically distributed. This assumption implies that the probability of having N earthquakes with magnitude exceeding M during time interval $(0, t)$ equals:

$$p_N = [\exp(-\nu_M t)(\nu_M t)^N]/N! \tag{6.11}$$

where ν_M is the mean rate of exceedance of magnitude M in the given volume. If N is taken equal to zero in eq. 6.11, one obtains that the probability distribution of the maximum magnitude during time interval t is equal to $\exp(-\nu_M t)$. If ν_M is given by eq. 6.6, the extreme type-I distribution is obtained.

Some weaknesses of this model become evident in the light of statistical information and of an analysis of the physical processes involved: the Poisson assumption implies that the distribution of the waiting time to the next event is not modified by the knowledge of the time elapsed since the last one, while physical models of gradually accumulated and suddenly released energy call for a more general renewal process such that, unlike what happens in the Poisson process, the expected time to the next event decreases as time goes on (Esteva, 1974). Statistical data show that the Poisson assump-

tion may be acceptable when dealing with large shocks throughout the world (Ben-Menahem, 1960), implying lack of correlation between seismicities of different regions; however, when considering small volumes of the earth, of the order of those that can significantly contribute to seismic risk at a site, data often contradict Poisson's model, usually because of clustering of earthquakes in time. the observed numbers of short intervals between events are significantly higher than predicted by the exponential distribution, and values of Poisson's index of dispersion are well above unity (Figs. 6.12 and 6.13). In some instances, however, deviations in the opposite direction have been observed: waiting times tend to be more nearly periodic, Poisson's index of dispersion is smaller than one, and the process can be represented by a renewal model. This condition has been reported, for instance, in the southern coast of Mexico (Esteva, 1974), and in the Kamchatka and Pamir—Hindu Kush regions (Gaisky, 1966 and 1967). The models under discussion also fail to account for clustering in space (Tsuboi, 1958; Gajardo and Lomnitz, 1960), for the evolution of seismicity with time, and for the systematic shifting of active sources along geologic accidents (Allen, Chapter 3 of this book). On account of its simplicity, however, the Poisson process model provides a valuable tool for the formulation of some seismic-risk-related decisions, particularly of those that are sensitive only to magnitudes of events having very long return periods.

6.3 3.2 Trigger models

Statistical analysis of waiting times between earthquakes does not favor the adoption of the Poisson model or of other forms of renewal processes, such as those that assume that waiting times are mutually independent with lognormal or gamma distributions (Shlien and Toksoz, 1970). Alternative models have been developed, most of them of the 'trigger type' (Vere-Jones, 1970), i e. the overall process of earthquake generation is considered as the superposition of a number of time series, each having a different origin, where the origin times are the events of a Poisson process. In general, let N be the number of events that take place during time interval $(0, t)$, τ_m = origin time of the mth series, $W_m(t, \tau_m)$ the corresponding number of events up to instant t_1 and n_t the random number of time series initiated in the interval $(0, t)$. The total number of events that occur before instant t is then:

$$N = \sum_{m}^{n_t} W_m(t, \tau_m) \tag{6.12}$$

If origin times are distributed according to a homogeneous Poisson process with mean rate ν, and all W_m's are identically distributed stochastic processes with respect to $(t - \tau_m)$, it can be shown (Parzen, 1962) that the mean and variance of N can be obtained from:

$$E(N) = \nu \int_0^t E[W(t, \tau)]\mathrm{d}\tau \tag{6.13}$$

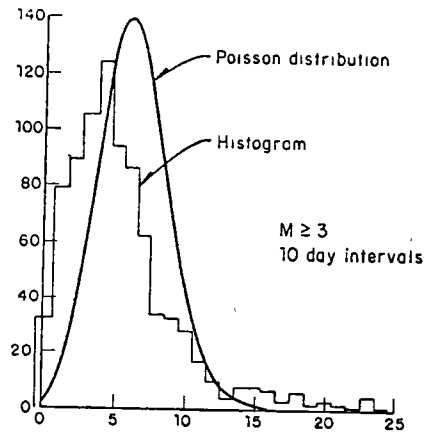

Fig. 6.12. Evaluation of Poisson process assumption (After Knopoff, 1964.)

$$\mathrm{var}\,(N) = \nu \int_0^t E[W^2(t, \tau)]\mathrm{d}\tau \tag{6.14}$$

Parzen (1962) gives also an expression for the probability generating function $\psi_N(Z; t)$ of the distribution of N in terms of $\psi_W(Z; t, \tau)$, the generat-

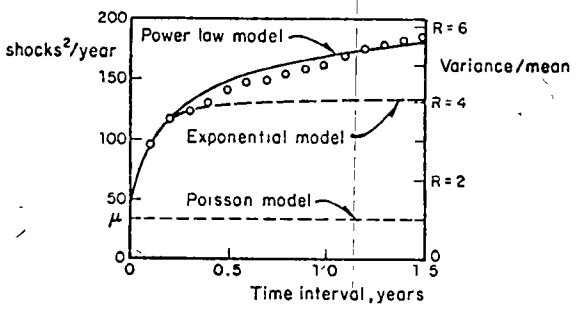

Fig. 6.13 Variance—time curve for New Zealand shallow shocks. (After Vere-Jones, 1966)

ing function of each of the component processes:

$$\psi_N(Z; t) = \exp\left[-\nu t + \nu \int_0^t \psi_W(Z; t, \tau)\mathrm{d}\tau\right] \tag{6.15}$$

where:

$$\psi_W(Z; t, \tau) = \sum_{n=0}^{\infty} Z^n \, P\{W(t, \tau) = n\} \tag{6.16}$$

and the probability mass function of N can be obtained from $\psi_N(Z; t)$ by recalling that:

$$\psi_N(Z; t) = \sum_{n=0}^{\infty} Z^n P\{N = n\}$$

expanding ψ_N in power series of Z, and taking $P\{N = n\}$ equal to the coefficient of Z^n in that expansion. For instance, if it is of interest to compute $P\{N = 0\}$, expansion of $\psi_N(Z; t)$ in a Taylor's series with respect to $Z = 0$ leads to:

$$\psi_N(Z; t) = \psi_N(0, t) + Z\psi'_N(0; t) + \frac{Z^2}{2!}\psi''_N(0; t) + \ldots \tag{6.17}$$

where the prime signifies derivative with respect to Z. From the definition of ψ_N, $P\{N = 0\} = \psi_N(0; t)$.

Because the component processes of 'trigger'-type time series appear overlapped in sample histories, their analytical representation usually entails study of a number of alternative models, estimation of their parameters, and comparison of model and sample properties — often second-order properties (Cox and Lewis, 1966).

Vere-Jones models. Applicability of some general 'trigger' models to represent local seismicity processes was discussed in a comprehensive paper by Vere-Jones (1970), who calibrated them mainly against records of seismic activity in New Zealand. In addition to simple and compound Poisson processes (Parzen, 1962), he considered Neyman-Scott and Bartlett-Lewis models, both of which assume that earthquakes occur in clusters and that the number of events in each cluster is stocastically independent of its origin time. In the Neyman-Scott model, the process of clusters is assumed stationary and Poisson, and each cluster is defined by p_N, the probability mass function of its number of events, and $\Lambda(t)$, the cumulative distribution function of the time of an event corresponding to a given cluster, measured from the cluster origin. The Bartlett-Lewis model is a special case of the former, where each cluster is a renewal process that ends after a finite number of renewals. In these models the conditional probability of an event taking place during the interval $(t, t + \mathrm{d}t)$, given that the cluster consists of N shocks, is equal to $N\lambda(t)\mathrm{d}t$, where $\lambda(t) = \partial\Lambda(t)/\partial t$.

Because clusters overlap in time they cannot easily be identified and separated. Estimation of process parameters is accomplished by assuming different sets of those parameters and evaluating the corresponding goodness of fit with observed data.

Various alternative forms of Neyman-Scott's model were compared by Vere-Jones with observed data on the basis of first- and second-order statistics: hazard functions, interval distributions (in the form of power spectra) and variance time curves. The statistical record comprises about one thousand New Zealand earthquakes with magnitudes greater than 4.5, recorded from 1942 to 1961. Figures 6.13—6.15 show results of the analysis for shallow New Zealand shocks as well as the comparison of observed data with sev-

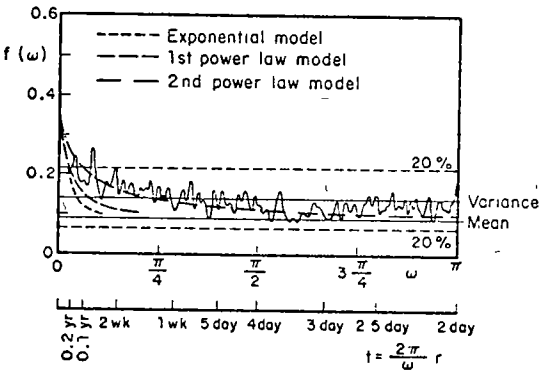

Fig. 6.14. Smoothed periodogram for New Zealand shallow shocks. (After Vere-Jones, 1966.)

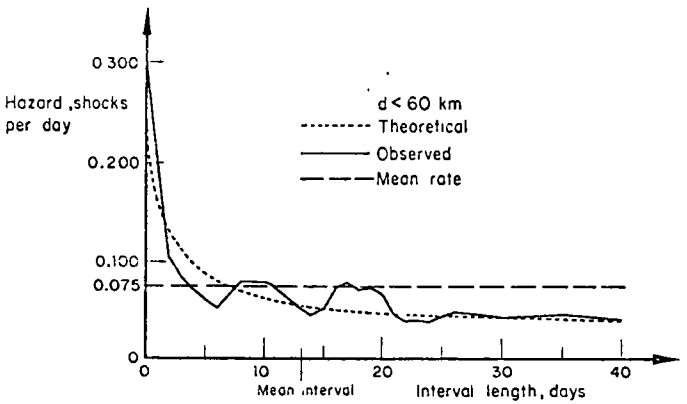

Fig 6.15. Hazard function for New Zealand shallow shocks (After Vere-Jones, 1970)

eral alternative models. The process of cluster origins is Poisson in all cases, but the distributions of cluster sizes (N) and of times of events within clusters differ among the various instances: in the Poisson model no clustering takes place (the distribution of N is a Dirac delta function centered at $N = 1$) while in the exponential and in the power-law models the distribution of N is extremely skewed towards $N = 1$, and $\Lambda(t)$ is taken respectively as $1 - e^{-\lambda t}$

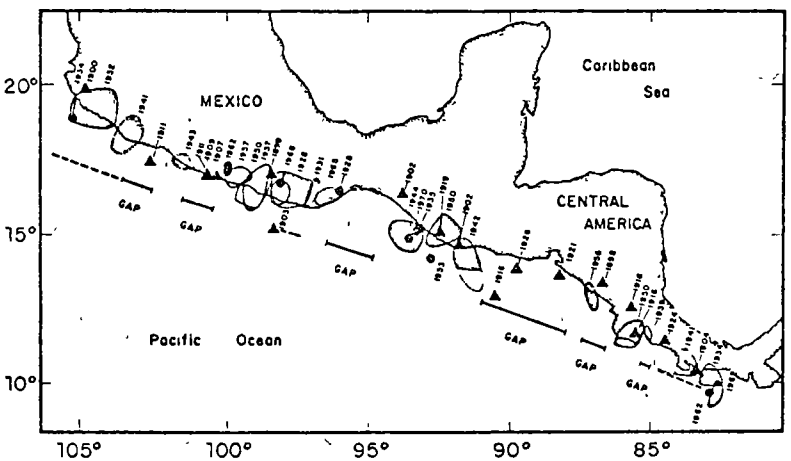

Fig. 6 16. Rupture zones and epicenters of large shallow Middle American earthquakes of this century. (After Kelleher et al., 1973.)

and $1 - [c/(c + t)]^{\delta}$ for $t \geqslant 0$, and as zero for $t < 0$, where λ, c, and δ are positive parameters. In Figs. 6.13—6.15, $\delta = 0.25$, $c = 2.3$ days, and $\lambda = 0.061$ shocks/day. The significance of clustering is evidenced by the high value of Poisson's dispersion index in Fig. 6.13, while no significant periodicity can be inferred from Fig. 6.14. Both figures show that the power-law model provides the best fit to the statistics of the samples. A similar analysis for New Zealand's deep shocks shows much less clustering. Poisson's dispersion index equals 2, and the hazard function is nearly constant with time.

Still, data reported by Gaisky (1967) have hazard functions that suggest models where the cluster origins as well as the clusters themselves may be represented by renewal processes. Mean return periods are of the order of several months, and hence these processes do not correspond, at least in the time scale, to the process of alternate periods of activity and quiescense of some geological structures cited by Kelleher et al. (1973), which have led to the concept of 'temporal seismic gaps', discussed below.

Simplified trigger models. Shlien and Toksoz (1970) proposed a simple particular case of the Neyman-Scott process; they lumped together all earthquakes taking place during non-overlapping time intervals of a given length and defined them as clusters for which $\lambda(t)$ was a Dirac delta function. Working with one-day intervals, they assumed the number of events per cluster to be distributed in accordance with the discrete Pareto law and applied a maximum-likelihood criterion to the information consisting of 35 000 earthquakes reported by the USCGS from January 1971 to August 1968. The model proposed represents reasonably well both the distribution of the number of earthquakes in one-day intervals and the dispersion index. However, owing to the assumption that no cluster lasts more than one day, the model fails to represent the autocorrelation function of the daily numbers of shocks for small time lags. The degree of clustering is shown to be a regional function, and to diminish with the magnitude threshold value and with the focal depth.

Aftershock sequences The trigger processes described have been branded as reasonable representations of regional seismic activity, even when aftershock sequences and earthquake swarms are suppressed from statistical records, however arbitrary that suppression may be. The most significant instances of clustering are related, however, to aftershock sequences which often follow shallow shocks and only rarely intermediate and deep events. Persistence of large numbers of aftershocks for a few days or weeks has propitiated the detailed statistical analysis of those sequences since last century. Omori (1894) pointed out the decay in the mean rate of aftershock occurrence with t, the time elapsed since the main shock, he expressed that rate as inversely proportional to $t + q$, where q is an empirical constant. Utsu (1961) proposed a more general expression, proportional to $(t + c)^{-\zeta}$ where ζ is a constant, Utsu's proposal is consistent with the power-law expression for $\Lambda(t)$ presented above.

Lomnitz and Hax (1966) proposed a clustering model to represent aftershock sequences; it is a modified version of Neyman and Scott's model, where the process of cluster origins is non-homogeneous Poisson with mean rate decaying in accordance with Omori's law, the number of events in each cluster has a Poisson distribution, and $\Lambda(t)$ is exponential. All the results and methods of analysis described by Vere-Jones (1970) for the stationary process of cluster origins can be applied to the nonstationary case through a transformation of the time scale. Fitting of parameters to four aftershock sequences was accomplished through use of the second-order information of the sample defined on a transformed time scale. By applying this criterion to earthquake sets having magnitudes above different threshold values it was noticed that the degree of clustering decreases as the threshold value increases.

The magnitude of the main shock influences the number of aftershocks and the distribution of their magnitudes and, although the rate of activity decreases with time, the distribution of magnitudes remains stable throughout each sequence (Lomnitz, 1966, Utsu, 1962, Drakopoulos, 1971). Equation 6.6 represents fairly well the distribution of magnitudes observed in most aftershock sequences. Values of β range from 0.9 to 3.9 and decrease as the depth increases. Since values of β for regular (main) earthquakes are usually estimated from relatively small numbers of shocks generated throughout crust volumes much wider than those active during aftershock sequences, no relation has been established among β-values for series of both types of events. The parameters of Utsu's expression for the decay of aftershock activity with time have been estimated for several sequences, for instance those following the Aleutian earthquake of March 9, 1957, the Central Alaska earthquake of April 7, 1958, and the Southeastern Alaska earthquake of July 10, 1958 (Utsu, 1962), with magnitudes equal to 8.3, 7.3, and 7.9, respectively; c (in days) was 0.37, 0.40, and 0.01, while ζ was 1.05, 1.05 and 1.13, respectively. The relationship of the total number of aftershocks whose magnitude exceeds a given value with the magnitude of the main shock was studied by Drakopoulos (1971) for 140 aftershock sequences in Greece from 1912 to 1968. His results can be expressed by $N(M) = A \exp(-\beta M)$, where $N(M)$ is the total number of aftershocks with magnitude greater than M, and A is a function of M_0, the magnitude of the main shock:

$$A = \exp(3.62\,\beta + 1.1 M_0 - 3.46) \qquad (6.18)$$

Formulation of stochastic process models for given earthquake sequences is feasible once this relationship and the activity decay law are available for the source of interest. For seismic-risk estimation at a given site the spatial distribution of aftershocks may be as significant as the distribution of magnitudes and the time variation of activity, particularly for sources of relatively large dimensions.

6.3.3 3 Renewal process models

The trigger models described are based on information about earthquakes with magnitudes above relatively low thresholds recorded during time intervals of at most ten years. The degrees of clustering observed and the distributions of times between clusters cannot be extrapolated to higher magnitude thresholds and longer time intervals without further study.

Available information shows beyond doubt that significant clustering is the rule, at least when dealing with shallow shocks. However, there is considerable ground for discussion on the nature of the process of cluster origins during intervals of the order of one century or longer. While lack of statistical data hinders the formulation of seismicity models valid over long time intervals, qualitative consideration of the physical processes of earthquake generation may point to models which at least are consistent with the state of knowledge of geophysical sciences. Thus, if strain energy stored in a region grows in a more or less systematic manner, the hazard function should grow with the time elapsed since the last event, and not remain constant as the Poisson assumption implies. The concept of a growing hazard function is consistent with the conclusions of Kelleher et al. (1973) concerning the theory of periodic activation of *seismic gaps*. This theory is partially supported by results of nearly qualitative analysis of the migration of seismic activity along a number of geological structures. An instance is provided by the southern coast of Mexico, one of the most active regions in the world Large shallow shocks are generated probably by the interaction of the continental mass and the subductive oceanic Cocos plate that underthrusts it and by compressive or flexural failure of the latter (Chapter 2) Seismological data show significant gaps of activity along the coast during the present century and not much is known about previous history (Fig 6 16). Along these gaps, seismic-risk estimates based solely on observed intensities are quite low, although no significant difference is evident in the geological structure of these regions with respect to the rest of the coast, save some transverse faults which divide the continental formation into several blocks. Without looking at the statistical records a geophysicist would assign equal risk throughout the area. On the basis of seismicity data, Kelleher et al have concluded that activity migrates along the region, in such a manner that large earthquakes tend to occur at seismic gaps, thus implying that the hazard function grows with time since the last earthquake. Similar phenomena have been observed in other regions; of particular interest is the North Anatolian fault where activity has shifted systematically along it from east to west during the last forty years (Allen, 1969).

Conclusions relative to activation of seismic gaps are controversial because the observation periods have not exceeded one cycle of each process. Nevertheless, those conclusions point to the formulation of stochastic models of seismicity that reflect plausible features of the geophysical processes.

These considerations suggest the use of renewal-process models to rep-

resent sequences of individual shocks or of clusters. Such models are characterized because times between events are independent and identically distributed. The Poisson process is a particular renewal model for which the distribution of the waiting time is exponential. Wider generality is achieved, without much loss of mathematical tractability, if inter-event times are supposed to be distributed in accordance with a gamma function:

$$f_T(t) = \frac{\nu}{(k-1)!}(\nu t)^{k-1}\, e^{-\nu t} \tag{6.19}$$

which becomes the exponential distribution when $k = 1$. If $k < 1$, short intervals are more frequent and the coefficient of variation is greater than in the Poisson model; if $k > 1$, the reverse is true. Shlien and Toksöz (1970) found that gamma models were unable to represent the sequences of individual shocks they analyzed; but these authors handled time intervals at least an order of magnitude shorter than those referred to in this section.

On the basis of hazard function estimated from sequences of small shocks in the Hindu-Kush, Vere-Jones (1970) deduces the validity of 'branching renewal process' models, in which the intervals between cluster centers, as well as those between cluster members, constitute renewal processes.

Owing to the scarcity of statistical information, reliable comparisons between alternate models will have to rest partially on simulation of the process of storage and liberation of strain energy (Burridge and Knopoff, 1967; Veneziano and Cornell, 1973).

6.3.4 Influence of the seismicity model on seismic risk

Nominal values of investments made at a given instant increase with time when placing them at compound interest rates, i.e. when capitalizing them. Their real value — and not only the nominal one — will also grow, provided the interest rate overshadows inflation. Conversely, for the purpose of making design decisions, nominal values of expected utilities and costs inflicted upon in the future have to be converted into present or actualized values, which can be directly compared with initial expenditures. Descriptions of seismic risk at a site are insufficient for that purpose unless the probability distributions of the times of occurrence of different intensities — or magnitudes at neighbouring sources — are stipulated; this entails more than simple magnitude-recurrence graphs or even than maximum feasible magnitude estimates.

Immediately after the occurrence of a large earthquake, seismic risk is abnormally high due to aftershock activity and to the probability that damage inflicted by the main shock may have weakened natural or man-made structures if emergency measures are not taken in time. When aftershock activity has ceased and damaged systems have been repaired, a normal risk level is attained, which depends on the probability-density functions of the waiting times to the ensuing damaging earthquakes.

For the purpose of illustration, let it be assumed that a fixed and deterministically known damage D_0 occurs whenever a magnitude above a given value is generated at a given source. If $f(t)$ is the probability-density function of the waiting time to the occurrence of the damaging event, and if the risk level is sufficiently low that only the first failure is of concern, the expected value of the actualized cost of damage is (see Chapter 9):

$$\bar{D} = D_0 \int_0^\infty e^{-\gamma t} f(t)\,dt \tag{6.20}$$

where γ is the discount (or compound interest) coefficient and the overbar denotes expectation. If the process is Poisson with mean rate ν, then $f(t)$ is exponential and $\bar{D} \cong D_0\ \nu/\gamma$, however, if damaging events take place in clusters and most of the damage produced by each cluster corresponds to its first event, the computation of $\bar{D}$ should make use of the mean rate ν corresponding to the clusters, instead of that applicable to individual events. Table 6.II shows a comparison of seismic risk determined under the alternative assumptions of a Poisson and a gamma model ($k = 2$), both with the same mean return period, k/ν (Esteva, 1974). Three descriptions of risk are presented as functions of the time t_0 elapsed since the last damaging event: T_1, the expected time to the next event, measured from instant t_0, the expected value of the present cost of failure computed from eq. 6.20, and the hazard function (or mean failure rate). Since clustering is neglected, risk of aftershock occurrence must be either included in D_0 or superimposed on that displayed in the table.

This table shows very significant differences among risk levels for both processes. At small values of t_0, risk is lower for the gamma process, but it

TABLE 6.II

Comparison of Poisson and gamma processes

$t_0\,\nu/k$	$\bar{T}_1\,\nu/k$	Poisson process, $k = 1$		hk/ν	$T_1\,\nu/k$	Gamma process, $k = 2$		hk/ν
		D/D_0				D/D_0		
		$\gamma k/\nu = 10$	$\gamma k/\nu = 100$			$\gamma k/\nu = 10$	$bk/\nu = 100$	
0					1.0	0 0278	0.0004	0
0.1					0 92	0 0511	0 0036	0 367
0.2					0.86	0.0675	0 0059	0 667
0.5					0 75	0.0973	0 0100	1 333
1	1.0	0.0909	0.0099	1.0	0.67	0.120	0 0132	2 000
2					0 60	0.139	0 0158	2 667
5					0.54	0 154	0 0179	3 333
10					0 52	0.160	0 0187	3 633
					0 50	0.167	0 0196	4 000

grows with time, until it outrides that for the Poisson process, which remains constant. The differences shown clearly affect engineering decisions.

6.4 ASSESSMENT OF LOCAL SEISMICITY

Only exceptionally can magnitude-recurrence relations for small volumes of the earth's crust and statistical correlation functions of the process of earthquake generation be derived exclusively from statistical analysis of recorded shocks. In most cases this information is too limited for that purpose and it does not always reflect geological evidence. Since the latter, as well as its connection with seismicity, is beset with wide uncertainty margins, information of different nature has to be evaluated, its uncertainty analyzed, and conclusions reached consistent with all pieces of information. A probabilistic criterion that accomplishes this is presented here: on the basis of geotectonic data and of conceptual models of the physical processes involved, a set of alternate assumptions can be made concerning the functions in question (magnitude recurrence, time, and space correlation) and an initial probability distribution assigned thereto, statistical information is used to judge the likelihood of each assumption, and a posterior probability distribution is obtained. How statistical information contibutes to the posterior probabilities of the alternate assumptions depends on the extent of that information and on the degree of uncertainty implied by the initial probabilities. Thus, if geological evidence supports confidence in a particular assumption or range of assumptions, statistical information should not greatly modify the initial probabilities. If, on the other hand, a long and reliable statistical record is available, it practically determines the form and parameters of the mathematical model selected to represent local seismicity.

6.4.1 Bayesian estimation of seismicity

Bayesian statistics provide a framework for probabilistic inference that accounts for prior probabilities assigned to a set of alternate hypothetical models of a given phenomenon as well as for statistical samples of events related to that phenomenon. Unlike conventional methods of statistical inference, Bayesian methods give weight to probability measures obtained from samples or from other sources; numbers, coordinates and magnitudes of earthquakes observed in given time intervals serve to ascertain the probable validity of each of the alternative models of local seismicity that can be postulated on the grounds of geological evidence. Any criterion intended to weigh information of different nature and different degrees of uncertainty should lead to probabilistic conclusions consistent with the degree of confidence attached to each source of information. This is accomplished by Bayesian methods.

Let H_i ($i = 1, \ldots, n$) be a comprehensive set of mutually exclusive assumptions concerning a given, imperfectly known phenomenon and let A be the observed outcome of such a phenomenon. Before observing outcome A we assign an initial probability $P(H_i)$ to each hypothesis. If $P(A|H_i)$ is the probability of A in case hypothesis H_i is true, then Bayes' theorem (Raiffa and Schlaifer, 1968) states that:

$$P(H_i|A) = P(H_i)\frac{P(A|H_i)}{\sum_j P(H_j)P(A|H_j)} \tag{6.21}$$

The first member in this equation is the (posterior) probability that assumption H_i is true, given the observed outcome A.

In the evaluation of seismic risk, Bayes' theorem can be used to improve initial estimates of $\lambda(M)$ and its variation with depth in a given area as well as those of the parameters that define the shape of $\lambda(M)$ or, equivalently, the conditional distribution of magnitudes given the occurrence of an earthquake. For that purpose, take $\lambda(M)$ as the product of a rate function $\lambda_L = \lambda(M_L)$ by a shape function $G^*(M,B)$, equal to the conditional complementary distribution of magnitudes given the occurrence of an earthquake with $M \geqslant M_L$, where M_L is the magnitude threshold of the set of statistical data used in the estimation, and B is the vector of (uncertain) parameters $B_1, \ldots, B_r$ that define the shape of $\lambda(M)$. For instance, if $\lambda(M)$ is taken as given by eq. 6.8, B is a vector of three elements equal respectively to β, β_1, and M_U, if eq. 6.9 is adopted, B is defined by k and M_U.

The initial distribution of seismicity is in this case expressed by the initial joint probability density function of λ_L and B: $f'(\lambda_L, B)$. The observed outcome A can be expressed by the magnitudes of all earthquakes generated in a given source during a given time interval. For instance, suppose that N earthquakes were observed during time interval t and that their magnitudes were $m_1, m_2, \ldots, m_N$. Bayes' expression takes the form:

$$f''(\lambda_L, B|m_1, \ldots, m_N; t) = f'(\lambda_L, B)\frac{P[m_1, m_2, \ldots, m_N; t|\lambda_L, B]}{\int\int P[m_1, m_2, \ldots, m_N, t|l, b]f'(l,b)\mathrm{d}l\mathrm{d}b} \tag{6.22}$$

where $f''(.)$ is the posterior probability density function, and l and b are dummy variables that stand for all values that may be taken by λ_L and B, respectively. Estimation of λ_L can usually be formulated independently of that of the other parameters The observed fact is then expressed by N_L, the number of earthquakes with magnitude above M_L during time t, and the following expression is obtained, as a first step in the estimation of $\lambda(M)$:

$$f''(\lambda_L|N_L, t) = f'(\lambda_L)\frac{P(N_L; t|\lambda_L)}{\int P(N_L; t|l)f'(l)\mathrm{d}l} \tag{6.23}$$

6.4.1.1 Initial probabilities of hypothetical models

Where statistical information is scarce, seismicity estimates will be very

sensitive to initial probabilities assigned to alternative hypothetical models, the opinions of geologists and geophysicists about probable models, about the parameters of these models, and the corresponding margins of uncertainty should be adequately interpreted and expressed in terms of a function f', as required by equations similar to 6.22 and 6.23. Ideally, these opinions should be based on the formulation of potential earthquake sources and on their comparison with possibly similar geotectonic structures. This is usually done by geologists, more qualitatively than quantitatively, when they estimate M_U. Initial estimates of λ_L are seldom made, despite the significance of this parameter for the design of moderately important structures (see Chapter 9).

Analysis of geological information must consider local details as well as general structure and evolution. In some areas it is clear that all potential earthquake sources can be identified by surface faults, and their displacements in recent geological times measured. When mean displacements per unit time can be estimated, the order of magnitude of creep and of energy liberated by shocks and hence of the recurrence intervals of given magnitudes can be established (Wallace, 1970, Davies and Brune, 1971), the corresponding uncertainty evaluated, and an initial probability distribution assigned. The fact that magnitude-recurrence relations are only weakly correlated with the size of recent displacements is reflected in large uncertainties (Petrushevsky, 1966).

Application of the criterion described in the foregoing paragraph can be unfeasible or inadequate in many problems, as in areas where the abundance of faults of different sizes, ages, and activity, and the insufficient accuracy with which focal coordinates are determined preclude a differentiation of all sources. Regional seismicity may then be evaluated under the assumption that at least part of the seismic activity is distributed in a given volume rather than concentrated in faults of different importance. The same situation would be faced when dealing with active zones where there is no surface evidence of motions. Hence, consideration of the overall behavior of complex geological structures is often more significant than the study of local details.

Not much work has been done in the analysis of the overall behavior of large geological structures with respect to the energy that can be expected to be liberated per unit volume and per unit time in given portions of those structures. Important research and applications should be expected, however, since, as a result of the contribution of plate-tectonics theory to the understanding of large-scale tectonic processes, the numerical values of some of the variables correlated with energy liberation are being determined, and can be used at least to obtain orders of magnitude of expected activity along plate boundaries. Far less well understood are the occurrence of shocks in apparently inactive regions of continental shields and the behavior of complex continental blocks or regions of intense folding, but even there some

progress is expected in the study of accumulation of stresses in the crust.

Knowledge of the geological structure can serve to formulate initial probability distributions of seismicity even when quantitative use of geophysical information seems beyond reach. Initial probability distributions of local seismicity parameters λ_L, B in the small volumes of the earth's crust that contribute significantly to seismic risk at a site, can be assigned by comparison with the average seismicity observed in wider areas of similar tectonic characteristics, or where the extent and completeness of statistical information warrant reliable estimates of magnitude-recurrence curves (Esteva, 1969). In this manner we can, for instance, use the information about the average distribution of the depths of earthquakes of different magnitudes throughout a seismic province to estimate the corresponding distribution in an area of that province, where activity has been low during the observation interval, even though there might be no apparent geophysical reason to account for the difference. Similarly, the expected value and coefficient of variation of λ_L in a given area of moderate or low seismicity (as a continental shield) can be obtained from the statistics of the motions originated at all the supposedly stable or aseismic regions in the world.

The significance of initial probabilities in seismic risk estimates, against the weight given to purely statistical information, becomes evident in the example of Fig. 6.16. If Kelleher's theory about activation of seismic gaps is true, risk is greater at the gaps than anywhere else along the coast; if Poisson models are deemed representative of the process of energy liberation, the extent of statistical information is enough to substantiate the hypothesis of reduced risk at gaps. Because both models are still controversial, and represent at most two extreme positions concerning the properties of the actual process, risk estimates will necessarily reflect subjective opinions.

6.4.1.2 Significance of statistical information

Estimation of λ_L. Application of eq. 6.23 to estimate λ_L independently of other parameters will be first discussed, because it is a relatively simple problem and because λ_L is usually more uncertain than M_U and much more so than β.

A model as defined by eq. 6.19 will be assumed to apply. If the possible assumptions concerning the values of λ_L constitute a continuous interval, the initial probabilities of the alternative hypotheses can be expressed in terms of a probability-density function of λ_L. If, in addition, a certain assumption is made concerning the form of this probability-density function, only the initial values of $E(\lambda_L)$ and $V(\lambda_L)$ have to be assumed. It is advantageous to assign to $\nu = k/E(T)$ a gamma distribution. Then, if ρ and μ are the parameters of this initial distribution of ν, if k is assumed to be known, and if the observed outcome is expressed as the time t_n elapsed during $n+1$ consecutive events (earthquakes with magnitude $\geq M_L$), application of eq. 6.23 leads to the conclusion that the posterior probability function of ν is

also gamma, now with parameters $\rho + nk$ and $\mu + t_n$. The initial and the posterior expected values of ν are respectively equal to ρ/μ, and to $(\rho + nk)/(\mu + t_n)$. When initial uncertainty about ν is small, ρ and μ will be large and the initial and the posterior expected values of ν will not differ greatly. On the other hand, if only statistical information were deemed significant, ρ and μ should be given very small values in the initial distribution, and $E(\nu)$, and hence λ_L, will be practically defined by n, k, and t_n. This means that the initial estimates of geologists should not only include expected or most probable values of the different parameters, but also statements about ranges of possible values and degrees of confidence attached to each.

In the case studied above only a portion of the statistical information was used. In most cases, especially if seismic activity has been low during the observation interval, significant information is provided by the durations of the intervals elapsed from the initiation of observations to the first of the $n + 1$ events considered, and from the last of these events until the end of the observation period. Here, application of eq. 6.23 leads to expressions slightly more complicated than those obtained when only information about t_n is used.

The particular case when the statistical record reports no events during *at least* an interval $(0, t_0)$ comes up frequently in practical problems The probability-density function of the time T_1 from t_0 to the occurrence of the first event must account for the corresponding shifting of the time axis. Furthermore, if the time of occurrence of the last event before the origin is unknown, the distribution of the waiting time from $t = 0$ to the first event coincides with that of the *excess life* in a renewal process at an arbitrary value of t that approaches infinity (Parzen, 1962). For the particular case when the waiting times constitute a gamma process, T_1 is measured from $t = 0$, T is the waiting time between consecutive events, and it is known that $T_1 \geqslant t_0$, the conditional density function of $\tau_1 = (T_1 - t_0)/E(T)$ is given by eq. 6.24 (Esteva, 1974), where $u_0 = t_0/E(T)$:

$$f_{\tau_1}(u|T_1 \geqslant t_0) = \frac{\sum_{m=1}^{k} \frac{k}{(m-1)!} [k(u+u_0)]^{m-1}}{\sum_{m=1}^{k} \sum_{n=1}^{m} \frac{1}{(n-1)!} (ku_0)^{n-1}} e^{-ku} \qquad (6.24)$$

Consider now the implications of Bayesian analysis when applied to one of the seismic gaps in Fig. 6.16, under the conditions implicit in eq. 6.24. An initial set of assumptions and corresponding probabilities was adopted as described in the following. From previous studies referring to all the southern coast of Mexico, local seismicity in the gap area (measured in terms of λ for $M \geqslant 6.5$) was represented by a gamma process with $k = 2$. An initial probability density function for ν was adopted such that the expected value of $\lambda(6.5)$ for the region coincided with its average throughout the complete seismic province. Two values of ρ were considered: 2 and 10, which correspond to coefficients of variation of 0.71 and 0.32, respectively. Values in Table 6.III were obtained for the ratio of the final to the initial expected values of ν, in terms of u_0.

The last two columns in the table contain the ratios of the computed values of $E''(T_1)$ and $E'(T)$ when ν is taken as equal respectively to its initial or to its posterior expected value. This table shows that, for $\rho = 10$, that is, when uncertainty attached to the geologically based assumptions is low, the expected value of the time to the next event keeps decreasing, in accordance with the conclusions of Kelleher et al. (1973). However, as time goes on and no events occur, the statistical evidence leads to a reduction in the estimated risk, which shows in the increased conditional expected values of T_1. For $\rho = 2$, the geological evidence is less significant and risk estimates decrease at a faster rate.

6 4.1.3 Bayesian estimation of jointly distributed parameters

In the general case, estimation of B will consist in the determination of the posterior Bayesian joint probability function of its components, taking as statistical evidence the relative frequencies of observed magnitudes. Thus, if event A is described as the occurrence of N shocks, with magnitudes $m_1, ..., m_N$, and b_i $(i = 1, ..., r)$ are values that may be adopted by the components of vector B being estimated, eq. 6.21 becomes:

$$f''_B(b_1, ..., b_r|A) = \frac{f'_B(b_1, ..., b_r)P(A|b_1, ..., b_r)}{\int ... \int f'_B(u_1, ..., u_r)P(A|u_1, ..., u_r)du_1, ..., du_r} \qquad (6.25)$$

where $P(A|u_1, ..., u_r)$ is proportional to

$$\prod_{i=1}^{N} g(m_i|u_1, ..., u_r)$$

and $g(m) = -\partial G^*(m)/\partial m$.

Closed-form solutions for f'' as given by eq. 6.25 are not feasible in general. For the purpose of evaluating risk, however, estimates of the posterior first and second moments of f'' can be obtained from eq. 6.25, making use of available first-order approximations (Benjamin and Cornell, 1970, Rosenblueth, 1975) Thus, the posterior expected value of B_i is given by $\int f''_{B_i}(u)\, u\, du$, where $f''_{B_i}(u_i) = \int ... \int f''_B(u_1, ..., u_r)\, du_1, ..., du_n$ and the multiple integral is of order $r - 1$, because it is not extended to the dominion of B_i. Hence:

$$E''(B_i) = \frac{E'_B[B_i P(A|B_1, ..., B_r)]}{E'_B[P(A|B_1, ..., B_r)]} \qquad (6.26)$$

TABLE 6 III

Bayesian estimates of seismicity in one seismic gap

$\tilde{u}_0 = t_0/E'(T)$	$E''(\nu)/E'(\nu)$		$E''(T_1 \mid T_1 > t_0)/E'(T)$	
	$\rho = 2$	$\rho = 10$	$\rho = 2$	$\rho = 10$
0	1.0	1.0	0.75	0 75
0.1	0 95	0 99	0 76	0.74
0 5	0.75	0 94	0.91	0 71
1	0 58	0 87	1 14	0.73
5	0 20	0.54	3 11	1 05
10	0 11	0 36	5.47	1 55
20	0.06	0 22	10.50	2 48

where E' and E'' stand for initial and posterior expectation, and subscript B means that expectation is taken with respect to all the components of B. Likewise, the following *posterior moments* can be obtained:

Covariance of B_i and B_j

$$\mathrm{Cov}''(B_i, B_j) = \frac{E'_B[B_i B_j P(A|B_1, \ldots, B_r)]}{E'_B[P(A|B_1, \ldots, B_r)]} - E''(B_i)E''(B_j) \tag{6.27}$$

Expected value of $\lambda(M)$

$$E''[\lambda(M)] = E''(\lambda_1)E''[G^*(M, B)] = E''(\lambda_1)\frac{E'_B[G^*(M, B)P(A|B_1, \ldots, B_r)]}{E'_B[P(A|B_1, \ldots, B_r)]} \tag{6.28}$$

Marginal distributions The posterior expectation of $\lambda(M)$ is in some cases all that is required to describe seismicity for decision-making purposes Often, however, uncertainty in $\lambda(M)$ must also be acounted for. For instance, the probability of exceedance of a given magnitude during a given time interval has to be obtained as the expectation of the corresponding probabilities over all alternative hypotheses concerning $\lambda(M)$. In this manner it can be shown that, if the occurrence of earthquakes is a Poisson process and the Bayesian distribution of λ_L is gamma with mean $\bar{\lambda}_L$ and coefficient of variation V_L, the marginal distribution of the number of earthquakes is negative binomial with mean $\bar{\lambda}_L$. In particular, the marginal probability of zero events during time interval t — equivalently, the complementary distribution function of the waiting time between events — is equal to $(1 + t/t'')^{-r''}$, where $r'' = V_L^{-2}$ and $t'' = r''/\bar{\lambda}_L$. The marginal probability-density function of the waiting time, that should be substituted in eq. 6.20, is $\bar{\lambda}_L(1 + t/t'')^{-r''-1}$, which tends to the exponential probability function as r'' and t'' tend to infinity (and $V_L \to 0$) while their ratio remains equal to $\bar{\lambda}_L$.

Bayesian uncertainty tied to the joint distribution of all seismicity parameters ($\lambda_L, B_1, \ldots, B_r$) can be included in the computation of the probability of occurrence of a given event Z by taking the expectation of that probability with respect to all parameters:

$$P(Z) = E_{\lambda_L, B}[P(Z); \lambda_L, B_1, \quad, B_r)] \tag{6.29}$$

When the joint distribution of λ_L, B stems from Bayesian analysis of an initial distribution and an observed event, A, this equation adopts the form:

$$P'(Z) = \frac{E'_{\lambda_L, B}[P(Z|\lambda_L, B)P(A|\lambda_L, B)]}{E'_{\lambda_L, B}[P(A|\lambda_L, B)]} \tag{6.30}$$

where ' and " stand for initial and posterior, respectively.

Spatial variability. Figure 6.17 shows a map of geotectonic provinces of Mexico, according to F. Mooser. Each province is characterized by the large-scale features of its tectonic structure, but significant local perturbations to the overall patterns can be identified. Take for instance zone 1, whose seismotectonic features were described above, and are schematically shown in Fig. 6.18 (Singh, 1975): the Pacific plate underthrusts the continental block and is thought to break into several blocks, separated by faults transverse to the coast, that dip at different angles. The continental mass is also

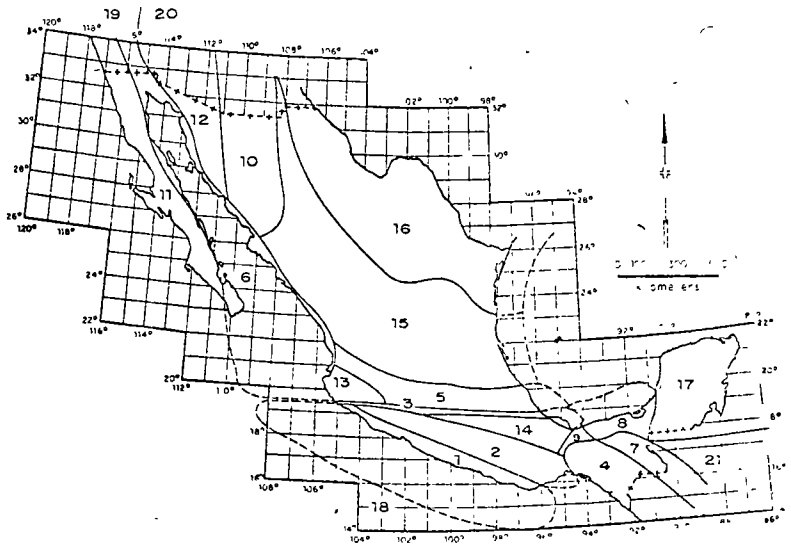

Fig. 6 17. Seismotectonic provinces of Mexico (After F. Mooser.)

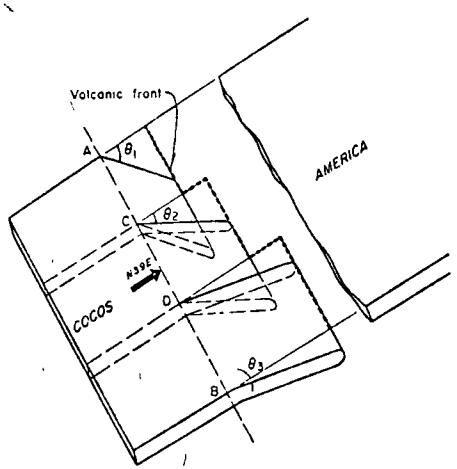

Fig. 6.18. Schematic drawing of the segmenting of Cocos plate as it subducts below American plate. (After Singh, 1974.)

made up of several large blocks. Seismic activity at the underthrusting plate or at its interface with the continental mass is characterized by magnitudes that may reach very high values and by the increase of mean hypocentral depth with distance from the coast; small and moderate shallow shocks are generated at the blocks themselves. Variability of statistical data along the whole tectonic system was discussed above and is apparent in Fig 6.10. Bayesian estimation of local seismicity averaged throughout the system is a matter of applying eq. 6.21 or any of its special forms (eqs. 6.22 and 6.23), taking as statistical evidence the information corresponding to the whole system. However, seismic risk estimates are sensitive to values of local seismicity averaged over much smaller volumes of the earth's crust, hence the need to develop criteria for probabilistic inference of possible patterns of space variability of seismicity along tectonically homogeneous zones.

On the basis of seismotectonic information, the system under consideration can first be subdivided into the underthrusting plate and the subsystem of shallow sources; each subsystem can then be separately analyzed. Take for instance the underthrusting plate and subdivide it into s sufficiently small equal-volume subzones. Let ν_L be the rate of exceedance of magnitude M_L throughout the main system, ν_{L_i} the corresponding rate at each subzone, and define p_i as ν_{L_i}/ν_L, with p_i independent of ν_L (p_i is equal to the probability that an earthquake known to have been generated in the overall system originated at subzone i). Initial information about possible space variability of

ν_{L_i} can be expressed in terms of an initial probability distribution of p_i and of the correlation among p_i and p_j for any i and j. Because $\Sigma\nu_{L_i} = \nu_L$, one obtains $\Sigma p_i = 1$. This imposes two restrictions on the initial joint probability distribution of the p_i's: $E'(p_i) = 1$, $\text{var}'\ \Sigma p_i = 0$. If all p_i's are assigned equal expectations and all pairs p_i, p_j, $i \neq j$ are assumed to possess the same correlation coefficient $\rho_{ij} = \rho'$, the restrictions mentioned lead to $E'(p_i) = 1/s$ and $\rho' = -1/(s-1)$. Posterior values of $E(p_i)$ and ρ_{ij} are obtained according to the same principles that led to eqs 6.25—6.28. Statistical evidence is in this case described by N, the total number of earthquakes generated in the system, and n_i ($i = 1, \ldots, s$) the corresponding numbers for the subzones. Given the p_i's, the probability of this event is the multinomial distribution:

$$P[A|p_1, \ldots, p_s] = \frac{N!}{n_1!, \ldots, n_s!}\, p_1^{n_1} \ldots p_s^{n_s} \tag{6.31}$$

If the correlation coefficients among seismicities of the various subzones can be neglected, each p_i can be separately estimated. Because p_i has to be comprised between 0 and 1, it is natural to assign it a beta initial probability distribution, defined by its parameters n_i' and N_i', such that $E'(p_i) = n_i'/N_i'$ and $\text{var}'(p_i) = n_i'(N_i' - n_i')/[N_i'^2(N_i' + 1)]$ (Raiffa and Schlaifer, 1968). The parameters of the posterior distribution will be

$$n_i'' = n_i' + n_i, N_i'' = N_i' + N$$

Take for instance a zone whose prior distribution of λ_L is assumed gamma with expected value λ_L' and coefficient of variation V_L'. Suppose that, on the basis of geological evidence and of the dimensions involved, it is decided to subdivide the zone into four subzones of equal dimensions; a-priori considerations lead to the assignment of expected values and coefficients of variation of p_i for those subzones, say $E'(p_i) = 0\ 25$, $V'(p_i) = 0\ 25$ ($i = 1, \ldots, 4$). From previous considerations for $s = 4$ take $\rho_{ij}' = -1/3$ for $i \neq j$. Suppose now that, during a given time interval t, ten earthquakes were observed in the zone, of which 0, 1, 3, and 6 occurred respectively in each subzone. If the Poisson process model is adopted, λ_L' and V_L' can be expressed in terms of a fictitious number of events $n' = V_L'^{-2}$ occurred during a fictitious time interval $t' = n'/\bar{\lambda}_L'$; after observing n earthquakes during an interval t, the Bayesian mean and coefficient of variation of λ_L will be $\bar{\lambda}_L'' = (n' + n)/(t' + t)$, $V_L'' = (n' + n)^{-1/2}$ (Esteva, 1968). Hence,

$$\lambda_L'' = (V_L'^{-2} + 10)/(V_L'^{-2}\bar{\lambda}_L'^{-1} + t), \qquad V_L'' = (V_L'^{-2} + 10)^{-1/2}$$

Local deviations of seismicity in each subzone with respect to the average λ_L can be analyzed in terms of p_i ($i = 1, \ldots, 4$); Bayesian analysis of the proportion in which the ten earthquakes were distributed among the subzones proceeds according to:

$$E''(p_i|A) = \frac{E'[p_i P(A|p_i, \ldots, p_4)]}{E'[P(A|p_i, \ldots, p_4)]} \tag{6.32}$$

The expectations that appear in this equation have to be computed with respect to the initial joint distribution of the p_i's. In practice, adequate approximations are required. For instance, Benjamin and Cornell's (1970) first-order approximation leads to $E''(p_1) = 0.226$, $E''(p_4) = 0.294$.

If correlation among subzone seismicities is neglected, and statistical information of each subzone is independently analyzed, when the p_i's are assigned beta probability-density functions with means and coefficients of variation as defined above, one obtains $E''(p_1) = 0.206$, $E''(p_4) = 0.311$, which are not very different from those formerly obtained; however, when $E'(p_i) = 0.25$ and $V'(p_i) = 0.5$, the first criterion leads to $E''(p_i) = 0.206$, $E''(p_4) = 0.314$, while the second produces 0.131 and 0.416, respectively. Part of the difference may be due to neglect of ρ'_{ij}, but probably a significant part stems from inaccuracies of the first-order approximation to the expectations that appear in eq. 6.32, alternate approximations are therefore desirable.

Incomplete data Statistical information is known to be fairly reliable only for magnitudes above threshold values that depend on the region considered, its level of activity, and the quality of local and nearby seismic instrumentation. Even incomplete statistical records may be significant when evaluating some seismicity parameters; their use has to be accompanied by estimates of detectability values, that is, of ratios of the numbers of events recorded to total numbers of events in given ranges (Esteva, 1970; Kaila and Narain, 1971).

6.5 REGIONAL SEISMICITY

The final goal of local seismicity assessment is the estimation of regional seismicity, that is, of probability distributions of intensities at given sites, and of probabilistic correlations among them. These functions are obtained by integrating the contributions of local seismicities of nearby sources, and hence their estimates reflect Bayesian uncertainties tied to those seismicities. In the following, regional seismicity will be expressed in terms of mean rates of exceedance of given intensities; more detailed probabilistic descriptions would entail adoption of specific hypotheses concerning space and time correlations of earthquake generation.

6.5.1 Intensity-recurrence curves

The case when uncertainty in seismicity parameters is neglected will be discussed first. Consider an elementary seismic source with volume dV and local seismicity $\lambda(M)$ per unit-volume, distant R from a site S, where intensity-recurrence functions are to be estimated. Every time that a magnitude M shock is generated at that source, the intensity at S equals:

$$Y = \epsilon Y_p = \epsilon b_1 \exp(b_2 M) g(R) \qquad (6.33)$$

(see eqs. 6.4 and 6.5), where ϵ is a random factor and Y and Y_p stand for actual and predicted intensities, b_1 and b_2 are given constants, and $g(R)$ is a function of hypocentral distance. The probability that an earthquake originating at the source will have an intensity greater than y is equal to the probability that $\epsilon Y_p > y$. If Y_p is expressed in terms of M and randomness in ϵ is accounted for, one obtains:

$$\nu(y) = \int_{\alpha_u}^{\alpha_L} \nu_p(y/u) f_\epsilon(u) du \qquad (6.34)$$

where ν and ν_p are respectively mean rates at which actual and predicted intensities exceed given values, $\alpha_U = y/y_U$, $\alpha_L = y/y_L$, y_U, and y_L are the predicted intensities that correspond to M_U and M_L, and f_ϵ the probability-density function of ϵ. If eq. 6.33 is assumed to hold:

$$\nu_p(y) = K_0 + K_1 y^{-r_1} - K_2 y^{-r_2} \qquad (6.35)$$

where:

$$K_i = [b_1 g(R)]^{r_i} A_i \lambda_L dV \quad (i = 0, 1, 2) \qquad (6.36)$$

$$r_0 = 0, \quad r_1 = \beta/b_2, \quad r_2 = (\beta - \beta_1)/b_2 \qquad (6.37)$$

Substitution of eq. 6.35 into 6.34, coupled with the assumption that $\ln \epsilon$ is normally distributed with mean m and standard deviation σ leads to:

$$\nu(y) = c_0 K_0 + c_1 K_1 y^{-r_1} - c_2 K_2 y^{-r_2} \qquad (6.38)$$

where:

$$c_i = \exp(Q_i) \left[\phi\left(\frac{\ln \alpha_L - u_i}{\sigma}\right) - \phi\left(\frac{\ln \alpha_U - u_i}{\sigma}\right) \right] \qquad (6.39)$$

ϕ is the standard normal cumulative distribution function, $Q_i = 1/2\ \sigma^2 r_i^2 + m r_i$, and $u_i = m + \sigma^2 r_i$. Similar expressions have been presented by Merz and Cornell (1973) for the special case of eq. 6.8 when $\beta_1 \to \infty$ and for a quadratic form of the relation between magnitude and logarithm of exceedance rate. Closed-form solutions in terms of incomplete gamma functions are obtained when magnitudes are assumed to possess extreme type-III distributions (eq. 6.9).

Intensity-recurrence curves at given sites are obtained by integration of the contributions of all significant sources. Uncertainties in local seismicities can be handled by describing regional seismicity in terms of means and variances of $\nu(y)$ and estimating these moments from eq. 6.34 and suitable first- and second-moment approximations. Influence of these uncertainties in design decisions has been discussed by Rosenblueth (in preparation).

6 5 2 Seismic probability maps

When intensity-recurrence functions are determined for a number of sites with uniform local ground conditions the results are conveniently represented by sets of seismic probability maps, each map showing contours of intensities that correspond to a given return period. For instance, Figs. 6.19 and 6 20 show peak ground velocities and accelerations that correspond to 100 years return period on firm ground in Mexico. These maps form part of a set that was obtained through application of the criteria described in this chapter. Because the ratio of peak ground accelerations and velocities does not remain constant throughout a region, the corresponding design spectra will not only vary in scale but also in shape (frequency content), in other words, seismic risk will usually have to be expressed in terms of at least the values of two parameters (for instance, as in this case, peak ground accelerations and velocities that correspond to various risk levels (return periods)).

6.5.3 Microzoning

Implicit in the above criteria for evaluation of regional seismicity is the adoption of intensity attenuation expressions valid on firm ground. Scatter of actual intensities with respect to predicted values was ascribed to differences in source mechanisms, propagation paths, and local site conditions; at least the latter group of variables can introduce systematic deviations in the

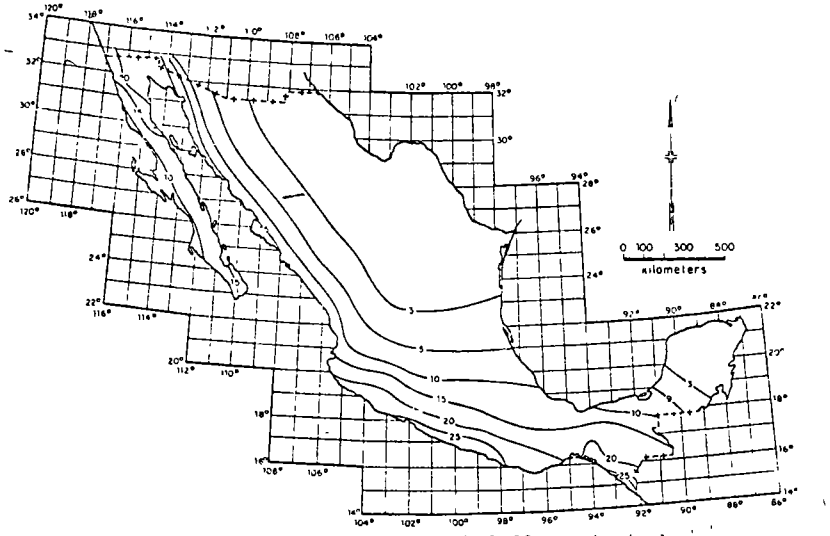

Fig 6.19. Peak ground velocities with return period of 100 years (cm/sec).

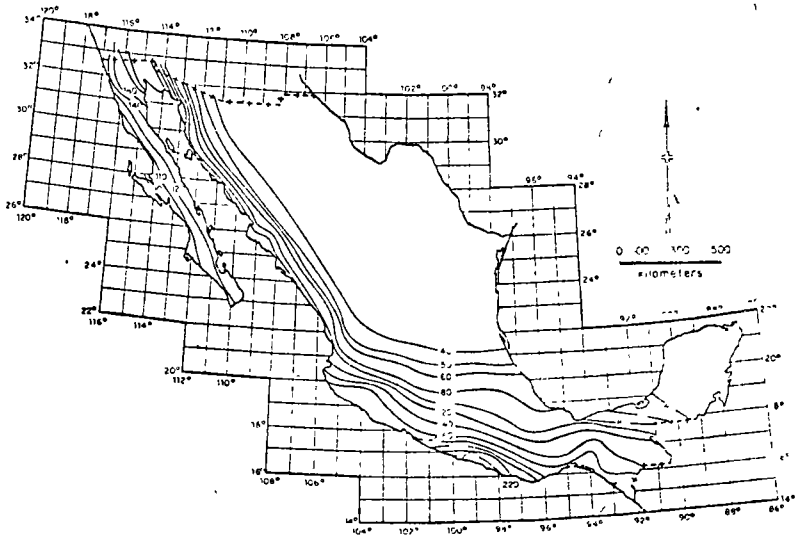

Fig. 6 20 Peak ground accelerations with return period of 100 years (cm/sec^2).

ratio of actual to predicted intensities; and geological details may significantly alter local seismicity in a small region, as well as energy radiation patterns, and hence regional seismicity in the neighbourhood. These systematic deviations are the matter of microzoning, that is, of local modification of risk maps similar to Figs. 6.19 and 6.20.

Most of the effort invested in microzoning has been devoted to study of the influence of local soil stratigraphy on the intensity and frequency content of earthquakes (see Chapter 4). Analytical models have been practically limited to response analysis of stratified formations of linear or nonlinear soils to vertically traveling shear waves. The results of comparing observed and predicted behavior have ranged from satisfactory (Herrera et al , 1965) to poor (Hudson and Udwadia, 1972). Topographic irregularities, as hills or slopes of firm ground formations underlying sediments, may introduce significant systematic perturbations in the surface motion, as a consequence of wave focusing or dynamic amplification. The latter effect was probably responsible for the exceptionally high accelerations recorded at the abutment of Pacoima dam during the 1971 San Fernando earthquake.

Present practice of microzoning determines seismic intensities or design parameters in two steps. First the values of those parameters on firm ground are estimated by means of suitable attenuation expressions and then they are amplified according to the properties of local soil; but this implies an arbitrary decision to which seismic risk is very sensitive: selecting the boundary between soil and firm ground. A specially difficult problem stems when

trying to fix that boundary for the purpose of predicting the motion at the top of a hill or the slope stability of a high cliff (Rukos, 1974).

It can be concluded that rational formulation of microzoning for seismic risk is still in its infancy and that new criteria will appear that will probably require intensity attenuation models which include the influence of local systematic perturbations. Whether these models are available or the two-step process described above is acceptable, intensity-recurrence expressions can be obtained as for the unperturbated case, after multiplying the second member of eq. 6.34 by an adequate intensity-dependent corrective factor.

REFERENCES

Aki, K., 1963. *Some Problems in Statistical Seismology.* University of Tokyo, Geophysical Institute.

Allen, C.R., 1969. Active faulting in northern Turkey. *Calif. Inst. Tech., Div. Geol. Sci., Contrib.* 1577.

Allen, C.R., St. Amand, P., Richter, C.F. and Nordquist, J.M., 1965. Relationship between seismicity and geologic structure in the southern California region. *Bull. Seismol. Soc. Am.*, 55 (4): 753–797.

Ambraseys, N.N., 1973. Dynamics and response of foundation materials in epicentral regions of strong earthquakes. *Proc. 5th World Conf. Earthquake Eng., Rome.*

Ananin, I.V., Bune, V.I., Vvedenskaia, N.A., Kirillova, I.V., Reisner, G.I. and Sholpo, V.N., 1968. *Methods of Compiling a Map of Seismic Regionalization on the Example of the Caucasus.* C. Yu. Schmidt Institute of the Physics of the Earth, Academy of Sciences of the USSR, Moscow.

Benjamin, J.R. and Cornell, C.A., 1970. *Probability, Statistics and Decision for Civil Engineers.* McGraw-Hill, New York.

Ben-Menahem, A., 1960. Some consequences of earthquake statistics for the years 1918–1955. *Gerlands Beitr. Geophys.*, 69: 68–72.

Bollinger, G.A., 1973. Seismicity of the southeastern United States. *Bull. Seismol. Soc. Am.*, 63: 1785–1808.

Bolt, B.A., 1970. Causes of earthquakes. In: R.L. Wiegel (editor), *Earthquake Engineering.* Prentice-Hall, Englewood Cliffs.

Brune, J.N., 1968. Seismic moment, seismicity and rate of slip along major fault zones. *J. Geophys. Res.*, 73: 777–784.

Burridge, R. and Knopoff, L., 1967. Model and theoretical seismicity. *Bull. Seismol. Soc. Am.*, 57: 341–371.

Cornell, C.A. and Vanmarcke, E.H., 1969. The major influences on seismic risk. *Proc. 4th World Conf. Earthquake Eng. Santiago.*

Crouse, C.B., 1973. Engineering studies of the San Fernando earthquake. *Calif. Inst. Technol., Earthquake Eng. Res. Lab.* Rep. 73-04.

Cox, D.F. and Lewis, P.A.W., 1966. *The Statistical Analysis of Series of Events.* Methuen, London.

Davenport, A.G., 1972. A statistical relationship between shock amplitude, magnitude and epicentral distance and its application to seismic zoning. *Univ. Western Ontario, Faculty Eng. Sci.*, BLWT-4-72.

Davies, G.F. and Brune, J.N., 1971. Regional and global fault slip rates from seismicity. *Nature*, 229: 101–107.

Drakopoulos, J.C., 1971. A statistical model on the occurrence of aftershocks in the area of Greece. *Bull. Int. Inst. Seismol. Earthquake Eng.*, 8: 17–39.

Esteva, L., 1968. Bases para la formulación de decisiones de diseño sísmico. *Natl. Univ. Mexico, Inst. Eng. Rep.* 182.

Esteva, L., 1969. Seismicity prediction: a bayesian approach. *Proc. 4th World Conf. Earthquake Eng. Santiago.*

Esteva, L., 1970. Consideraciones prácticas en la estimación bayesiana de riesgo sísmico. *Natl. Univ. Mexico, Inst. Eng., Rep.* 248.

Esteva, L., 1974. Geology and probability in the assessment of seismic risk. *Proc. 2nd Int. Congr. Int. Assoc. Eng. Geol., Sao Paulo.*

Esteva, L. and Villaverde, R., 1973. Seismic risk, design spectra and structural reliability. *Proc. 5th World Conf. Earthquake Eng., Rome*, pp. 2586–2597.

Figueroa, J., 1963. Isosistas de macrosismos mexicanos. *Ingeniería*, 33 (1): 45–68.

Gaisky, V.N., 1966. The time distribution of large, deep earthquakes from the Pamir–Hindu-Kush. *Dokl. Akad. Nauk Tadjik S.S.R.*, 9 (8): 18–21.

Gaisky, V.N., 1967. On similarity between collections of earthquakes, the connections between them, and their tendency to periodicity. *Fiz. Zemli*, 7: 20–28 (English transl., pp. 432–437).

Gajardo, E. and Lomnitz, C., 1960. Seismic provinces of Chile. *Proc. 2nd World Conf. Earthquake Eng., Tokyo*, pp. 1529–1540.

Gutenberg, B. and Richter, C.F., 1954. *Seismicity of the Earth.* Princeton University Press, Princeton.

Gzovsky, M.G., 1962. Tectonophysics and earthquake forecasting. *Bull. Seismol. Soc. Am.*, 52 (3): 485–505.

Herrera, I., Rosenblueth, E. and Rascón, O.A., 1965. Earthquake spectrum prediction for the Valley of Mexico. *Proc. 3rd Int. Conf. Earthquake Eng., Auckland and Wellington*, 1: 61–74.

Housner, G.W., 1969. Engineering estimates of ground shaking and maximum earthquake magnitude. *Proc. 4th World Conf. Earthquake Eng., Santiago.*

Hudson, D.E., 1971. *Strong Motion Instrumental Data on the San Fernando Earthquake of February 9, 1971.* California Institute of Technology, Earthquake Engineering Research Laboratory.

Hudson, D.E., 1972a. Local distributions of strong earthquake ground shaking. *Bull. Seismol. Soc. Am.*, 62 (6).

Hudson, D.E., 1972b. *Analysis of Strong Motion Earthquake Accelerograms, III, Response Spectra, Part A.* California Institute of Technology, Earthquake Engineering Research Laboratory.

Hudson, D.E. and Vdwadia, F.E., 1973. Local distribution of strong earthquake ground motions. *Proc. 5th World Conf. Earthquake Eng., Rome*, pp. 691–700.

Kaila, K.L. and Narain, H., 1971. A new approach for preparation of quantitative seismicity maps as applied to Alpide Belt–Sunda Arc and adjoining areas. *Bull. Seismol. Soc. Am.*, 61 (5): 1275–1291.

Kaila, K.L., Gaur, V.K. and Narain, H., 1972. Quantitative seismicity maps of India. *Bull. Seismol. Soc. Am.*, 62 (5): 1119–1132.

Kaila, K.L., Rao, N.M. and Narain, H., 1974. Seismotectonic maps of southwest Asia region comprising eastern Turkey, Caucasus, Persian Plateau, Afghanistan and Hindukush. *Bull. Seismol. Soc. Am.*, 64 (3): 657–669.

Kelleher, J., Sykes, L. and Oliver, J., 1973. Possible criteria for predicting earthquake locations and their application to major plate boundaries of the Pacific and the Caribbean. *J. Geophys. Res.*, 78 (14): 2547–2585.

Knopoff, L., 1964. The statistics of earthquakes in southern California. *Bull. Seismol. Soc. Am.*, 54: 1871–1873.

Lomnitz, C., 1966. Magnitude stability in earthquake sequences. *Bull. Seismol. Soc. Am.*, 56: 247–249.

Lomnitz, C. and Hax, A., 1966. Clustering in aftershock sequences. In: J.S. Steinhart and T. Jefferson Smith (editors), *The Earth Beneath the Continents.* Am. Geophys. Union, pp. 502-508.

McGuire, R.K , 1974. Seismic structural response risk analysis incorporating peak response regressions on earthquake magnitude and distance *Mass Inst Technol , Dep Civ Eng* , R74-51

Merz, H A and Cornell, C A , 1973 Seismic risk analysis based on a quadratic magnitude—frequency law. *Bull. Seismol Soc Am.*, 63 (6) 1999—2006.

Milne, W G. and Davenport, A G , 1969 Earthquake probability *Proc 4th World Conf. Earthquake Eng , Santiago.*

Mogi, K , 1962 Study of elastic shocks caused by the fracture of heterogeneous materials and its relations to earthquake phenomena *Bull Earthquake Res Inst Tokyo*, 40 125—173.

Molnar, P. and Sykes, L R , 1969. Tectonics of the Caribbean and Middle America regions from focal mechanisms and seismicity *Geol Soc Am Bull* , 80 1639

Newark, N M. and Rosenblueth, E., 1971. *Fundamentals of Earthquake Engineering* Prentice-Hall, Englewood Cliffs

Omori, F., 1894. On the aftershocks of earthquakes. *J. Coll Sci Imp Univ Tokyo*, 7: 111—200

Parzen, E., 1962 *Stochastic Processes* Holden Day, San Francisco.

Petrushevsky, B A , 1966 *The Geological Fundamentals of Seismic Zoning* Scientific Translation Service, order 5032, Ann Arbor, USA.

Raiffa, H and Schlaifer, R , 1968 *Applied Statistical Decision Theory*, MIT Press.

Rosenblueth, E , 1964 Probabilistic design to resist earthquakes *Am Soc. Civ Eng , J. Eng Mech Div.*, 90 (EM5) 189—249

Rosenblueth, E., 1969 Seismicity and earthquake simulation. *Rep. NSF-UCEER Conf. Earthquake Eng. Res , Pasadena;* pp. 47-64.

Rosenblueth, E , 1975 *Point Estimates for Probability Moments* National University of Mexico, Institute of Engineering, Mexico City.

Rosenblueth, E , in preparation Optimum design for infrequent disturbances.

Rukos, E., 1974. *Análysis dinamico de la margen izquierda de Chicoasén* National University of Mexico, Institute of Engineering, Mexico City.

Salt, P.E., 1974 Seismic site response *Bull N. Z Natl. Soc Earthquake Eng* , 7 (2) 63—77

Scholz, C.H , 1968 The frequency—magnitude relation of microfracturing and its relation to earthquakes *Bull. Seismol. Soc. Am.*, 58. 399—417.

Shlien, S. and Toksoz, M.N., 1970. A clustering model for earthquake occurrences *Bull Seismol Soc Am* , 60 (6) 1765—1787

Singh, S K , 1975 *Mexican Volcanic Belt Some Comments on a Model Proposed by F Mooser.* National University of Mexico, Institute of Engineering, Mexico City.

Trifunac, M D , 1973. Characterization of response spectra by parameters governing the gross nature of earthquake source mechanisms. *Proc. 5th World Conf Earthquake Eng* , Rome, pp. 701—704

Tsuboi, C , 1958 Earthquake province. Domain of sympathetic seismic activities *J Phys. Earth.*, 6 (1) 35—49

Utsu, T., 1961. A statistical study on the occurrence of aftershocks *Geophys Mag , Tokyo*, 30 521—605

Utsu, T , 1962 On the nature of three Alaska aftershock sequences of 1957 and 1958. *Bull Seismol. Soc Am* , 52 179—297

Veneziano, D. and Cornell, C.A., 1973. Earthquake models with spatial and temporal memory for engineering seismic risk analysis *Mass Inst Technol , Dep. Civ Eng.*

Vere-Jones, D , 1970. Stochastic models for earthquake occurrence *J R. Stat. Soc* , 32 (1) 1—45.

Wallace, R E , 1970 Earthquake recurrence intervals on the San Andreas Fault *Geol Soc Am. Bull* , 81 2875—2890.

Yegulalp, T M. and Kuo, J T , 1974. Statistical prediction of the occurrences of maximum magnitude earthquakes *Bull Seismol Soc. Am.*, 64 (2): 393—414.

DIRECTORIO DE ASISTENTES AL CURSO: SISMOLOGIA Y SISMICIDAD
(DEL 5 AL 21 DE JULIO DE 1977

	NOMBRE Y DIRECCION	EMPRESA Y DIRECCION
1.	ING. JOSE FRIAS DIAZ	UNIVERSIDAD AUTONOMA DEL ESTADO DE MEXICO.
2.	ING. ALBERTO GARCIA RUBIO	INSTITUTO MEXICANO DEL PETROLEO Av. de los 100 Metros # 152 México, D. F.
3.	ING. ARTURO QUIROZ SOTO Sur 109 # 705 Col. Sector Popular México 13, D. F. Tel. 582-43-35	UNIVERSIDAD AUTONOMA METROPOLITANA Av. San Pablo s/n Azcapotzalco, D. F. Tel. 561-37-33 Ext. 200
4.	ALFREDO RAMIREZ ANGELES Inguarán # 3651 Col. Río Blanco Mexico 14, D. F.	DGETENAL San Antonio Abad # 124 Col. Tránsito México 14, D. F. Tel. 578-62-00 Ext. 7276
5.	ING. CARLOS VALDESPINO PONCE Roble #29 Col. Casa Blanca Toluca, Edo. de Méx. Tel. 438-87	UNIVERSIDAD AUTONOMA DEL ESTADO DE MEXICO. F. I Cerro Coatepec Toluca Edo. de Méx. Tel. 545-12